NASA CR 182112

LARGE-SCALE ADVANCED PROP-FAN (LAP) FINAL REPORT

(NASA-CR-182112) LARGE-SCALE ADVANCED
PROP-FAN (LAP) Final Report (Hamilton
Standard) 255 p CSCL 21E

N88-20306

Unclas
G3/07 0134586

By: C.L. DeGeorge

HAMILTON STANDARD DIVISION
UNITED TECHNOLOGIES

Prepared for
National Aeronautics and Space Administration
NASA-Lewis Research Center
Contract NAS3-23051

NASA CR 182112

ORIGINAL CONTAINS
COLOR ILLUSTRATIONS

NASA

LARGE-SCALE ADVANCED PROP-FAN (LAP) FINAL REPORT

By: C.L. DeGeorge

HAMILTON STANDARD DIVISION
UNITED TECHNOLOGIES

Prepared for
National Aeronautics and Space Administration
NASA-Lewis Research Center
Contract NAS3-23051

CONTENTS

SUBJECT PAGE

1.0 SUMMARY 1

2.0 INTRODUCTION 3

3.0 SR-7L BLADE DESIGN 11

- 3.1 Blade Configuration 11
- 3.2 Design Requirements and Goals 11
  - 3.2.1 Design Requirements 12
  - 3.2.2 Design Goals 14
- 3.3 Finite Element Modeling 16
- 3.4 Steady-State Analysis 17
  - 3.4.1 Application of Loads 17
  - 3.4.2 Pre-Deflection Design 17
  - 3.4.3 Final Calculations 18
- 3.5 Vibratory Response Analysis 18
  - 3.5.1 Origin of the Once-Per-Revolution Excitation 18
  - 3.5.2 Calculation of Vibratory Response 18
- 3.6 Stress vs Strength Evaluation 19
  - 3.6.1 Method of Combining Steady-State and Vibratory Stresses 19
  - 3.6.2 High Cycle Fatigue 20
  - 3.6.3 Low Cycle Fatigue 21
- 3.7 Resonant Frequencies and Mode Shapes 22
  - 3.7.1 Calculation Method 22
  - 3.7.2 Results 22
- 3.8 Stability 24
  - 3.8.1 Unstalled Flutter Analysis 24
  - 3.8.2 Stall Flutter Evaluation 26

PR. NG PAGE BLANK NOT FILMED

PAGE INTENTIONALLY BLANK

CONTENTS (Continued)

SUBJECT PAGE

3.9 Foreign Object Damage 27
- 3.9.1 Calculation Procedure 27
- 3.9.2 Effect On Blade 27

3.10 Blade Trunnion Design 28
- 3.10.1 Blade Trunnion Loading and Fatigue Strength 28

4.0 SR-7L HUB AND BLADE RETENTION DESIGN 37

4.1 Configuration 37
4.2 Design Requirements 37
4.3 Retention and Hub Loads 38
- 4.3.1 Retention Loads 38
- 4.3.2 Tailshaft Loads 39

4.4 Blade Retention Stress Analysis 39
4.5 Hub Stress Analysis 39
4.6 Tailshaft Stress Analysis 40
4.7 Retention Stiffness Analysis 40

5.0 SR-7L SPINNER DESIGN 47

5.1 Configuration 47
5.2 Design Requirements 47
5.3 Finite Element Model 47
5.4 Steady Loads 48
5.5 Vibratory Loads 48
5.6 Spinner Stress Analysis 48
5.7 Spinner Natural Frequencies 48
5.8 Spinner Foreign Object Damage Analysis 48
5.9 Spinner Removability 49

6.0 SR-7L PITCH CHANGE ACTUATOR AND CONTROL DESIGN 53

6.1 Configuration 53
6.2 Design Requirements 54
6.3 Actuator Design 54
- 6.3.1 Servo and Ballscrew 54

CONTENTS (Continued)

SUBJECT PAGE

6.3.2 Pitchlock Screw 55
6.3.3 Beta Valve 55
6.3.4 ΔP Valve 56
6.3.5 Stationary Piston and Translating Cylinder 56

6.4 Control Design 58

6.4.1 Hydraulic Pumps 58
6.4.2 Main and Standby Regulating Valve with Orifice Pack 58
6.4.3 Governor 59
6.4.4 Feather Valve 59
6.4.5 Control Input Linkage 60
6.4.6 Gearing 60
6.4.7 Transfer Bearing 61
6.4.8 Auxiliary Pump and Motor 61

6.5 Control Dynamic Analysis 62
6.6 Beta Control 62

7.0 SR-7L SYSTEM DESIGN AND INTEGRATION 75

7.1 Consistency of Design Loads 75
7.2 Hardware Compatibility 76
7.3 Failure Mode and Effects Analysis 76

8.0 SR-7L PROP-FAN INSTRUMENTATION SYSTEM DESIGN 77

8.1 System Description 77
8.2 Design Goals and Criteria 78
8.3 Transducers 78

8.3.1 Strain Gages 78
8.3.2 Pressure Transducers 78
8.3.3 Blade Angle Potentiometer 79

8.4 Bridge Completion Boards 79
8.5 Programmable Connectors 79
8.6 Rotating Interface Board (RIB) 80
8.7 VCO Case 80
8.8 Rotating Power Supply 81
8.9 Slip Ring and Brush Block 82
8.10 Detranslator/Discriminator System 82

CONTENTS (Continued)

SUBJECT PAGE

9.0 SR-7A AEROELASTIC MODEL DESIGN 87

9.1 Design Goals and Requirements 87
9.2 Blade and Retention Design 87

9.2.1 Blade Finite Element Analysis 89
9.2.2 Steady State Analysis and Results 89
9.2.3 Blade Resonant Frequencies and Mode Shapes 90
9.2.4 Blade Stability 90

9.3 SR-7A Hub and Spinner Design 91

9.3.1 Hub Stress Analysis 91

9.4 Pitch Change Mechanism Design 92

10.0 MANUFACTURING AND QUALITY ASSURANCE 99

10.1 Manufacturing 99

10.1.1 SR-7L Blade Fabrication 99
10.1.2 SR-7L Hub Fabrication 99
10.1.3 SR-7L Spinner Fabrication 100
10.1.4 SR-7L Pitch Control and Actuator 100
10.1.5 SR-7L Prop-Fan Assembly Procedures and Tools 100
10.1.6 SR-7A Aeroelastic Model Blade Fabrication 100

10.2 Quality Assurance 101

10.2.1 Configuration and Change Control 101
10.2.2 Procurement Source Control 102
10.2.3 Material and Process Control 102
10.2.4 Control of Nonconforming Material 102

11.0 SUB-COMPONENT TESTING 109

11.1 Main & Standby Valve and Orifice Pack 109
11.2 Transfer Bearing 111
11.3 Pump Tests 113

CONTENTS (Continued)

SUBJECT PAGE

12.0 RETENTION STIFFNESS TEST 121

12.1 Test Description 121
12.2 Test Results 121
12.3 Comparison of Data and Analytical Predictions 122

13.0 WHIRL RIG TEST 127

13.1 Test Description 127

13.1.1 Feather Test 127
13.1.2 Speed Set Point and Dead Band Test 128
13.1.3 Governor Gain Test 128
13.1.4 Blade Angle Cycling Endurance Test 128
13.1.5 Maximum CTM Endurance Test 128
13.1.6 Blade Angle Pitchlock Test 129

13.2 Test Results 129

13.2.1 Feathering Test 129
13.2.2 Speed Set Point and Dead Band Test 129
13.2.3 Governor Gain Test 129
13.2.4 Maximum CTM Endurance Test 130
13.2.5 Blade Angle Cycling Endurance Test 130
13.2.6 Blade Angle Pitchlock Test 130

13.3 Comparison of Data with Analytical Predictions 130

14.0 Blade ESA and Fatigue Testing 137

14.1 Test Description 137

14.1.1 Blade ESA Test 137
14.1.2 Blade Fatigue Test 138

14.2 Test Results 139

14.2.1 Blade ESA Test 139
14.2.2 Blade Fatigue Test 140

14.3 Discussion of Results 141

14.3.1 Blade ESA Test 141
14.3.2 Blade Fatigue Test 141

CONTENTS (Continued)

SUBJECT PAGE

15.0 HUB ESA AND FATIGUE TESTING 151

15.1 Test Description 151

15.1.1 Hub ESA Test 151
15.1.2 Hub Fatigue Test 152

15.2 Test Results 152

15.2.1 Hub ESA Test 152
15.2.2 Hub Fatigue Test 154

16.0 STATIC ROTOR TEST 159

16.1 Test Description 159

16.1.1 Aerodynamic Performance Testing 160
16.1.2 Structural Dynamic Testing 160
16.1.3 Blade Steady State Strain and Deflection Measurement 162
16.1.4 Blade Surface Steady Pressure Testing 163
16.1.5 Blade Surface Unsteady Pressure Testing 165

16.2 Results and Discussion 167

16.2.1 Aerodynamic Performance 167
16.2.2 Structural Dynamic Test Results 168
16.2.3 Blade Steady Strain and Deflection 169
16.2.4 Blade Surface Steady Pressure Results 170
16.2.5 Blade Surface Unsteady Pressure Results 170

17.0 HIGH SPEED WIND TUNNEL TEST 189

17.1 Test Description 189

17.1.1 Test Facility 189
17.1.2 Spinner/Centerbody Drag Test 190
17.1.3 Aerodynamic Performance Testing 192
17.1.4 Structural Dynamic Testing 193
17.1.5 Blade Surface Steady Pressure Testing 194
17.1.6 Blade Surface Unsteady Pressure Testing 194

CONTENTS (Continued)

SUBJECT PAGE

17.2 Test Results 194

17.2.1 Spinner/Centerbody Drag Test 194
17.2.2 Aerodynamic Performance Testing 195
17.2.3 Structural Dynamic Testing 196
17.2.4 Blade Surface Steady Pressure Testing 197
17.2.5 Blade Surface Unsteady Pressure Testing 197

18.0 SR-7A AEROELASTIC MODEL WIND TUNNEL TEST 213

18.1 SR-7A Aeroelastic Model Instrumentation 213
18.2 SR-7A Aeroelastic Model Wind Tunnel Test Procedure 213

18.2.1 Static and Low Speed Testing 213
18.2.2 Intermediate and High Speed Testing 214

18.3 SR-7A Aeroelastic Model Test Results 215

18.3.1 Static and Low Speed Test Results 215
18.3.2 Intermediate and High Speed Test Results 216

19.0 INTERFACE COORDINATION 227

19.1 Installation Drawing 227
19.2 Prop-Fan Physical Properties 227
19.3 Interconnections and Utilities 228

19.3.1 Mechanical 228
19.3.2 Electrical 228

20.0 CONCLUSIONS AND RECOMMENDATIONS 237

20.1 Conclusions 237
20.2 Recommendations 239

REFERENCES 241

APPENDIX A FAILURE MODE AND EFFECT ANALYSIS 243

ILLUSTRATIONS

FIGURE		PAGE
2.1	Summary of Prop-Fan Wind Tunnel Models	7
2.2	Flight Operating Envelope	8
2.3	Large Scale Advanced Prop-Fan	9
3.1	SR-7L Blade Design Configuration	29
3.2	SR-7L Blade Finite Element Model	30
3.3	SR-7L Element Model Restraints	31
3.4	Cyclic Aerodynamic Loading	32
3.5	Typical Goodman Diagram	33
3.6	Calculated Modal Frequencies	34
3.7	Blade Trunnion Assembly	35
4.1	LAP Hub	42
4.2	Cross Section - LAP Hub and Blade Retention	43
4.3	Blade Loading Coordinate System	44
4.4	Subsurface Stress, Hub Retention Bearing Race	45
4.5	Tailshaft Stresses	46
5.1	Spinner Configuration	50
5.2	Spinner Assembly - Analytical Model	50
5.3	Spinner Stress Analysis Results	51
5.4	Spinner Natural Frequency Criteria	52
6.1	LAP Control Schematic	63
6.2	LAP Actuator	65
6.3	LAP Control	66
6.4	Beta Valve Flow and Pressure Gain	67
6.5	SR-7L Centrifugal and Aerodynamic Twisting Moment, (100% speed)	68
6.6	Actuator Pressure Spectrum for a Typical Flight	69
6.7	Governor Linkage Schematic	70
6.8	LAP Control Gear Train Schematic - View Looking Aft	71
6.9	Transfer Bearing Modifications	72
6.10	LAP System Functional Block Diagram	73
6.11	Motor Driven Pitch Control Mechanism	74
8.1	LAP Instrumentation Schematic	83
8.2	LAP Instrumentation Hardware Assembly	84
8.3	Bridge Completion Board Installation	85
8.4	Programmable Connector Wiring	86
9.1	SR-7A Blade Construction	93
9.2	Deflection Contour Plots, 35000 ft Altitude, Cruise Condition	94
9.3	SR-7A Blade Stress Analysis Results	95
9.4	Comparison of SR-7A and SR-7L Blade Natural Frequencies	96
9.5	SR-7A Blade Retention, Hub and Pitch Change Mechanism	97
10.1	SR-7L Blade in Resin Injection Die	104
10.2	Foaming Mold for SR-7A Aeroelastic Model Blade	105
10.3	SR-7A Spar/Foam Assembly	106
10.4	Resin Injection Mold	107
11.1	Main & Standby Valve Test Arrangement	114

PRECEDING PAGE BLANK NOT FILMED

PAGE X INTENTIONALLY BLANK

ILLUSTRATIONS (Continued)

FIGURE		PAGE
11.2	Effect of Leakage on Main & Standby Valve Performance	115
11.3	Test Arrangement, Main and Standby Valve and Orifice Pack	116
11.4	Transfer Bearing Test Schematic	117
11.5	Transfer Bearing Deflection Due to Pressure Loading, Original Design	118
11.6	Pump 100 Hour Endurance Test Results	119
12.1	Retention Stiffness Test Arrangement	123
12.2	Stub Natural Frequency vs RPM	124
12.3	Stub Natural Frequency vs Retention Stiffness	125
12.4	Retention Stiffness vs Centrifugal Load	126
13.1	Whirl Rig Test Arrangement	131
13.2	LAP Installed in the G-5 Whirl Rig	132
13.3	Input Lever Position vs Governing Speed	133
13.4	Blade Pitch Rate vs % Speed Error, Set Point = 1698 RPM	134
13.5	Pitchlock Test Results 1780 RPM	135
14.1	Stresscoat Test Arrangement - Edgewise Mode	142
14.2	Strain Gage Arrangement for Static and Dynamic Testing	143
14.3	Dynamic Strain Gage Test Configuration	144
14.4	Zero Mean Stress Fatigue Test Arrangement	145
14.5	Mean Stress Fatigue Test Configuration	146
14.6	Stresscoat Results, Face Side	147
14.7	Stresscoat Results, Camber Side	148
14.8	Static Strain Gage ESA - Spanwise Strain Distribution Along Spar	149
14.9	Static Strain Gage ESA - Spanwise Strain Distribution Along Sheath	150
15.1	Hub ESA Test Arrangement	155
15.2	Loading Configurations for Hub ESA Testing	156
15.3	Brittle Lacquer Indication Centrifugal Loading	157
16.1	SR-7L Prop-Fan on WPAFB Whirl Rig	172
16.2	Active Strain Gage Arrangement for Flutter and Critical Speed Testing	173
16.3	Active Strain Gage Arrangement for Steady Strain and Blade Deflection Testing	174
16.4	Steady Pressure Blade, Pressure Tap Numbering and Locations	175
16.5	Unsteady Pressure Blade, Transducer Locations	176
16.6	SR-7L Corrected Thrust and Power vs Blade Angle	177
16.7	SR-7L Prop-Fan, Comparison of Measured and Predicted Curves of Blade Angle vs Power Coefficient and Thrust Coefficient vs Power Coefficient	178
16.8	SR-7L Static Rotor Test Summary	179
16.9	SR-7L Blade Natural Frequencies	180
16.10	The Effect of Blade Angle on Blade Natural Frequency for the SR-7L	181
16.11	SR-7L Steady Strain Radial Distribution During WPAFB Overspeed Test, $\beta_{3/4} = 25.8°$, 2038 RPM, Strain Normalized to Maximum Strain Gage 417	182

ILLUSTRATIONS (Continued)

FIGURE		PAGE
16.12	SR-7L Steady Strain During the Overspeed Test, β3/4 = 25.8°, 2038 RPM	183
16.13	Blade Tip Twist Deflection vs Rotational Speed β3/4 = 25.8°	184
16.14	Comparison of Measured & Predicted Blade Twist Deflection β3/4 = 32°, N = 1700 RPM	185
16.15	SR-7 Pressure Distribution, r/R = 0.287	186
16.16	SR-7 Pressure Distribution, r/R = 0.963	187
16.17	Pressure Data, Transducer PT21C, Plate Obstruction, β3/4 = 32°, 1200 RPM	188
17.1	Prop-Fan Drive System ONERA S1 Wind Tunnel	199
17.2	Centerbody Pressure Tap Locations, High Speed Wind Tunnel Test	200
17.3	Spinner Drag Test Arrangement	201
17.4	Prop-Fan Two, Four and Eight Blade Configurations, High Speed Wind Tunnel Tests	202
17.5	Strain Gage Arrangements - High Speed Wind Tunnel Test	203
17.6	Tap Locations, Steady Pressure Blade, High Speed Wind Tunnel Test	204
17.7	Prop-Fan Steady Pressure Test Set-Up	205
17.8	LAP Spinner Drag Coefficient vs Mach Number	206
17.9	Centerbody Drag Coefficient vs Mach Number	207
17.10	Comparison of Measured and Predicted Performance, 4 Blades	208
17.11	Comparison of Measured and Predicted Performance, 8 Blades	209
17.12	Steady Pressure Data - Nominal Static Case	210
17.13	Steady Pressure Data - High Mach No., Low Power Case	211
17.14	Unsteady Pressure Data, High Speed Wind Tunnel Test	212
18.1	SR-7A Strain Gage Arrangement	218
18.2	SR-7A Installed in 9 X 15 Low Speed Wind Tunnel	219
18.3	SR-7A Model Prop-Fan in 8 X 6 Foot NASA-Lewis Wind Tunnel	220
18.4	SR-7A High Vibratory Strain Operating Limits	221
18.5	Comparison of High Vibratory Strain Operating Boundaries for SR-7A and SR-7L	222
18.6	1P Vibratory Strain Response as a Function of Inflow Angle	223
18.7	SR-7A Blade Natural Frequency vs RPM	224
18.8	Mid-Blade 1P Vibratory Strain vs Inflow angle	225
18.9	Mid-Blade Vibratory Strain vs RPM	226
19.1	PF8T60 Prop-Fan Installation Drawing	231
19.2	LAP Reverse Thrust Produced and Power Absorbed	233
19.3	LAP Drag, Feathered Configuration	234
19.4	LAP Windmilling Drag	235

TABLES

TABLE		PAGE
3-1	Primary Required Design Conditions Analyzed to Assure Structural Adequacy	12
3-2	Additional Secondary Conditions Evaluated	15
3-3	Table of Spring Rates to be Simulated	16
3-4	High Cycle Fatigue Stress/Strength Comparison	20
3-5	Low Cycle Fatigue Stress/Strength Comparison	21
3-6	SR-7L Blade Resonant Frequency Summary	23
3-7	Predicted Flutter Mach Number for Ten SR-7L Operating Conditions	25
3-8	Stall Flutter Onset Prediction Summary	26
4-1	Retention Loads	38
4-2	Comparison of 2-D and 3-D Barrel Stiffness Results	40
4-3	Comparison of Retention Stiffness Results	41
5-1	Revised Spinner Shell Thickness	49
6-1	Actuator Sizing Criteria	56
8-1	VCO Sub-Carrier Frequencies	81
9-1	SR-7A Design Conditions	89
12-1	Comparison of Measured and Calculated Retention Stiffnesses	122
13-1	Control Dead Band Data	129
14-1	Stresscoat ESA Test Results	139
14-2	Comparison of Measured and Predicted Resonant Frequencies	140
15-1	Stresscoat Indications Found at Tested Load Conditions	153
15-2	% of Allowable Hub Stress For 10^8 Cycles	154
16-1	Test Points for Aerodynamic Performance and Structural Dynamic Testing	161
16-2	Steady State Structural Test Points	162
16-3	Steady Pressure Test Points	164
16-4	Blade Surface Unsteady Pressure Test Points	166
17-1	Spinner/Centerbody Drag Test Points	191
18-1	Low Speed Test Points for which the Blade 1P Response was Calculated	214
18-2	High Speed Test Points for which the Blade 1P Response was Calculated	214

PRECEDING PAGE BLANK NOT FILMED

PAGE XIV INTENTIONALLY BLANK

1.0 SUMMARY

The Large Scale Advanced Prop-Fan (LAP) Program accomplished the successful design, fabrication and ground testing of a full scale, flightworthy Prop-Fan system capable of operation at Mach .8 and 35,000 feet altitude. An aeroelastic model of the full scale Prop-Fan was also successfully fabricated and tested. Extensive quantities of test data were collected, analyzed and compared with theoretical predictions. This served to prove out the LAP hardware, confirmed the validity of the analytical techniques used in the design and amassed a data base that will be useful as a guide in the design of future Prop-Fans.

The specific Prop-Fan components that were designed and fabricated during the course of the Large Scale Advanced Prop-Fan Program were the blade, hub, spinner, actuator and control. The element of the Prop-Fan design that allows it to operate efficiently at Mach numbers up to 0.8 are the thin highly swept and highly loaded blades. Hamilton Standard was able to design and build these blades using design tools, materials and fabrication techniques that had previously proven successful on more conventional military and commercial propellers along with new techniques developed during Prop-Fan model testing over the past 10 years. The hub, spinner, actuator and control did not incorporate significant new technology and their design and fabrication proceeded along the lines of standard propellers.

Significant hardware development testing was accomplished on the Prop-Fan system components to ensure their suitability for Static Rotor and High Speed Wind Tunnel Testing in this contract and Static Engine and Flight Testing in the follow on PTA Program (reference contract NAS3-24339). The hardware development testing included sub-component testing of selected control components, blade retention stiffness testing, whirl rig testing of the Prop-Fan with stub blades and fatigue and Experimental Stress Analysis testing of the blade and hub. None of these tests uncovered any problems that would impede the completion of static rotor, high speed wind tunnel, static engine or flight testing.

Static rotor and high speed wind tunnel testing provided extensive data on the static and dynamic structural behavior and the aerodynamic performance of the Prop-Fan system. Among the significant findings of this testing were: a stall buffet phenomenon prevented the Prop-Fan from absorbing design power at design operating RPM static conditions; unstalled flutter was not encountered anywhere in the portion of the flight envelope tested; the importance of tip and leading edge vortex flow in determining the blade surface pressure distribution for static and low Mach number operating conditions; the importance of shocks attached to the blade camber surface in determining the blade surface pressure distribution near the tip at intermediate and high subsonic Mach numbers.

The structural dynamic performance of the aeroelastic model during aerodynamic performance and acoustic testing in the NASA LeRC 8' X 6' and 9' X 15' wind tunnels correlated well with that of the Large Scale Advanced Prop-Fan. This demonstrated the utility of using an aeroelastically scaled model to predict the structural dynamic performance of a full scale Prop-Fan.

2.0 INTRODUCTION

National energy demand has outpaced domestic supply, creating an increased U.S. dependence on foreign sources. This was dramatized by the OPEC oil embargo in the winter of 1973 to 1974. The embargo triggered a rapid rise in the cost of fuel which brought about increased emphasis on energy conservation. Later, in 1979 worldwide shortages caused an additional steep rise in the cost of oil. These events, of course, affected the air transport industry as well as other high energy consuming industries.

In 1975, at the request of Congress, NASA established the Aircraft Energy Efficiency (ACEE) Program directed at reducing fuel consumption of commercial subsonic air transports. Besides saving fuel, the technology developed under the program would help U.S. aircraft manufacturers retain their dominant role in the world commercial aircraft market. One element of the ACEE Program offering the greatest potential fuel savings is the Advanced Turboprop Program (ATP). Turboprops, with their inherently higher propulsive efficiency, have provided efficient transportation for years at speeds of about Mach 0.6 and altitudes around 20,000 feet. However, in order to be compatible with the current and future commercial aircraft operational structure, future turboprop-powered aircraft will be required to cruise at speeds of Mach 0.7 to 0.8 and altitudes of 30,000 feet and higher, while maintaining a comfortable cabin environment.

Studies have shown that the inherent efficiency advantage of turboprop propulsion systems over turbofan systems at low speed may be extended to high subsonic speeds by use of highly loaded, multi-bladed, swept-tip propellers, (sometimes called Prop-Fans). Turboprop aircraft with this type of propeller have the potential of obtaining fuel savings of 15 to 20 percent relative to turbofans with an equivalent level of core engine technology. This translates into a 30 to 40 percent fuel savings relative to current in-service turbofan-powered aircraft.

Initial work under the ATP concentrated on small aerodynamic models of Prop-Fans. Beginning in 1976 Hamilton Standard and NASA collaborated on a series of these models which were tested in NASA and United Technologies Corporation wind tunnels. The models were used to evaluate the aerodynamic performance and structural dynamic characteristics of various Prop-Fan designs over a range of Mach numbers up to 0.8 Mn. Figure 2.1 describes the design of the various wind tunnel models that were tested and summarizes the results that were obtained. These tests demonstrated that an advanced turboprop propulsion system that could achieve propulsive efficiencies above 80% at Mach 0.8 could be designed. Based on the performance obtained with the various aerodynamic models, and structural and aerodynamic lessons learned, the design of the SR-3 Prop-Fan blade was found to be most appropriate as the basis for a full scale Prop-Fan design.

PRECEDING PAGE BLANK NOT FILMED

PAGE 2 INTENTIONALLY BLANK

2.0 (Continued)

In 1981 Hamilton Standard initiated work under NASA contract NAS3-22394 to perform design studies for a Large Scale Advanced Prop-Fan (LAP). The detail tasks undertaken in this program were:

- The selection of the LAP Prop-Fan configuration (referred to as SR-7L)
- The Aerodynamic/Acoustic design of the SR-7L blade
- Preliminary mechanical design of the SR-7L blade
- Concept design of the testbed Prop-Fan System
- Preliminary design of a scale aeroelastic model of the LAP.

The work conducted by Hamilton Standard under contract NAS3-22394 provided the basis from which to proceed with a full fledged design and development program for the Large Scale Advanced Prop-Fan.

In 1983 Hamilton Standard began work on the Large Scale advanced Prop-Fan program under NASA contract NAS3-23051. The objectives undertaken by Hamilton Standard under this contract were to:

1. Design and fabricate large-scale, flightworthy, advanced technology Prop-Fan blades for testing and evaluation.
2. Evaluate Prop-Fan blade structural characteristics (natural frequencies and modes, strength, fatigue life, and FOD tolerance) through specimen and large-scale blade tests.
3. Design and fabricate flightworthy hub, pitch change mechanism, and pitch control hardware for use in Prop-Fan system testing.
4. Experimentally determine the operating characteristics of the hub, blade retension, pitch change mechanism, and pitch control at simulated operating conditions.
5. Experimentally determine the Prop-Fan performance, overspeed characteristics, and stall flutter boundaries at static (zero forward speed) conditions.
6. Experimentally evaluate the Prop-Fan high-speed flutter characteristics.
7. Design, fabricate and test an aeroelastic model Prop-Fan having the same aerodynamic characteristics and similar aeroelastic characteristics as the large-scale Prop-Fan.
8. Deliver Prop-Fan assemblies for planned flight testing with a drive system.

2.0 (Continued)

The design parameters for the Large Scale Advanced Prop-Fan included 8 blades and a 9 foot diameter disk with a design blade tip speed of 800 ft/sec. The SR-7L Prop-Fan is designed for a maximum takeoff power of 4413 kw (6000 horsepower) and a cruise power of 1906 kw (2592 horsepower) at an altitude of 10,668 meters (35000 ft) and Mach 0.8. The design performance goals of the LAP were to achieve a configuration that was free of flutter through the flight envelope defined in Figure 2.2, a net propulsive efficiency of 78.6% at the design cruise condition, a near field noise level of 144 dB at the design cruise condition and a far field noise level on takeoff meeting FAR-36 minus 10 dB.

The design, fabrication and testing procedures employed during the LAP program were intended to produce a flight representative test article. The structural and mass properties of the Prop-Fan hardware, the safety features designed into the Prop-Fan system, the quality and product assurances procedures used during the manufacturing cycle and the planned component testing were all focused on ensuring that the SR-7L would be suitable for engine and flight testing at the completion of the Large Scale Advanced Prop-Fan program. If achievement of the design goals discussed above could be demonstrated, using a flightworthy test article, a significant step would be taken in proving the readiness of Prop-Fan technology for introduction into the commercial aviation marketplace.

The scope of the work undertaken in the Large Scale Advanced Prop-Fan Program included the design and fabrication of the Prop-Fan hardware, the flight instrumentation system, assembly tooling and procedures and an aeroelastic wind tunnel model of the Prop-Fan. Hardware development and proof of concept testing were conducted for both the SR-7L Prop-Fan and the aeroelastic model. System design and integration, interface coordination and parametric data tasks were also undertaken.

The detail SR-7L Prop-Fan components designed and fabricated were the blade, the hub and retention, the control and actuator and the spinner. These components are illustrated in Figure 2.3.

Since many of the features of the SR-7L Prop-Fan differ from those of Hamilton Standard's production propellers, design and fabrication of a set of assembly tools and fixtures unique to the Prop-Fan was required. Assembly and test procedures were also documented in an assembly and test specification.

The planned testing and research to be conducted with the Large Scale Advanced Prop-Fan established a need for the capability to monitor a large number of parameters on the rotating side of the Prop-Fan. The electronic instrumentation system conceived for the SR-7L provided 32 channels for transmitting information from the rotating to the stationary field. The system employed multiplexed FM signals, transmitted through a brush block and slip ring arrangement.

2.0 (Continued)

The design of the SR-7L blade incorporated a thin airfoil section, a highly swept planform and lightweight composite construction. These characteristics made the SR-7L blade more likely to encounter flutter than the heavier and stiffer metal blades used on standard propellers. For this reason a small scale aeroelastic model of the SR-7L was designed and constructed. The characteristics of the aeroelastic model were scaled so as to yield the same aeroelastic performance as the SR-7L. The aeroelastic response obtained with the SR-7L and aeroelastic model could be compared for the same test condition to confirm the validity of the model. The aeroelastic model was also used to explore the aeroelastic response to operating conditions that could not be obtained with the SR-7L due to test facility limitations. Aerodynamic performance and acoustic tests of the model were conducted by NASA.

Testing conducted under the LAP program could be classified under two categories, hardware development testing and proof of concept testing. Hardware development testing was intended to confirm the suitability of certain critical components for use in the SR-7L Prop-Fan. Hardware development testing included control sub-component testing, experimental stress analysis and fatigue testing of the hub and blade, and whirl rig testing of the Prop-Fan with stubs substituted for the blades. Proof of concept testing was intended to evaluate the performance of the Prop-Fan system at various operating conditions. Proof of concept testing included the SR-7L Static Rotor Test, the SR-7L High Speed Wind Tunnel Test and the aeroelastic model wind tunnel test.

The tasks conducted as part of the system design and integration effort were intended to coordinate the designs of the major SR-7L components illustrated in Figure 2.3. This effort included coordinating all interface dimensions to ensure proper clearances and fit, ensuring consistency of design loads at all component interfaces and the preparation of a failure mode and effects analysis for the entire Prop-Fan System.

Interface coordination was conducted in preparation for possible future flight testing that would follow the completion of the LAP program. The purpose of this effort was to determine and document Prop-Fan characteristics that would be required by airframe and engine designers and manufacturers in preparation for a flight test of the SR-7L Prop-Fan.

The parametric data package prepared under the LAP contract (reference 1) presented estimates of aerodynamic and acoustic performance of the SR-7L Prop-Fan. The data was presented in dimensionless form so that aerodynamic and acoustic performance can be computed for a broad range of operating parameters.

This report summarizes all of the work performed and results obtained during the Large Scale Advanced Prop-Fan Program (Contract NAS3-23051). Overall program conclusions and recommendations are also presented.

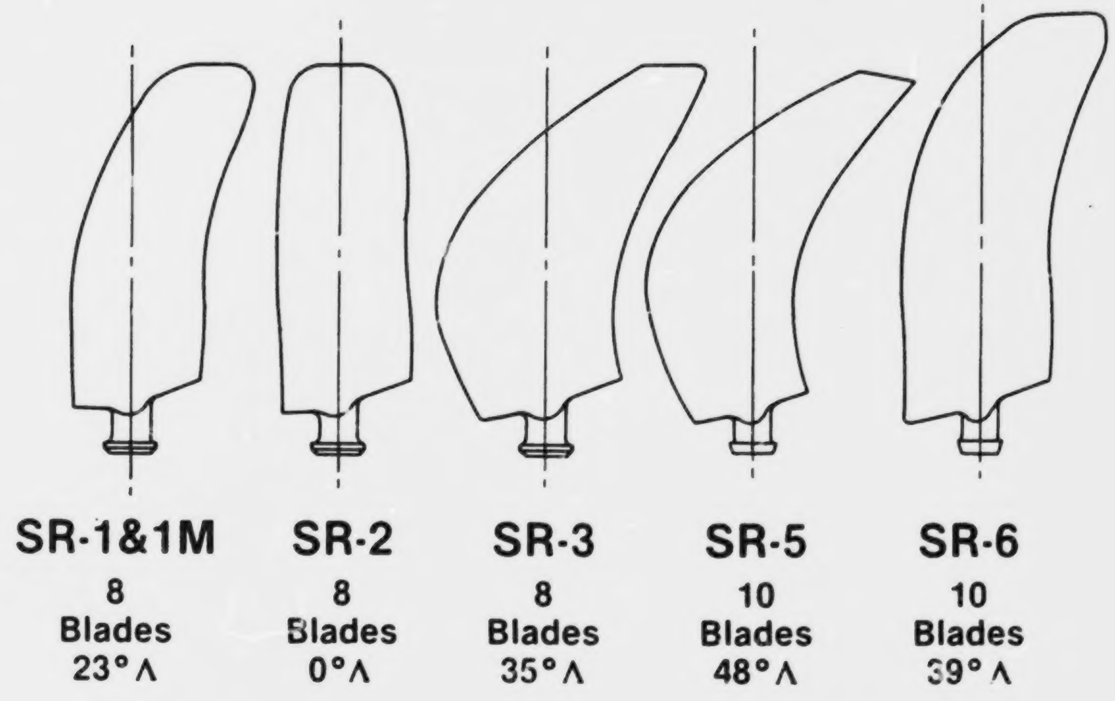
SR-1&1M
8
Blades
23° Λ
SR-2
8
Blades
0° Λ
SR-3
8
Blades
35° Λ
SR-5
10
Blades
48° Λ
SR-6
10
Blades
39° Λ

Altitude 35,000 Ft, Mach Number 0.8

Configuration	No. of Blades	SHP/D2	Tip Speed fps	ηmeas %	ηcalc %	$\Delta\eta$ %
SR-2	8	37.5	800	75.8	76.4	0.6
SR-1	8	37.5	800	76.2	75.9	−0.3
SR-3	8	37.5	800	78.2	78.4	0.2
SR-1M	8	37.5	800	77.7	77.5	−0.2
SR-6(1)	10	30.0	700	77.8	80.6	2.8(2)
SR-5	10	26.0	600	77.9(3)	78.6	−0.5

(1) NASA's aero/acoustic design

(2) Calculation does not reflect root choke evident in test data

(3) Extrapolation of test data as bending-torsion flutter phenomenon prevented testing at design conditions.

FIGURE 2.1 SUMMARY OF PROP-FAN WIND TUNNEL MODELS

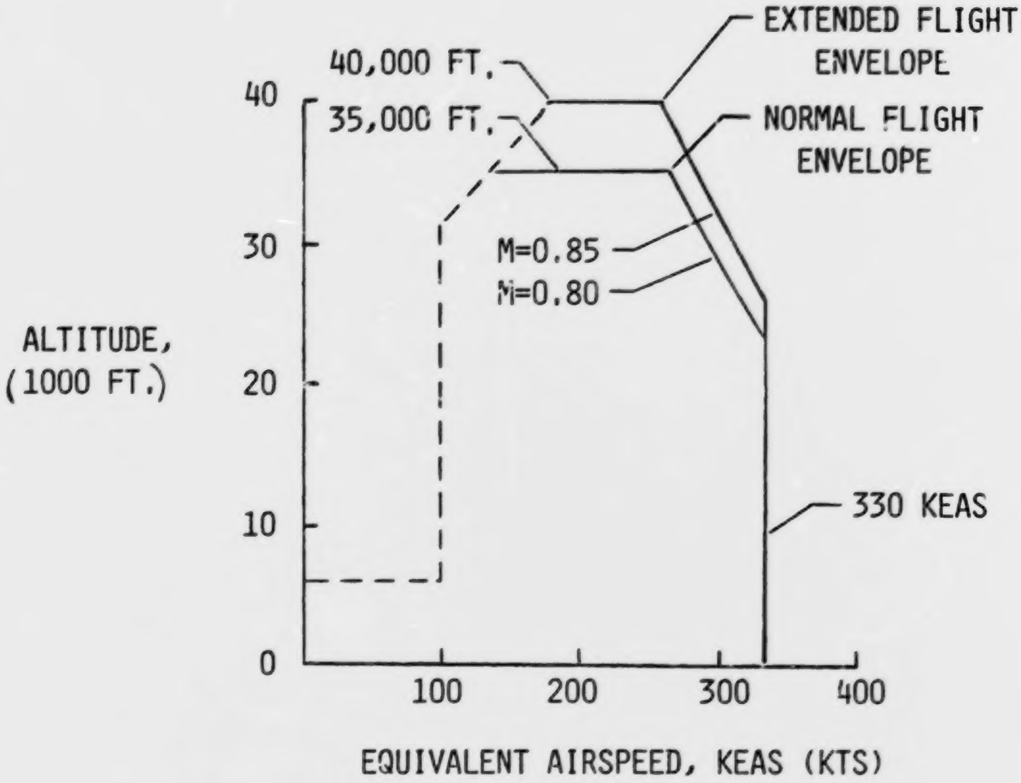

FIGURE 2.2 LAP FLIGHT OPERATING ENVELOPE

ORIGINAL PAGE IS
OF POOR QUALITY

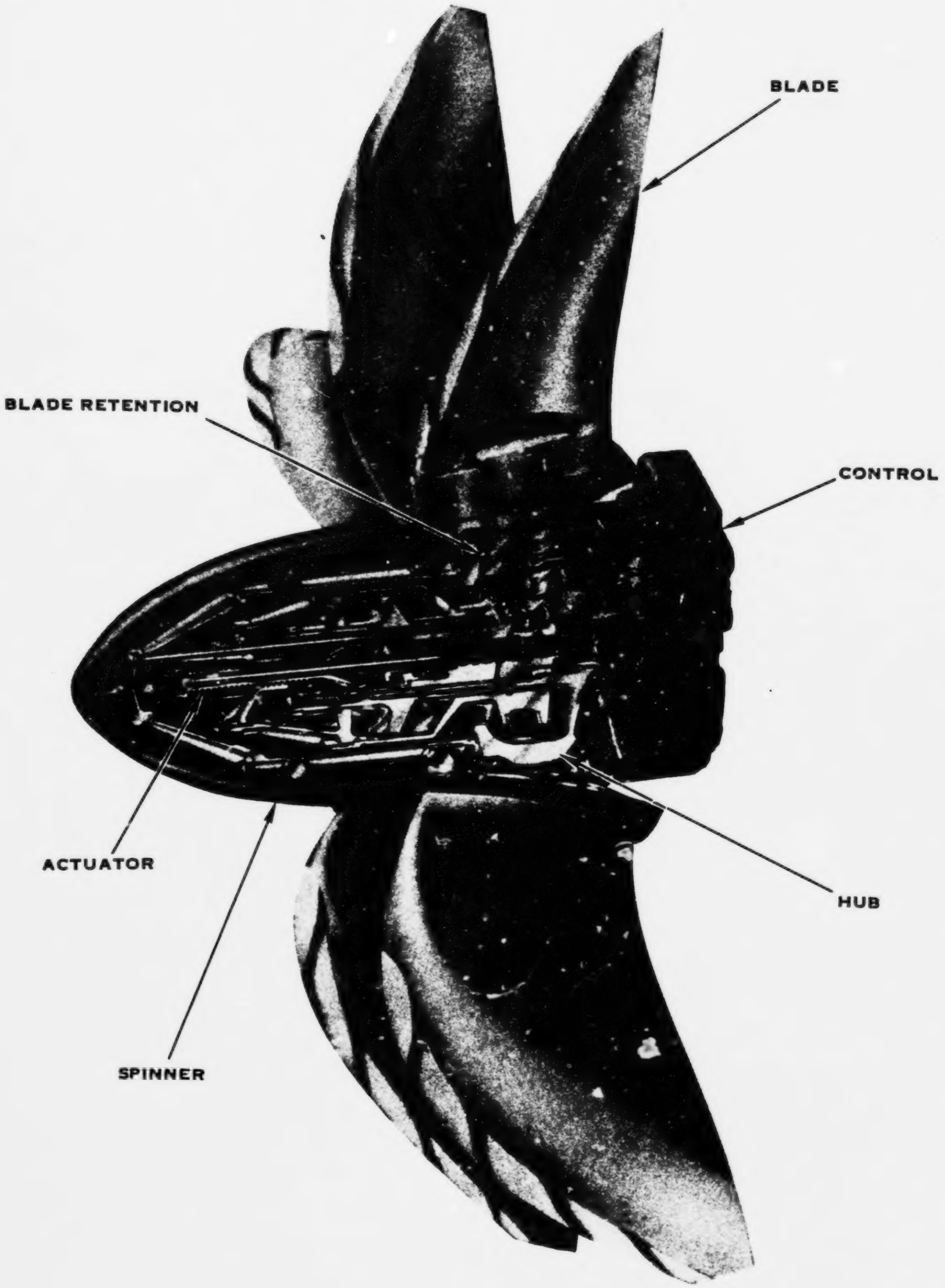
BLADE
BLADE RETENTION
CONTROL
ACTUATOR
HUB
SPINNER

FIGURE 2.3 LARGE SCALE ADVANCED PROP-FAN

E-37990

3.0 SR-7L BLADE DESIGN

3.1 BLADE CONFIGURATION

The structural configuration of the SR-7L blade consists of a central aluminum spar, a fiberglass shell which overhangs the leading and trailing edges of the spar and a nickel sheath that covers the leading edge of the outer two thirds of the blade. The remaining internal cavities are filled with low density rigid foam. The outboard portion of the spar is intentionally moved toward the leading edge of the blade to increase stability while at the same time increasing the resistance of the leading edge to foreign object damage. The thickness of the fiberglass shell is varied by adding plies of fiberglass as needed to meet the stiffness and strength requirements of the design. The blade design makes use of a NACA Series 16 airfoil outboard and a NACA Series 65 circular arc airfoil inboard. The blade has an activity factor of 227 with 37° of blade sweep at the tip. The blade design is illustrated in Figure 3.1.

The combination of an aluminum spar fiberglass shell, and foam fill is a service proven design, used by Hamilton Standard on several commercial and military propellers. It was chosen because it allowed the design requirements and goals to be achieved with a minimum of technical risk.

3.2 DESIGN REQUIREMENTS AND GOALS

As mentioned in the introduction, the aerodynamic and acoustic design of the blade was accomplished under a previous contract. The results of this design effort are reported in references 2 and 3. The design effort conducted under this contract is reported in detail in reference 4. A series of requirements and goals for the blade design phase of this contract were established. The design requirements were characteristics that had to be attained in the design while the design goals were desired characteristics, the attainment of which was not mandatory.

PRECEDING PAGE BLANK NOT FILMED

PAGE 10 INTENTIONALLY BLANK

3.2.1 Design Requirements

The design requirements can be divided into five categories. These categories along with the requirements of each follow. A description of the operating conditions for which the primary design requirements were evaluated is given in Table 3-1. These four conditions were used to determine the structural adequacy of the design.

TABLE 3-1

PRIMARY REQUIRED DESIGN CONDITIONS
ANALYZED TO ASSURE STRUCTURAL ADEQUACY

Case	D1	D2	D3	D4
Condition	Design/ Cruise	Take-off/ Climb	25 pct. overspeed	40 pct. overspeed
Power loading, * kw/meter^2 (HP/foot^2)	253 (32.0)	586 (74.1)	0.0 (0.0)	0.0 (0.0)
Forward velocity, Mach no.	0.80	0.20	**	**
Altitude, meters (feet)	10,575 (35,000)	sea level	**	**
Tip speed, meters/second (feet/second)	244 (800)	244 (800)	305 (1,000)	342 (1,120)
Rotation speed, rev./min.	1,698	1,698	2,122	2,371
Excitation factor	4.5	4.5	0.0	0.0
Beta 3/4, degrees	57.57	38.26	57.57	57.57
Power, kilowatts (horsepower)	1,906 (2,592)	4,413 (6,000)	**	**
Thrust, newtons (pounds)	6,490 (1,459)	33,649 (7,565)	**	**

* based on blade tip diameter squared.

** Overspeed conditions were evaluated as 125% and 140% design/cruise RPM, while maintaining airloads and blade angle setting of the design/cruise condition.

3.2.1.1 Flutter Limits - The Prop-Fan assembly shall be free of flutter instabilities over a normal flight profile shown in Figure 2.2 for a representative aircraft installation and for normal operating conditions.

3.2.1.2 Critical Speed Margins - For the two-per-revolution (2-P) excitation at 244 meters per second (800 feet per second) tip rotational speed, the critical speed margin shall be a minimum of ten percent of propeller speed and resonant frequency. This margin shall be reduced inversely as the exciting order is increased from 3-P to 5-P. No 1-P critical speeds shall be permitted in the operating speed range and the minimum 1-P margin shall be 40 percent of the maximum Prop-Fan operating speed. For ground operation, the 2-P critical speed margin shall be a minimum of twenty percent of the propeller speed and frequency. These margins shall include the effect of blade angle on frequency.

3.2.1.3 Stress Limits - The stress limits will be determined using Goodman diagrams which presents the allowable combinations of steady and cyclic stress for 10^8 cycles of life.

3.2.1.3.1 Normal Operation - All structural components of the blade shall be free of higher than allowable combined stresses during both the design/cruise and take-off/climb conditions. The high cycle fatigue stress limits for these conditions are based on 10^8 cycles, while the low cycle fatigue stress limits are based on 50,000 start-stop cycles.

3.2.1.3.2 Rotor Overspeeds - The blade shall be capable of operating to 125 percent (1.5 times the normal centrifugal load) of the maximum operating speed with no inelastic deformation. That is, all material stresses must fall below the yield strength.

The blade shall be capable of operating to 140 percent (2.0 times the normal centrifugal load) of the maximum operating speed with some allowable inelastic deformation, but no material separation (metal or composite). All material stresses must fall below the ultimate tensile strength.

3.2.1.4 Foreign Object Damage - The outer portion of the blade leading edge shall be covered with a partial chord width metal sheath for protection against erosion, such as from rain and sand.

3.2.1.5 Flight Representative Design - The blade shall be designed to have weight and structural characteristics that are representative of anticipated Prop-Fan systems for future aircraft applications.

3.2.2 Design Goals

The blade design goals can be divided into three categories. These categories along with the goals of each follow. In addition to the primary design conditions, eight additional secondary conditions were analyzed. These conditions are listed in Table 3-2. It was not mandatory that the design requirements be satisfied for these conditions, however, if the results of the evaluation placed severe limitations on planned testing, a revision of the blade design would have been considered.

3.2.2.1 Flutter Margin

3.2.2.1.1 Stall Flutter - The Prop-Fan shall be free of stall flutter at 100 percent of design take-off power at 100 percent design speed and take-off conditions (Mach no. = 0.0 to 0.2). The Prop-Fan shall also be free of stall flutter in reverse thrust.

3.2.2.1.2 Unstalled Flutter - The Prop-Fan shall be free of unstalled high speed flutter over the normal flight profile and range of power loadings with a 15 percent degradation in natural frequencies.

3.2.2.2 Foreign Object Damage (FOD)

3.2.2.2.1 Minor Impacts - Minor impacts are those due to sand, small stones, and birds up to .113 kilogram (four ounces). No structural damage allowed to the blade shell or sheath. Operation will continue without impediment.

3.2.2.2.2 Moderate Impacts - Moderate impacts are those due to 5.1 centimeter (two inch) hailstones and birds up to .907 kilogram (two pounds). Damage can include loss of material or airfoil distortion. Operation shall continue at 76 percent power for five minutes. No fragments (metal or composite) shall be lost which can penetrate the aircraft fuselage pressure shell. Roughness shall be tolerable and the rotor unbalance force due to damage to one or more blades shall be kept below 22,240 newtons (5,000 pounds).

3.2.2.2.3 Major Impacts - Major impacts are those due to a single bird up to 1.814 kilograms (four pounds). Damage can include loss of material or airfoil distortion. The ability to feather the Prop-Fan must be maintained. Shutdown must be accomplished without catastrophic effects on the airframe structure. The rotor unbalance force due to damage to one or more blades shall be kept below 111,200 newtons (25,000 pounds). No fragments (metal or composite) shall be lost which can penetrate the aircraft fuselage pressure shell.

3.2.2.3 Blade Design Life and Inherent Reliability

Replacement life with scheduled maintenance	35,000 hours
Mean time between unscheduled removals (8 blade set)	50,000 hours

Table 3-2

ADDITIONAL SECONDARY CONDITIONS EVALUATED

Case	1A	1B	1C	2	3	4	5	6	7	8
Condition	ONERA 8 Blade	ONERA 4 Blade	ONERA 2 Blade	Static Thrust	Reverse Thrust	Cruise Lo RPM	Cruise Hi RPM	Climb Mid Alt.	Dive Mid Alt.	Dive High Alt.
Power loading,* kw/meter^2 (HP/foot^2)	103 (13.0)	103 (13.0)	103 (13.0)	586 (74.1)	117 (14.8)	198 (25.0)	316 (40.0)	527 (66.7)	0.0 (0.0)	0.0 (0.0)
Forward velocity, Mach no.	0.80	0.80	0.80	0.00	0.00	0.80	0.85	0.50	0.60	0.80
Altitude, meters (feet)	4,270 (14,000)	4,270 (14,000)	4,270 (14,000)	sea level	sea level	10,675 (35,000)	10,675 (35,000)	3,050 (10,000)	6,100 (20,000)	10,675 (35,000)
Tip speed, meters/second (feet/second)	244 (800)	244 (800)	244 (800)	244 (800)	244 (800)	183 (600)	256 (840)	244 (800)	244 (800)	244 (800)
Rotational speed, rev./minute	1698	1698	1698	1698	1698	1273	1783	1698	1698	1698
Excitation factor	4.5	4.5	4.5	0.0	0.0	4.5	4.5	4.5	0.0	0.0

*based on blade tip diameter squared.

3.3 FINITE ELEMENT MODELING

Because of the swept geometry of the blade, considerable attention was given to the analytical techniques to be used in the design process. An in-house finite element analysis (FEA) code was used to represent the three-dimensional blade structure. During preliminary design iterations, the blade was modeled with a relatively coarse mesh of triangular plate elements, three layers deep through the thickness of the blade. Once an acceptable preliminary design was achieved, a finer mesh FEA model was constructed.

The detail design blade model had a fine mesh of triangular three-dimensional plate elements. As shown in Figure 3.2, two outer layers on each side of the blade (face and camber) were used to represent the fiberglass shell and the leading edge nickel sheath, while a central layer was used to represent the internal aluminum spar and leading and trailing edge foam filler (shell cavity) regions.

In order to obtain the compliance simulation necessary for static, modal, and forced response analyses, the blade retention was modeled using a system of spring elements and multi-point constraints. Each spring element was given a spring rate, position, and orientation such that the system of spring elements would reflect the compliance of the actual blade retention. The spring rates to be simulated are listed in Table 3-3 and illustrated in Figure 3.3.

TABLE 3-3

TABLE OF SPRING RATES TO BE SIMULATED

Type of Load Resisted	Description of Load	Spring Rate to be Simulated
Axial	Total centrifugal pull load	26.2 X 10^8 newtons/meter (22.4 X 10^6 pounds/inch)
Twisting	About pitch change axis	22.6 X 10^6 newton-meters/radian (200 X 10^6 inch-pounds/radian)
Bending	About out-of-plane axis	1.5 X 10^6 newton-meters/radian (13.4 X 10^6 inch-pounds/radian)
Bending	About in -plane axis	1.15 X 10^6 newton-meters/radian (10.2 X 10^6 inch-pounds/radian)

3.4 STEADY-STATE ANALYSIS

Four operating conditions were analyzed using the steady-state finite element blade model to check for compliance with the design requirements. These conditions were: design/cruise, take-off/climb, 25 percent overspeed, and 40 percent overspeed.

In addition to the four design requirement conditions, eight other operating conditions were analyzed. These conditions were the three ONERA S1 Wind Tunnel conditions, static and reverse thrust conditions, cruise at low and high rotational speeds, mid-altitude climb, and two dive conditions at mid and high altitude.

3.4.1 Application of Loads

The Prop-Fan blade is affected by two major types of loads: centrifugal and air. Centrifugal loads arise from the blade rotating about the axis of rotation. Airloads arise from the blade moving through the air.

3.4.1.1 Centrifugal Loads - Centrifugal loads result from the rotation of the blade about the Prop-Fan axis of rotation. The finite element program uses the mass properties of the blades, the radial distance from the centerline of rotation to the blade element centroids and the rotational speed of the Prop-Fan to compute the centrifugal forces on each element and distributes the forces to the model nodal points.

3.4.1.2 Airloads - The airloads used in this analysis were the result of aerodynamic calculations using lifting line theory. The aerodynamic loads are resolved into lift and drag loads at the radial stations of the blade that correspond to the rows of nodal points in the finite element model. The aerodynamic loads are then distributed to the nodal points in such a manner as to obtain the correct center of pressure on the blade surface.

3.4.2 Pre-Deflection Design

The undeflected shape of the blade was determined by an iterative process. The process began by modeling the blade in the desired configuration for the design cruise condition. The design cruise condition loads were applied to the model and the blade deflections were computed. The deflections were subtracted from the desired coordinates of the blade at the design cruise condition to obtain the undeflected shape of the blade. A new finite element model was formed using the new undeflected blade coordinates and the blade was reanalyzed for the design cruise loads. If this analysis indicated that the deflected shape of the blade was not the desired shape for the design cruise condition, this procedure was repeated until an undeflected blade shape was obtained that yielded the desired configuration at the design cruise condition. Seven iterations were required to obtain an undeflected shape that yielded an acceptable .023 centimeter error from the desired position of the blade tip leading edge at the design cruise condition.

3.4.3 Final Calculations

Twelve operating conditions were analyzed for steady state reactions, deflections and stresses. The stresses are combined with the vibratory stresses discussed in Section 3.5 for comparison to design allowables.

3.5 VIBRATORY RESPONSE ANALYSIS

A vibratory response analysis was performed for a once-per-revolution, or 1-P, aerodynamic excitation for eight of the twelve design conditions. These conditions were: design/cruise, take-off/climb, the three ONERA S1 Wind Tunnel conditions, the low and high rotational speed cruise conditions, and the 0.5 Mach number climb.

3.5.1 Origin Of The Once-Per-Revolution Excitation

The once-per-revolution (1-P) excitation occurs because of the angle (ψ) which the propeller axis of rotation makes with the forward direction of the aircraft, particularly during the climb condition, as illustrated in Figure 3.4.

This results in a difference in the relative angle of attack of two horizontal blades shown in the front view. That is, the advancing blade 1 sees a reduced angle of attack (α_1), while the retreating blade 5 sees an increased angle of attack (α_5). In the top and bottom positions, the angle of attack is equal. Therefore, a single blade experiences a sinusoidal variance in load during each revolution. The difference in load between blades 5 and 1 results in a small constant vertical force as shown in the front view, while the difference in thrust results in a propeller shaft bending moment as seen in the top view. Additionally, depending on the installation and the proximity of the Prop-Fan to a wing engine inlet, and/or fuselage, the Prop-Fan can operate in a flow field of varying velocity. This is more pronounced if the wing has considerable sweep.

3.5.2 Calculation of Vibratory Response

Cyclic airloads corresponding to a 4.5 excitation factor were used for the vibratory response analysis. The excitation factor is a measure of the severity of the 1P aerodynamic excitation and is defined by equation 3.1.

$$EF = \gamma \left[\frac{Ve}{348}\right]^2 \qquad (3.1)$$

where Ve = Equivalent Airspeed (KTS)
γ = angle of Prop-Fan Axis to Airflow (Radians)

A finite element code was used to evaluate the blade vibratory response based on the 4.5 excitation factor and a 1P excitation frequency. The cyclic stress response is combined with the steady stresses computed in Section 3.4 for comparison to design allowables on Goodman diagrams.

3.6 STRESS VS STRENGTH EVALUATION

3.6.1 Method of Combining Steady State and Vibratory Stresses

After completing both the steady-state and vibratory response analyses, the next step was to combine the 1-P vibratory stresses with the steady-state stresses to provide a structural evaluation of blade components. This was done for each of the cyclic load conditions analyzed.

A Goodman diagram was used to show the relationship of the combined stress of the vibratory response and the steady-state analysis with the design allowable limit. Figure 3.5 shows a calculation point plotted on a typical Goodman diagram.

Line A can be constructed on the Goodman diagram which connects a calculation point with the origin of the diagram. Line B can then be drawn coincident with the first line from the origin until it intersects the design limit line. The percent of the first line (origin to calculation point) with respect to the second line (origin to design allowable limit) represents the percent of the allowable limit of the combined stress state at that calculation point.

3.6.2 High Cycle Fatigue

High cycle fatigue is associated with the application of cyclic stress over a relatively long period of time. The application of this cyclic stress will often be in combination with a steady stress which may be much greater in magnitude. The steady stress field was calculated as part of the steady-state analysis. The cyclic stress levels were calculated for the 1-P excitation. For this evaluation, each of the blade components (spar, shell, sheath, and foam filler) is required to withstand at least 10^8 cycles under this combined stress condition. The maximum percent of allowable limit for each of the conditions analyzed is listed in Table 3-4.

TABLE 3-4

HIGH CYCLE FATIGUE STRESS/STRENGTH COMPARISON

		Percent of Allowable Limit*			
No.	Condition	Spar	Shell	Foam Filler	Sheath
D1	Design/Cruise	74	67	50	53
D2	Take-off/Climb	76	64	60	53
D3	25% Overspeed	42	61	29	41
D4	40% Overspeed	52	74	35	44
1A	ONERA, 8 Blade	33	76	58	41
1B	ONERA, 4 Blade	86	87	77	46
1C	ONERA, 2 Blade	97	93	86	49
2	Static Thrust	26	65	22	35
3	Reverse Thrust	43	67	18	79
4	Cruise, Low RPM	100	85	63	81
5	Cruise, Hi RPM	70	64	44	49
6	Climb, Mid Altitude	77	67	57	58
7	Dive, Mid Altitude	30	61	24	34
8	Dive, High Altitude	30	60	25	35

* Percent of allowable limit measured diagonally on Goodman diagram and based on 10^8 cycles endurance limit.

3.6.3 Low Cycle Fatigue

Low cycle fatigue (LCF), sometimes referred to as "start-stop" cycles, is associated with alternating between an unstressed state and the maximum stress state. For the low cycle fatigue stresses, the steady and cyclic stresses are combined to determine the maximum tensile or compressive stress.

For LCF evaluation, the steady and cyclic stresses are each assumed equal to half of this maximum value, and are then plotted on a modified Goodman diagram for comparison to the material allowable limits. For the low cycle fatigue conditions, each of the blade components must withstand at least $5x10^4$ stress cycles under this combined stress condition.

The highest percent of allowable limit for each of the conditions analyzed is listed in Table 3-5 for each of the blade components.

TABLE 3-5

LOW CYCLE FATIGUE STRESS/STRENGTH COMPARISON

		Percent of Allowable Limit* (Cycles to Allowable if Less Than 50,000)			
No.	Condition	Spar	Shell	Foam Filler	Sheath
D1	Design/Cruise	56	73	57	54
D2	Take-off/Climb	50	64	52	60
D3	25% Overspeed	71	102 (20,000)	67	58
D4	40% Overspeed	86	125 (80)	81	62
1A	ONERA, 8 Blade	58	81	67	50
1B	ONERA, 4 Blade	60	76	69	50
1C	ONERA, 2 Blade	60	77	71	53
2	Static Thrust	43	110 (1,300)	50	50
3	Reverse Thrust	71	113 (600)	41	113 (20,000)
4	Cruise, Low RPM	48	68	63	47
5	Cruise, Hi RPM	58	74	44	51
6	Climb, Mid Altitude	52	96	57	63
7	Dive, Mid Altitude	49	102 (25,000)	24	48
8	Dive, High Altitude	49	101 (35,000)	25	49

* Percent of allowable limit based on 50,000 start-stop cycles
Zero to max stress = (SS+CYC) ± (SS+CYC)/2
SS = Steady stress
CYC = Cyclic stress

3.7 RESONANT FREQUENCIES AND MODE SHAPES

The prediction and placement of the resonant frequencies of the Prop-Fan blades are important aspects of the design analysis process. The first few integer orders of design rotational speed are important areas to avoid resonance because excitation forces for these are highest, decreasing inversely as P-order increases. Dynamic magnification, if insufficiently damped, could cause undesirable vibration and stresses. Furthermore, for an eight-bladed propeller, the 2-P, 3-P, 4-P, and 5-P modes of vibration are reactionless, that is, vibration loads at the blade shank are reacted internally through the hub, and no component of vibration is transmitted to the propeller shaft. Thus the pilot has no direct sensory feedback of the vibratory condition of the propeller. For this reason, specific bands of resonant frequency avoidance are specified. These frequency avoidance bands decrease in size with increasing P-order since the magnitude of the excitation decreases as P-order increases. Strain gages will be mounted on the blade surface such that undesirable vibratory levels, should they occur, can be detected and avoided during operation.

3.7.1 Calculation Method

Because the NASTRAN eigenvalve solver is faster than the determinant search method used by the in-house finite element code (BESTRAN), the NASTRAN solver was used for this analysis.

3.7.2 Results

A listing of the first five modal frequencies for each of the twelve conditions analyzed is given in Table 3-6. The differences in resonant frequencies between operating conditions are caused primarily by differences in centrifugal stiffening, resulting from the various combinations of blade angle and RPM.

3.7.2 (Continued)

TABLE 3-6

SR-7L BLADE RESONANT FREQUENCY SUMMARY

Frequencies in Hz

No.	Condition	Mode 1	2	3	4	5
D1	Design/Cruise	43.2	80.1	101.0	148.2	168.6
D2	Take-off/Climb	45.7	77.2	103.2	147.5	170.4
1A	ONERA, 8 Blade	43.4	79.6	100.9	149.8	167.1
1B	ONERA, 4 Blade	43.4	79.7	100.8	149.6	167.2
1C	ONERA, 2 Blade	43.4	79.9	101.2	149.4	168.7
2	Static Thrust	46.4	76.3	103.1	148.4	169.6
3	Reverse Thrust	50.1	73.7	94.3	138.1	148.7
4	Cruise, Low RPM	38.8	77.6	95.6	143.2	155.9
5	Cruise, Hi RPM	44.0	80.7	101.9	149.0	169.4
6	Climb, Mid Altitude	44.1	78.9	102.0	148.8	169.5
7	Dive, Mid Altitude	44.7	77.0	102.2	150.1	168.6
8	Dive, High Altitude	44.0	77.3	101.6	149.5	168.2

The calculated modal frequencies for the required design conditions of design/cruise and take-off/climb are also plotted on a Campbell diagram in Figure 3.6. The Campbell diagram includes the integer order resonance avoidance bands specified in the design requirements. Static frequencies are also shown. These frequencies were calculated with a clamped blade shank, and therefore are not shown connected with the other modes that were calculated at speed.

As can be seen from the diagrams, all resonance placement requirements have been meet except for the second mode in the design/cruise condition which infringes slightly on the 3-P avoidance band. This is not of great concern since the second mode is edgewise, and is sensitive to retention stiffness. A reduction in frequency will accompany a reduction in stiffness. Experience has shown that predicted retention stiffnesses tend to be higher than actually observed. Therefore the actual second mode natural frequency may be lower than predicted and further removed from the avoidance band. In addition no source of 3-P excitation is projected for the second mode.

3.8 STABILITY

A stability analysis of the SR-7L blade was performed to assure structural integrity in terms of aeroelastic stability over the entire flight envelope and the wind tunnel test conditions. The requirements divide flutter into two categories: unstalled flutter and stalled flutter. These categories were established because there is a distinct difference in aerodynamics during unstalled and stalled operation. Unstalled flutter can occur when the Prop-Fan operates in an unstalled condition, such as during cruise at high forward speed. Stall flutter can occur when the Prop-Fan operates in a stalled condition, such as during take-off under high power and low forward speed. The combination of high power and low speed gives rise to a high airfoil angle of attack, causing the air to separate from the aerodynamic surface and to stall the blade. For this reason, stall flutter is often called separated flow flutter. Because each category of flutter involves a unique aerodynamic condition, they are examined using different analytical approaches.

3.8.1 Unstalled Flutter Analysis

The unstalled flutter stability of the SR-7L blade was examined using an aeroelastic stability analysis that was specifically developed to model the structural and aerodynamic complexities of a Prop-Fan (reference 5).

Briefly, the analysis is a linear modal formulation in which the structure is modeled with fully-coupled mode shapes obtained from finite element analysis and the unsteady aerodynamic loads are based on linear, compressible, two-dimensional theory. Because the aeroelastic analysis uses two-dimensional aerodynamic theory to model the three-dimensional flow about the blade, the application of the theory has been guided by existing model test results to give consistent and accurate predictions.

To ensure that the entire operating regime is free of instabilities, ten operating conditions were studied for stability. These conditions are listed in Table 3-7, along with their flutter Mach number. For each condition the calculated flutter Mach number was greater than the actual Mach number for that condition, indicating a stable configuration.

TABLE 3-7

PREDICTED FLUTTER MACH NUMBER FOR TEN SR-7L OPERATING CONDITIONS

Case	Condition	Operating Mach no.	Altitude, meters (feet)	RPM	Flutter Mach no.	Flutter mode
D1	Design/Cruise	.80	10,675 (35,000)	1,698	.95	3
D2	Take-off/Climb	.20	0 (0)	1,698	.60	3
1A	ONERA, 8 Blades	.80	4,270 (14,000)	1,698	.85	3
1B	ONERA, 4 Blades	.80	4,270 (14,000)	1,698	1.00	2
1C	ONERA, 2 Blades	.80	4,270 (14,000)	1,698	.95	2
4	Cruise, Low RPM	.80	10,675 (35,000)	1,273	1.00	-
5	Cruise, High RPM	.85	10,675 (35,000)	1,783	.92	3
6	Climb, Mid Altitude	.50	3,050 (10,000)	1,698	.76	3
7	Dive, Mid Altitude	.60	6,100 (20,000)	1,698	.92	3
8	Dive, High Altitude	.80	10,675 (35,000)	1,698	1.00	3

3.8.2 Stall Flutter Evaluation

To study stall flutter, two methods of analysis were used. One was a semi-empirical formulation that has been incorporated in the aeroelastic stability analysis computer program. The other method was a purely empirical method used for conventional propeller stall flutter analysis. Two methods were chosen for stall flutter analysis because the theoretical analysis of stall flutter is not a well-established procedure due to the complexity of the air flow about a stalled blade section.

3.8.2.1 Semi-Empirical Method - The semi-empirical method uses combined bending and torsion modes, but does not couple the modes since stall flutter is generally a single mode phenomenon. The unsteady airfoil coefficients are developed from steady-state empirical airfoil data. The results from this analysis give the onset of stall flutter, not the magnitude of the response, because large amplitude stall flutter response is non-linear while the analysis assumes a linear response.

Table 3-8 lists the conditions examined for stall flutter along with the resulting predictions. The predictions are in terms of blade angle because stall flutter occurs at high power when the blade is stalled and increasing power corresponds to increasing blade angle.

TABLE 3-8

STALL FLUTTER ONSET PREDICTION SUMMARY

	Take-off/Climb	Static Thrust	Reverse
Speed, RPM	1698	1698	1698
Mach no.	0.2	0.0	0.0
Nominal blade angle, deg	38.0	33.0	-10.0
Flutter blade angle, deg	40.0	31.0	No flutter
Flutter mode of vibration	4	4	No flutter

The predictions show that shall flutter occurs at a lower blade angle than required by the static thrust condition. The fourth mode, which is the first torsional mode, becomes unstable at a 31 degree blade angle.

When the blade is subjected to a small amount of forward flight speed, the stall flutter stability is greatly improved, as seen by the take-off/climb condition. This improvement in stability indicates that with the proper pitch change schedule, stall flutter will not be a problem at take-off.

3.8.2.2 Empirical Method - Since the SR-7L blade has a distinct torsional mode, and stall flutter was predicted for this mode, a stall flutter parameter was calculated for the blade. The stall flutter parameter is an empirical design factor that was developed for conventional propeller design to prevent the occurrence of torsional stall flutter. This parameter is calculated for a given configuration and plotted on a stall flutter design chart to see if torsional stall flutter is possible. The calculated stall flutter parameter for the SR-7L blade for a blade angle of 33.0 degrees is 1.35, which is well inside the stable region of a stall flutter design chart, indicating that no flutter will occur in the torsional mode.

The two methods used to predict the stall flutter stability of the SR-L blade give different results. The first method, the semi-empirical method which predicted the blade angle when flutter would occur, shows stall flutter occuring in a mode that the second method, using the stall parameter, showed to be stable. Therefore, the stall flutter results are inconclusive. The best procedure for determining stall flutter stability is testing.

3.9 FOREIGN OBJECT DAMAGE

To assess the FOD tolerance design goals, gross blade stresses resulting from moderate and major impacts were calculated for the SR-7L blade. A moderate impact is one with a bird of up to .907 kilogram (two pounds) while a major impact involves a bird of up to 1.814 kilogram (four pounds).

3.9.1 Calculation Procedure

A three-dimensional, computerized, impact analysis program was used to calculate the gross blade stresses due to a 1.814 kilogram (four pound) bird impact. A single flight condition was analyzed: 185 kilometers per hour (100 knots) take-off at a blade angle of 37 degrees. Impact was assumed to occur at 80% blade span, resulting in an impact velocity of 210 meters per second (689 feet per second).

3.9.2 Effect On Blade

For the bird impact, the blade appears to be in good shape. A sizeable portion of the bird hits the blade, while the remaining portion is separated. For moderate impacts, birds up to .907 kilogram (two pounds), both the spar and shell spanwise stresses are well below their respective strengths and thus there is no problem meeting the requirements for moderate impacts. For major impacts, birds up to 1.814 kilogram (four pounds), the spar begins to yield, spanwise, at about the 1.814 kilogram (four pound) level, while the shell is still slightly below its tensile strength. Again, there is no problem meeting the requirements.

3.10 BLADE TRUNNION DESIGN

The trunnion assembly provides the link between the blade and the blade pitch actuator. It transmits the torque generated by the blade to the actuator and translates actuator axial motion to blade rotation about the retention radial axis. The trunnion is bolted to the blade shank and the trunnion roller bearing mates with ears on the actuator yoke. The trunnion assembly is shown in Figure 3.7.

The trunnion is bolted to the blade shank in four places. Since the blade shank material is aluminum, threaded inserts were incorporated to take advantage of the increased shear and tensile stress areas of the oversized threads of the inserts. The threads in the blade shank are rolled to increase fatigue life. The blade shank and trunnion mounting faces are shotpeened also to increase fatigue life. The trunnion roller is through hardened steel and mates with surface hardened steel wear plates on the actuator.

3.10.1 Blade Trunnion Loading and Fatigue Strength

The blade trunnion was analyzed for the blade CTM (centrifugal twisting moment) ATM (aerodynamic twisting moment) and FTM (frictional twisting moment) corresponding to 100% RPM at sea level and a blade angle, $\beta 3/4$, of 38.5°. For high cycle fatigue analysis the total twisting moment is applied as a steady load and the ATM component is applied as a cyclic load. For low cycle fatigue, half of the total twisting moment was applied as a steady load and half as an alternating load. The loads acting at the centerline of the trunnion roller bearing for low cycle and high cycle fatigue analyses are listed below:

HCF = 46704 ± 5426 N (10500 + 1220 lb)
LCF = 23352 ± 23352 N (5250 ± 5250 lb)

Ample low and high cycle fatigue margins were obtained for the trunnion, blade shank and related hardware.

ORIGINAL PAGE IS
OF POOR QUALITY

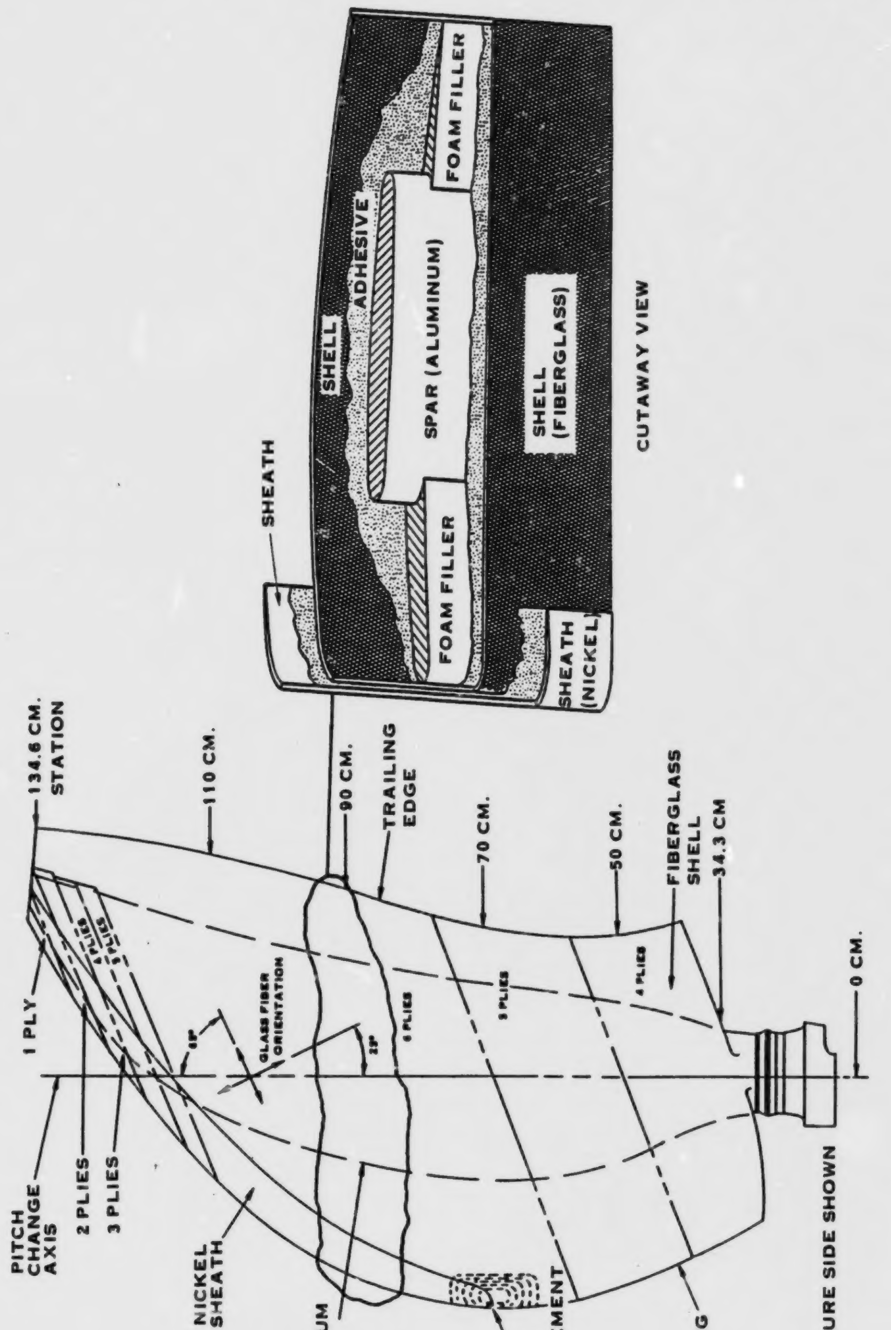
PITCH CHANGE AXIS
1 PLY
2 PLIES
3 PLIES
4 PLIES
5 PLIES
134.6 CM. STATION
110 CM.
90 CM.
TRAILING EDGE
70 CM.
50 CM.
FIBERGLASS SHELL
34.3 CM
0 CM.
GLASS FIBER ORIENTATION
6°
22°
6 PLIES
5 PLIES
4 PLIES
NICKEL SHEATH
ALUMINUM SPAR
ADDED PLIES FOR REINFORCEMENT
LEADING EDGE
PRESSURE SIDE SHOWN
SHEATH
SHELL
ADHESIVE
FOAM FILLER
SPAR (ALUMINUM)
FOAM FILLER
SHELL (FIBERGLASS)
SHEATH (NICKEL)
CUTAWAY VIEW

FIGURE 3.1 SR-7L BLADE DESIGN CONFIGURATION

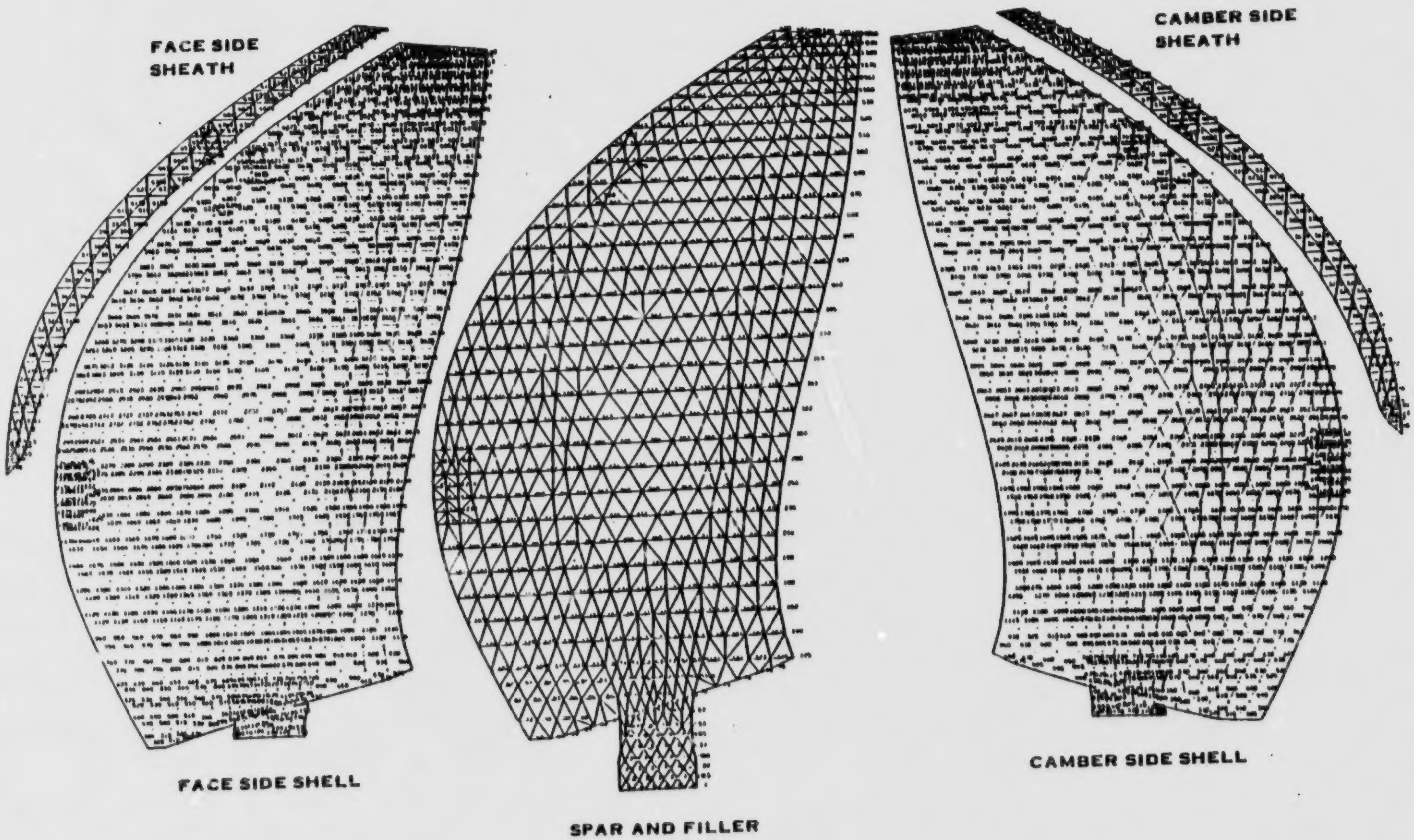
FACE SIDE SHEATH
CAMBER SIDE SHEATH
FACE SIDE SHELL
SPAR AND FILLER
CAMBER SIDE SHELL

FIGURE 3.2 SR-7L BLADE FINITE ELEMENT MODEL

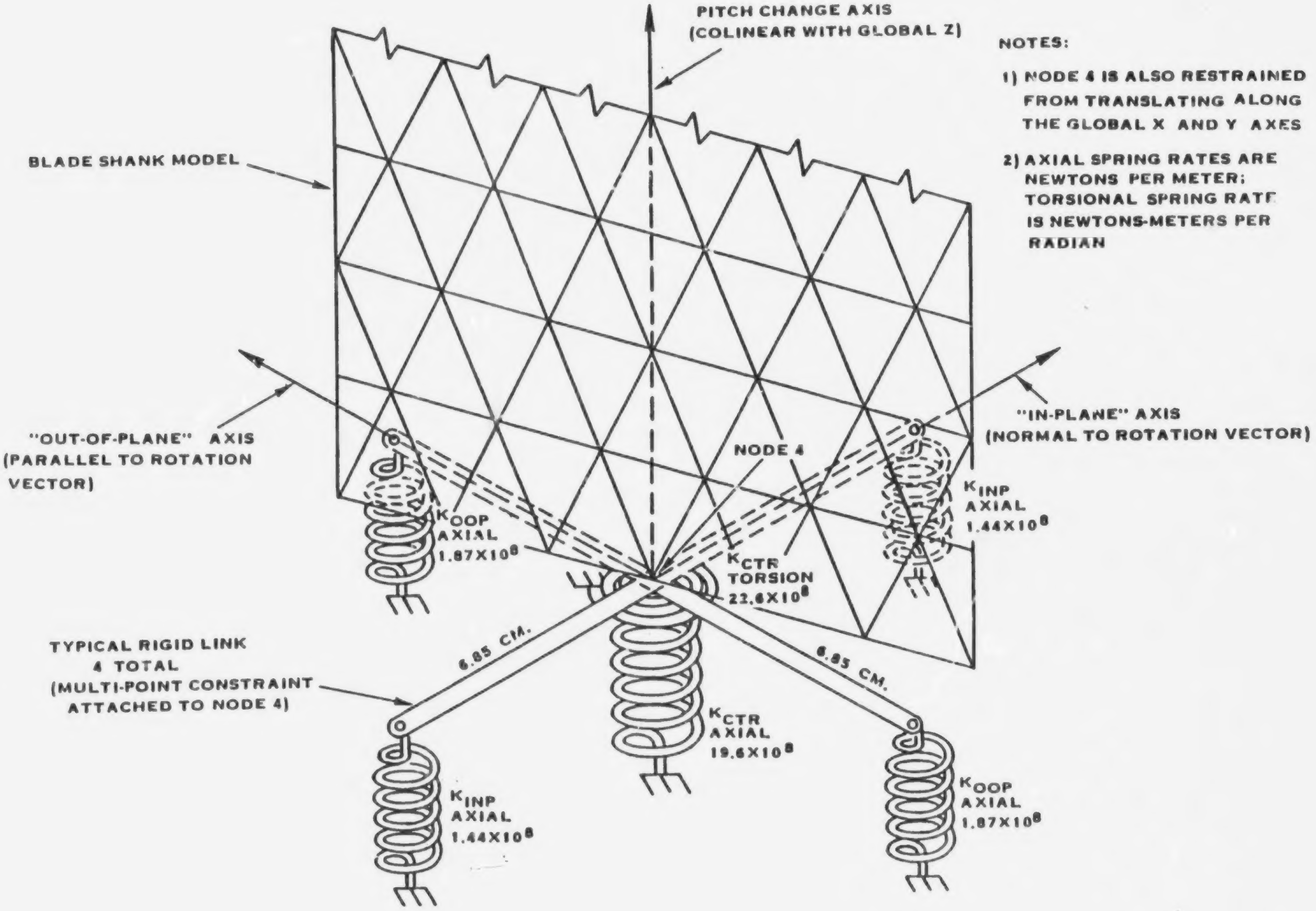
PITCH CHANGE AXIS
(COLINEAR WITH GLOBAL Z)
BLADE SHANK MODEL
"OUT-OF-PLANE" AXIS
(PARALLEL TO ROTATION
VECTOR)
"IN-PLANE" AXIS
(NORMAL TO ROTATION VECTOR)
NODE 4
K_{OOP}
AXIAL
1.87X10^8
K_{CTR}
TORSION
22.6X10^8
K_{INP}
AXIAL
1.44X10^8
TYPICAL RIGID LINK
4 TOTAL
(MULTI-POINT CONSTRAINT
ATTACHED TO NODE 4)
6.85 CM.
6.85 CM.
K_{CTR}
AXIAL
19.6X10^8
K_{INP}
AXIAL
1.44X10^8
K_{OOP}
AXIAL
1.87X10^8

NOTES:

1) NODE 4 IS ALSO RESTRAINED FROM TRANSLATING ALONG THE GLOBAL X AND Y AXES

2) AXIAL SPRING RATES ARE NEWTONS PER METER; TORSIONAL SPRING RATE IS NEWTONS-METERS PER RADIAN

FIGURE 3.3 SR-7L ELEMENT MODEL RESTRAINTS

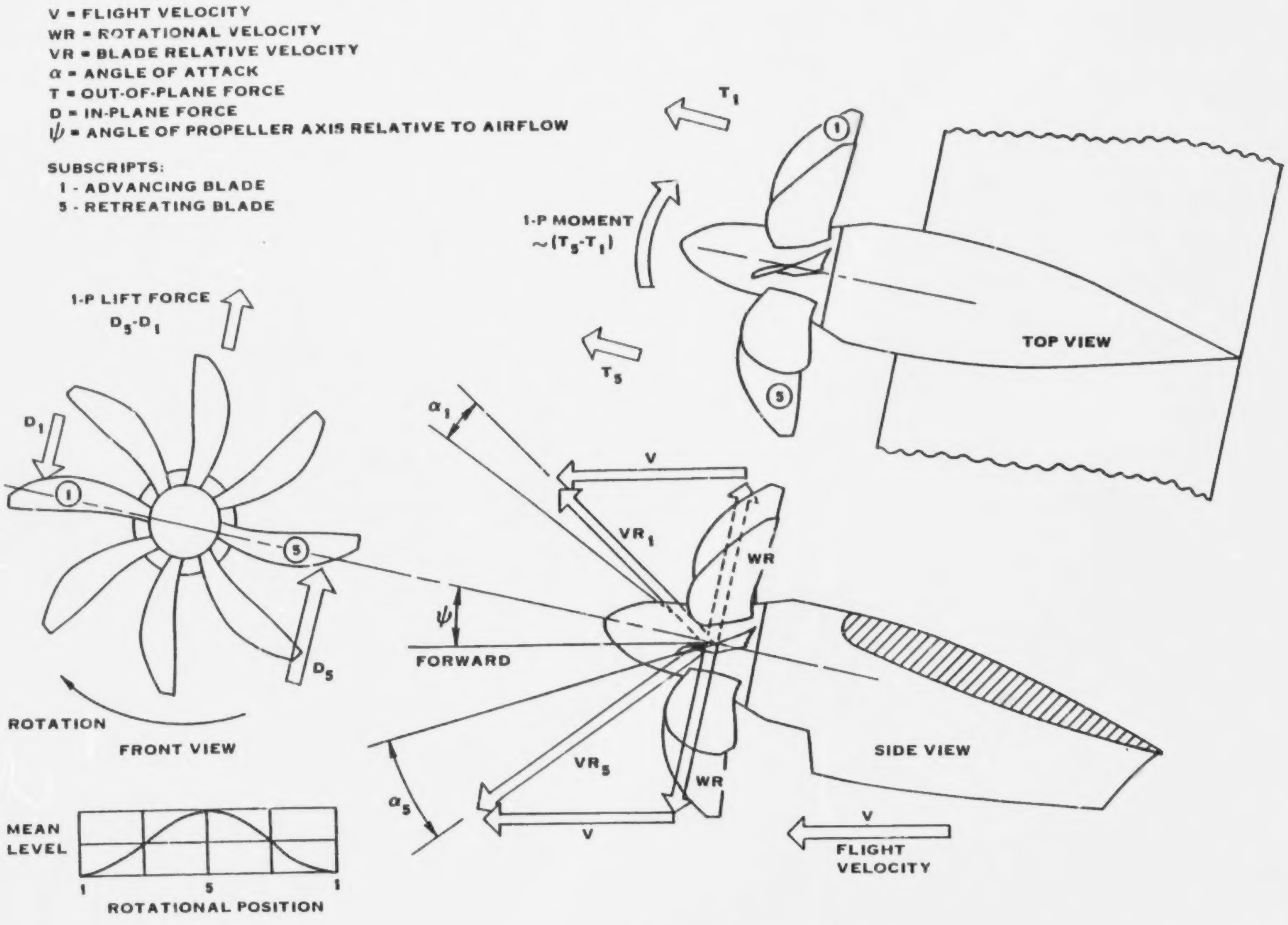
V = FLIGHT VELOCITY
WR = ROTATIONAL VELOCITY
VR = BLADE RELATIVE VELOCITY
α = ANGLE OF ATTACK
T = OUT-OF-PLANE FORCE
D = IN-PLANE FORCE
ψ = ANGLE OF PROPELLER AXIS RELATIVE TO AIRFLOW
SUBSCRIPTS:
1 - ADVANCING BLADE
5 - RETREATING BLADE
T_1
1-P MOMENT
$\sim (T_5 - T_1)$
T_5
TOP VIEW
1-P LIFT FORCE
$D_5 - D_1$
D_1
D_5
ROTATION
FRONT VIEW
α_1
V
VR_1
WR
ψ
FORWARD
VR_5
α_5
WR
V
SIDE VIEW
V
FLIGHT
VELOCITY
MEAN
LEVEL
1
5
1
ROTATIONAL POSITION

FIGURE 3.4 CYCLIC AERODYNAMIC LOADING

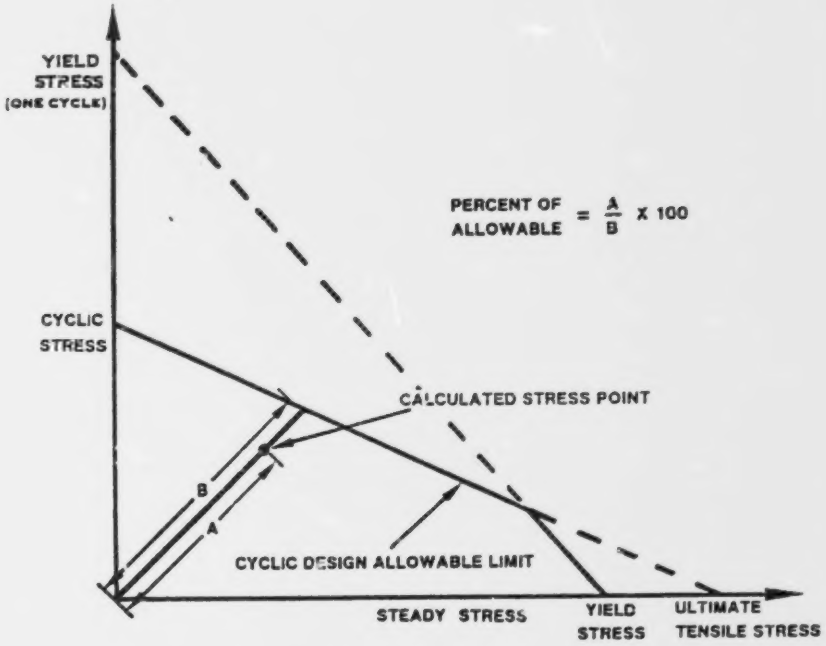
YIELD STRESS (ONE CYCLE)
PERCENT OF ALLOWABLE = A/B X 100
CYCLIC STRESS
CALCULATED STRESS POINT
B
A
CYCLIC DESIGN ALLOWABLE LIMIT
STEADY STRESS
YIELD STRESS
ULTIMATE TENSILE STRESS

FIGURE 3.5 TYPICAL GOODMAN DIAGRAM

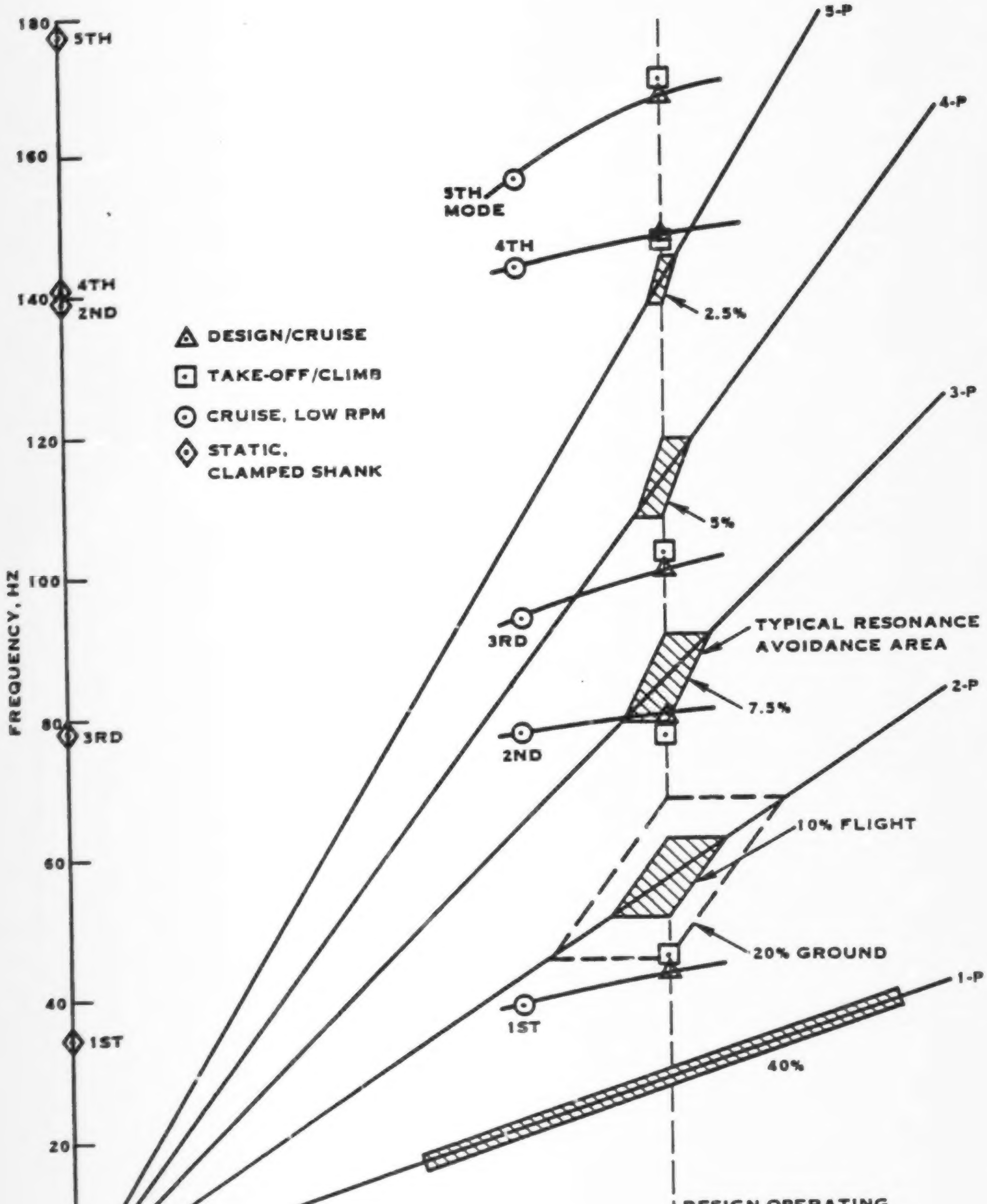

FIGURE 3.6 CALCULATED MODAL FREQUENCIES

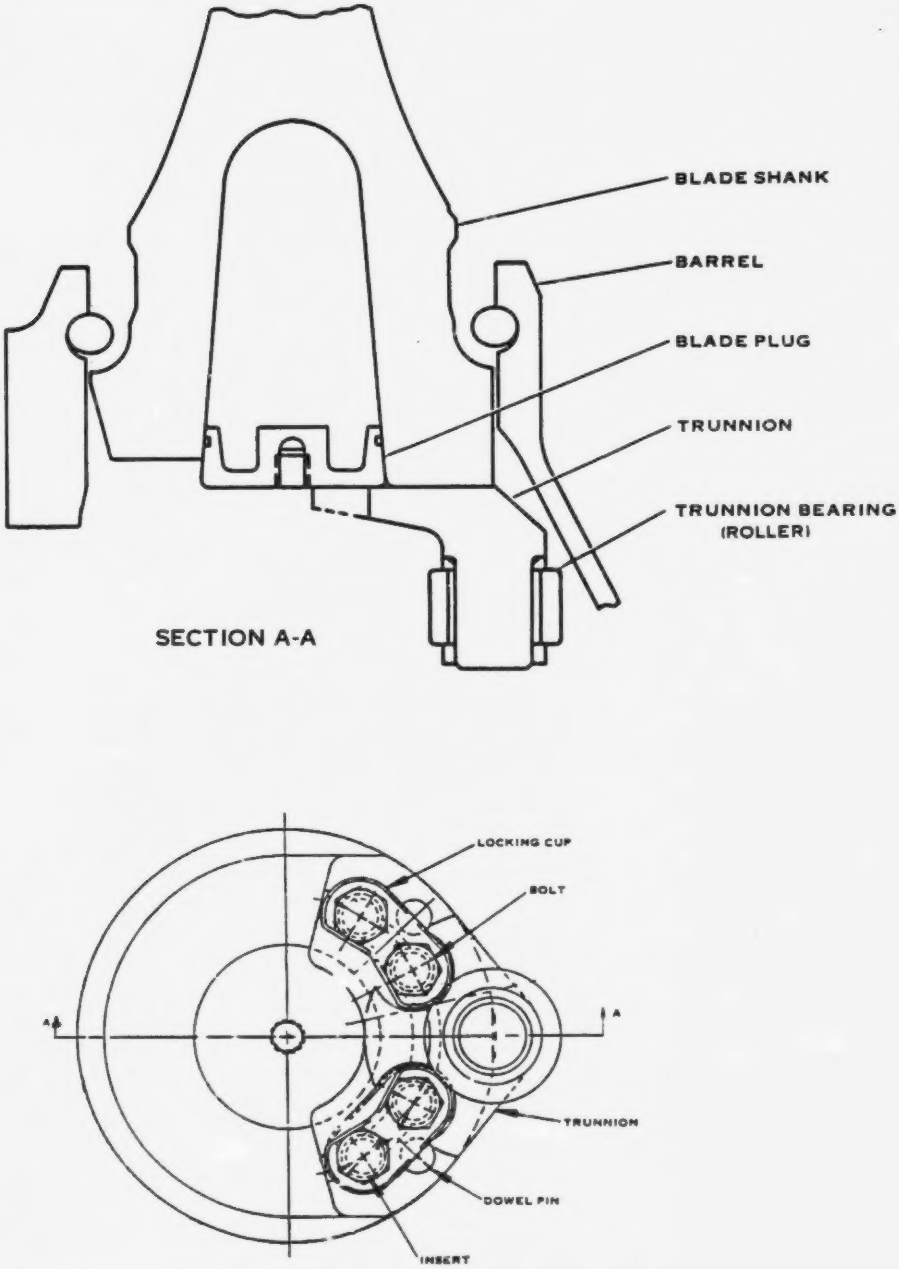
BLADE SHANK
BARREL
BLADE PLUG
TRUNNION
TRUNNION BEARING (ROLLER)
SECTION A-A
LOCKING CUP
BOLT
A
A
TRUNNION
DOWEL PIN
INSERT

FIGURE 3.7 BLADE TRUNION ASSEMBLY

4.0 SR-7L HUB AND BLADE RETENTION DESIGN

4.1 CONFIGURATION

The Large Scale Advanced Prop-Fan hub assembly forms a semi-rigid link between the blades, which provide thrust, and the engine shaft, which transmits torque. The hub and tailshaft is a one piece partially forged part which is carburized, heat treated and machined. A single row of ball bearings restrains each of the eight blades in the hub, while the tailshaft secures the propeller to the engine shaft with two cone seats that are preloaded against each other by the Prop-Fan retaining nut. The hub also forms the support for the pitch change actuator system, the control and the spinner. The hub is shown in Figure 4.1. The design effort is reported in detail in reference 6.

The retention transmits the loads from the blades to the hub while allowing changes in blade pitch. The single row ball bearing retention provides ease of maintenance by allowing individual blade replacement without disassembly of the hub. It has a through hardened inner race which seats against the aluminum blade shank and an outer race which is integral with the barrel. The outer race area is carburized to achieve the hardness necessary to support the ball loads. The balls are kept from contact with each other by a separator. The rotational speed of the propeller keeps the retention submerged in oil which is contained in the hub by a seal. A cross sectional view of the hub and retention are shown in Figure 4.2.

4.2 DESIGN REQUIREMENTS

The design requirements for the Large Scale Advanced Prop-Fan hub and retention are as follows:

- Combined steady and cyclic stresses experienced by the hub and retention for the operating conditions presented in Table 3-1 will be below a level that would yield 10^8 cycles of high cycle fatigue life and 50,000 cycle of low cycle fatigue life.
- The weight of the hub and retention must be representative of hardware that would be used in future production Prop-Fan systems.
- The stiffness of the hub and blade retention will be such as to prevent the propeller blade natural frequencies from impinging on the resonance avoidance zones discussed in Section 3.2.1.2.
- The fully hardened case depth of the hub blade retention race must exceed the depth at which the peak of the subsurface shear stress occurs.

PRECEDING PAGE BLANK NOT FILMED

PAGE 36 INTENTIONALLY BLANK

4.3 RETENTION AND HUB LOADS

4.3.1 Retention Loads

All the external loads on the retention and hub have their source in the blade loads. The retention loads used for the analysis of the hub and retention were derived from the finite element analysis of the blade discussed in Sections 3.4 and 3.5. The retention loads are the sum of the finite element model reactions to the steady centrifugal and aerodynamic loads and the vibratory response to the cyclic aerodynamic loads.

The aircraft climb condition has the highest flight vibratory loading and accumulates a large number of cycles over the life of the aircraft. The stress cycles accumulate at the rate of the Prop-Fan rotational speed. The climb condition therefore, was used for the hub design case. The retention loadings for the climb case are tabulated in Table 4-1.

TABLE 4-1
RETENTION LOADS

	Fx Newtons (lbs)	Fy Newtons (lbs)	Fz Newtons (lbs)	My Newton-meters (in-lbs)	Mz Newton-meter (in-lbs)
STDY + VIB	-368690 (-82890)	-35240 (-7922)	-14360 (-3229)	-3898 (-34499)	-2248 (-19893)
STDY - VIB	-368690 (-82890)	-29450 (-6620)	-2913 (-655)	1130 (10003)	-6449 (-57073)

The sign convention for the blade retention loads is illustrated in Figure 4.3. The lateral loads (Fx and Fy) have been found in the past to have negligible effect on hub stressing and thus were neglected in the analysis.

4.3.2 Tailshaft Loads

The loads which are applied to the tailshaft can be broken down into five categories: thrust, torque, engine shaft/tailshaft preload, blade centrifugal load, and shaft bending moment. Because of its high impressed moment and large number of cycles, the aircraft climb condition once again was determined to be the design limiting case.

The thrust generated by the propeller and torque applied to the propeller are fed through the tailshaft. Therefore, the tailshaft must be able to withstand the 32,995 newtons (7,418 lbs) of thrust and the 25,165 newton-meters (222,700 in-lbs) of torque the engine produces. Only a small portion of the blade centrifugal load is transmitted to the tailshaft, the majority being absorbed by the hub. The engine shaft/tailshaft interface is made up of two cones seated in the hub and preloaded against each other by the propeller retaining nut through the engine shaft. This nut is torqued to 3,390 newton-meters (30,000 in-lbs) producing a 298,906 newton (67,200 lb) axial preload on the cones. The moment load applied to the tailshaft is described in detail in the retention load section. This is a steady bending moment that produces once per revolution fully reversed bending stresses in the tailshaft because of its rotation. The moment magnitude is 8,645 newton-meters (76,500 in-lbs).

4.4 BLADE RETENTION STRESS ANALYSIS

The retention stresses were analyzed using a computerized analysis called H380. This analysis does a load balance on the bearing accounting for such parameters as number of balls, ball diameter, pitch diameter, forces, moments, material properties, and geometry. The results from this analysis that are used in retention design include Hertzian deflections and stresses, position of the ball contact pattern, and moment spring rate. For the loads listed in Table 4-1 a high cycle fatigue life in excess of 10^8 cycles and a low cycle fatigue life of 10,000 cycles were achieved. The 10,000 cycle LCF life is lower than the desired 50,000 cycles but is sufficient to complete all of the foreseeable testing with the SR-7L Prop-Fan The distribution of the subsurface shear stresses in the race are presented in Figure 4.4.

The specified fully hardened case depth of .104 cm (.041 inches) for the race exceeds the depth at which the peak of the shear stress distribution occurs. The analysis also showed that the ball patterns are on the race for all flight conditions.

4.5 HUB STRESS ANALYSIS

The stress analysis of the hub was conducted by splitting it into sections that could be analyzed by ring analysis and shell of revolution analysis computer programs. A 3-D finite element analysis of the hub was also conducted. Stresses obtained for the aircraft climb condition were low enough to allow both the 10^8 cycle HCF life and the 50,000 cycle LCF life to be obtained with significant margin.

4.6 TAILSHAFT STRESS ANALYSIS

The tail shaft was analyzed using a shell of revolution computer analysis. A radial deflection due to centrifugal load of .035 cm (.0014 in) was calculated for the tailshaft. The tailshaft model was predeflected by this amount to reproduce the effect of the centrifugal load. The remaining loads as explained in Section 4.3.2 were also applied to the model. The locations of the peak stresses are shown in Figure 4.5. The stresses are also shown plotted on a Goodman diagram, indicating significant strength margin.

4.7 RETENTION STIFFNESS ANALYSIS

The hub wall thickness is dictated by stiffness rather than strength considerations. A major function of the hub is to provide a retention stiffness that will place the natural frequencies of the propeller outside the restricted range illustrated in Figure 3.6. The retention stiffness was evaluated by a two-dimensional finite element analysis of the blade shank, the race, the ball, the shank/race interface and the hub. The hub stiffness was also evaluated using a 3-D finite element analysis.

A comparison of the in-plane and out-of-plane barrel stiffnesses determined by the 2-D and 3-D models is shown in Table 4-2.

TABLE 4-2

COMPARISON OF 2-D AND 3-D BARREL STIFFNESS RESULTS

	STIFFNESS	
	OOP (in-lb/rad)	IP (in-lb/rad)
MODEL		
2-D	61×10^6	55×10^6
3-D	70×10^6	37×10^6

4.7 (Continued)

The retention stiffness computed using the 2-D analysis of all of the hub and retention hardware is compared with the retention stiffness computed using the 3-D analysis of the hub and the 2-D analysis of the blade shank and race, and the ball and ball race interface in Table 4-3.

TABLE 4-3

COMPARISON OF RETENTION STIFFNESS RESULTS

	STIFFNESS	
	OOP (in-lb/rad)	IP (in-lb/rad)
MODEL		
2-D	15.5×10^6	13.7×10^6
3-D Hub, 2-D Blade and Retention	16.9×10^6	7.9×10^6

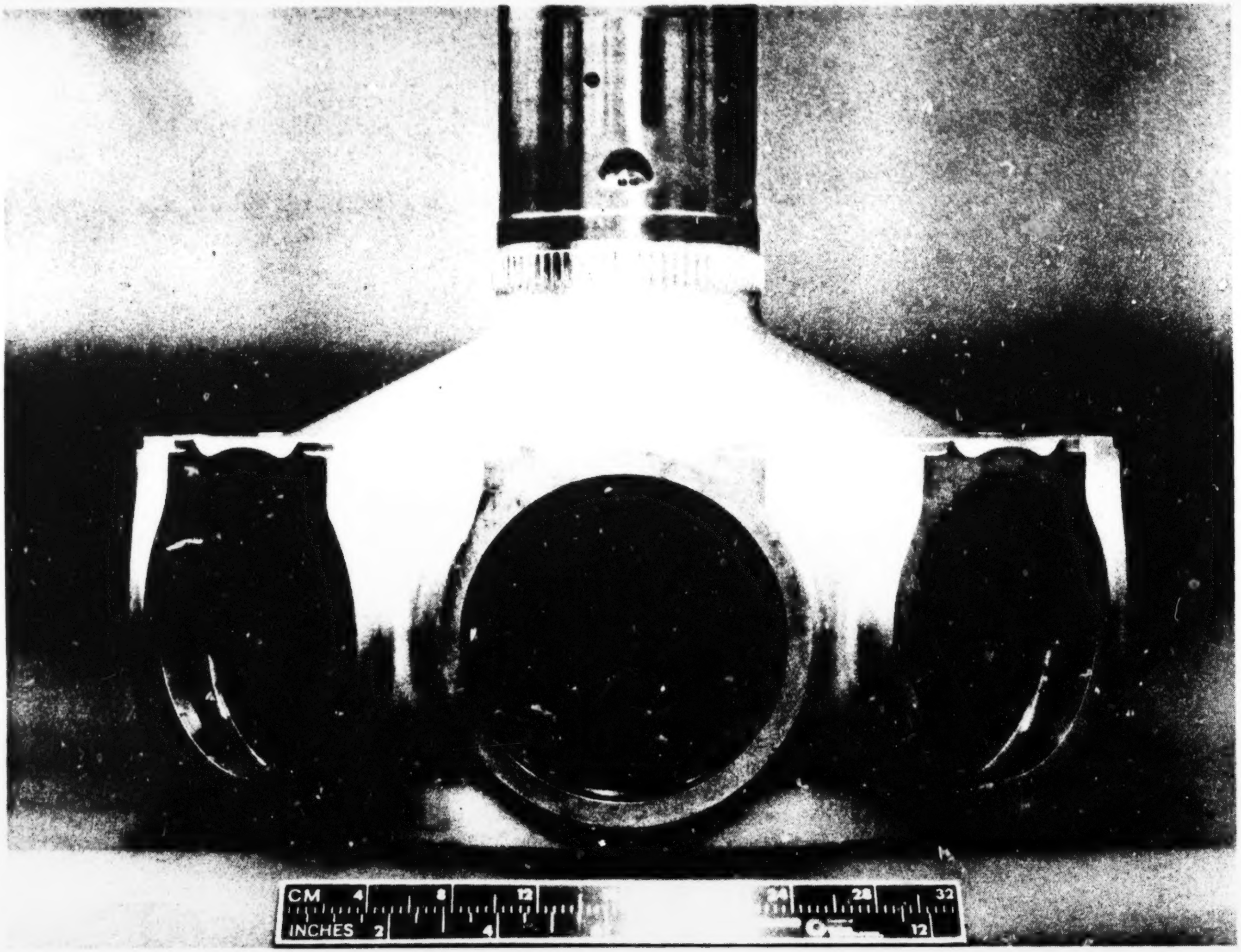
CM 4 8 12 24 28 32
INCHES 2 4 12

FIGURE 4.1 LAP HUB

RIGINAL PAGE IS
OF POOR QUALITY

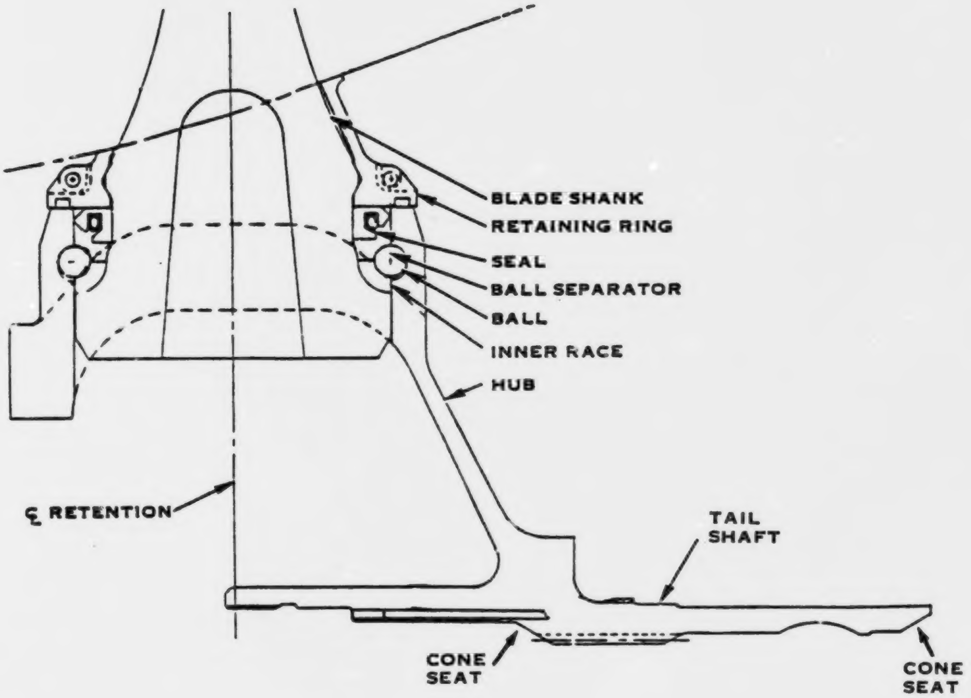
BLADE SHANK
RETAINING RING
SEAL
BALL SEPARATOR
BALL
INNER RACE
HUB
℄ RETENTION
TAIL SHAFT
CONE SEAT
CONE SEAT

FIGURE 4.2 CROSS SECTION, LAP HUB AND BLADE RETENTION

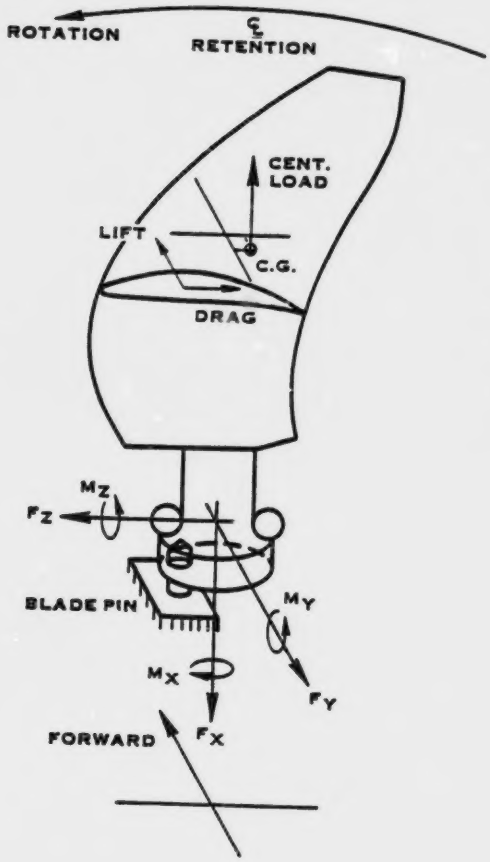
ROTATION
℄ RETENTION
CENT. LOAD
LIFT
C.G.
DRAG
MZ
FZ
BLADE PIN
MY
MX
FY
FORWARD
FX

FIGURE 4.3 BLADE LOADING COORDINATE SYSTEM

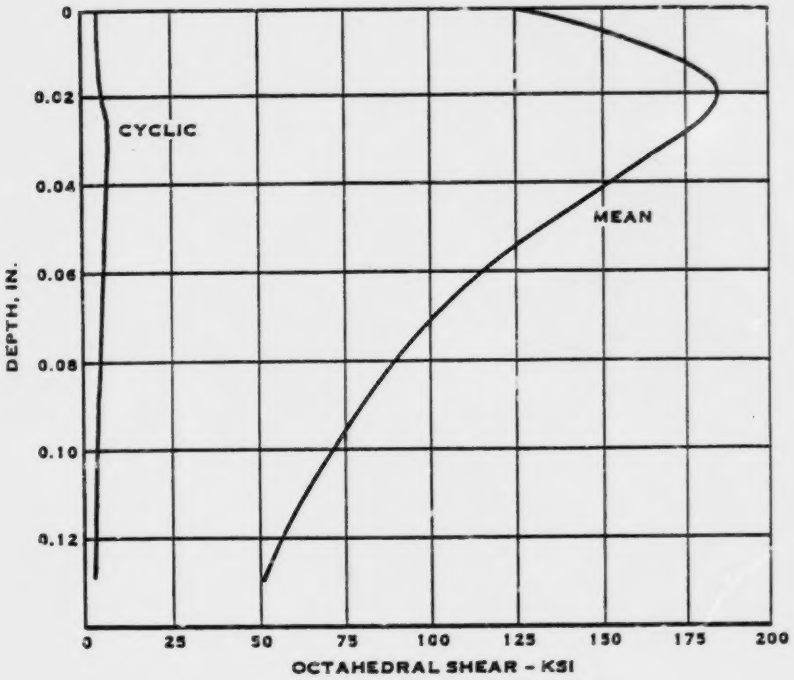

FIGURE 4.4 SUBSURFACE STRESS, HUB RETENTION BEARING RACE

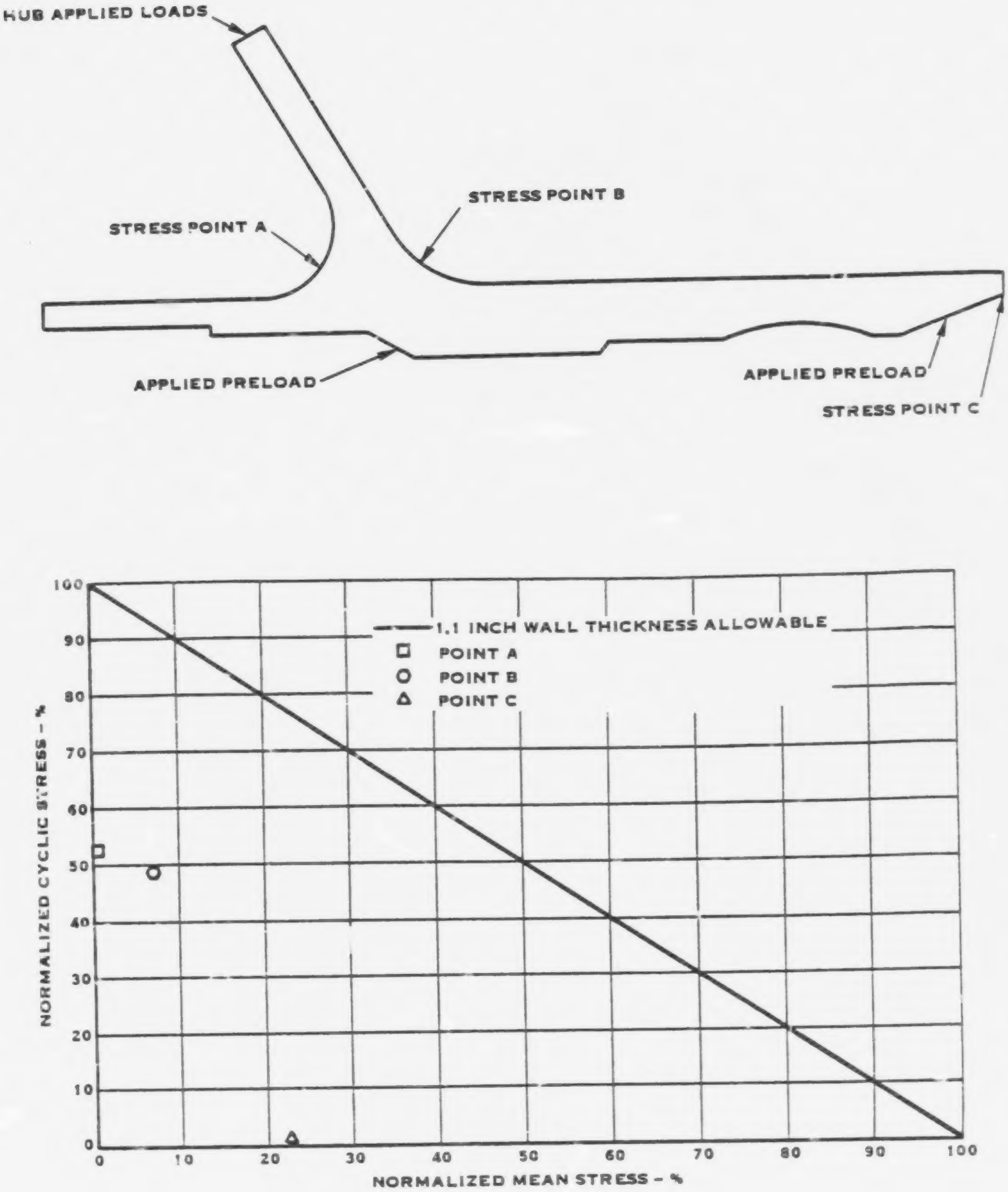

FIGURE 4.5 TAIL SHAFT STRESSES

5.0 SR-7L SPINNER DESIGN

5.1 CONFIGURATION

The LAP Spinner consists of a fiberglass shell with two integral bulkheads, eight tee-shaped fiberglass platforms and a rear bulkhead. The main structural supports are the two shell bulkheads which mount on the actuator dome and the rear bulkhead that mounts on the hub. The eight tee-shaped fiberglass platforms continue the spinner contour between the shell and the rear bulkhead and are fastened in place by two rows of screws. The contour of the spinner was chosen to provide the proper inflow to the Prop-Fan disc to attain optimum aerodynamic performance. The configuration of the Prop-Fan spinner is illustrated in Figure 5.1.

5.2 DESIGN REQUIREMENTS

The design requirements for the Large Scale Advanced Prop-Fan spinner are as follows:

- Combined steady and cyclic stresses experienced by the spinner will be below a level that will yield 10^8 cycles of high cycle fatigue life and 50,000 cycles of LCF life.
- The spinner first fore and aft and first lateral vibratory modes shall not have 7-P, 8-P or 9-P frequency crossovers within the Prop-Fan operating range of 1273-1698 RPM.
- The spinner must be removable with the blades at any pitch angle.
- The mass of the spinner must be representative of flight hardware.

5.3 FINITE ELEMENT MODEL

The spinner was analyzed using the NASTRAN finite element code. Modeling of the spinner was accomplished using triangular plate elements. The finite element model allowed the rubber O-Ring spinner mounts on the actuator dome and the screw attachments of the tee-platforms to be accurately modeled. The finite element model is illustrated in Figure 5.2. The model was used to calculate steady stresses and deflection, dynamic response stresses and normal modes and frequencies.

5.4 STEADY LOADS

The major steady load on the spinner is due to centrifugal force. Air pressure forces are very low and are neglected. The centrifugal forces are determined by the finite element computer code and vary with the element's centroidal radius and mass. The overall force on the element is distributed to the three corner nodes of the element.

5.5 VIBRATORY LOADS

The vibratory loads on the spinner arise from propeller excitation. These excitations are the result of out-of-plane blade deflections. The fore and aft mode and lateral mode excitation occur when their resonant frequencies cross the 7-P, 8-P and 9-P lines respectively. The degree to which the spinner responds is related to the excitation magnitude at the crossover point and the amount of damping. Since these parameters are not known exactly the spinner is analyzed for 10.0g fore and aft and 12.7g lateral excitations, at their corresponding resonant frequencies. This is known to be conservative because excitation as large as 10g's are not likely to occur at frequencies as high as 7-P.

5.6 SPINNER STRESS ANALYSIS

The combinations of steady and vibratory stresses for the various parts of the spinner are plotted on Goodman diagrams in Figure 5.3 for the 10g fore and aft excitation and 12.7g lateral excitation cases. The steady stresses include stress concentration effects which occur around shell and platform attachment points. The Goodman diagrams indicate that the tee-platforms are the most highly stressed portion of the spinner. However the platforms have significant margin for infinite fatigue life.

5.7 SPINNER NATURAL FREQUENCIES

A Campbell diagram for the spinner design is presented in Figure 5.4. The diagram shows plots of the spinner fore and aft and lateral natural frequencies overlayed on the P- order lines. The actual first fore and aft mode natural frequency is 251 Hz and crosses the 8-P line outside the operating RPM range. The actual first lateral natural frequency is 172 Hz and crosses the 9-P line outside the operating RPM range. However the lateral natural frequency crosses the 7-P line inside the operating RPM range. Since the 12.7g lateral vibratory loading was applied in the analysis at the 7-P crossover (172 Hz) with resulting stresses well below the allowable limit, operation over the range of 1273 to 1698 RPM is acceptable.

5.8 SPINNER FOREIGN OBJECT DAMAGE ANALYSIS

An analysis of the as designed spinner was conducted to determine its resistance to potential damage due to an in-flight impact by a bird or other foreign object.

The analysis was accomplished using the transient finite element analysis technique in NASTRAN using the following assumptions:

5.8 (Continued)

1. The bird weighs four pounds, has a length over diameter ratio of two, and has a density of .0249 pounds per cubic inch.

2. Maximum air speed at which a bird strike may occur is less than 150 knots.

3. Due to the fact that of the two bulkheads only the rear bulkhead carries a fore and aft load, a head-on collision is assumed to be the worst direction for impact.

The analysis revealed that the shell thickness would have to be increased in the nose area from the originally planned 0.050 inches.

Table 5-1 shows the total revised shell thickness for the nose area of the spinner. The maximum stress in the revised spinner is 67% of the Hamilton Standard design allowable.

TABLE 5-1

REVISED SPINNER SHELL THICKNESS

Axial Distance (Inches)	Total Thickness (Inches)
0.000	.100
.070	.100
.390	.100
.480	.100
.710	.100
.975	.150
1.275	.150
1.625	.200
1.975	.200
2.350	.200
2.765	.200
3.210	.200
3.745	.100
4.575	.100
5.625	.050

5.9 SPINNER REMOVABILITY

Removability of the spinner with the blade at any angle is achieved by selecting the pitch and length of the sixteen 1/4-28 flathead screws, that attach the 8 platforms to the aft bulkhead, to allow a clearance to the butt face of the blade.

ORIGINAL PAGE IS
OF POOR QUALITY

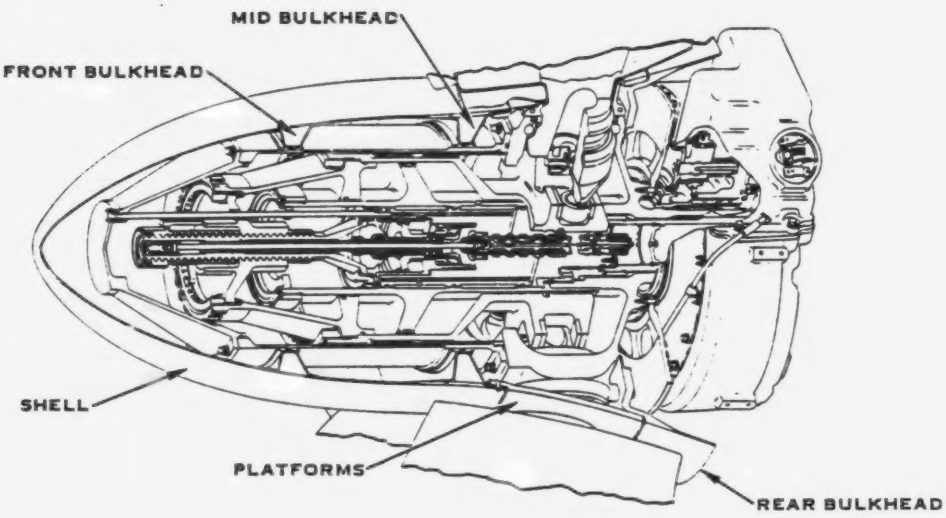
MID BULKHEAD
FRONT BULKHEAD
SHELL
PLATFORMS
REAR BULKHEAD

FIGURE 5.1 SPINNER CONFIGURATION

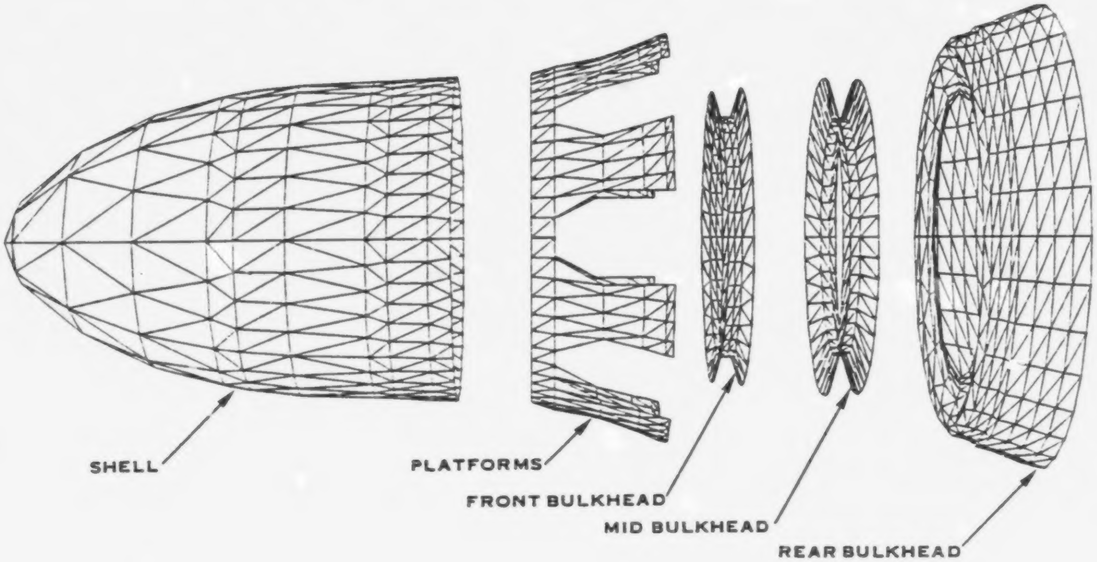
SHELL
PLATFORMS
FRONT BULKHEAD
MID BULKHEAD
REAR BULKHEAD

FIGURE 5.2 SPINNER ASSEMBLY - ANALYTICAL MODEL

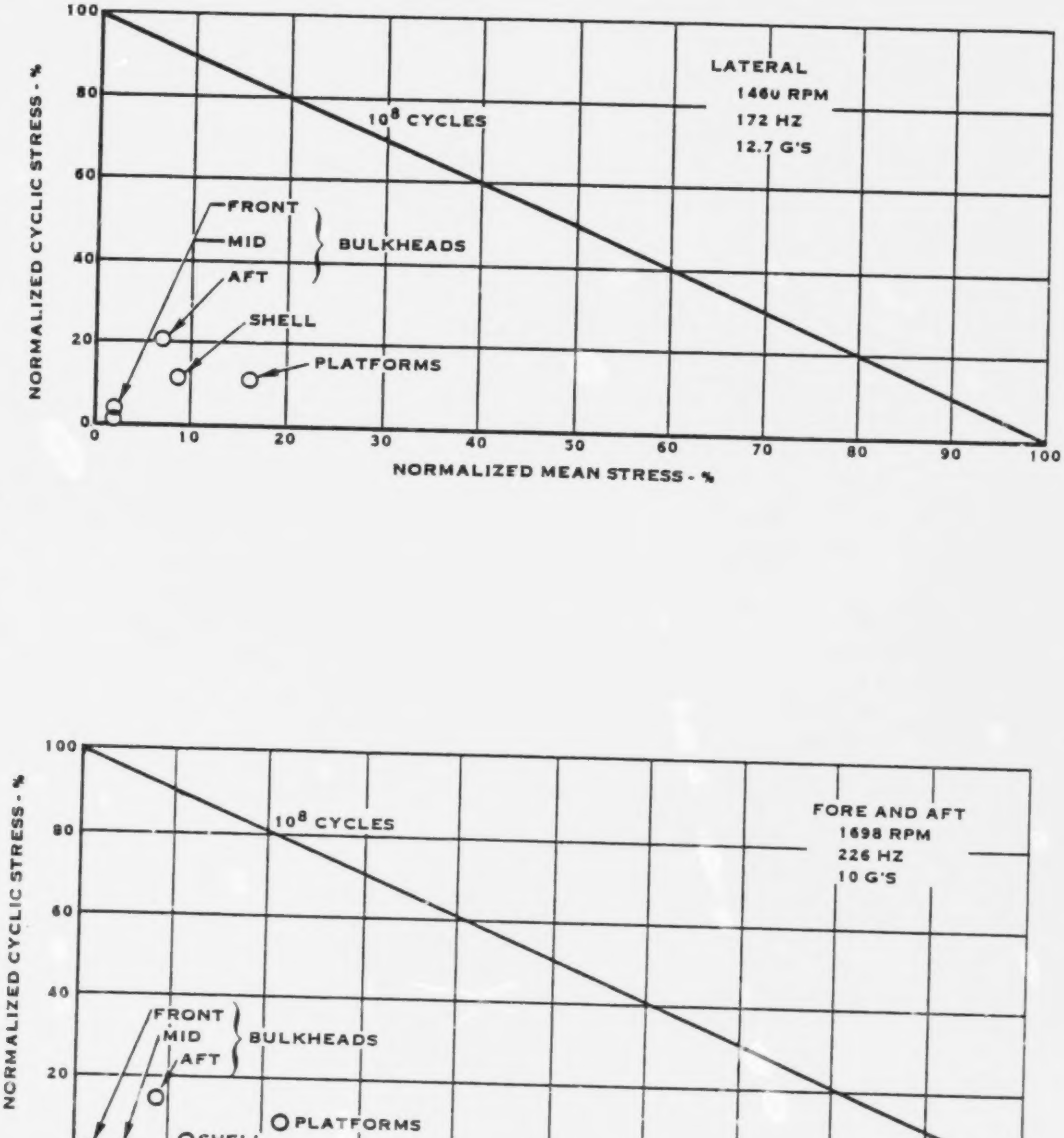

FIGURE 5.3 SPINNER STRESS ANALYSIS RESULTS

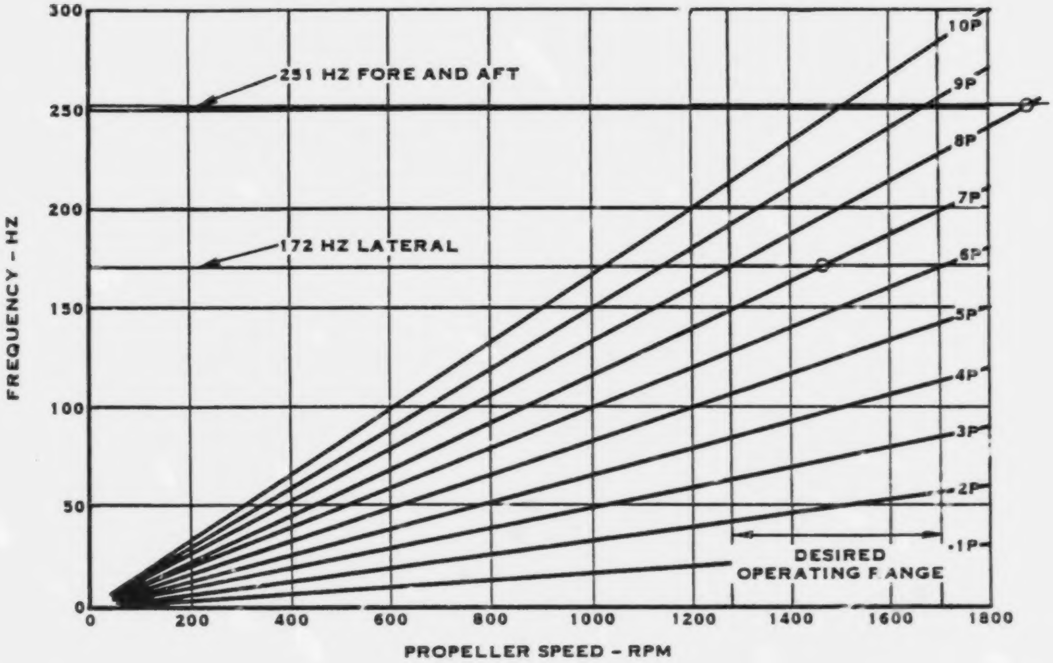

FIGURE 5.4 SPINNER NATURAL FREQUENCY CRITERIA

6.0 SR-7L PITCH CHANGE ACTUATOR AND CONTROL DESIGN

6.1 CONFIGURATION

The purpose of the control and actuator is to maintain a propeller RPM set point by varying blade angle to compensate for changes in engine power and inflow velocity at the propeller disc. The system is shown schematically in Figure 6.1. The design of the control and actuator is reported in detail in reference 7. The actuator is the prime mover for blade angle change. The actuator assembly mounts on the propeller hub and is illustrated in Figure 6.2. It consists of an internal stationary piston, a translating outer cylinder with an integral yoke that engages the blade trunnion and converts the translation to rotation of the blade, a centrally located pitchlock screw, a differential pressure regulating valve, a four way metering valve and a half area servo and ballscrew.

To change blade pitch, a pressure signal is generated by the propeller control and converted to a rotary signal by the servo and ballscrew. This rotary input is applied to a pitchlock screw. To increase pitch, the rotary signal drives the screw rearward a small amount relative to the cylinder assembly. This rearward motion temporarily decreases the pitchlock gap and moves the four-way valve rearward relative to the valve housing and sleeve. The valve stroke directs the supply oil to the increase pitch chamber of the actuator, and ports the decrease chamber to drain. This causes the actuator cylinder to move forward to increase the blade pitch toward feather. The motion of the actuator to increase pitch also carries the pitchlock screw forward returning the four-way valve to null and re-establishing the pitchlock gap.

The control is a modified version of the 54460 pitch control used on the Grumman E2-C2 aircraft. The control mounts on the hub tailshaft and is constrained from rotating by a lug on the engine gearbox. The control contains two major sub-assemblies, the pump housing assembly and the valve housing assembly. The pump housing assembly contains the hydraulic pumps that provide pressure for the actuator, the gearing that drives the pumps from the rotation of the prop shaft, the transfer bearing which transmits the hydraulic pressure across the rotating/stationary interface, and an auxiliary electric motor and pump to provide hydraulic pressure for static cycling of the blade angle. The valve housing contains a flyweight governor and governor valve, which control Prop-Fan RPM by generating the increase/decrease pitch hydraulic signal sent to the actuator, pressure regulating valves, a feather solenoid and valve and cams and linkages to adjust the governor and actuate the feather valve. The control sub-assemblies are illustrated in Figure 6.3.

6.2 DESIGN REQUIREMENTS

The purpose of the Large Scale Advanced Prop-Fan was to be a test vehicle for evaluating, the structural, aerodynamic and acoustic performance of the SR-7L blade. The actuator and control provide the capability to set blade angle and rotational speed for evaluation of the blade's performance and to provide a failsafe propulsion system in which any malfunction will cause the propeller to either pitchlock (maintain the current blade angle) or feather (increase blade angle to maximum pitch, 87.5°). The specific design requirements for the control and actuator are listed below:

- Governing Speed: 75-105%, Tip Speed: 183-256 meters/sec. (600-840 feet/sec.)
- Ground Adjustable Feather Stop: 87.5 ±2.5 Deg (ß 3/4)
- Ground Adjustable Low Pitch Stop: -10 to +40 Deg (ß 3/4)
- In-Place Pitchlock: 1.5 Deg. Max. Blade Angle Loss
- Slew Rate (Max): 9 Deg/Sec.
- Steady State Governing Accuracy: .22% Max. RPM
- Hysteresis: .15 Deg.

6.3 ACTUATOR DESIGN

The main components of the actuator are shown in Figure 6.2. The materials selected for the main structural elements are listed as well as some of the significant design parameters. This type of pitch change actuator and the materials used are typical of several Hamilton Standard production actuator designs.

6.3.1 Servo and Ballscrew

The servo and ballscrew convert a hydraulic signal from the control to a rotary input to the pitchlock screw. For an underspeed condition the governor would increase metered pressure which in turn changes the force balance in the servo driving it forward. The forward motion of the servo, which is axially attached to the ballscrew through a duplex ball bearing, rotates the ballscrew. The ballscrew is directly connected to the pitchlock screw through a splined quill and the rotary motion of the ballscrew is imparted to the pitchlock screw. The pitchlock screw translates forward displacing the beta valve which routes hydraulics to the decrease side of the actuator. For an overspeed condition this process is reversed. The governor at null regulates metered pressure at one-half of the supply pressure, therefore to maintain a force balance at the servo in an on-speed condition the area of the metered pressure side of the servo was designed to be twice that of the supply pressure side.

6.3.2 Pitchlock Screw

For normal operation the pitchlock screw is driven thru a quill shaft from the ballscrew. The quill shaft accommodates any angular or radial misalignment due to manufacturing tolerances between the ballscrew and the pitchlock screw. The quill shaft has a sliding spline at the pitchlock screw to accommodate the relative axial stroke of the ballscrew. The sliding spline on the pitchlock screw quill is nitrided and coated with a dry film lubricant. The mating internal spline is chrome-plated. The fixed spline on the quill is also nitrided. This combination for the quill shaft was selected for its compatibility with the existing ballscrew spline and is based on experience with similar applications.

6.3.3 Beta Valve

The beta valve is a four way, force compensated, spool valve with direct mechanical feedback from the actuator. The steel sleeve and spool are manufactured as a flow matched set. Their running surfaces are carburized to prevent erosion wear at the metering lands.

Motion of the valve aft of the null position meters oil to the increase pitch side of the actuator cylinder, and allows flow out of the decrease pitch side of the cylinder. This causes blade motion to increase pitch through the yoke and blade trunnion rollers. Since the valve's inner spool is attached to the actuator cylinder via the connecting rod, motion of the actuator brings the beta valve back to the null position. Conversely, forward motion of the valve moves the blades toward decrease pitch.

Pressure gain and flow gain are the two important hydraulic characteristics of the Beta valve. Pressure gain is the change in the ratio of high or low pitch pressure to main pump (supply) pressure with a change in valve displacement. The pressure gain determines the dead band hysteresis of the actuator. Flow gain is the change in hydraulic flow to the actuator with valve displacement. The flow gain determines the actuator time constant. The flow and pressure gain requirements for the Beta valve are shown in Figure 6.4. The flow and pressure gain requirements were chosen based on previous experience with other propellers.

6.3.4 ΔP Valve

The purpose of the ΔP valve is to limit the output force of the servo under extremes of metered pressure.

The ΔP regulating valve is a double-acting relief valve. It has the same area ratio as the servo and has control metered pressure acting on the larger area and supply pressure on the small area. The valve is preloaded such that for small changes in control metered pressure nothing changes. If the ratio of metered pressure to supply increases beyond 59%, the valve opens (i.e., moves to the right). Pressure to the servo is then regulated between the valve and the fixed orifice to approximately 59% of supply pressure. Conversely, if the signal pressure changes below 42% of supply, the valve moves to the left and maintains pressure to the servo at approximately 42%. By controlling the relationship between metered and supply pressure in this band, the output force of the servo can also be controlled at the desired level.

6.3.5 Stationary Piston and Translating Cylinder

6.3.5.1 Actuator Sizing - The size of the actuator is determined by the blade loads that must be reacted by the pitch change system. The three types of blade loads that must be reacted are centrifugal twisting moment (CTM), aerodynamic twisting moment (ATM) and friction twisting moment (FTM). CTM is the predominant load and results from the tendency of a centrifugal field to turn the blades toward flat pitch. ATM results from the distribution of air loads on the blade and may either add to or subtract from CTM. FTM results from the friction of the blade retention and acts to oppose blade angle change. CTM and ATM are plotted as a function of blade angle for 100% RPM in Figure 6.5. FTM is 1.419×10^5 Nm/blade at 100% speed. ATM, CTM and FTM are also functions of RPM^2.

The actuator was sized according to the blade loads generated by three flight conditions. The conditions and the required operating criteria are listed below.

TABLE 6-1

ACTUATOR SIZING CRITERIA

Case	V-Kts EAS	% RPM	Alt.	Kw (SHP)	Criteria
1. Overspeed	333	110%	SLSD	0	Must be able to change pitch
2. V_{max}	333	100%	SLSD	3580 Kw (4800)	Pitch rate = 9°/sec
3. Overspeed	333	125%	1520 meters (5,000 Ft)	2237 Kw (3,000)	Must be able to change pitch

6.3.5.1 (Continued)

The stall output of the actuator is calculated with 1050 psi at the increase pitch side of the actuator and 30 psi drain pressure at the decrease side. The actuator output at 9°/sec. was calculated with 700 psi at the increase pitch side to account for pressure drops.

6.3.5.2 Structural Criteria - The stationary piston and translating cylinder were analyzed using a finite element shelf of revolution program. The analyses were used to determine if the stress levels in the components and their axial and radial deflection were acceptable. The actuator was analyzed for the pressure spectrum presented in Figure 6.6. The results of the analysis indicate a possible maximum loss of .56° blade angle on the low pitch stop due to deflection caused by pressure loading, which is considered acceptable. The fatigue life criteria for the actuator was also met.

6.4 CONTROL DESIGN

In order to minimize development cost and time, the LAP pitch control design was derived from an existing propeller control. Based on the type of engine and gearbox anticipated to be used, the Hamilton Standard 54460 control was selected. A number of modifications in the control components were necessary to accommodate the higher RPM and opposite hand rotation of the LAP and the different type of actuator. A description of both the existing components and the design changes follows. The function of the control components are shown schematically in Figure 6.1.

6.4.1 Hydraulic Pumps

The main and standby pumps provide the hydraulic flow sent to the actuator. The scavange pump draws oil from the control atmospheric sump and pressurizes the control pressurized sump. These pumps are modified versions of the 54460 pump. The modifications were made to accommodate the change in direction of the propeller rotation. This was accomplished by interchanging the drive and driven gears on the pumps and designing a new front cover for the pump housings. The pumps run at approximately 12% higher RPM in the LAP control and the normal operating pressure is also higher. The suitability of these pumps for the LAP application was ensured by an accelerated endurance test which is discussed in Section 11.3 of this report.

6.4.2 Main and Standby Regulating Valve with Orifice Pack

The purpose of the main and standby regulating valve is to provide the system with a relatively constant supply pressure over a wide range of system flow conditions. The valve balances the force due to supply pressure on one end of the valve against a spring and a fixed reference pressure on the other end. Pressure regulation occurs in response to a change in actuator flow requirements. Under conditions of low flow demand, most of the combined flow of the main and standby pumps is diverted to the pressurized sump. With an increase in demand the supply pressure drops slightly causing a displacement of the plunger. The plunger motion closes the main pump metering window, restricting flow to drain, and results in an increase in supply flow to the actuator. When the flow to the system approaches the flow capacity of the main pump, the plunger has displaced sufficiently to completely close the main metering window and begins to meter across the standby land. Under this condition the standby pressure increases to the same value as supply pressure and opens the check valve located upstream of the regulating valve. In this manner the standby pump augments main pump flow to meet high system flow demand while allowing it to operate at lower pressure and heat generation levels during low demand conditions.

The purpose of the orifice pack is to provide the desired reference pressure to balance the valve spool. This is accomplished by connecting two orifices in series between supply and pressurized sump. The reference pressure is taken between the first and second orifice.

6.4.3 Governor

The purpose of the governor is to maintain a desired propeller speed under all aerodynamic conditions. This is accomplished by maintaining equilibrium between the flyweight force and speed set spring. The flyweight assembly, driven by the transfer bearing gear, rotates in direct proportion to the propeller speed. This rotation of the flyweights develops a force as a function of the rpm squared. An error in governing speed alters the force balance between the flyweights and speeder spring moving the governor valve from null. This valve stroke results in a change in metered pressure which changes the force balance in the half area servo, thus driving it in the direction of the unbalanced load. The blade angle change is made in the direction that corrects the speed error returning the governor valve back to null. The governing speed is selected by changing the preload on the speeder spring.

The governor's ability to accurately govern at a constant speed is dependent on the effective governor pressure gain at the servo. Before motion occurs at the servo to correct speed errors the pressure level must be increased to overcome system friction. The pressure gain of the valve is the increase in metered pressure as a function of valve stroke. The pressure gain of the valve, discounting external leakage, is 1.56×10^8 Pa/mm (576,000 psi/in). The calculated governing accuracy is .205% based on the estimated actuator friction and calculated pressure gain.

The flow gain of the valve is the volume of metered flow supplied by the governor to the servo valve as a function of valve stroke. There are two requirements that have to be met by the flow gain. Based on experience the flow gain should result in a blade angle rate of 2.5 deg/sec/%rpm around the null position. In addition, with the valve wide open the flow of the valve should provide for a slewing rate of the servo equal to or slightly higher than the actuator slewing rate of 9 deg/sec.

6.4.4 Feather Valve

The feather valve enables the hydraulic system to bypass normal control signals, from the governor, to feather the propeller. The feather valve can be actuated mechanically through the input linkage or hydraulically through the electric feather solenoid valve. The electric signal to the solenoid is either a result of a pilot command to feather or activated by the engine overspeed governor.

The basic function of the feather valve is to dump metered pressure to drain. Dumping metered pressure drives the servo and beta valve which moves the actuator in the increase pitch (feather) direction.

6.4.5 Control Input Linkage

The aircraft interface is the control input lever. Figure 6.7 is a schematic representation of the control linkage. The input schedule was designed with 2.5356° of input lever rotation equivalent to a 1% change in RPM. The input lever rotation is transmitted to the speed-setting cam by a set of spur gears such that 1° of input rotation results in 2.8824° of cam rotation. The speed-setting cam rise is translated to the speeder spring by a series of levers. Beyond the governing range the cam radius remains constant. Rotating the input lever to the feather position causes the feather cam to activate the feather linkage and displace the feather valve spool.

6.4.6 Gearing

The configuration of the LAP geartrain is similar to the 54460 geartrain. The system was designed with the intention of keeping the speeds of the pumps and governor as close as possible to the present speeds of the 54460 components. The system was also designed to accommodate left hand rotation, which is the opposite of the 54460, with minimum control modifications. A schematic of the geartrain is shown in Figure 6.8.

The transfer bearing gear, used to drive the pumps and idler, was enlarged in order to achieve the desired gear ratios. This was accomplished by machining off the old gear and riveting on a new gear. Twelve 1/8 in. rivets were used and the resulting stress on each rivet based on a transfer bearing gear torque of 89NM (789 in.-lbs), is 10^7PA (1450 psi).

The differential geartrain, used to run the governor and for beta feedback in the 54460 control, was replaced by a compound idler gear. To minimize modifications to the governor assembly, the governor gear utilized in the 54460 control is incorporated into the system and the resulting increase in RPM is only 15.78%.

The control gears have been sized per allowables established by Hamilton Standard for gears in this type of application based on experience in both large aircraft gearbox design and for control hardware, such as the 54460 control. The stress levels established represent a $\bar{X}$ - 3.0 sigma deviation from data, or 1 failure in 1000.

The gear material for the transfer bearing, pumps, and idler is AMS 6260, all carburized with the exception of the idler gear that meshes with the governor gear. This is because the governor gear in the 54460 control is not presently carburized. The gears are splash lubricated with MIL-H-5606, hydraulic oil.

6.4.7 Transfer Bearing

The transfer bearing supplies hydraulic flow to the rotating propeller from the stationary control. The transfer bearing provides three passages across the rotating interface for supply pressure, metered pressure and drain pressure. The LAP transfer bearing is a modified version of the 54460 bearing. The design is depicted in Figure 6.9.

Leakage of metered hydraulic pressure would adversely affect control performance. In order to minimize this leakage the diametral clearance at land A of the bearing was reduced. An additional radial hole and seal were added to the bearing rotating sleeve. This diverted metered pressure beneath the rotating sleeve at land A, which reduced the tendency of the bearing to deflect under the higher pressures of the LAP application. This deflection tended to increase the clearance and thus the leakage at land A.

A stiffer barrel support ring was also used in the LAP application. The purpose of the barrel support ring is to limit radial growth of the hub tailshaft, when it is tightened onto the engine shaft. This radial growth could tend to reduce the bearing clearances.

6.4.8 Auxiliary Pump and Motor

The auxiliary pump and motor are the same hardware used on the E2/C2 control. The pump output is used for ground handling and to feather the propeller in case of main and standby pump failure. The auxiliary pump supplies hydraulic flow to the actuator during static operation. The auxiliary pump is a two element pump. The main element supplies .0132 M^3/MM @ 9.48 x 10^6 PA (14 qpm at 1375 psi) to the supply system and the second element acts as a scavenge to return drain oil from the atmospheric sump to the pressurized sump. The auxiliary pump is driven, through a geartrain, by a 200 volt, 400 Hz, 3 phase electric motor. The motor limits the duty cycle to 20 seconds on at 3350 watts (4.5 horsepower), and 15 minutes off.

6.5 CONTROL DYNAMIC ANALYSIS

The LAP system dynamic analysis was accomplished with the development and use of a non-linear computer simulation model. This simulation model was needed to help understand the dynamic inter-relationships among sub-systems within the overall LAP system and to relate these dynamic inter-relationships to system stability and overall transient performance. The model was used to determine the appropriate value of pitch change governor gain and to analyze dynamic performance characteristics of this Prop-Fan system.

A simplified LAP system block diagram consisting of the Allison 501-M78 engine and controls, the LAP control and actuator and the Prop-Fan is shown in Figure 6.10. This functional signal flow diagram shows the input/output relationship of each turboprop subsystem. The dynamic engine and fuel control models were created with the use of a steady state engine cycle deck and fuel control block diagram. The Prop-Fan control model simulates the control governor, the actuator servo and ball screw and the beta valve. The Prop-Fan model uses power and thrust coefficient maps which are functions of blade angle and advance ratio. The power turbine torque output, accessory torque and Prop-Fan torque absorbed are summed to determine the torque available to accelerate the Prop-Fan power turbine and gearbox inertias to determine Prop-Fan speed.

The LAP system dynamic control model was used to evaluate the system response to large and small changes in engine power. The analysis found the system to be stable for all of the conditions analyzed. However all engine power setting changes should be input slowly to avoid large Prop-Fan speed overshoot. The tendency for a significant speed overshoot is the result of the blade slew rate being limited to 9°/sec.

6.6 BETA CONTROL

The SR-7L was tested on the static test rig at Wright Field to explore the stall flutter boundary and in the Modane wind tunnel to explore the high speed flutter boundary. For these tests it was desirable to operate the Prop-Fan with direct blade angle control and not with speed control. These boundaries are established by varying speed over a range while holding blade angle constant. This procedure is repeated for many different blade angles.

To incorporate blade angle control on the LAP, the rotary input to the pitchlock screw from the servo is replaced by a D.C. motor and gearhead. This arrangement replaces the governing mode configuration and is shown in Figure 6.11.

ORIGINAL PAGE
COLOR PHOTOGRAPH

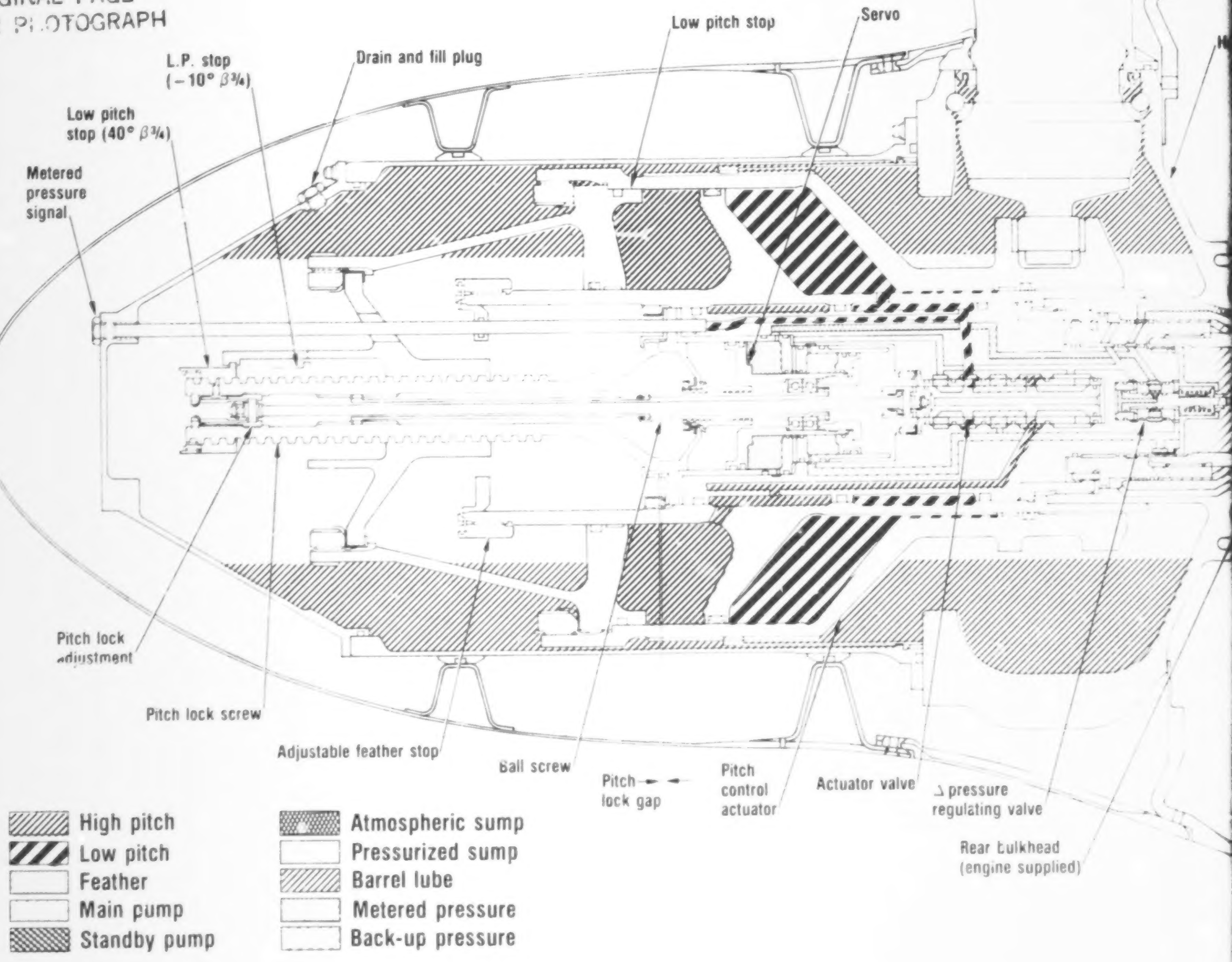
Low pitch stop
Servo
L.P. stop
(−10° β¾)
Drain and fill plug
Low pitch
stop (40° β¾)
Metered
pressure
signal
Pitch lock
adjustment
Pitch lock screw
Adjustable feather stop
Ball screw
Pitch lock gap
Pitch
control
actuator
Actuator valve
Δ pressure
regulating valve
Rear bulkhead
(engine supplied)
▨ High pitch
▨ Low pitch
☐ Feather
☐ Main pump
▨ Standby pump
▨ Atmospheric sump
☐ Pressurized sump
▨ Barrel lube
☐ Metered pressure
☐ Back-up pressure

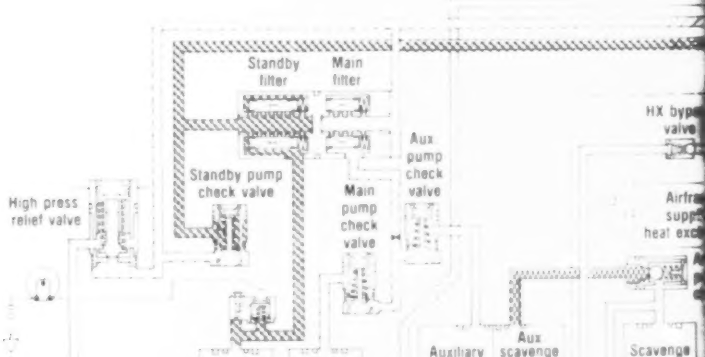
Standby
filter
Main
filter
HX byp
valve
Aux
pump
check
valve
Standby pump
check valve
High press
relief valve
Main
pump
check
valve
Airfra
supp
heat exc
Standby
pump
Main
pump
Auxiliary
pump
Aux
scavenge
pump
Scavenge
pump
Auxiliary
motor
Pressurized sump
Atmospheric

FOLDOUT FRAME

ORIGINAL PAGE
COLOR PHOTOGRAPH

2 FOLDOUT FRAME

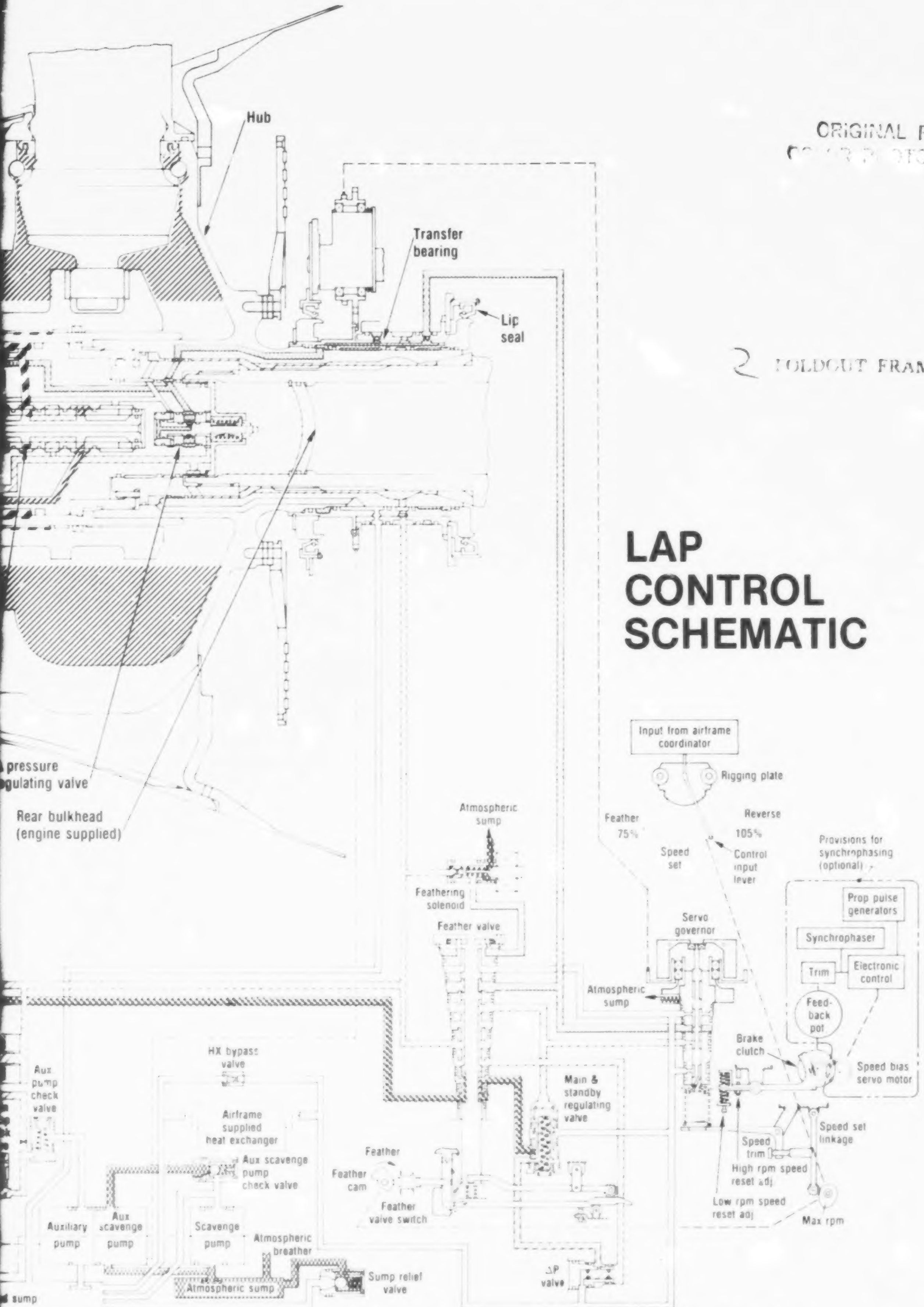
Hub
Transfer bearing
Lip seal
pressure
gulating valve
Rear bulkhead (engine supplied)
Input from airframe coordinator
Rigging plate
Feather
75%
Reverse
105%
Speed set
Control input lever
Provisions for synchrophasing (optional)
Prop pulse generators
Synchrophaser
Trim
Electronic control
Feed-back pot
Servo governor
Atmospheric sump
Brake clutch
Speed bias servo motor
Speed set linkage
Speed trim
High rpm speed reset adj
Low rpm speed reset adj
Max rpm
Atmospheric sump
Feathering solenoid
Feather valve
Main & standby regulating valve
Feather
Feather cam
Feather valve switch
ΔP valve
HX bypass valve
Aux pump check valve
Airframe supplied heat exchanger
Aux scavenge pump check valve
Auxiliary pump
Aux scavenge pump
Scavenge pump
Atmospheric breather
Atmospheric sump
Sump relief valve
sump

LAP CONTROL SCHEMATIC

FIGURE 6-1. LAP CONTROL SCHEMATIC

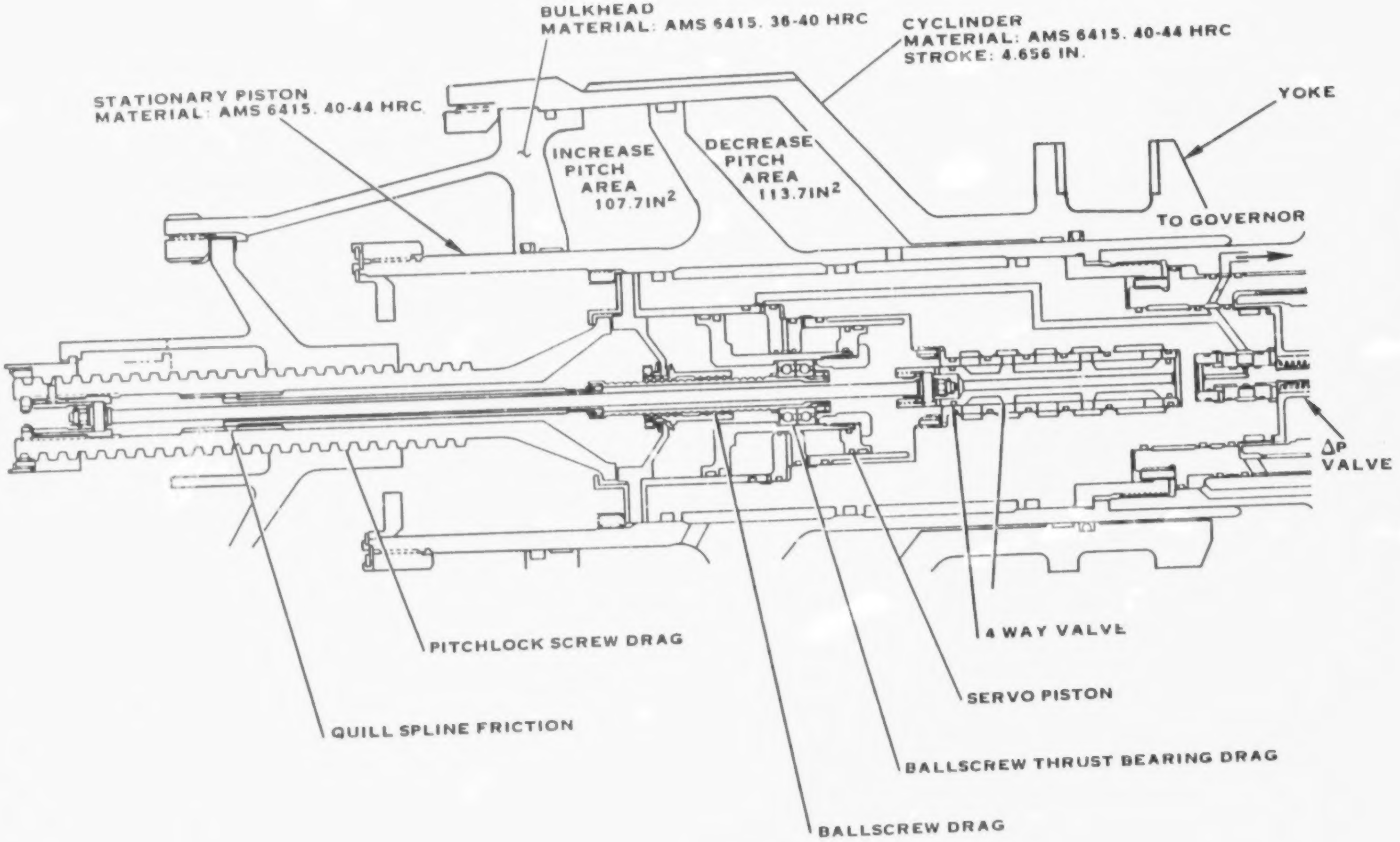
BULKHEAD
MATERIAL: AMS 6415. 36-40 HRC
CYCLINDER
MATERIAL: AMS 6415. 40-44 HRC
STROKE: 4.656 IN.
STATIONARY PISTON
MATERIAL: AMS 6415. 40-44 HRC
YOKE
INCREASE PITCH AREA 107.7IN²
DECREASE PITCH AREA 113.7IN²
TO GOVERNOR
ΔP VALVE
PITCHLOCK SCREW DRAG
4 WAY VALVE
SERVO PISTON
QUILL SPLINE FRICTION
BALLSCREW THRUST BEARING DRAG
BALLSCREW DRAG

FIGURE 6.2 LAP ACTUATOR

ORIGINAL PAGE IS
OF POOR QUALITY

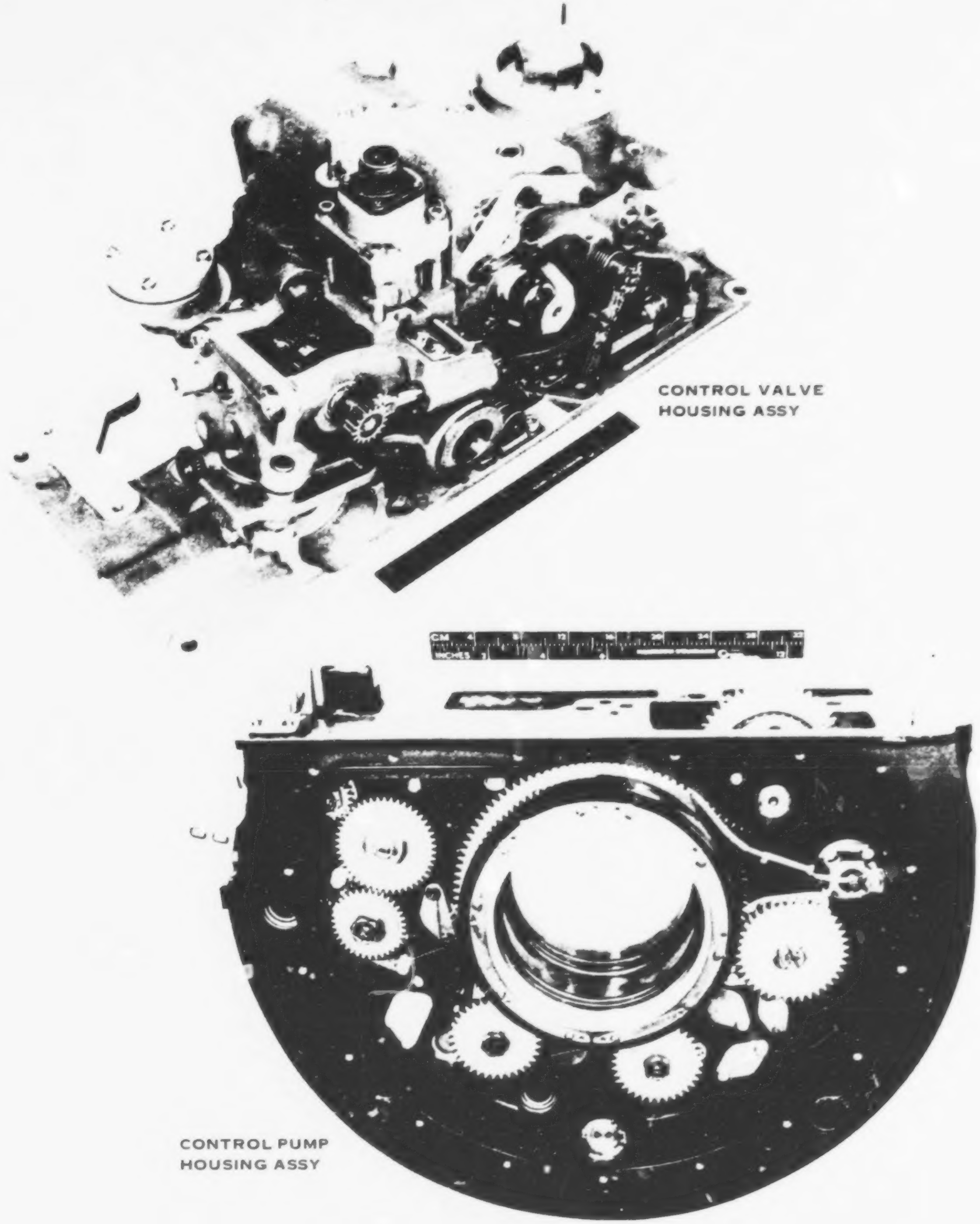
CONTROL VALVE
HOUSING ASSY
CONTROL PUMP
HOUSING ASSY

FIGURE 6.3 LAP CONTROL

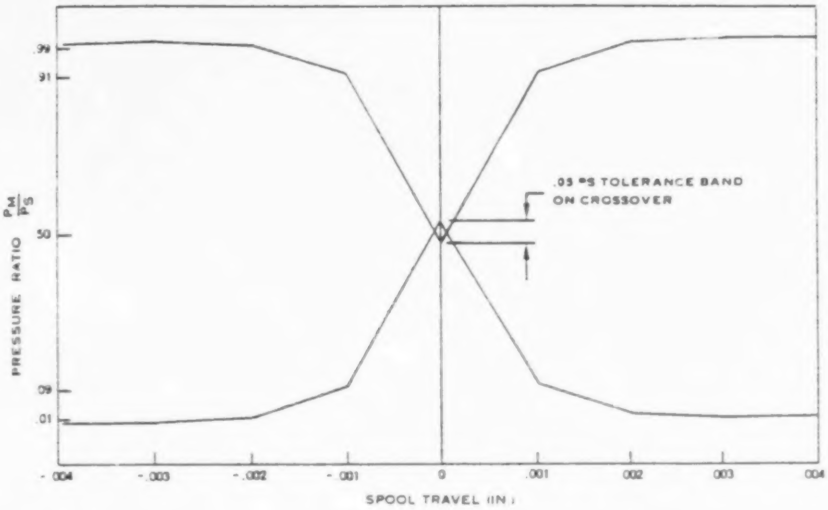

PRESSURE GAIN CHARACTERISTICS OF BETA VALVE

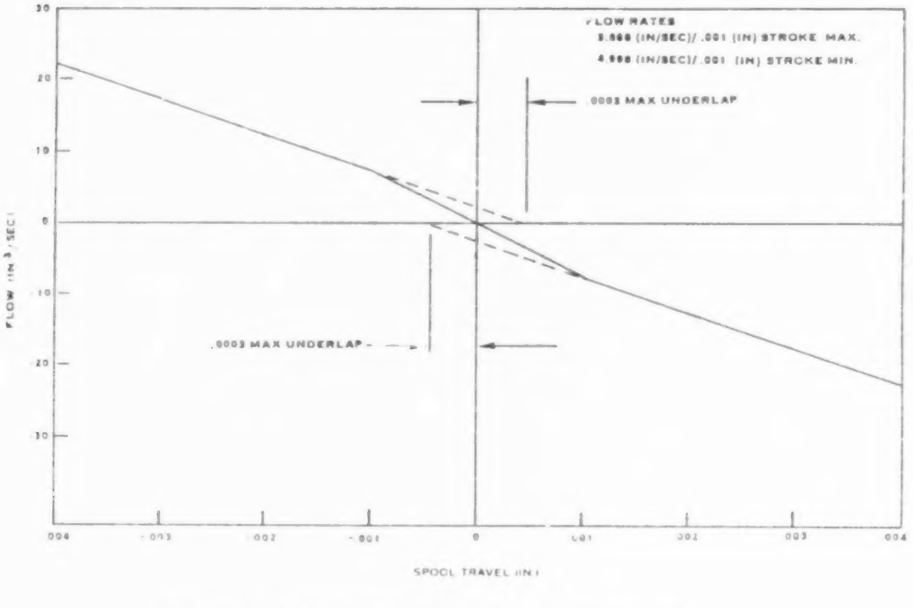

FLOW GAIN CHARACTERISTICS OF BETA VALVE

FIGURE 6.4 BETA VALVE FLOW AND PRESSURE GAIN

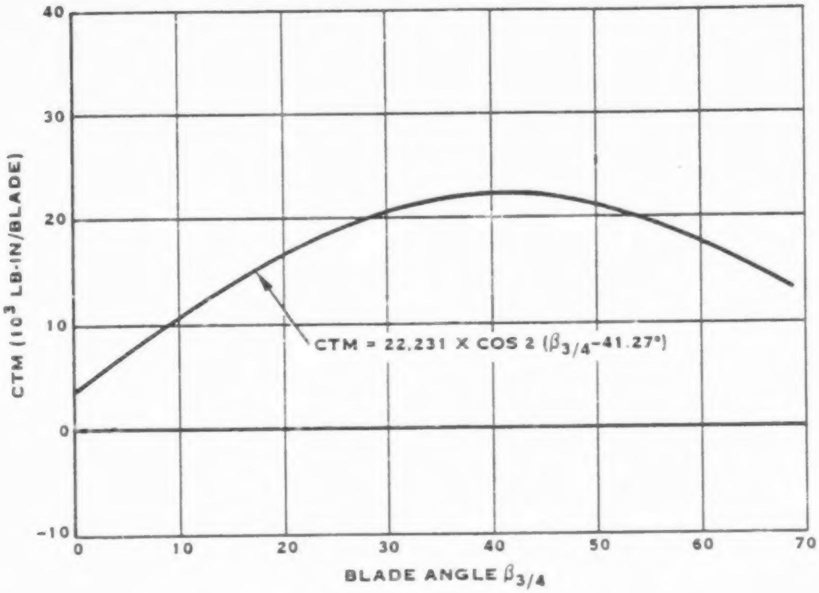

CENTRIFUGAL TWISTING MOMENT (CTM)-100% SPEED

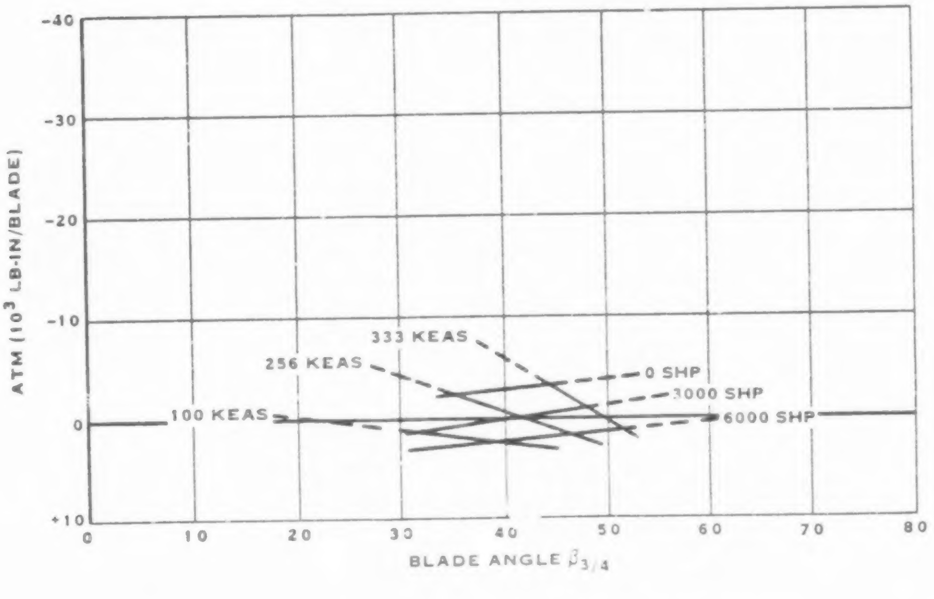

AERODYNAMIC TWISTING MOMENT (ATM) - 100% SPEED (5,000 FT)
(+ TOWARD HIGH PITCH)

FIGURE 6.5 SR-7L CENTRIFUGAL AND AERODYNAMIC TWISTING MOMENT, (100% SPEED)

Pitch Change Actuator
Life/Load Spectrum

Start-Stop Cycles	10,000	0 - 9.48×10^6 PA	(0 - 1375 PSI)
Flight Cycle	500,000	$6.55 \times 10^6 \pm 1.65 \times 10^6$ PA	(950 ± 240 PSI)
Pressure Pulsations	Life	$7.93 \times 10^6 \pm 1.21 \times 10^6$ PA	(1150 ± 175 PSI)
Proof		11.72×10^6 PA	(1700 PSI)
Burst		17.58×10^6 PA	(2550 PSI)

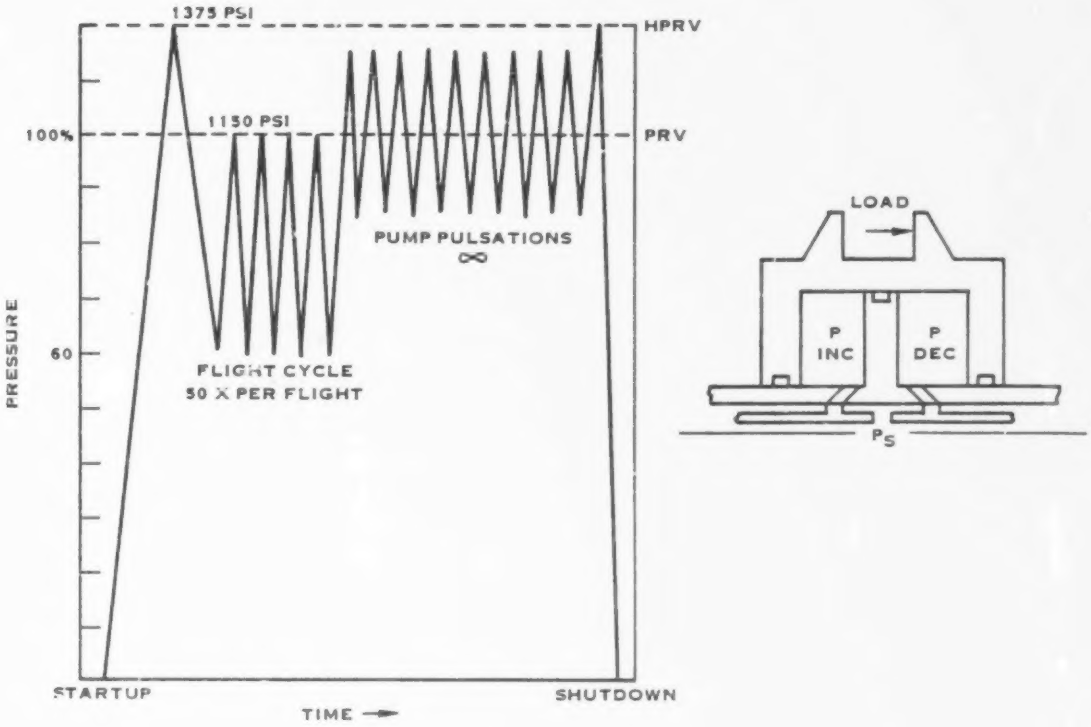

FIGURE 6.6 ACTUATOR PRESSURE SPECTRUM FOR A TYPICAL FLIGHT

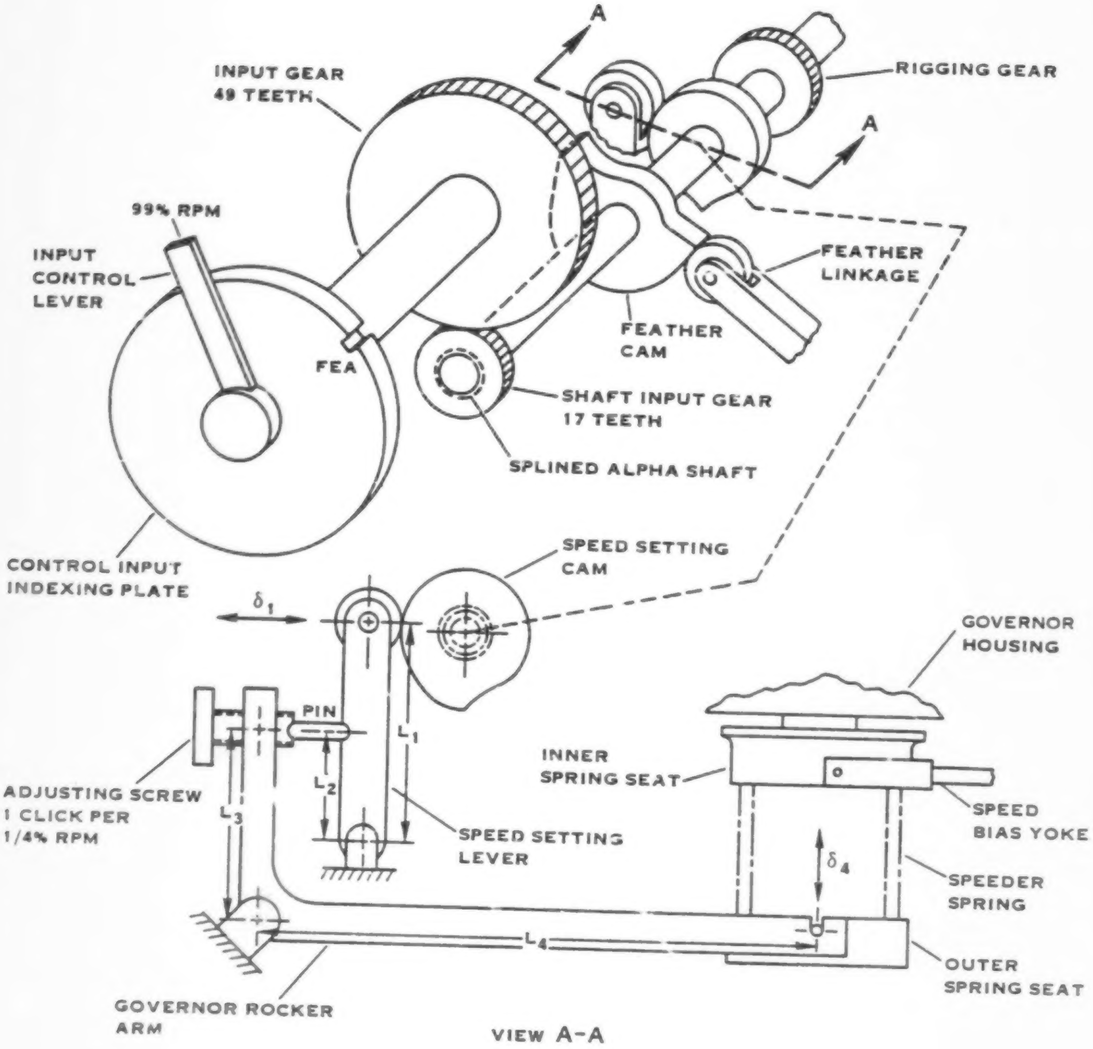
A
A
INPUT GEAR
49 TEETH
RIGGING GEAR
99% RPM
INPUT
CONTROL
LEVER
FEATHER
LINKAGE
FEA
FEATHER
CAM
SHAFT INPUT GEAR
17 TEETH
SPLINED ALPHA SHAFT
CONTROL INPUT
INDEXING PLATE
SPEED SETTING
CAM
δ1
GOVERNOR
HOUSING
PIN
L1
L2
L3
INNER
SPRING SEAT
ADJUSTING SCREW
1 CLICK PER
1/4% RPM
SPEED
BIAS YOKE
SPEED SETTING
LEVER
δ4
SPEEDER
SPRING
L4
OUTER
SPRING SEAT
GOVERNOR ROCKER
ARM
VIEW A-A

TABLE OF LENGTHS AND RATIOS

L_1 = 2.2037 IN.

L_2 = 1.00 IN.

L_3 = 1.38 IN.

L_4 = 4.18 IN.

$\delta_4 = 1.3746\,\delta_1$

GEAR RATIO = 2.8824 (° CAM/° INPUT)

FIGURE 6.7 GOVERNOR LINKAGE SCHEMATIC

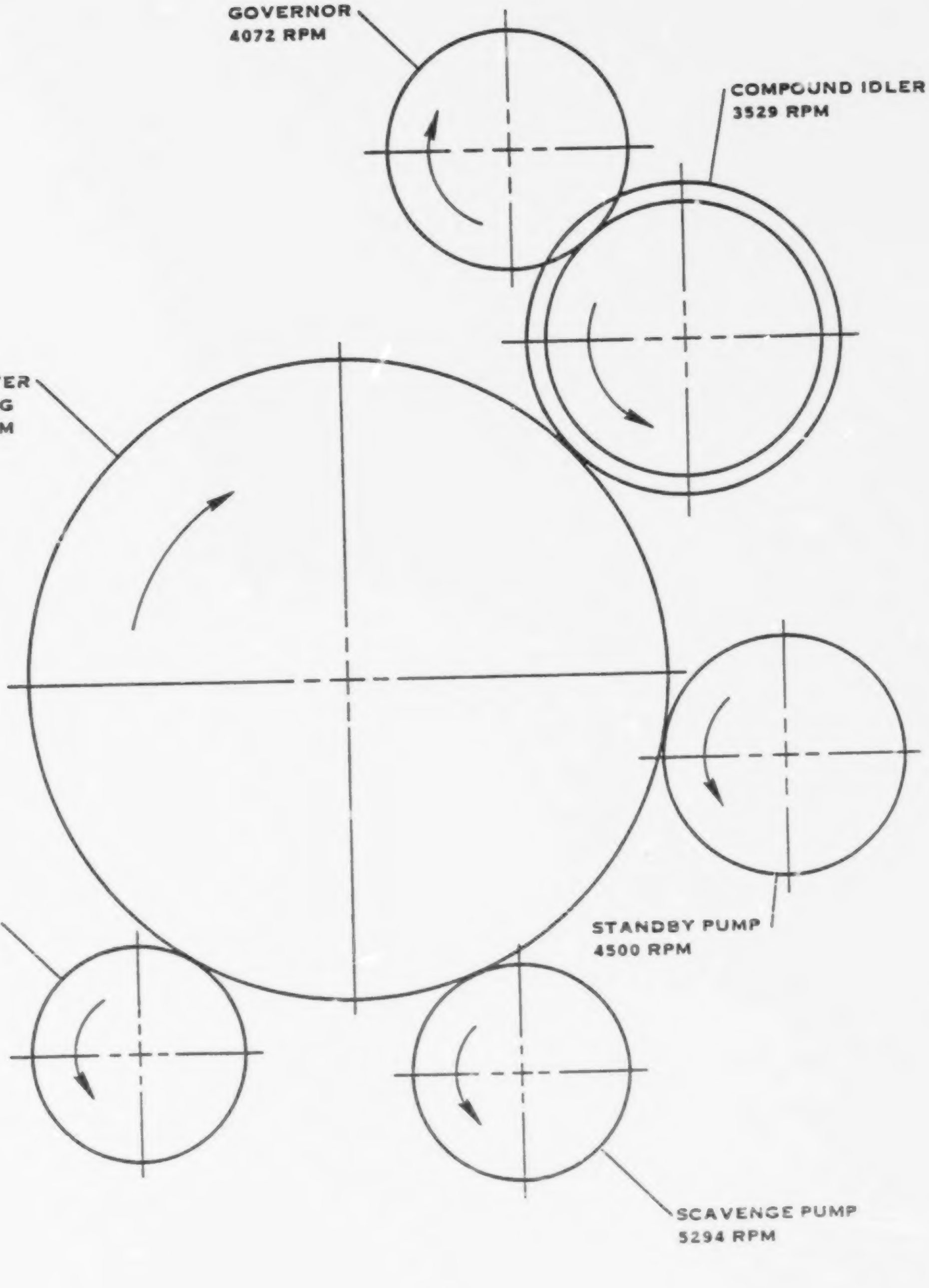
GOVERNOR
4072 RPM
COMPOUND IDLER
3529 RPM
TRANSFER
BEARING
1698 RPM
MAIN PUMP
5294 RPM
STANDBY PUMP
4500 RPM
SCAVENGE PUMP
5294 RPM

FIGURE 6.8 LAP CONTROL GEAR TRAIN SCHEMATIC - VIEW LOOKING AFT

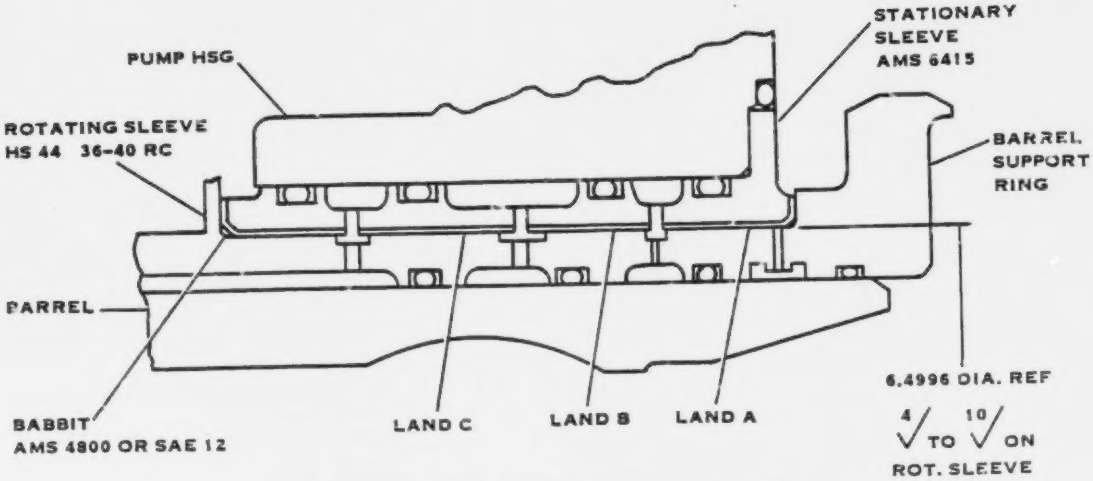
STATIONARY SLEEVE AMS 6415
PUMP HSG
ROTATING SLEEVE HS 44 36-40 RC
BARREL SUPPORT RING
BARREL
6.4996 DIA. REF
BABBIT AMS 4800 OR SAE 12
LAND C
LAND B
LAND A
4√ TO 10√ ON ROT. SLEEVE

DIAMETER CLEARANCE (IN)		
LAND	LAP	E2/C2
A	0.00155-0.00175	0.0035-0.0040
B	0.00155-0.00175	0.00155-0.00175
C	0.00155-0.00175	0.00165-0.00185

FIGURE 6.9 TRANSFER BEARING MODIFICATIONS

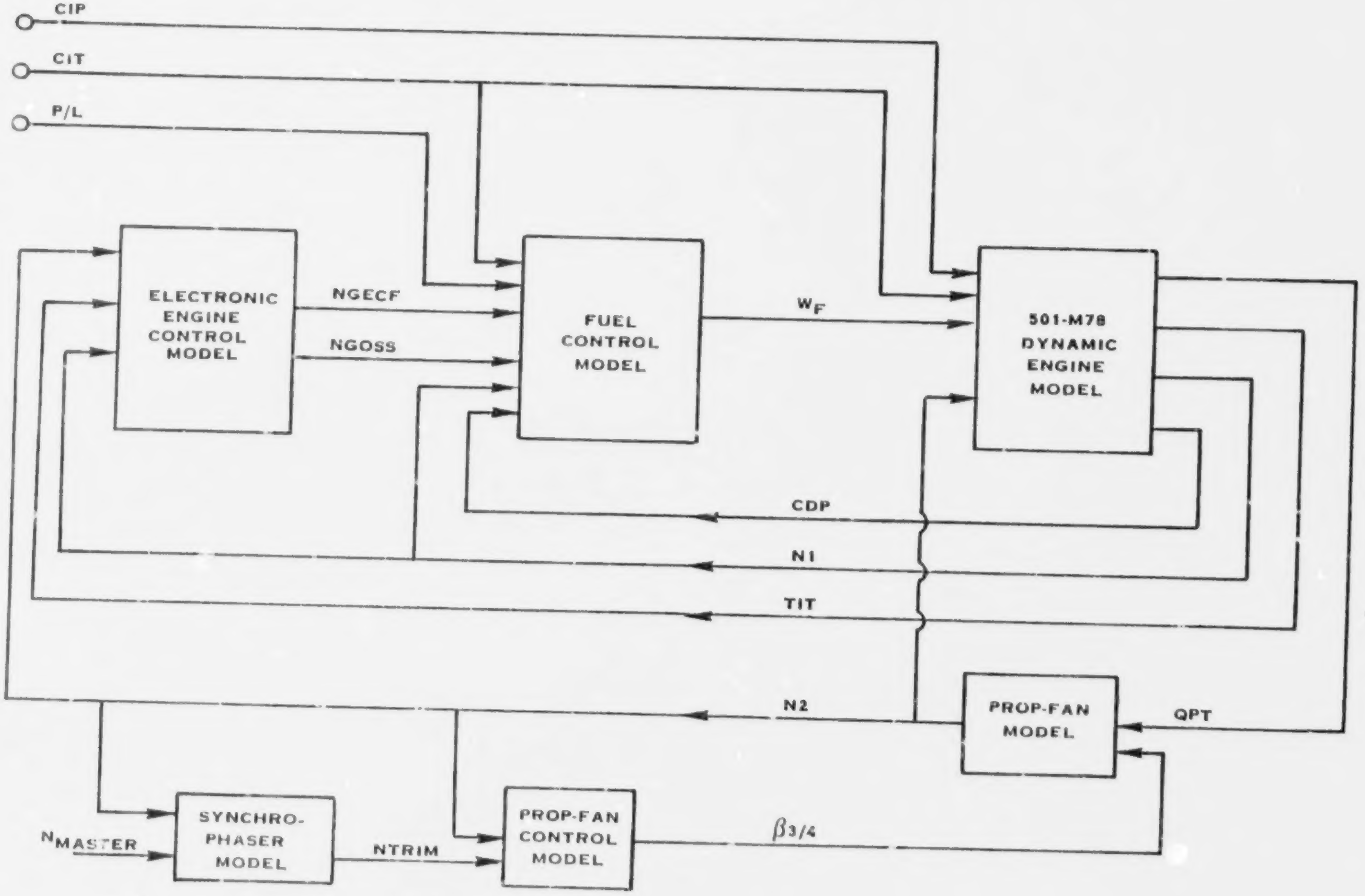
CIP
CIT
P/L
ELECTRONIC ENGINE CONTROL MODEL
NGECF
NGOSS
FUEL CONTROL MODEL
W_F
501-M78 DYNAMIC ENGINE MODEL
CDP
N1
TIT
N2
PROP-FAN MODEL
QPT
SYNCHRO-PHASER MODEL
N_{MASTER}
NTRIM
PROP-FAN CONTROL MODEL
$\beta_{3/4}$

FIGURE 6.10 LAP SYSTEM FUNCTIONAL BLOCK DIAGRAM

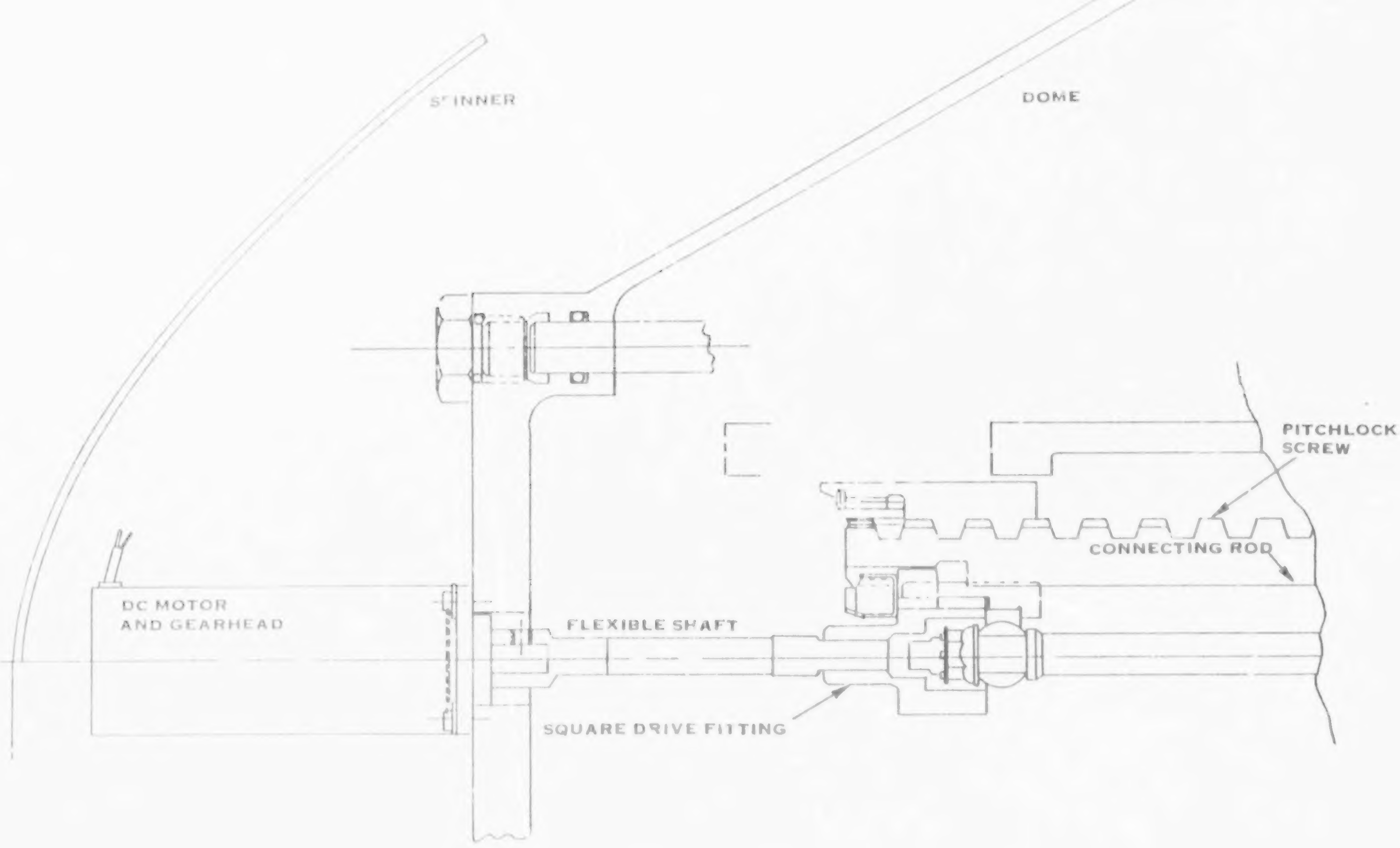
SPINNER
DOME
PITCHLOCK SCREW
CONNECTING ROD
DC MOTOR AND GEARHEAD
FLEXIBLE SHAFT
SQUARE DRIVE FITTING

FIGURE 6.11 MOTOR DRIVEN PITCH CONTROL MECHANISM

7.0 SR-7L SYSTEM DESIGN AND INTEGRATION

The efforts conducted under the system design and integration portion of the LAP contract were reported in detail in reference 8, and accomplished in three phases. The first two phases were intended to ensure the smooth operation and assembly of the Large Scale Advanced Prop-Fan. The first phase involved coordination of the design loads at the system interfaces. This was done to ensure the consistency of the loads used in the design process. The second phase of the effort was related to the physical dimension of the hardware at the system interfaces. The objective was to ensure that no dimensional interferences were present in the design. The third phase of the effort was the preparation of the failure modes and effect analysis (FMEA). The purpose of the FMEA was to isolate significant problems of a systems nature.

7.1 CONSISTENCY OF DESIGN LOADS

As specified under contract NAS3-23051, the Prop-Fan hub, retention and pitch control system design has been coordinated to ensure proper operation within the spinner envelope. The first step was to verify that the design loads used at the various system interfaces were consistent. The retention transfers the blade centrifugal, bending and shear loads to the hub. The trunnion transfers the blade torsional load to the actuator, and the tailshaft transfers the hub loads to the engine shaft. The loads at these interfaces must, therefore, be consistent. Given sufficient time, complete consistency in the design loads would have been possible. However, the demands of the schedule made this impossible. The components had to be designed in parallel, so the final loads were not usually available when needed. Therefore, some of the loads used to size the component interfaces were best estimates based on a preliminary analysis and previous experience.

As the analysis was refined, the loads were revised. As time permitted or if the initial analysis was not conservative, the affected hardware was re-analyzed. If however, the initial load was conservative and the results were acceptable, there was no re-analysis. Thus, the loads used in the analyses were not always consistent but they were conservative.

7.2 HARDWARE COMPATIBILITY

The first step in the Design/Drafting loop was the creation of the layouts. As the designers created their layouts, they communicated among themselves to define the system interfaces and envelopes. When the layout was complete, it was put through a series of design reviews. After receiving final approval, the layout was sent to drafting. The layout was the vehicle used to formally communicate design requirements to drafting.

Drafting took the layout and created the detail drawings. If a problem arose, drafting worked with design engineering to resolve the problem without compromising the design. Before the drawing was released, it was checked to ensure that all the design requirements had been satisfied and that the proper fits and clearances had been maintained. If the adjacent hardware had not been detailed, a Cavity Sketch Layout (CSL) was created to define the mating interfaces and the checking was then completed. The detail drawings were thoroughly reviewed again and signed by design, drafting, materials and project engineering. As a final check, a system assembly layout was created. Special attention was devoted to all system interfaces. No interference or assembly problems were found during this process.

7.3 FAILURE MODE AND EFFECTS ANALYSIS

The Failure Mode and Effects Analysis (FMEA) contained in Appendix A was used by Hamilton Standard to evaluate the potential reliability of the Large-Scale Advanced Prop-Fan (LAP).

The primary objective of this "functional" FMEA was to highlight critical failure areas so that susceptibility to such failures could be removed from the system during the design phase. In this analysis, each potential functional failure was considered in light of the probability of occurrence and evaluated as to the probable effect on safety and mission success.

Since the LAP is a research and development unit to explore the structural and acoustic characteristics of highly loaded, thin, swept blades at high Mach numbers, the philosophy was to have failures in the actuation system result in either blade pitch lock or feather.

The conclusions reached are based upon experience with similar products. Representatives from the reliability, design and project functions have reviewed this FMEA and concur that it properly described the LAP at the time.

8.0 SR-7L PROP-FAN INSTRUMENTATION SYSTEM DESIGN

8.1 SYSTEM DESCRIPTION

The rotating instrumentation system for the SR-7L Large Scale Advanced Prop-Fan, reported on in detail in reference 9, provides the capacity to transmit 33 channels of information from electronic measurement devices on the rotating side of the Prop-Fan to data collection equipment in the stationary field. The measurement devices include 30 strain gages for measuring stress in the blade structure, two pressure transducers for measuring high and low pitch hydraulic pressure in the Prop-Fan actuator and a potentiometer for measuring the blade pitch angle. A schematic of the instrumentation system is shown in Figure 8.1. The instrumentation hardware is shown in Figure 8.2.

Each of the eight blades on the Large Scale Advanced Prop-Fan may be instrumented with up to ten strain gages. Bridge completion for these gages is accomplished by a printed circuit board in the cuff of each blade. Programmable connectors are used to interface between the bridge completion boards and the rotating interface board (RIB).

The 30 strain gages from which data is collected are selected by the programmable connectors. The RIB board provides signal and power interconnections between the components of the instrumentation system.

Electric power for the rotating instrumentation and instrumentation signals are transmitted across the rotary/stationary interface by a brush block and slip rings. The physical arrangement of the LAP allowed for only eight slip rings. The need to transmit 33 channels of information necessitated the use of multiplexing. The signals from the strain gages and pressure transducers were divided into two groups of 16 and were converted to frequency modulated signals by two sets of voltage controlled oscillators (VCO's). Each group was then multiplexed by a mixer, allowing 32 channels to be transmitted through two slip rings. This left six slip rings available for transmitting the blade pitch angle signal, instrumentation power, and power for the Beta control electric motor.

Each of the two groups of 16 multiplexed channels are detranslated into four groups of four channels for recording in the stationary field by a dual 16 channel detranslator system. Both real time and playback monitoring capabilities are provided.

8.2 DESIGN GOALS AND CRITERIA

The design goals and criteria for the LAP rotating instrumentation system were as follows:

- Achieve noise immunity through the use of frequency modulated data transmission.
- Provide 33 data channels for blade strain gages, actuator pressure transducers and a blade angle transducer.
- Achieve a system accuracy of ±3% RSS.
- Attain a time correlation between channels of ±5%.
- Provide a system frequency response of DC to 1000 Hz.
- Provide a operating temperature range of -55 °C to 80 °C.

8.3 TRANSDUCERS

The transducers used in the SR-7L Prop-Fan rotating instrumentation system include strain gages, pressure transducers and a potentiometer.

8.3.1 Strain Gages

The strain gages have a 1000 ohm gage resistance. Bridge completion resistance were selected to reduce power consumption. The gages have a nominal gage factor of two and are self temperature compensated. A three wire system was selected for the strain gages to reduce the effect of voltage drop changes in the gage lead wires.

8.3.2 Pressure Transducers

The pressure transducers are a bonded strain gage type with a zero to 1500 PSI range. The transducers use a four wire system (2 signal wires, 2 excitation wires) with a 5 volt excitation.

8.3.3 Blade Angle Potentiometer

The blade angle sensor is a wirewound potentiometer that is mechanically coupled to a pulley. The pulley in turn is coupled to the blade shank via a monofilament (nylon) line so that as the blade rotates it causes the potentiometer to rotate. Nylon is used because of its low modulus to help take up any relative motion between the blade and spinner bulkhead and avoid errors in the output signal due to this effect.

The potentiometer is 2,000 ohms and excited by 12 VDC so that a high level output is developed at the potentiometer wiper. This signal is transmitted directly from the rotating side to the stationary side via slip rings for recording or display. Calibration is accomplished after installation using a blade angle protractor and voltmeter to obtain a graph of angle versus output voltage. The ratio of blade shank diameter to pulley diameter is approximately 3 so that 97 degrees of blade rotation gives about 300 degrees of potentiometer rotation to optimize dynamic range.

8.4 BRIDGE COMPLETION BOARDS

The bridge completion printed circuit boards are mounted in the cuff of each blade and provide up to ten channels of either half bridge or full bridge completion. Provisions are also included for full scale standardization, bridge balancing and bridge attenuation. The installation of the bridge completion boards is illustrated in Figure 8.3.

8.5 PROGRAMMABLE CONNECTORS

The programmable connectors are standard 55 pin connectors that are mounted on the forward face of the Prop-Fan hub adjacent to each arm bore. The installation of the programmable connector is illustrated in Figure 8.4. The purpose of the connector is to select the strain gage that will be connected to each data channel. Strain gage selection for a specific channel is accomplished by adding jumper wires between pairs of pins on the connector. The following limitations apply when selecting strain gage arrangements.

A. The maximum number of available channels is 32.

B. The bridge completion board limits the maximum number of gages to 10 on each blade.

C. VCO Case A limits the maximum number of gages selected from blades 1-4 to 16. VCO Case B limits the maximum of gages selected from blades 5-8 to 16.

D. Gages on blades 1 and 3 may only be programmed for VCO Case A -channels 1 through 10. Therefore, the total number of gages selected from both of these blades must not exceed 10.

8.5 (Continued)

E. Gages on blades 2 and 4 may only be programmed for VCO Case A -channels 7 through 16. Therefore, the total number of gages selected from both of these blades must not exceed 10.

F. Gages on blades 5 and 7 may only be programmed for VCO Case B -channels 1 through 10. Therefore, the total number of gages selected from both of these blades must not exceed 10.

G. Gages on blades 6 and 8 may only be programmed for VCO Case B -channels 7 through 16. Therefore, the total number of gages selected from both of these blades must not exceed 10.

H. Maximum channel capacity may only be achieved if the following blade pairs have a sum total of selected channels greater than or equal to 6 and less than or equal to 10:

1) 1 and 3
2) 2 and 4
3) 5 and 7
4) 6 and 8

8.6 ROTATING INTERFACE BOARD (RIB)

The rotating interface board is a five layered printed circuit board. Its primary purpose is to minimize rotating system cabling by interconnecting all rotating electronic components. All connections to this board are soldered and a convenient set of power voltage test points are included for troubleshooting purposes.

8.7 VCO CASE

The LAP instrumentation system utilizes two identical VCO cases. Each case contains 16 VCO's and matching preamplifiers, 1 mixing amplifier/line driver, VCO and line driver connectors and input and output connectors.

Each VCO accepts conditioned strain gage or pressure transducer signals from the RIB board and generates an FM signal with a unique sub-carrier frequency. The matched preamplifier for each VCO has a gain of 250 to accommodate the condition signals. All 16 VCO outputs in each case are then fed to the mixer amplifier/line driver where they are mixed into a single 16 channel frequency multiplexed signal. The VCO sub-carrier frequencies are all IRIG A constant bandwidth channels with a ± 2 KHz deviation as shown in Table 8-1.

TABLE 8-1

VCO SUB-CARRIER FREQUENCIES

IRIG CHANNEL NUMBER	CENTER FREQUENCY (KHz)
DEVIATION ±2 KHz	
1A	16
2A	24
3A	32
4A	40
5A	48
6A	56
7A	64
8A	72
9A	80
10A	88
11A	96
12A	104
13A	112
14A	120
15A	128
16A	136

8.8 ROTATING POWER SUPPLY

The rotating power supply accepts DC power from the primary power supply in the stationary field and conditions it to supply the following voltages.

1) floating 10 VDC excitation for the strain gages

2) ground referenced +25.5 VDC for the rotating electronic

3) ground referenced 12.0 VDC for blade angle excitation

The power supply is designed so that none of the output voltages will vary by more than .2% over the entire temperature operating range.

8.9 SLIP RING AND BRUSH BLOCK

The slip ring and brush block provide the interface between the rotating and stationary portions of the instrumentation system. The slip ring assembly consists of eight concentric rings ranging in diameter from 34.7 cm (13.65 in.) to 46.9 cm (18.45 in.). The rings are fabricated from plate bronze and are hard silver plated. The slip ring assembly mounts on the Prop-Fan aft spinner bulkhead.

The brush block assembly mounts on the Prop-Fan control and provides for easy replacement of brushes. The brush block is designed with two brushes riding on each of the inner four rings and four brushes riding on each of the outer four rings. More brushes are employed where the relative velocity between the rings and brushes is higher. The material for the brushes is silver graphite. The 1 per rev sensor also mounts on the brush block and is triggered by a target attached to the rotating power supply.

8.10 DETRANSLATOR/DISCRIMINATOR SYSTEM

The Detranslator/Discriminator System is contained in two modular racks, each containing a 16 channel subsystem. Each rack contains a 50 KHz reference oscillator for tape speed compensation, a group frequency detranslator, a reference discriminator and four data discriminators. The detranslators decompose the 16 channel multiplexed signal to four groups of four channels (IRIG STANDARD 1A thru 4A). These groups of four channels are recorded on a tape recorder. Each of the data discriminators is tuned to one of the IRIG Standard center frequencies. The discriminators separate the groups of 4 multiplexed channels into individual signals and demodulates them for display on a 4 channel oscilloscope.

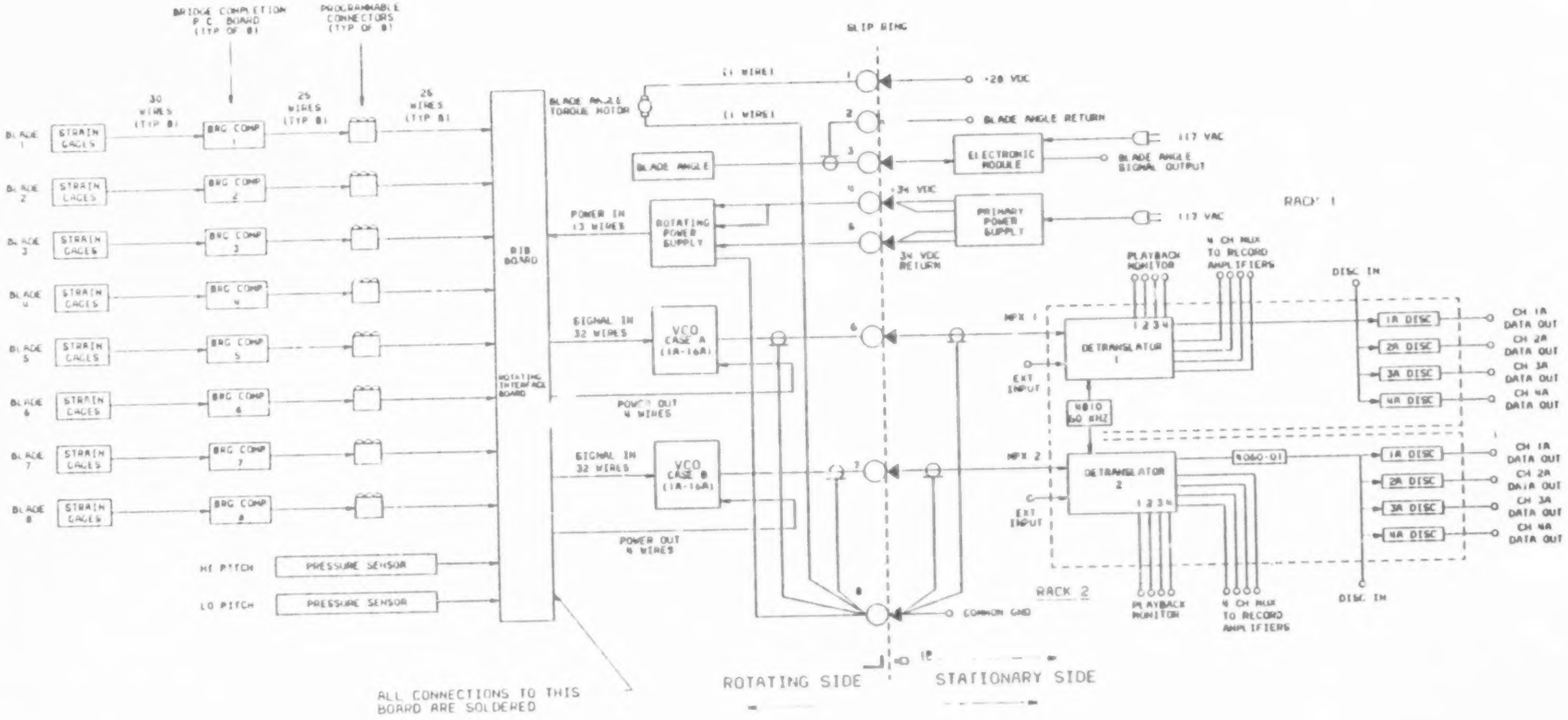
BRIDGE COMPLETION
P C BOARD
(TYP OF 8)
PROGRAMMABLE
CONNECTORS
(TYP OF 8)
30
WIRES
(TYP 8)
25
WIRES
(TYP 8)
26
WIRES
(TYP 8)
BLADE 1
BLADE 2
BLADE 3
BLADE 4
BLADE 5
BLADE 6
BLADE 7
BLADE 8
STRAIN GAGES
BRG COMP 1
BRG COMP 2
BRG COMP 3
BRG COMP 4
BRG COMP 5
BRG COMP 6
BRG COMP 7
BRG COMP 8
HI PITCH
LO PITCH
PRESSURE SENSOR
PRESSURE SENSOR
RIB BOARD
ROTATING INTERFACE BOARD
ALL CONNECTIONS TO THIS
BOARD ARE SOLDERED
BLADE ANGLE
TORQUE MOTOR
BLADE ANGLE
POWER IN
13 WIRES
ROTATING
POWER
SUPPLY
SIGNAL IN
32 WIRES
VCO
CASE A
(1A-16A)
POWER OUT
4 WIRES
SIGNAL IN
32 WIRES
VCO
CASE B
(1A-16A)
POWER OUT
4 WIRES
(1 WIRE)
(1 WIRE)
SLIP RING
1
2
3
4
5
6
7
8
+28 VDC
BLADE ANGLE RETURN
ELECTRONIC
MODULE
117 VAC
BLADE ANGLE
SIGNAL OUTPUT
+34 VDC
34 VDC
RETURN
PRIMARY
POWER
SUPPLY
117 VAC
RACK 1
PLAYBACK
MONITOR
4 CH MUX
TO RECORD
AMPLIFIERS
DISC IN
MPX 1
DETRANSLATOR
1
1 2 3 4
EXT
INPUT
4810
60 KHZ
1A DISC
2A DISC
3A DISC
4A DISC
CH 1A
DATA OUT
CH 2A
DATA OUT
CH 3A
DATA OUT
CH 4A
DATA OUT
MPX 2
DETRANSLATOR
2
1 2 3 4
EXT
INPUT
4060-01
1A DISC
2A DISC
3A DISC
4A DISC
CH 1A
DATA OUT
CH 2A
DATA OUT
CH 3A
DATA OUT
CH 4A
DATA OUT
DISC IN
RACK 2
PLAYBACK
MONITOR
4 CH MUX
TO RECORD
AMPLIFIERS
COMMON GND
ROTATING SIDE
STATIONARY SIDE

FIGURE 8.1 LAP INSTRUMENTATION SCHEMATIC

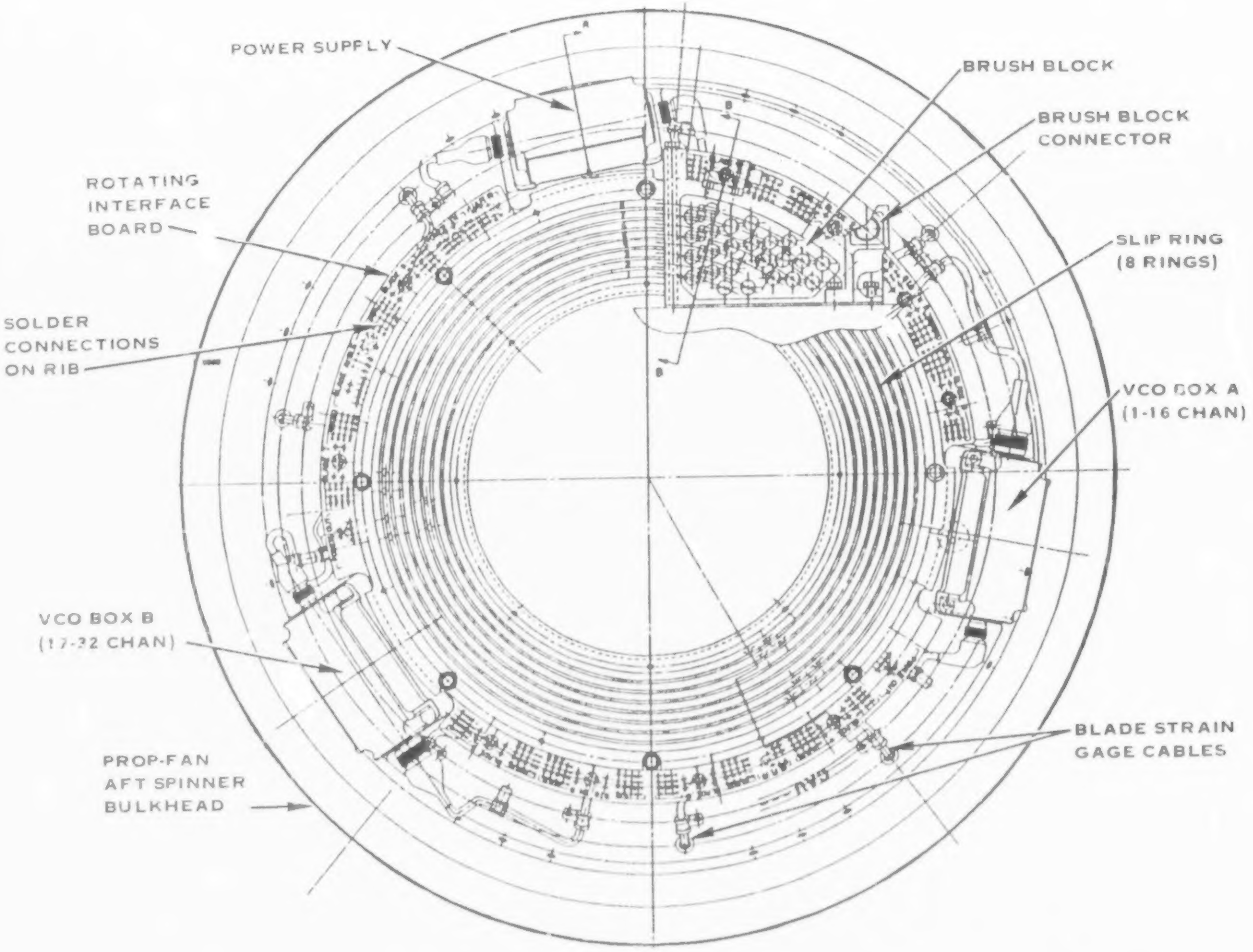
POWER SUPPLY
BRUSH BLOCK
BRUSH BLOCK CONNECTOR
ROTATING INTERFACE BOARD
SLIP RING (8 RINGS)
SOLDER CONNECTIONS ON RIB
VCO BOX A (1-16 CHAN)
VCO BOX B (17-32 CHAN)
BLADE STRAIN GAGE CABLES
PROP-FAN AFT SPINNER BULKHEAD

FIGURE 8.2 LAP INSTRUMENTATION HARDWARE ASSEMBLY

ORIGINAL PAGE IS
OF POOR QUALITY

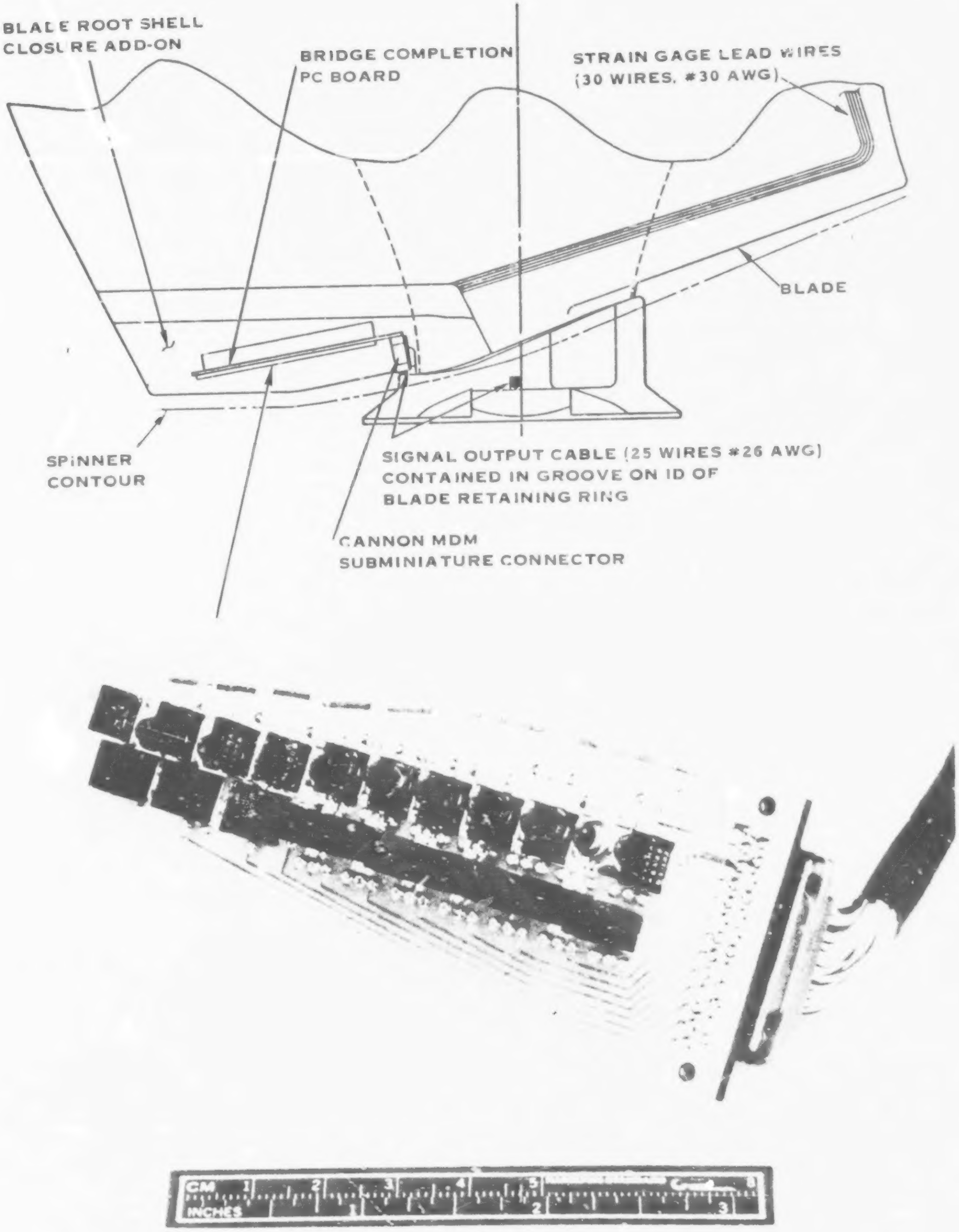
BLADE ROOT SHELL
CLOSURE ADD-ON
BRIDGE COMPLETION
PC BOARD
STRAIN GAGE LEAD WIRES
(30 WIRES, #30 AWG)
BLADE
SPINNER
CONTOUR
SIGNAL OUTPUT CABLE (25 WIRES #26 AWG)
CONTAINED IN GROOVE ON ID OF
BLADE RETAINING RING
CANNON MDM
SUBMINIATURE CONNECTOR
CM 1 2 3 4 5 6
INCHES 1 2 3

FIGURE 8.3 BRIDGE COMPLETION BOARD INSTALLATION

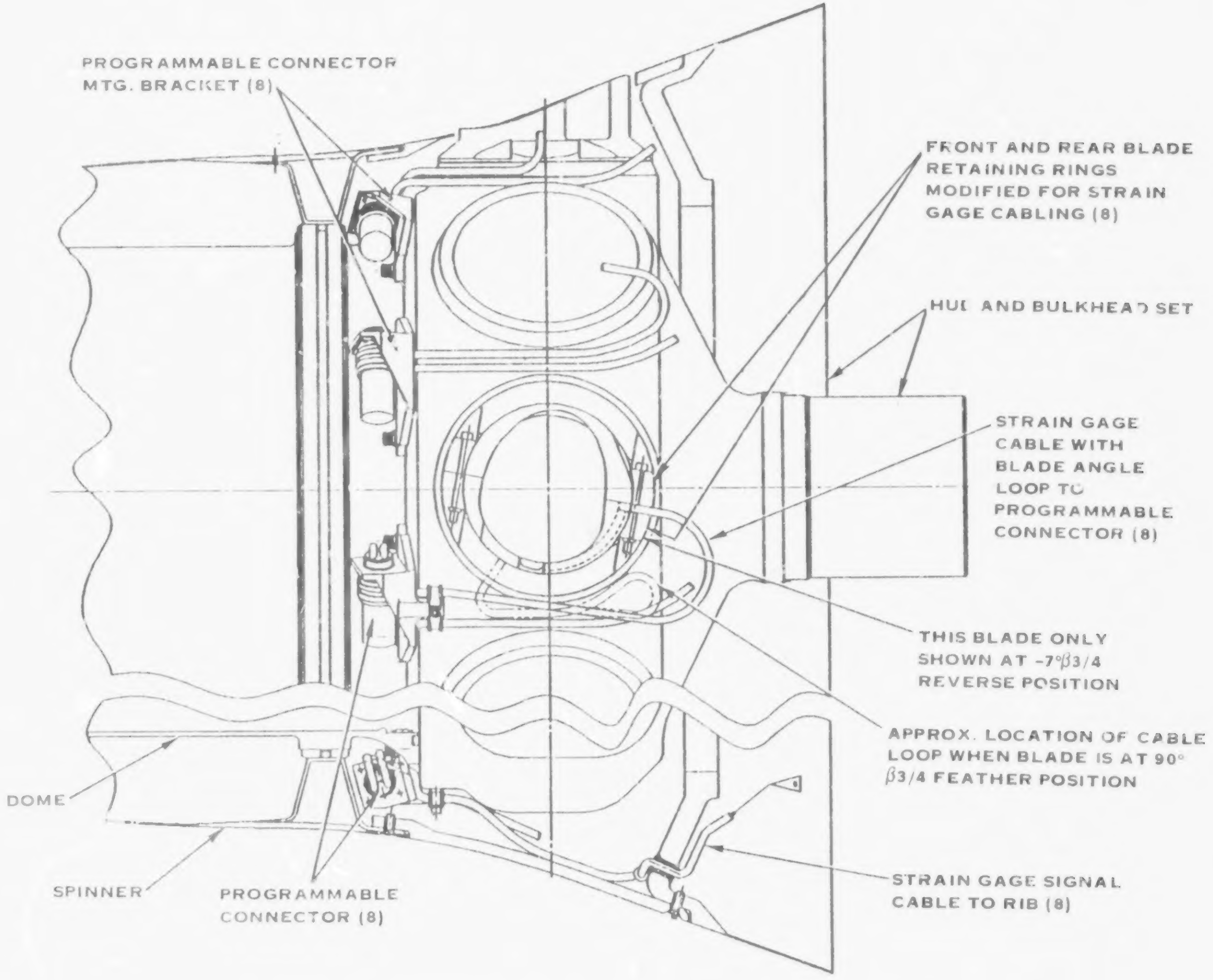
PROGRAMMABLE CONNECTOR MTG. BRACKET (8)
FRONT AND REAR BLADE RETAINING RINGS MODIFIED FOR STRAIN GAGE CABLING (8)
HUB AND BULKHEAD SET
STRAIN GAGE CABLE WITH BLADE ANGLE LOOP TO PROGRAMMABLE CONNECTOR (8)
THIS BLADE ONLY SHOWN AT -7°β3/4 REVERSE POSITION
APPROX. LOCATION OF CABLE LOOP WHEN BLADE IS AT 90° β3/4 FEATHER POSITION
DOME
SPINNER
PROGRAMMABLE CONNECTOR (8)
STRAIN GAGE SIGNAL CABLE TO RIB (8)

FIGURE 8.4 PROGRAMMABLE CONNECTOR INSTALLATION

9.0 SR-7A AEROELASTIC MODEL DESIGN

The SR-7A is a .62 meter (2 foot) diameter scale model of the SR-7L Large Scale Advanced Prop-Fan. Its intended use was as a research tool to gain preliminary information about the aeroelastic behavior of the SR-7L Prop-Fan. In order to accomplish this goal, structural and aerodynamic scaling principles were applied in the design of the SR-7A so that its structural dynamic and aerodynamic characteristics would be similar to the SR-7L. The SR-7A model design also included a pitch change mechanism that would allow the blade pitch angle to be precisely adjusted and set. The pitch change mechanism was only required to provide the capability for changing blade angle while the model was not rotating. The SR-7A was originally intended for wind tunnel testing and testing mounted on a Lockheed Jetstar aircraft. The detail design of the model is described in reference 10.

9.1 DESIGN GOALS AND REQUIREMENTS

The design goals and requirements for the SR-7A Prop-Fan aeroelastic model were as follows:

- The SR-7A spinner and blade contours were to be direct scales of the SR-7L contours. The scale factor is the ratio of the blade tip diameter of the SR-7A and SR-7L, (62.23/274.32 = .22685).
- SR-7A blade natural frequencies and mode shapes must match those of the SR-7L as closely as possible.
- The SR-7A must be structurally adequate for operation at blade tip speeds of 290 meters/second.
- The SR-7A must exhibit aeroelastic stability at wind tunnel operating condition up to Mach .8

9.2 BLADE AND RETENTION DESIGN

The scaling of the aeroelastic model design was based on the consideration of such parameters as the Reynolds Number, Lock Number, Cauchy Number, Reduced Frequency and Froude Number. The main results obtained from analyses using these parameters were, that if the SR-7A blade geometry was directly scaled from the SR-7L, the ratio of air density to the structural density of the blade (ρ/σ) would have to remain the same and the ratios of the edgewise and torsional stiffnesses to the flatwise stiffness would also have to be the same as the SR-7L.

The retention stiffnesses were scaled directly proportional to the blade loads. The blade bending moments are a function of the tip diameter to the third power. Therefore the ratio of the SR-A to SR-7L bending stiffness was calculated as follows:

$$(62.23/274.32)^3 = .01167$$

9.2 (Continued)

Similarly the thrust, tangential and radial stiffnesses are scaled from the SR-7L by the ratio of the tip diameters squared as follows:

$$(62.23/274.32)^2 = .05146$$

It was determined that a scale model of the SR-7L blade, using the same materials and construction composition as the SR-7L would meet the scaling criteria discussed above. However this was not considered a practical approach from a manufacturing standpoint. An alternate design was used which had an external geometry that was a direct scale of the SR-7L blade but had a different construction that could be readily fabricated.

The aeroelastic model blade is composed of three structural layers: a central spar-and-filler layer enveloped by two graphite-reinforced fiberglass shell outer layers (face and camber). Four plies of fiberglass cloth, each .140 mm (0.0055 inch) thick with fiber orientations of -25 degrees and +65 degrees to the blade axis, cover most of the blade. The shells are locally reinforced over the spar with three layers of graphite, each .178 mm (.007 inch) thick, sandwiched between fiberglass plies, with alternating ply orientations at 0 degree and 30 degrees to the blade axis. The construction of the SR-7A blade is illustrated in Figure 9.1.

The titanium spar is somewhat narrower and thinner than a scaled down SR-7L aluminum spar. Also, because of space limitations inside the shell cavity, the spar is truncated inboard of the tip, at the 25.07 cm (9.87 inch) station. Two graphite reinforcing plies extend beyond the tip of the spar to provide stiffness continuity, simulating that of the SR-7L full-length spar. Outboard of the 22.86 cm (9 inch) station, center layer cavities contain solid fiberglass fill. The solid fiberglass fill helps compensate for the lack of spar mass at the tip. Low density foam, .128 gms/cm^3 (8 lbs per cu. ft.), fills the cavities fore and aft of the spar inboard of the 22.86 cm (9 inch) station.

Due to space limitations within the hub, and the fact that critical bearing tolerances do not scale directly, a ball bearing retention such as used on the SR-7L could not be used on the SR-7A model. Since the bending spring rate of the ball bearing is much lower than the other retention spring rates, it has the greatest effect on the blade natural frequencies and mode shapes. Therefore, ways of simulating the bearing bending spring rate on the model were investigated. The approach selected was to rigidly clamp the model blade at the root and use a long, slendor shank to simulate bending of the retention bearing. No attempt was made to match thrust and shear spring rates. The 1.727 cm (.68 in) shank diameter is considerably smaller than a scaled aluminum SR-7L shank would be. However since the shank is titanium it provides the desired retention stiffness.

C-2

9.2.1 Blade Finite Element Analysis

The SR-7A blade finite element model was constructed in a similar manner to the SR-7L blade model as discussed in Section 3.3. Since the retention stiffness of the SR-7L was simulated by the stiffness of the SR-7A blade shank, there was no need to model the retention stiffness as a collection of spring elements. Rather the model nodal points at the inboard end of the blade shank were restrained in all six degrees of freedom. The centrifugal and air loads were also applied to the finite element model of the SR-7A in the same manner as the SR-7L.

9.2.2 Steady State Analysis and Results

The steady state deflections and stresses of the SR-7A blade were calculated using the finite element model for the operating conditions listed in Table 9-1. The deflections provide an indication of how well the stiffness and mass distribution of the SR-7L and SR-7A blade are matched. The stresses are used to evaluate the structural integrity of the blade.

TABLE 9-1

SR-7A DESIGN CONDITIONS

CONDITION	PROP SPEED, RPM	β, DEG	CENTRIFUGAL FORCE, FZ NEWTONS (LBS)
10,668 M Cruise (35,000 Ft)	7484	57.57	17,392 (3,910)
Wind Tunnel - Cond. 1	8622	57.57	23,179 (5,211)
Wind Tunnel - Cond. 2	8886	57.57	26,620 (5,535)
Takeoff Climb	7484	38.36	17,392 (3,910)
Vacuum Condition	8886	37.57	24,402 (5,485)

9.2.2 (Continued)

Theoretically the deflection of the SR-7A blade should be equal to the deflections of the SR-7L blade multiplied by the model scale factor (62.23/274.32 = .22685). A comparison of the calculated maximum deflections of the SR-7L and the scaled calculated deflection of the SR-7A are shown in Figure 9.2. Good agreement was obtained.

Since several iterations were required to arrive at the final blade design, it was not practical to perform a complete stress analysis for each iteration. Design of the blade was concerned with achieving the desired aeroelastic behavior. Once this was achieved the stress analysis was performed. Figure 9.3 shows the maximum calculated steady stresses in the blade spar and shell plotted on a Goodman Diagram. The resulting allowable cyclic stresses are indicated.

9.2.3 Blade Resonant Frequencies and Mode Shapes

The SR-7A blade natural frequencies and mode shapes were calculated using the NASTRAN eigenvalve solver, which was also used for the SR-7L. The calculated SR-7A and SR-7L natural frequencies are compared on a modified Campbell Diagram in Figure 9.4. The Diagram was modified to account for the difference in RPM between the SR-7A and SR-7L. This was accomplished by plotting frequency times tip radius versus propeller RPM times tip radius. In general the model natural frequencies were higher than the SR-7L natural frequencies. However all of the first five SR-7A natural frequencies were within 10% of the SR-L frequencies, which was considered acceptable. The comparison of the first five SR-7A mode shapes with the first five SR-7L mode shapes also showed acceptable similarity.

9.2.4 Blade Stability

The unstalled stability of the SR-7A blade was analyzed for the design cruise case using the same computerized analysis applied to the SR-7L and described in Section 3.8.1. The SR-7A was predicted to go unstable in mode 3 at a .95 Mach number, the same as was predicted for the SR-7L (reference Table 3-7). This meets the design requirements for the SR-7A and illustrates the aeroelastic similarity between the SR-7A and SR-7L.

9.3 SR-7A HUB AND SPINNER DESIGN

A schematic drawing of the hub/spinner retention design is shown in Figure 9.5. From Figure 9.5 it can be seen that the hub/spinner assembly consists of three structural members. These components are the spinner, forward hub half, and rear hub half. The spinner which is the forward most part is made of aluminum. The primary function of the spinner is to establish a smooth flow path for the air stream prior to impingement on the blades.

The spinner is fastened to the forward half of the hub by a left-handed screw thread. A left-handed thread is used because the inertial moment acting on the spinner tends to generate a tightening torque when the hub is accelerated. To guard against potential loosening of the spinner during deceleration, three nylon inserts are installed 120 degrees apart in the spinner threads.

The remaining aerodynamic contour in the vicinity of the blades is formed by the external surfaces of the front and rear halves of the hub. The split hub concept facilitates installation and removal of the blades in the hub cavities. Both hub halves are made of steel.

The front and rear halves of the hub assembly are aligned by three pins. The pins are located such that there is only one position at which the two hub halves can be assembled. The pins are sized to be non-load carrying members.

To hold the front and rear hub halves together, eight alignment bolts were used. The bolts are serialized to assure that they are always assembled in the same hole. Dynamic balance of the spinner/hub assembly is accomplished by removal of material (by drilling) on the back face of the rear hub half.

9.3.1 Hub Stress Analysis

The spinner hub assembly was analyzed for the vacuum spin design condition at 8886 RPM. The combination of blade centrifugal force and steady bending moment for this condition result in the highest radial force acting on the hub. The blade contacts the hub circumferentially along a fillet radius at the inboard end of the shank. A matching convex radius in the hub is adjusted such that contact occurs at a nominal static angle of 45°.

The contact stresses between the hub and the blade shank were calculated to be 31,567 newtons/cm^2 (45,800 psi) using a computerized analysis method. This stress level was only 25% of the allowable for low cycle fatigue life of the titanium blade shank. A higher margin is achieved for the steel hub. The hub lip region (ref. Figure 9.5) was also analyzed using a shell of revolution finite element program. Hoop and radial stresses were in the order of 5000 N/cm^2 (7250 psi) and thus a large low cycle fatigue margin was also obtained for this analysis.

9.4 PITCH CHANGE MECHANISM DESIGN

The pitch change mechanism for the aeroelastic model is also illustrated in Figure 9.7. The system is designed for static pitch adjustment only, i.e., when the model is non-rotating. Two identical locking pins are used to prevent rotation of the face gear relative to the forward hub. All blades are indexed to the common face gear by individual blade segments gears, attached to the butt end of each blade with dowel pins.

Multiple holes are provided in the forward hub half and in the face gear to accept the two locking pins. The holes are varied to provide a vernier pitch adjustment which permits fixed incremental changes in blade angle setting. The holes in both components are arranged in pairs, exactly 180 degrees apart, to permit the use of two identical locking pins. This provides structural redundancy while preserving the overall mass balance of the model at any angular setting.

Blade pitch angle adjustments are accomplished by unscrewing the spinner and extracting both pitch locking pins. With the pins removed, the face gear becomes free to rotate and the pitch of all blades can be changed simultaneously. The vernier adjustment scheme used in the blade pitch change design consists of 24 holes in the face gear and 26 holes in the forward half hub. Based on the vernier combination and the blade gear to face gear ratio, the normal blade angle settings are integer multiples of 2.885 degrees. Finer blade angle adjustments can be obtained by re-indexing the alignment of the face gear to the blade segment gears. The smallest increment possible using this method is .577 degrees.

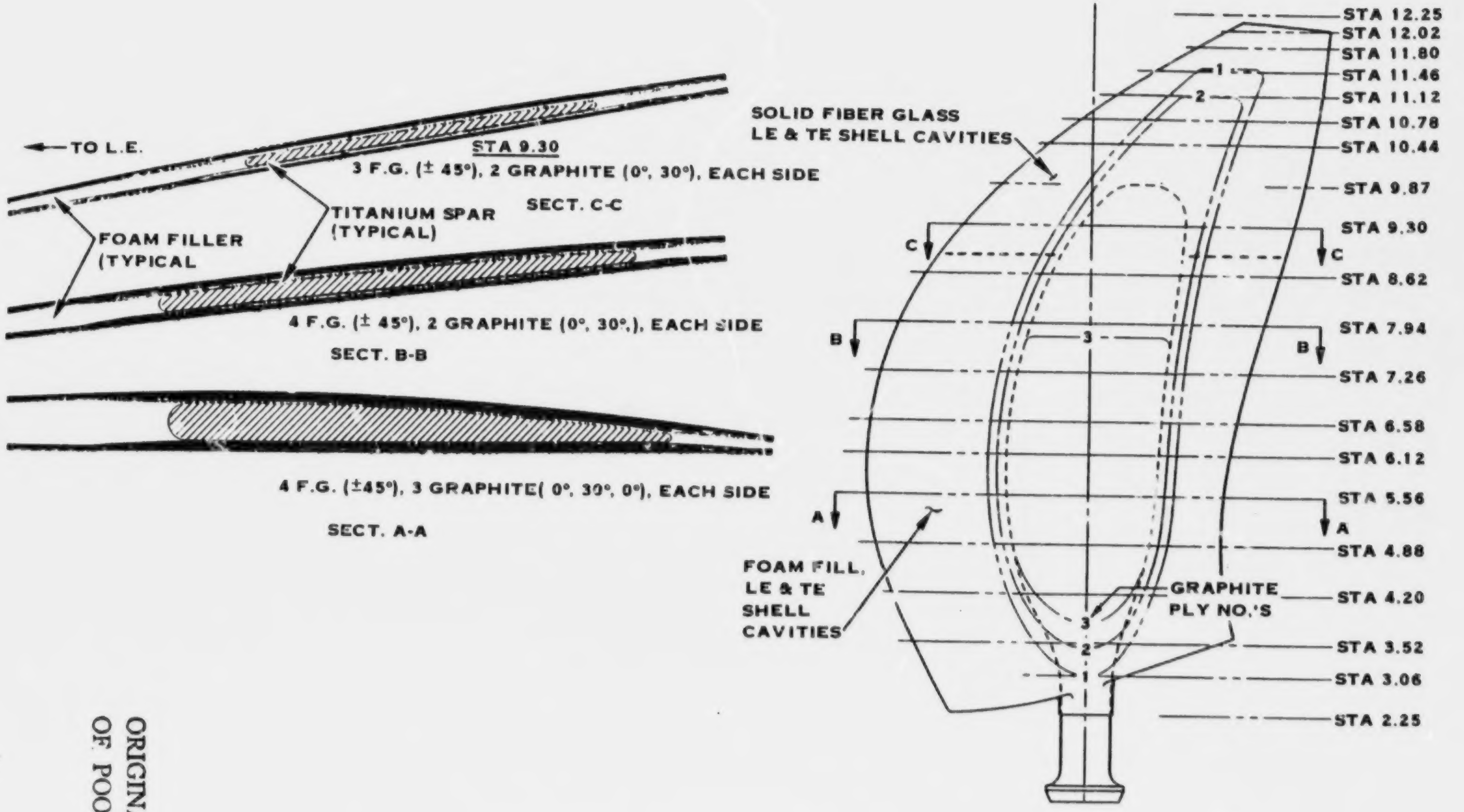
TO L.E.
STA 9.30
3 F.G. (± 45°), 2 GRAPHITE (0°, 30°), EACH SIDE
SECT. C-C
TITANIUM SPAR
(TYPICAL)
FOAM FILLER
(TYPICAL
4 F.G. (± 45°), 2 GRAPHITE (0°, 30°,), EACH SIDE
SECT. B-B
4 F.G. (±45°), 3 GRAPHITE(0°, 30°, 0°), EACH SIDE
SECT. A-A
SOLID FIBER GLASS
LE & TE SHELL CAVITIES
FOAM FILL,
LE & TE
SHELL
CAVITIES
GRAPHITE
PLY NO.'S
1
2
3
C
C
B
B
A
A
STA 12.25
STA 12.02
STA 11.80
STA 11.46
STA 11.12
STA 10.78
STA 10.44
STA 9.87
STA 9.30
STA 8.62
STA 7.94
STA 7.26
STA 6.58
STA 6.12
STA 5.56
STA 4.88
STA 4.20
STA 3.52
STA 3.06
STA 2.25

FIGURE 9.1 SR-7A BLADE CONSTRUCTION

ORIGINAL PAGE IS
OF POOR QUALITY

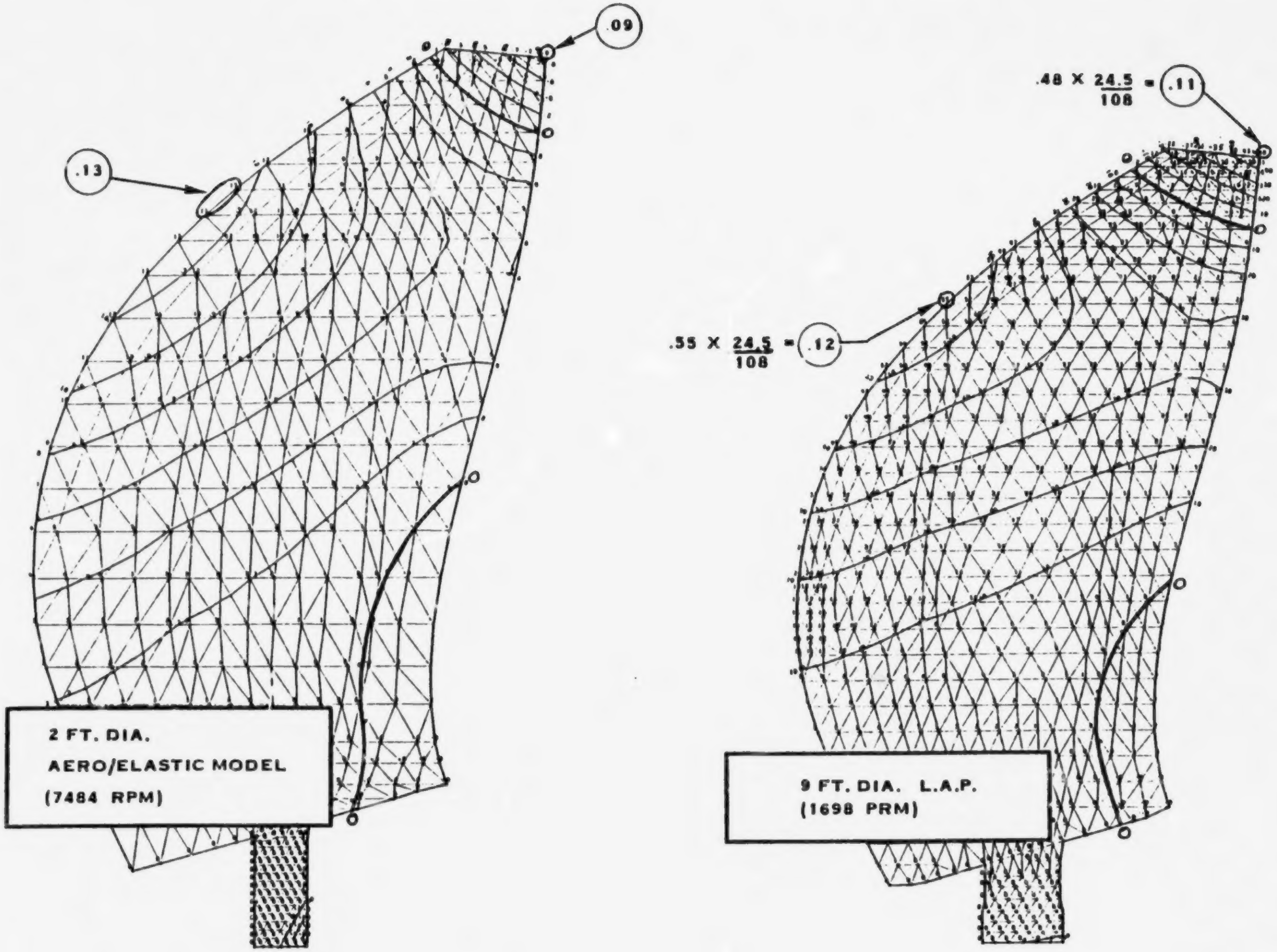

FIGURE 9.2 DEFLECTION CONTOUR PLOTS 35000 FT ALTITUDE CRUISE CONDITION

ORIGINAL PAGE IS
OF POOR QUALITY

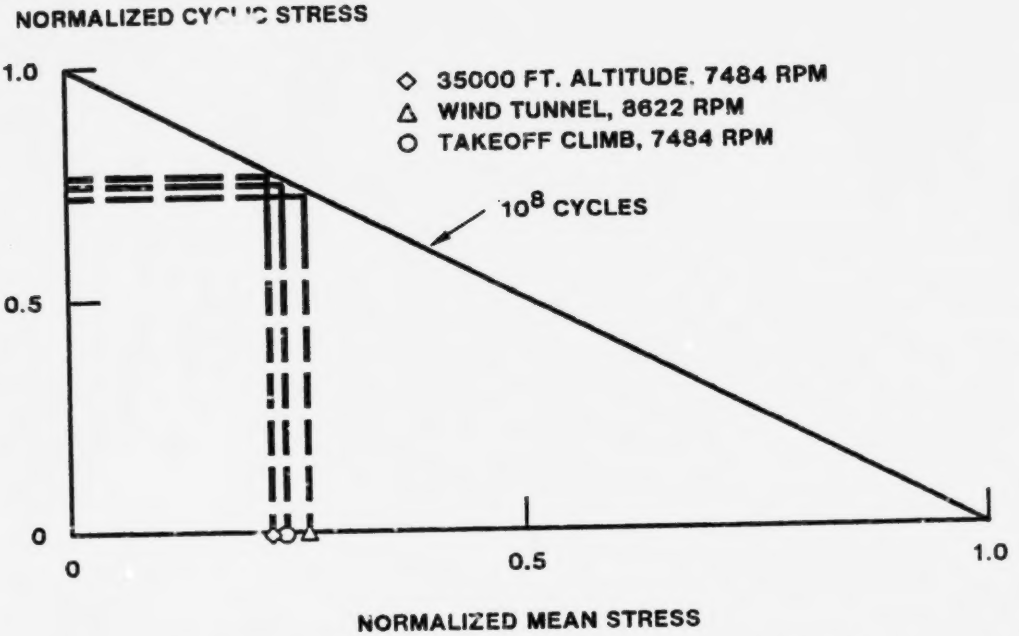

GOODMAN DIAGRAM SPAR TENSILE STRESS - SHANK AREA
TITANIUM (6A1-4V) GLASS BEAD PEENED

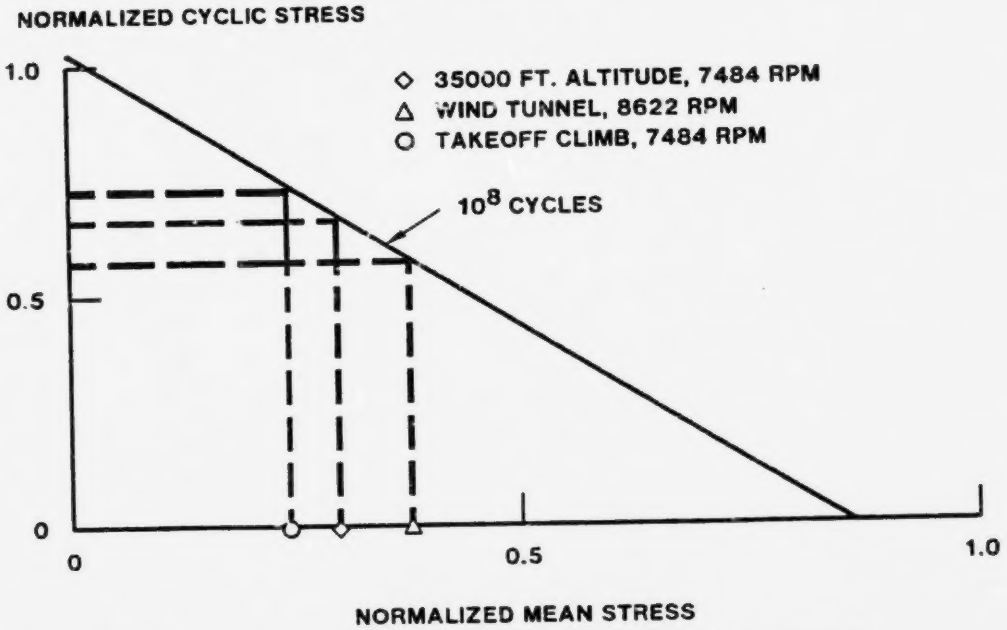

GOODMAN DIAGRAM SHELL TENSILE STRESS GRAPHITE 0°, 30°

FIGURE 9.3 SR-7A BLADE STRESS ANALYSIS RESULTS

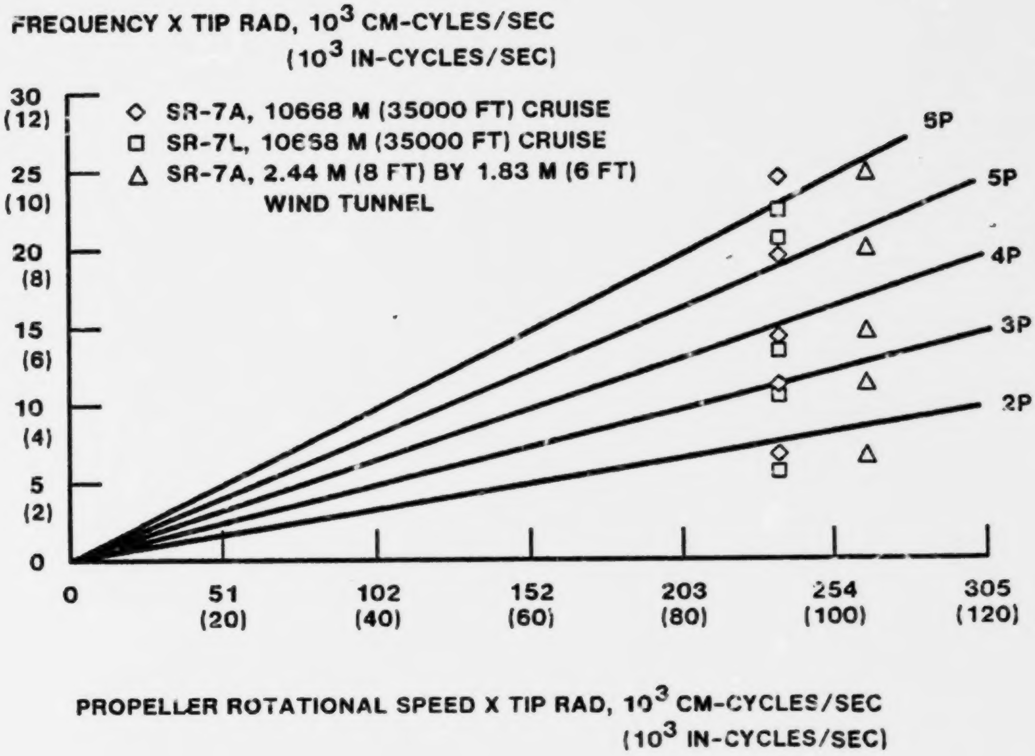

FIGURE 9.4 COMPARISON OF SR-7A AND SR-7L BLADE NATURAL FREQUENCIES

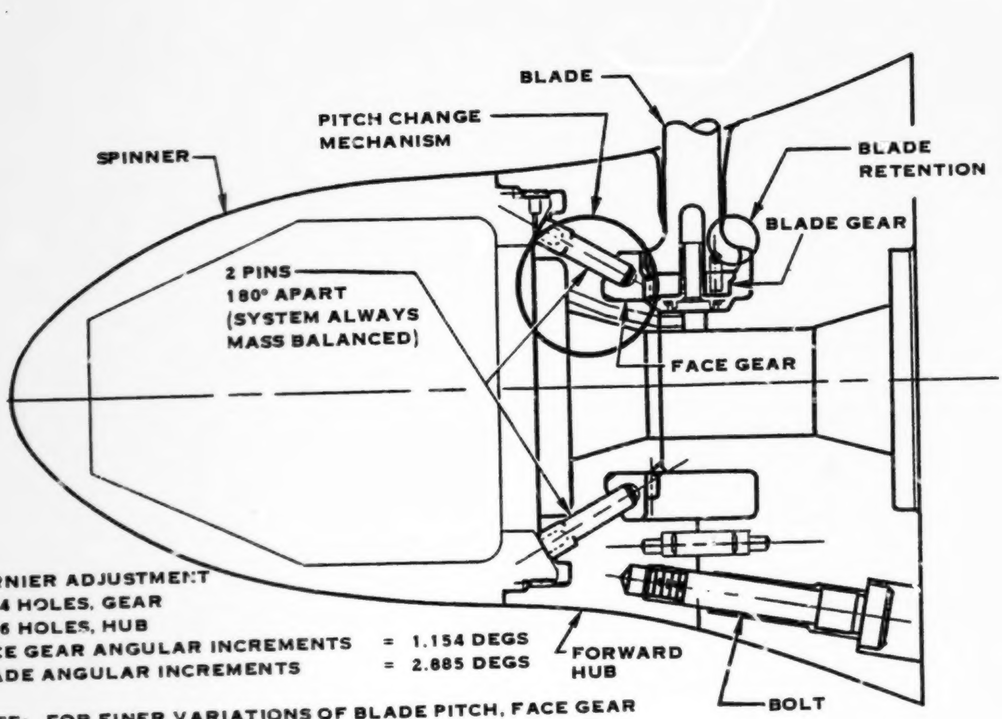
BLADE
PITCH CHANGE MECHANISM
SPINNER
BLADE RETENTION
BLADE GEAR
2 PINS 180° APART (SYSTEM ALWAYS MASS BALANCED)
FACE GEAR
FORWARD HUB
BOLT

VERNIER ADJUSTMENT
24 HOLES, GEAR
26 HOLES, HUB
FACE GEAR ANGULAR INCREMENTS = 1.154 DEGS
BLADE ANGULAR INCREMENTS = 2.885 DEGS

NOTE: FOR FINER VARIATIONS OF BLADE PITCH, FACE GEAR MAY BE RE-INDEXED TO BLADE GEAR (AFTER HUB DIS-ASSEMBLY) TO PROVIDE AS LOW AS 0.577 DEGREE BLADE INCREMENTS.

FIGURE 9.5 SR-7 BLADE RETENTION, HUB AND PITCH CHANGE MECHANISM

10.0 MANUFACTURING AND QUALITY ASSURANCE

10.1 MANUFACTURING

10.1.1 SR-7L Blade Fabrication

The SR-7L blade was manufactured using a vacuum injection fabrication method. The injection molding process inherently results in repeatable blades since the airfoil is produced by matched dies fabricated from a close tolerance master blade. The injection molding process is also used to fabricate Hamilton Standards 24PF, 14RF and 14SF propeller blades.

Manufacture of the blade began with fabrication of the spar. The spar is an aluminum forging, which was finish machined to obtain the proper airfoil contour and shank configuration. The low blade thickness to chord ratio, swept leading edge and the large amount of the blade twist increased the complexity of the spar fabrication process. In the injection molding process urethane foam was formed around the spar in matched dies. Fiberglass cloth was laid up over the spar/foam assembly, a formed sheath was positioned over the outboard leading edge, and an integral deicing heater was assembled to the inboard leading edge. Both the spar and sheath were previously coated with adhesive in areas which form a bond joint at assembly. This assembly was placed in a two-piece female die and epoxy resin was injected into the fiberglass and cured at an elevated temperature. A blade is shown being removed from the dies in Figure 10.1.

The high temperature cure not only cures the epoxy resin but provides it with elevated temperature resistance needed during operation. All of the high temperature cures during the blade manufacture were accomplished with the blade restrained in matched dies to preclude any airfoil distortion. Following the final resin cure in the injection molding die, the blade was not exposed to temperatures greater than those experienced in operation. Inspection of the airfoil was accomplished using airfoil templates to confirm conformance to the aerodynamic shape. The complete blade aerodynamic shape; contour, angle, leading edge alignment, face alignment, thickness and width were inspected at each design station. The blade was then painted with erosion coating.

10.1.2 SR-7L Hub Fabrication

The LAP hub was fabricated using conventional techniques which are used in the manufacture of Hamilton Standard's 54460 and 54H60 propeller hubs. The hub was fabricated from a steel forging which was heat treated to obtain the desired mechanical properties. A wood pattern of the hub was fabricated and the external contour of the hub was hydrotelled using the wood pattern as the master. The eight holes for the blades were bored and the races were rough machined. The races were hardened using a carburization process and then finish ground. A development program was conducted to determine the optimum parameters for the carburization process.

PRECEDING PAGE BLANK NOT FILMED

PAGE 98 INTENTIONALLY BLANK

10.1.3 SR-7L Spinner Fabrication

The shell of the LAP spinner was fabricated using an injection molding technique and hard tooling. Fiberglass cloth was layed up on a male mandrel, the female mandrel was placed on top and resin was injected into the tooling. The front and mid spinner bulkheads (reference Figure 5.1) were fabricated by laying up fiberglass cloth over rigid foam forms and then bonding these assemblies to the ID of the spinner shell. The rear spinner bulkhead was also fabricated by injection molding using hard tooling. The interconnecting platforms between the front and rear spinners were injection molded using soft tooling. Hard tooling was required for the spinner shell and aft bulkhead because of the complexity of their shapes.

10.1.4 SR-7L Pitch Control and Actuator

The pitch control and actuator were fabricated using conventional techniques which are commonly used in aerospace manufacturing. Many of the components were acquired from vendors who produce similar production hardware for Hamilton Standard. Some of the control components are common with the 54460 military control or were fabricated by modifying 54460 control components.

10.1.5 SR-7L Prop-Fan Assembly Procedures and Tools

Assembly procedures were written and assembly tools fabricated or procured for both the pitch control assembly and Prop-Fan assembly. The assembly procedures defined the correct sequence, methodology and tools to be used for assembling the Prop-Fan and control. Functional test procedures were also defined for the Prop-Fan and control as well as their sub-assemblies. Because a non-modular design was adapted for the Prop-Fan, in order to allow use of certain existing hardware, extensive assembly tooling was required for the actuator. Most of the assembly tools for the control were standard 54460 tools. A few unique control assembly tools were also fabricated.

10.1.6 SR-7A Aeroelastic Model Blade Fabrication

Fabrication of the SR-7A blade began with the manufacture and preparation of the titanium blade spar. The spars were machined using a 6X tracing master, constructed from stacked airfoil templates, to guide the grinding operation. The spar contours were inspected using 10X comparator charts. The bonding surface of the spar was prepared by passivation and application of an epoxy based adhesive. After cure the adhesive coated surfaces were abraded by sand blasting to enhance bonding.

The next step in the fabrication process was construction of the spar/foam sub-assembly. This was accomplished using a foaming mold. The foaming mold defined the leading and trailing edge foam cavities, held the spar in the correct spatial orientation with respect to the leading and trailing edge foam pieces and provided holes for injection and venting of the foam. The foaming mold is depicted in Figure 10.2. The airfoil surfaces of the foam mold were coated with epoxy based adhesive, which was partially cured.

10.1.6 (Continued)

The mold was then bolted together with the spar properly aligned in the mold cavity. Foam was injected into the leading and trailing edge cavities under vacuum and the assembly was cured in an oven. The assembly was extracted from the mold and the flashing was removed by a hand operation. The spar/foam sub-assembly is shown in Figure 10.3.

The shell was constructed using the resin injection mold shown in Figure 10.4. A layup of dry glass cloth and unidirectional graphite fibers were cut and stitched for both the face and camber sides of the blade. The face and camber shell pads were then located on the spar/foam assembly and sewn in place. This assembly was placed in the resin injection mold. Epoxy resin was injected into the mold and the resin was cured in an oven. The blade assembly was removed from the mold, trimmed and painted with erosion coating. Non destructive testing of the blades included X-ray and tap testing to detect the pressure of any foam voids and delaminations. The first blade manufactured was destructively examined to prove out the manufacturing process.

10.2 QUALITY ASSURANCE

The quality system employed during the fabrication of the Large Scale Advanced Prop-Fan was in compliance with MIL-Q-9858A, MIL-STD-45662 and MIL-STD-1535A. The quality program assured that proper materials, processes, tolerances and manufacturing methods were used throughout all phases of the manufacturing cycle. Fabrication and procurement of all the LAP hardware, except the test instrumentation was conducted under this system. The major areas of concern for the quality system were configuration and change control, procurement source control, material and process control and control and disposition of nonconforming hardware.

10.2.1 Configuration and Change Control

Once drawings or specifications were released for manufacture or procurement, no alterations were allowed to the documents without the issuance of a formal engineering change, processed through the Hamilton Standard change control board. The change board, composed of quality engineering, manufacturing engineering and liason engineering personnel, reviewed the change from the viewpoint of manufacturability and compliance with contractual and technical requirements and also obtained customer approval for the change either from NASA or NASA's delegated representative. Once engineering changes were approved and incorporated in the applicable documents, production control initiated disposition of the parts per the requirements of the change. Final inspection verified that all components incorporated into each Prop-Fan unit were in accordance with latest engineering change.

10.2.2 Procurement Source Control

Procurement source control was accomplished by one or more of the following means:

- Inspection of characteristics by a supplier, who has demonstrated the capability to maintain required quality levels (accredited vendor).
- Inspection of characteristics at the suppliers facility by a Hamilton Standard field inspector (source inspection).
- Inspection of characteristics upon receipt of material at Hamilton Standard (receiving inspection).

Vendor accreditation is granted based on Hamilton Standard's evaluation of the vendor's quality system and compliance with quality procedures, as well as the vendor performance evaluation. Accreditation is only granted to vendors whose quality system is deemed at least equivalent to Hamilton Standard's. Auditing of accredited vendors is maintained on a continuing basis to determine whether the vendor is still eligible for accreditation.

Procurement of LAP hardware was conducted under the guidelines of Hamilton Standard specification HS1000, "General Quality Control Requirements for Suppliers".

10.2.3 Material and Process Control

Material and process control assured compliance to quality requirements of new materials and processes such as machining, heat treatment, plating, bonding and assembly. This was accomplished by lab testing of material properties, dimensional inspection of parts and auditing of procedures. The applicable test procedures and inspection techniques were defined by Hamilton Standard engineering and quality control specifications.

10.2.4 Control of Nonconforming Material

Deviations from specification or blueprint requirements were documented on a material rejection ticket. The dispositions available for discrepant material were scrap, rework, repair or "accept as is". If the material was obviously not salvagable, quality personnel could immediately specify that it be scrapped. If by additional processing, discrepant material could be brought into full compliance with print or specification requirement, then a rework disposition was appropriate. Quality personnel were also permitted to make the rework disposition. If by additional processing, the material could be brought to a functionally acceptable form, that did not entirely comply with print or specification requirements, the repair disposition was used. The repair disposition required the concurrence of the Hamilton Standard Material Review Board and the customer. If the discrepant material was functionally acceptable without further processing, the "accept as is"

10.2.4 (Continued)

disposition could be used. This also required concurrence of the Material Review Board and customer. The Material Review Board was composed of quality and engineering personnel who reviewed the proposed disposition from the view point of safety, reliability, durability, performance and compliance with the program objectives. If the Material Review Board concurred that repair of the material was appropriate, the approval of NASA or its designated representative was obtained prior to proceeding with the repair.

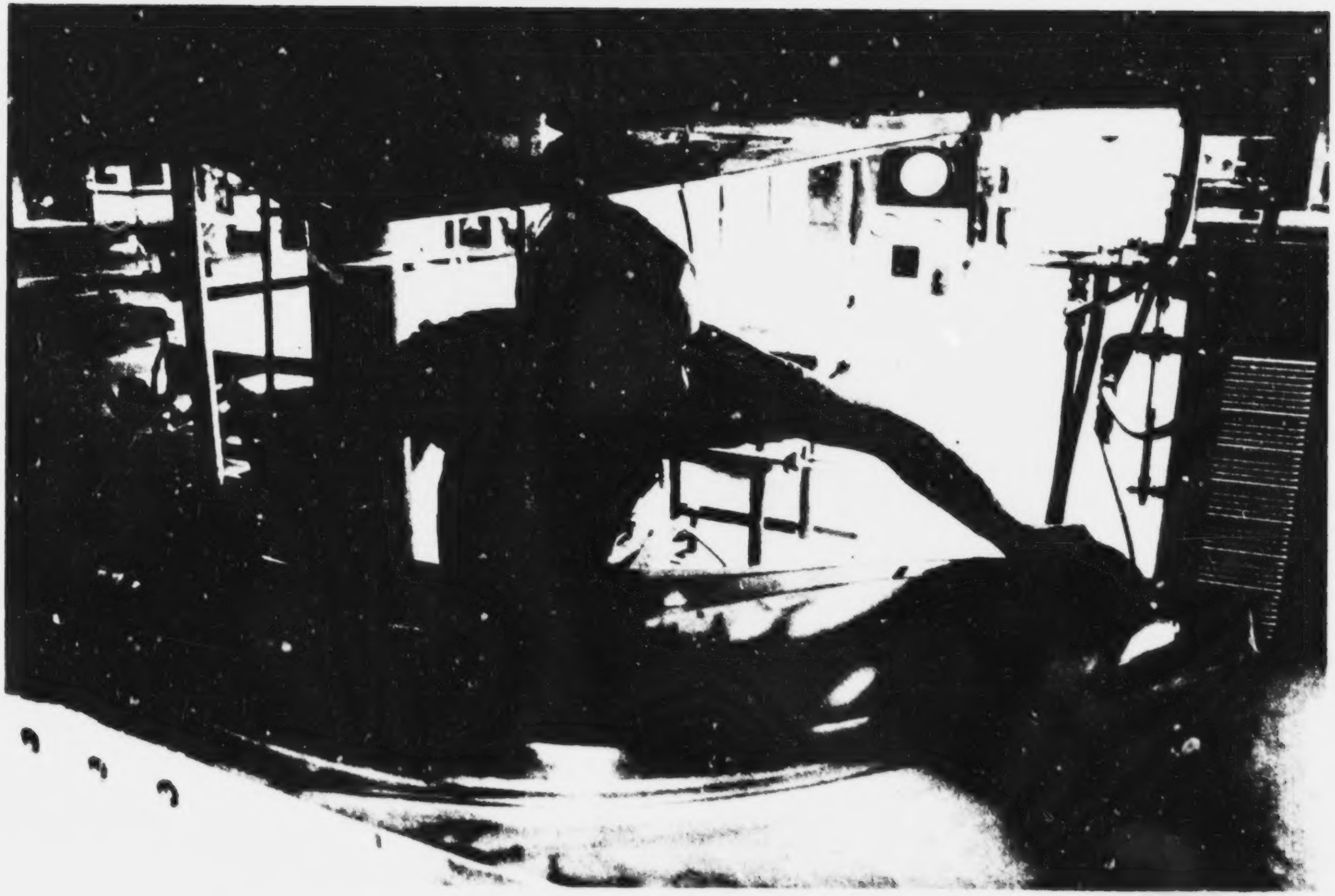

FIGURE 10.1 SR-7L BLADE IN RESIN INJECTION DIE

E-37993

ORIGINAL PAGE IS
OF POOR QUALITY

ORIGINAL PAGE IS
OF POOR QUALITY

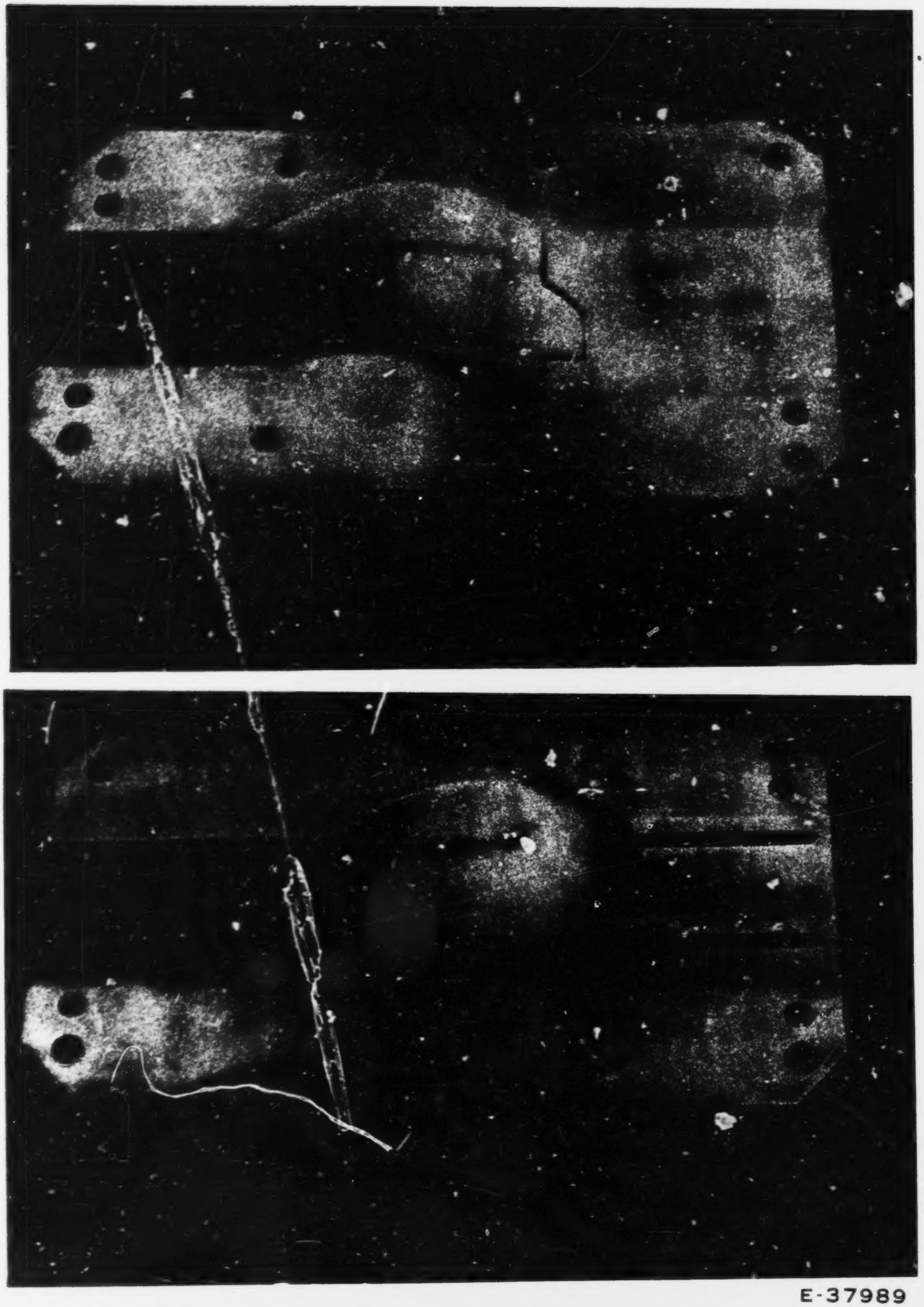

E-37989

FIGURE 10.2 FOAMING MOLD FOR SR-7A AEROELASTIC MODEL BLADE

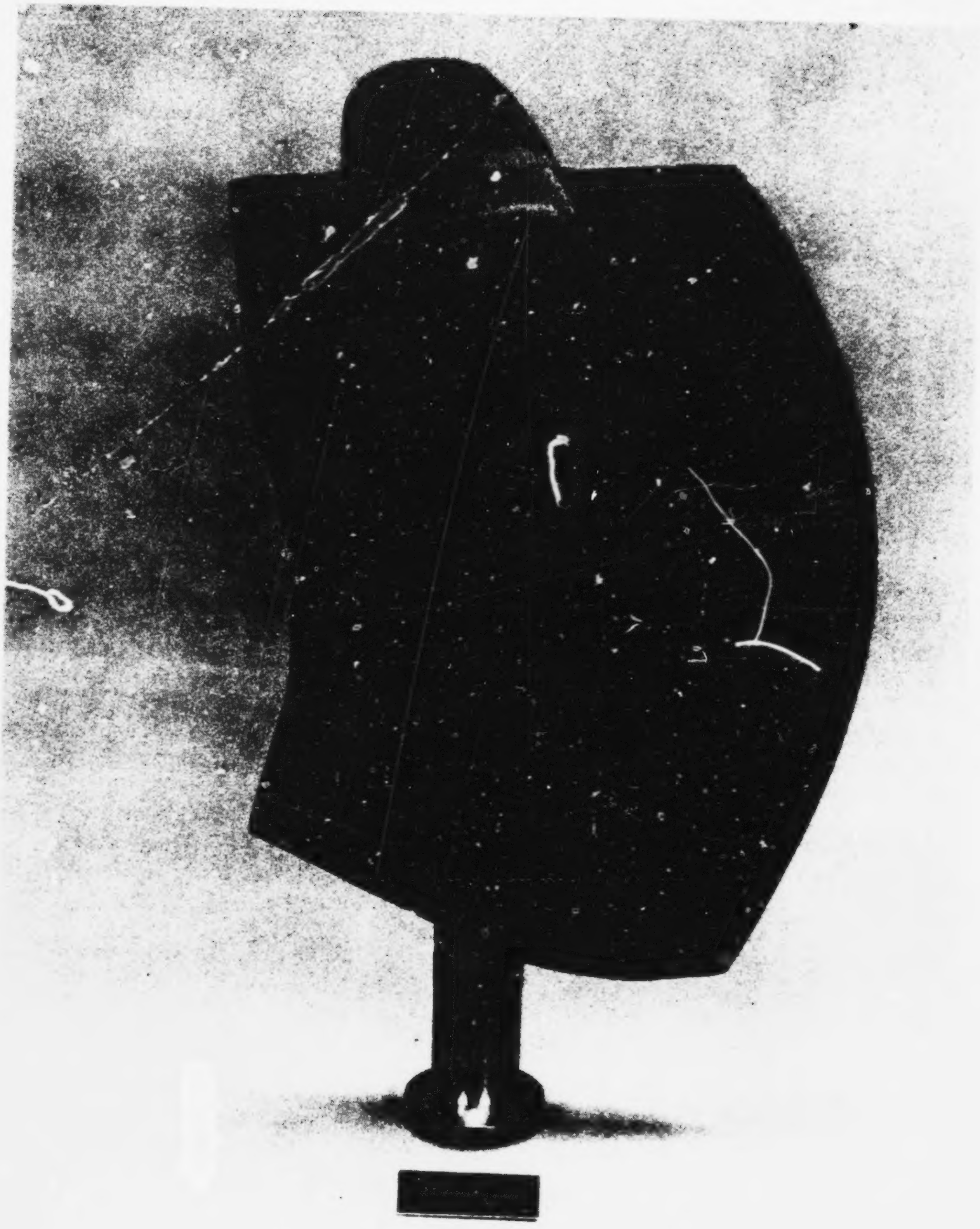

FIGURE 10.3 SR7A SPAR/FOAM ASSEMBLY E-37992

ORIGINAL PAGE IS
OF POOR QUALITY

ORIGINAL PAGE IS
OF POOR QUALITY

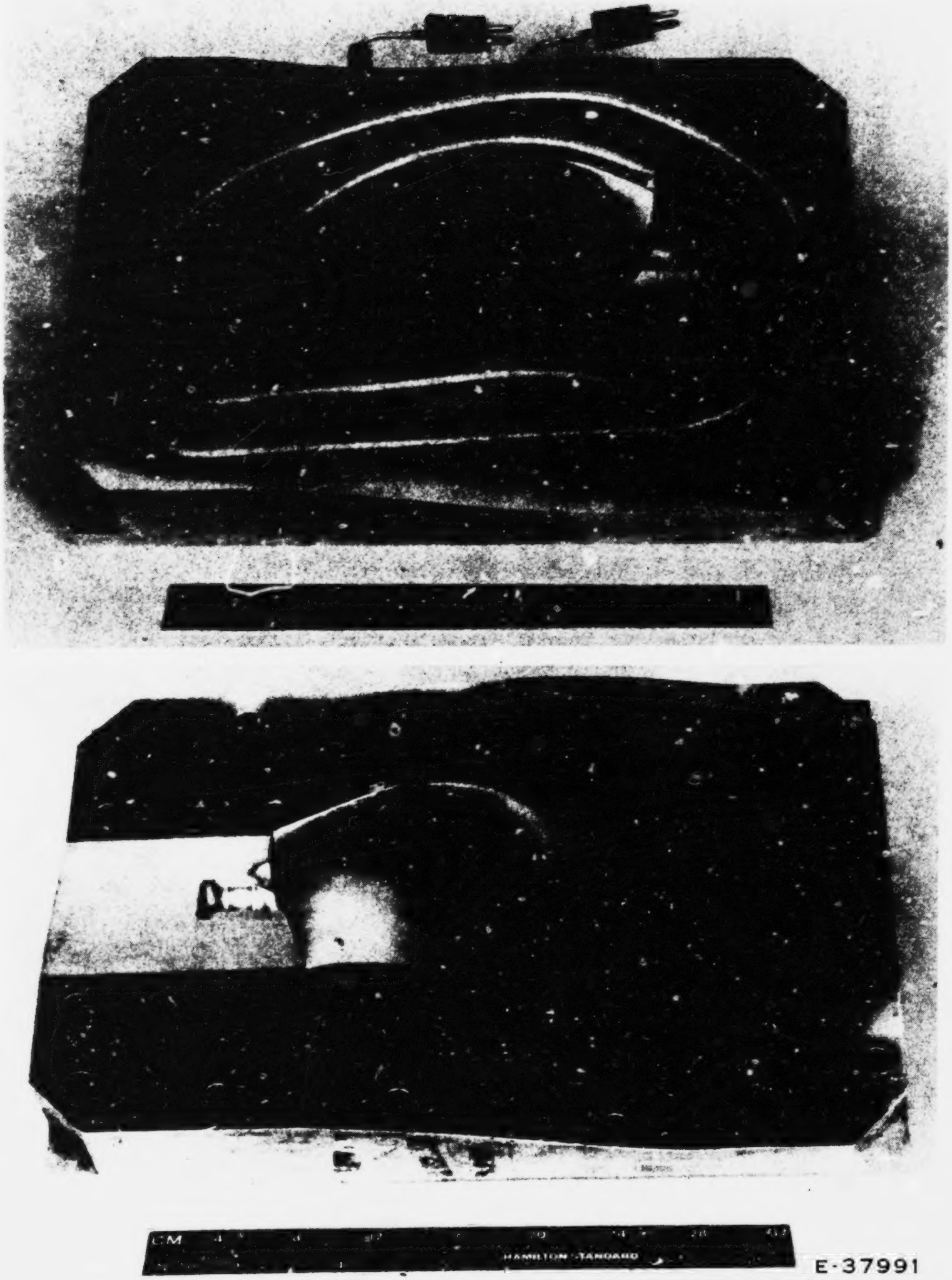
CM
HAMILTON STANDARD

E-37991

FIGURE 10.4 RESIN INJECTION MOLD FOR SR-7A AEROELASTIC MODEL BLADE

11.0 SUB-COMPONENT TESTING

The Large Scale Advanced Prop-Fan pitch control is a modified version of the 54460 military propeller control which has been produced by Hamilton Standard for over twenty years. In order to meet the performance requirements of the Prop Fan, the RPM and normal hydraulic pressure at which the control operates were increased significantly. Many of the 54460 control components were modified or redesigned for the LAP application. The modifications included the reduction of critical clearances in certain components. This combination of design changes and more severe operating parameters dictated that several of the control sub-components undergo testing to ensure that their performance and durability are adequate for the control to meet its design requirements. The critical sub-components for which testing was deemed necessary included the main and standby valve and orifice pack, the transfer bearing and the main, standby and scavenge hydraulic pumps.

11.1 MAIN & STANDBY VALVE AND ORIFICE PACK

The function of the Main and Standby valve in the LAP control was discussed in section 6.4.2 of this report. The purpose of the main and standby valve in the LAP control is to maintain supply pressure at a nearly constant level of 1140 psi over the entire range of actuator flow demand. This contrasts with the 54460 application where the main and standby valve maintains supply pressure at a level 150 psi higher than either high or low pitch pressure. In the LAP control the valve reference pressure is taken between two orifices connected in series and operating between supply pressure and pressurized sump. In the 54460 control the reference pressure is equal to the higher of high pitch or low pitch pressure.

The manufacturing tolerances on the area of the two orifices that constitute the orifice pack are ± 2%. The reference pressure is a function of the ratio of the orifice areas squared. Therefore depending on the tolerance stack up the reference pressure and thus the supply pressure regulated by the main and standby valve can vary significantly. The variation in supply pressure caused by the orifice tolerance variation can be compensated for by placing a shim between the main & standby valve spring and plunger.

The purpose of the main and standby valve test was to ensure the valve functioned properly in conjunction with the orifice pack, and to ensure that the supply pressure could be set to 1140 psi with reasonable precision by shimming the valve.

Initial testing of the valve was accomplished employing the test set up shown in Figure 11.1. The orifice pack was simulated using two micrometering valves in series. The valves were adjusted to yield the same flow and pressure drops for which the orifice pack was designed. The micrometering valves also allowed the tolerance in orifice area to be simulated.

PRECEDING PAGE BLANK NOT FILMED

PAGE 108 INTENTIONALLY BLANK

11.1 (Continued)

Simulation of the main and standby valve operation began by adjusting valves 3 and 9 to supply 22.4 quarts per minute (QPM) of oil to the main pump port and 39.8 QPM to the standby pump port. This simulated the condition where blade angle was not changing and all the hydraulic flow is being returned to sump. The flow to the main pump port was then reduced in 5 QPM intervals to simulate actuator flow demand. When the flow supplied to the main pump port was reduced to zero, valve 9 was opened all the way to equalize the pressure at the main and standby ports, simulating opening of the system check valve. Flow to the standby port was then reduced to simulate additional flow demand. This testing was repeated simulating the range of orifice area tolerances.

Two observations were made during the valve testing. First, the range of tolerances in the orifice areas could be compensated for with a shim of .080 maximum thickness. The .080 shim thickness was within limits that would allow the valve to go full open without the spring being compressed to solid height. Second there was a tendency for the main and standby valve to close completely and cease regulating when the pressures at the main and standby ports equalized. The tendency of the valve to cease regulating was caused by internal leakage within the valve between the reference pressure and standby pressure ports. This leakage increased the flow through the upstream orifice, reducing the reference pressure. When the standby pressure is increased to the level of supply pressure, the direction of leakage between standby and reference pressure changes, reducing the flow through the upstream orifice and reducing the pressure differential between supply and reference pressure below the level that would hold the valve open. The affect of leakage on valve performance is illustrated in Figure 11.2.

The tendency of the valve to cease regulating at the high flow demand conditions was corrected by two design changes. The diametrical clearance between the main and standby valve spool and sleeve was reduced to .0051 to .0102 mm (.0002 in to .0004 in) in order to minimize internal valve leakage. The size of the orifices were also both increased, keeping the same area ratio, in order to increase the orifice flow. Therefore leakage would be a much smaller percentage of the total flow through the upstream orifice and would have mush less affect on valve performance.

The main and standby valves and orifice packs used in the serial number one and two controls were tested using the fixture illustrated in Figure 11.3. This fixture allowed the valve and orifice pack to be tested as a matched set and the thickness required for the valve shim to be determined. These valves and orifice packs, which incorporated the design changes discussed above, did not exhibit a tendency to cease regulating under high flow demand operating conditions.

11.2 TRANSFER BEARING

The function of the transfer bearing was described in section 6.4.7 of this report. The purpose of the testing conducted was to determine if the bearing would function satisfactorily at the higher rotational speeds and hydraulic pressure at which the LAP control operates and with the bearing diametral clearance at land A reduced (reference Figure 6.9).

The initial testing of the transfer bearing was accomplished with a modified 54460 transfer bearing. Land A of the rotating sleeve was chrome plated then remachined to obtain the same diametric clearance to be used in the LAP transfer bearing. The stiffer barrel support ring discussed in section 6.4.7 was also used. A schematic of the test arrangement is shown in Figure 11.4. The transfer bearing was installed in a 54460 control pump housing and mounted on a 54460 propeller hub. The test assembly was installed in a propeller whirl rig in the Hamilton Standard engineering lab. Hydraulic oil flow for the test was provided by an external pump. Instrumentation allowed the monitoring of oil pressures and temperature and the oil flow across each bearing land.

The specific objectives of the test were to measure the amount of leakage across land A as a function of metered pressure and to observe the effect of 40 hours of running at the LAP operating conditions on the bearing.

The measured metered leakage was larger than predicted by analysis but was within limits that would not limit the governing performance of the control. The babbitted surface of the stationary sleeve did show signs of light wear after 40 hours of operation. An analysis of the wear resulted in the conclusion that the wear was caused by insufficient break-in running of the bearing. A break in procedure was devised for the transfer bearings to be used in the LAP controls. The procedure consisted of increasing running speed and oil pressure slowly so that any initial wear between the rotating sleeve and the stationary babbitted sleeve would not generate significant heat.

Break in running of the LAP transfer bearings was accomplished using the same test arrangement as shown in Figure 11.4. During break-in running a higher babbitt wear rate and higher leakage of metered hydraulic flow, than occurred during the initial testing, was noted. Additional testing and analysis were conducted, to determine the source of this problem. The analysis included the construction of a finite element model of the bearing stationary and rotating sleeves. The model was used to determine the effect deflection of the sleeves under pressure and centrifugal load had on the bearing diametral clearance. A complete dimensional inspection of the bearing hardware was also conducted.

11.2 (Continued)

The increased wear and leakage rate were found to be the result of a combination of factors. The hydraulic pressure distribution in the LAP bearing resulted in a 50% reduction in diametral clearance at lands B and C and a 50% increase in diametral clearance at land A. The calculated deflected shape of the bearing is shown in Figure 11.5. Insufficient clearance between the bearing rotating sleeve and the hub tail shaft was also found. This allowed the deflection of the tail shaft, which occurs when the prop nut is tightened, to distort the bearing rotating sleeve.

Several design changes were made to correct the problems discussed above. These changes include:

- Increasing the piloting I.D. of the bearing rotating sleeve by .05 mm (.002 in.) to provide more diametral clearance with tail shaft.
- An additional O-Ring was added to the rotating sleeve I.D. and a radial hole through the rotating sleeve at the metered pressure port was also added. This change introduced metered pressure below land A of the rotating sleeve, reducing inward deflection and the tendency of the diametral clearance at land A to increase under pressure load.
- The bearing diametral clearance at land C was increased by .005 mm (.0002 in.) because the maximum reduction in bearing diametral clearance due to pressure loading occurs at that land.

The bearings were retested following incorporation of the design changes listed above. No wear of the bearing babbitted surface was noted after incorporation of the design changes. The leakage of metered hydraulic pressure was also significantly reduced and the flows across the bearing lands corresponded well with analytical predictions.

11.3 PUMP TESTS

As discussed in section 6.4.1 of this report, the main, standby and scavenge pumps for the LAP control were similar to the pumps used in the 54460 control. The most significant alteration was interchanging the drive and driven pump shafts to accommodate the change in direction of rotation. However the rotational speed of the pumps on average is 12% higher in the LAP application than in the 54460 application. In addition the main pump will operate at a normal output pressure of 7.86X10^{6}Pa (1140 psi) in the LAP application versus 4.14X10^6 Pa (600 psi) in the 54460 application. The standby pump will intermittently see the same pressure as the main pump. Due to the more severe operating conditions experienced by the LAP main and standby pumps, a qualification test was run on one main pump and one standby pump. The qualification test consisted of an endurance run and an overspeed test. The endurance run was 100 hours of operation at the pump design speed and the maximum pressure seen by the pumps 9.5X10^{6}Pa (1375 PSI). The output flow of the pump and the drive torque were monitored continuously throughout the test. The acceptance criterion was that the pump output flow remain above the minimum allowable throughout the test. The overspeed test consisted of one hour of operation at 120% of design speed and 7.86X10^{6}Pa (1140 PSI) output pressure. The acceptance criterion for this test required that when the pump speed is returned to 100% design speed, the output flow must be above the minimum acceptable flow.

The scavenge pump is very similar in construction to the main pump and operates at the same speed and a much lower output pressure than the main pump. Therefore it was not deemed necessary to run a qualification test for the scavenge pump.

The flow output of the main and standby pumps as a function of operating time during the endurance test is shown in Figure 11.6.A 3% to 4% reduction in pumps output was noted over the course of the 100 hours of operation. Most of the reduction occurred over the first 40 hours of the test. The output reduction is attributed to the initial wear on the I.D. of the pump casing caused by the pump gears during break-in. No measurable difference in pump output was noted after the completion of the overspeed test.

At the conclusion of qualification testing each pump was disassembled for inspection. There was no sign of wear or damage on the gear teeth of the pumps. The I.D.'s of the pump casings were measured and an increase in diameter of from .023mm to .030mm (.0009 in to .0012 in) was measured. The pump manufacturer considered this to be normal break-in wear.

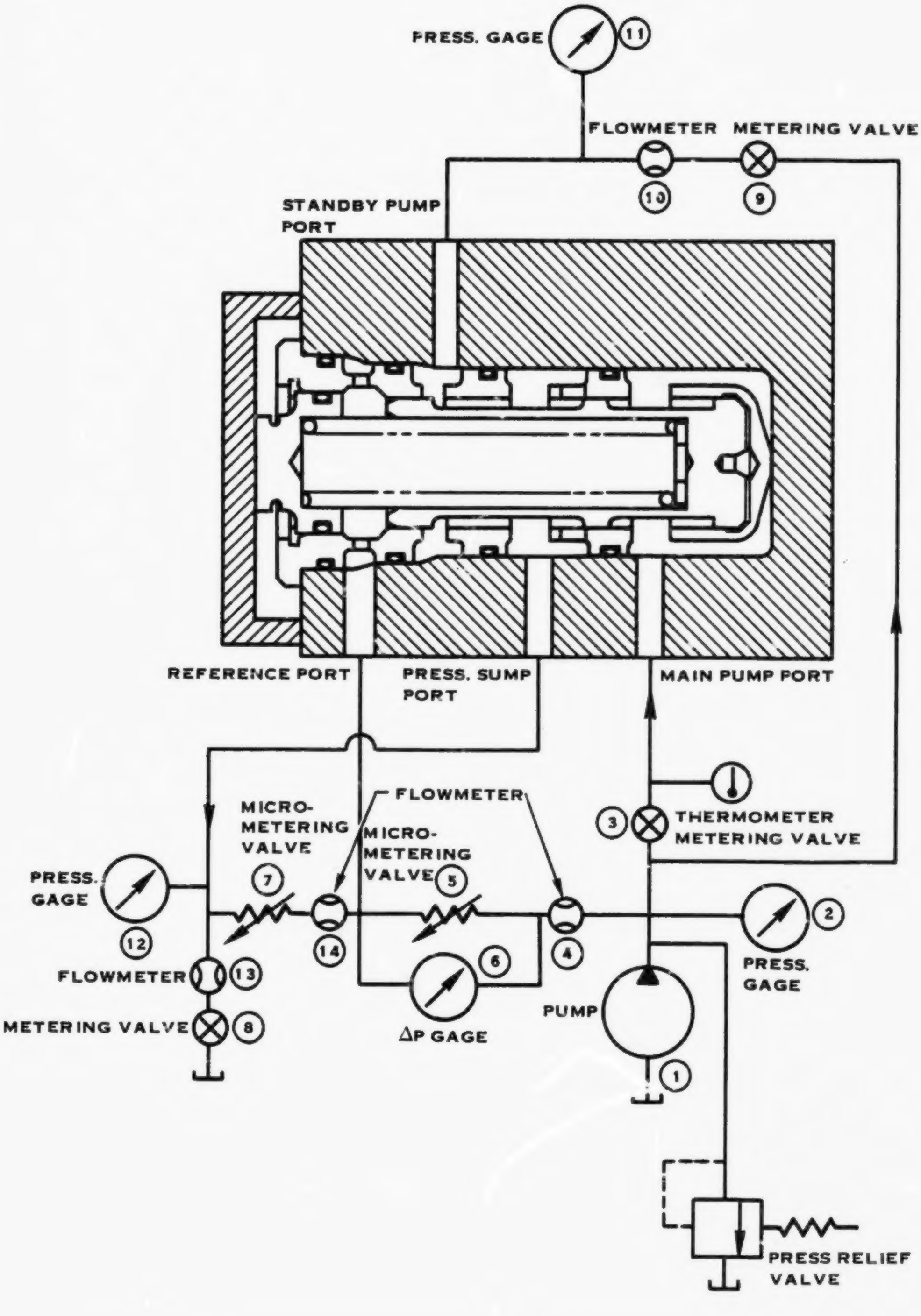
PRESS. GAGE
11
FLOWMETER
METERING VALVE
10
9
STANDBY PUMP PORT
REFERENCE PORT
PRESS. SUMP PORT
MAIN PUMP PORT
FLOWMETER
MICRO-METERING VALVE
MICRO-METERING VALVE
7
5
THERMOMETER
METERING VALVE
3
PRESS. GAGE
12
14
4
2
PRESS. GAGE
FLOWMETER
13
6
METERING VALVE
8
ΔP GAGE
PUMP
1
PRESS RELIEF VALVE

FIGURE 11.1 MAIN & STANDBY VALVE TEST ARRANGEMENT

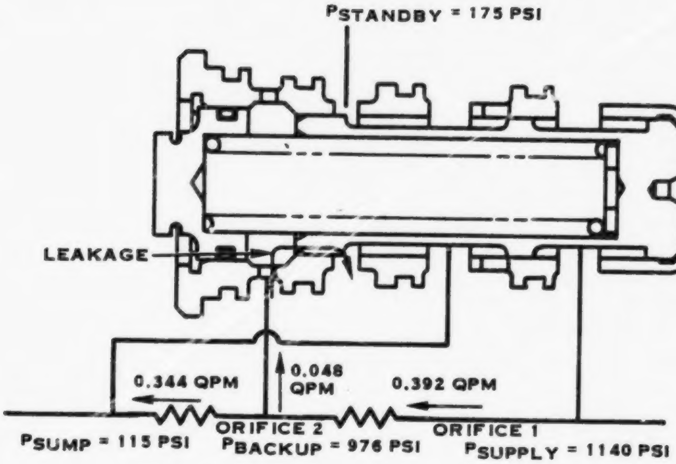
PSTANDBY = 175 PSI
LEAKAGE
0.344 QPM
0.048 QPM
0.392 QPM
ORIFICE 2
ORIFICE 1
PSUMP = 115 PSI
PBACKUP = 976 PSI
PSUPPLY = 1140 PSI

STANDBY PUMP CHECK VALVE CLOSED

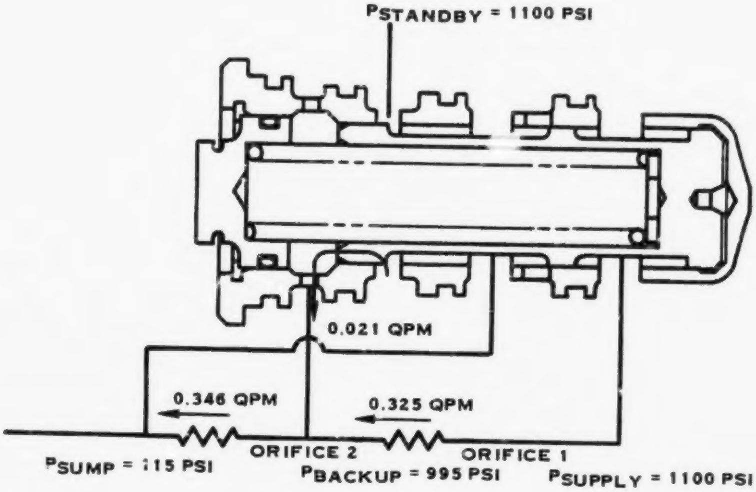
PSTANDBY = 1100 PSI
0.021 QPM
0.346 QPM
0.325 QPM
ORIFICE 2
ORIFICE 1
PSUMP = 115 PSI
PBACKUP = 995 PSI
PSUPPLY = 1100 PSI

STANDBY PUMP CHECK VALVE OPEN

FIGURE 11.2 EFFECT OF LEAKAGE ON MAIN & STANDBY VALVE PERFORMANCE

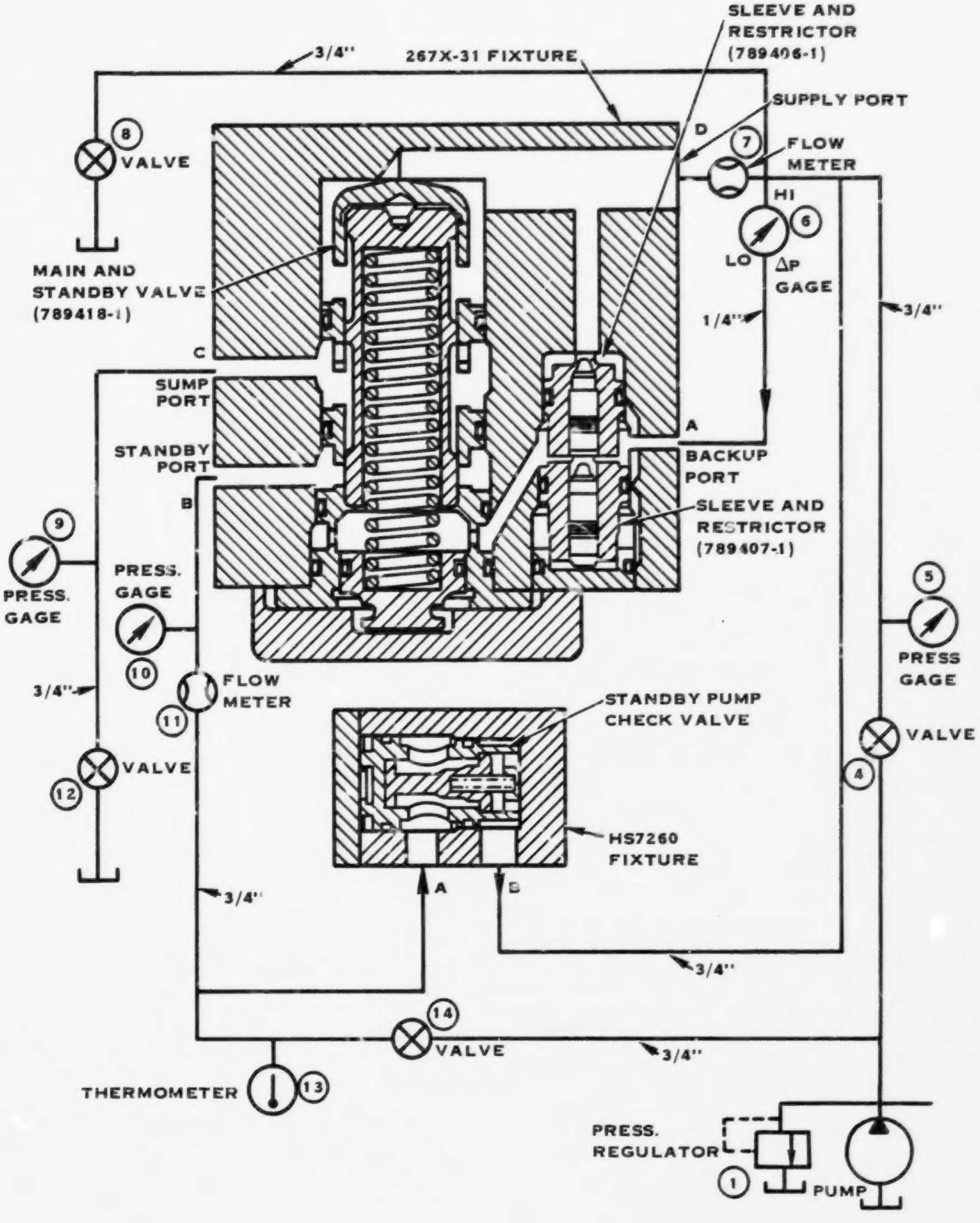
SLEEVE AND RESTRICTOR (789406-1)
3/4"
267X-31 FIXTURE
SUPPLY PORT
D
7
FLOW METER
8
VALVE
HI
6
LO
ΔP GAGE
MAIN AND STANDBY VALVE (789418-1)
1/4"
3/4"
C
SUMP PORT
A
STANDBY PORT
BACKUP PORT
B
SLEEVE AND RESTRICTOR (789407-1)
9
PRESS. GAGE
PRESS. GAGE
10
5
PRESS GAGE
3/4"
FLOW METER
11
STANDBY PUMP CHECK VALVE
VALVE
12
VALVE
4
HS7260 FIXTURE
3/4"
A
B
3/4"
14
VALVE
3/4"
THERMOMETER
13
PRESS. REGULATOR
1
PUMP

FIGURE 11.3 TEST ARRANGEMENT, MAIN AND STANDBY VALVE AND ORIFICE PACK

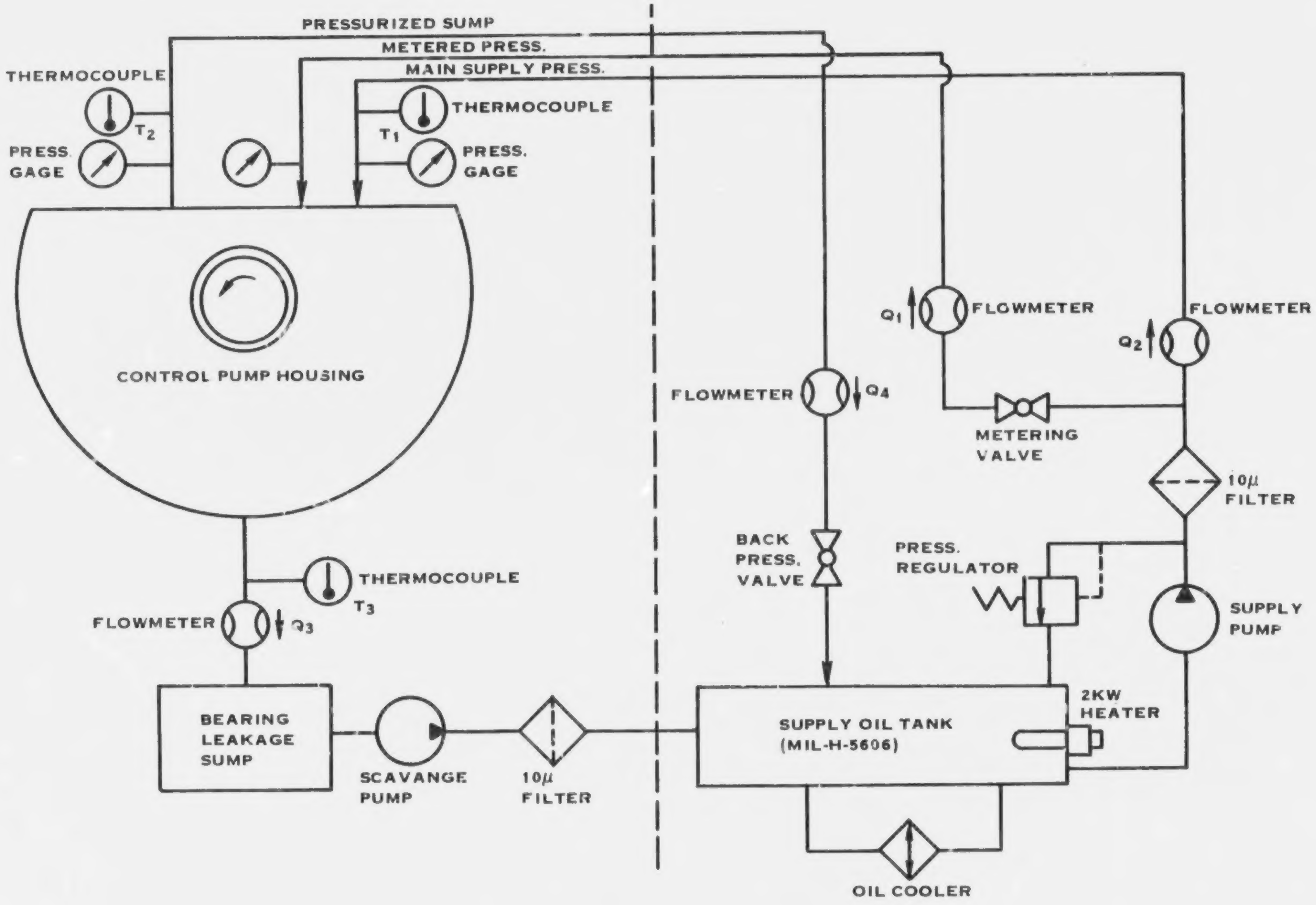
PRESSURIZED SUMP
METERED PRESS.
MAIN SUPPLY PRESS.
THERMOCOUPLE
T_2
PRESS. GAGE
THERMOCOUPLE
T_1
PRESS. GAGE
CONTROL PUMP HOUSING
THERMOCOUPLE
T_3
FLOWMETER
Q_3
BEARING LEAKAGE SUMP
SCAVANGE PUMP
10μ FILTER
FLOWMETER
Q_4
BACK PRESS. VALVE
Q_1
FLOWMETER
METERING VALVE
Q_2
FLOWMETER
10μ FILTER
PRESS. REGULATOR
SUPPLY PUMP
SUPPLY OIL TANK (MIL-H-5606)
2KW HEATER
OIL COOLER

FIGURE 11.4 TRANSFER BEARING TEST SCHEMATIC

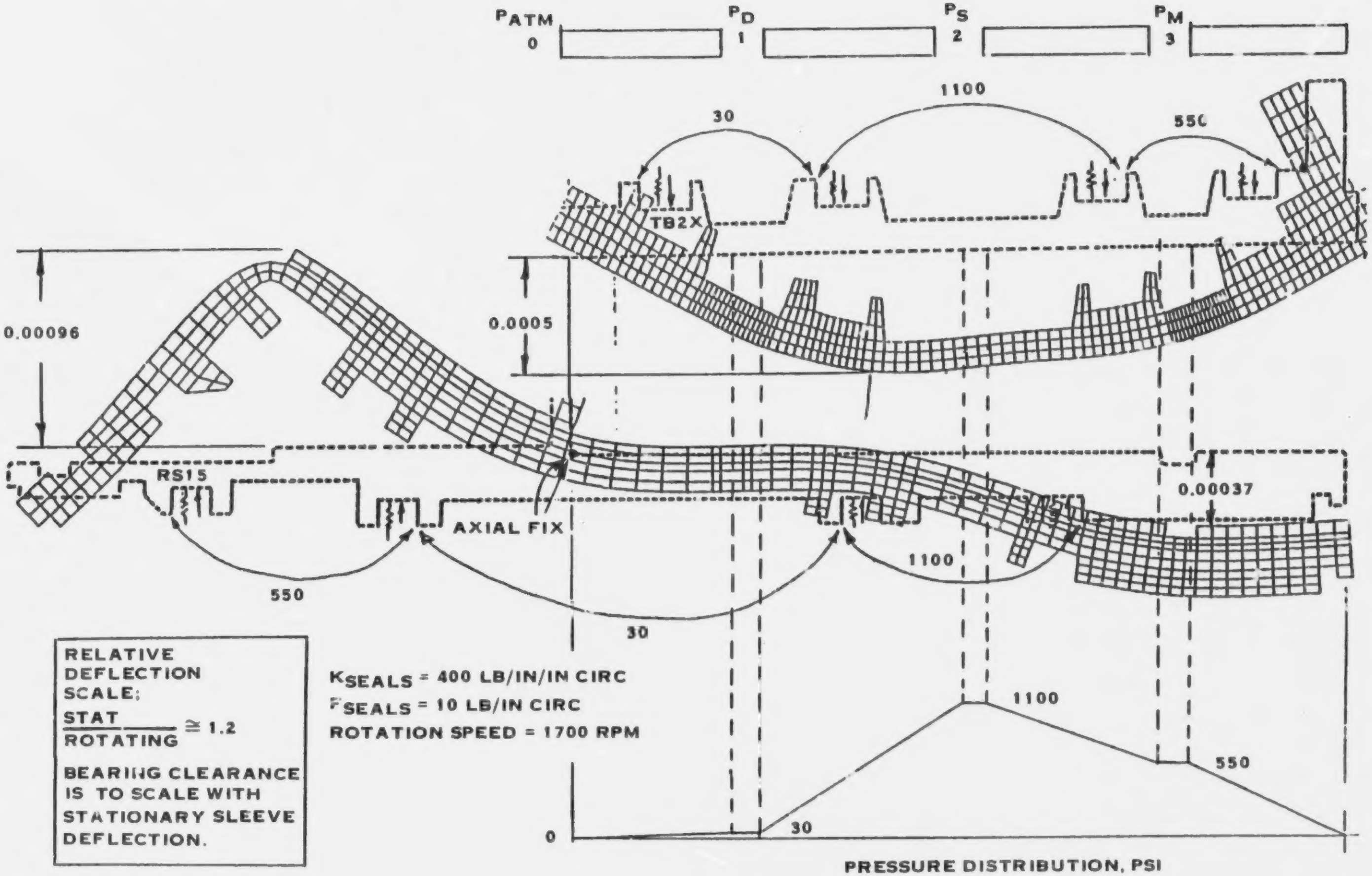
P_{ATM}
0
P_D
1
P_S
2
P_M
3
30
1100
550
TB2X
0.0005
0.00096
RS15
AXIAL FIX
0.00037
550
1100
30
RELATIVE DEFLECTION SCALE;
$\frac{\text{STAT}}{\text{ROTATING}} \cong 1.2$
BEARING CLEARANCE IS TO SCALE WITH STATIONARY SLEEVE DEFLECTION.
K_{SEALS} = 400 LB/IN/IN CIRC
F_{SEALS} = 10 LB/IN CIRC
ROTATION SPEED = 1700 RPM
0
30
1100
550
PRESSURE DISTRIBUTION, PSI

FIGURE 11.5 TRANSFER BEARING DEFLECTION DUE TO PRESSURE LOADING, ORIGINAL DESIGN

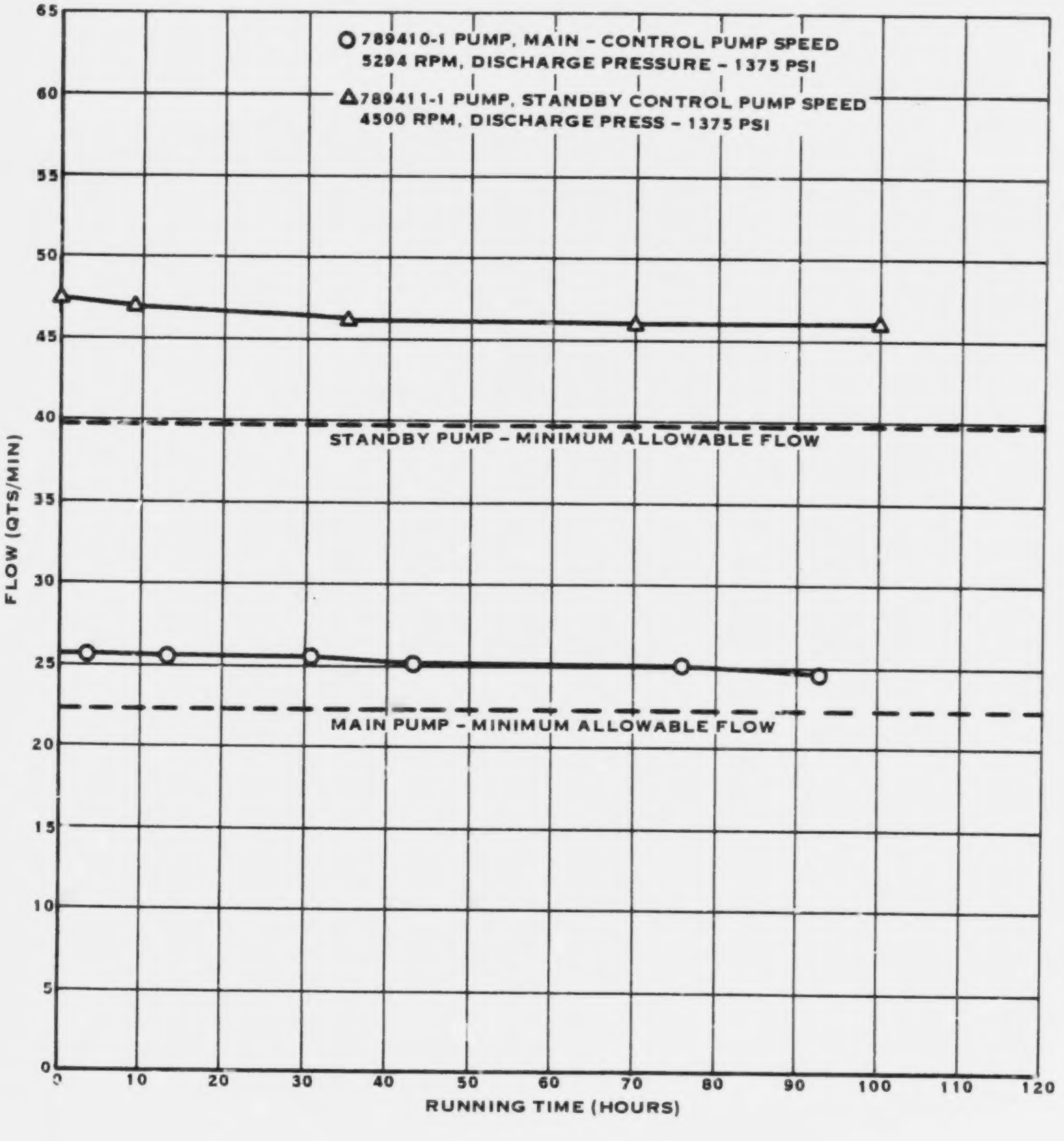

FIGURE 11.6 PUMP 100 HOUR ENDURANCE TEST RESULTS

12.0 RETENTION STIFFNESS TEST

12.1 TEST DESCRIPTION

The purpose of the retention stiffness test was to experimentally determine the combined stiffness of the hub and blade retention. The hub, blade retention hardware and actuator dome were installed in an electric motor driven whirl rig with dummy blade stubs substituting for the blades. The stubs were designed to apply the same centrifugal force to the hub and retention as the blades. The test installation is depicted in Figure 12.1.

Rotation of the test assembly in the whirl rig results in excitation of the blade stubs due to random air turbulence. Strain gages were applied to the stubs to measure the in-plane and out-of-plane vibrational response to the excitation. Spectral analysis of the strain gage data allowed the natural frequencies of the propeller to be determined.

The test assembly natural frequencies are a function of the retention stiffness, the dynamic characteristics of the stubs and the propeller RPM. The stubs are essentially solid metal cylinders. As such they are simple structures that are easy to analyze. The stub natural frequencies are calculated and plotted as a function of retention stiffness for a range of rotational speeds. Therefore when the stub natural frequency is experimentally measured at a particular rotational speed, a retention stiffness corresponding to that natural frequency can then be determined.

12.2 TEST RESULTS

When testing was initiated, it was observed that the natural air turbulence in the test cell was providing a very low level of excitation for the stubs. Therefore it was necessary to combine the data from several stubs to enhance the data quality. Since the phase of the individual stubs was known for the mode of interest, the data signals were combined by simple addition and subtraction to provide a signal amplified by a factor of four. The data signals from alternate stubs were combined as follows:

TOTAL OUTPUT = STUB 1 - STUB 3 + STUB 5 - STUB 7

Figure 12.2 shows experimentally determined propeller in-plane and out-of-plane natural frequencies plotted as a function of RPM. The heat generated by rotation of the stubs in the test cell resulted in a rapid air temperature rise that precluded operation above 1599 RPM. However the smooth variation of natural frequency with speed would allow extrapolation of the data to higher RPM's. The experimentally determined curves of natural frequency versus RPM are shown overlayed on the calculated curves of natural frequency versus retention stiffness in Figure 12.3. The intersections of these curves define the retention stiffness as a function of centrifugal load, which is plotted in Figure 12.4. The data is extrapolated out to a load of 369184N (83000 lbs) which corresponds to the design rotational speed of 1698 RPM.

12.3 COMPARISON OF DATA AND ANALYTICAL PREDICTIONS

As discussed in section 4.6 of the report, the hub retention stiffness was calculated using both two dimensional and three dimensional analytical techniques. The results of the retention stiffness test are compared with the results obtained using both of these analytical techniques in Table 12-1.

TABLE 12-1

COMPARISON OF MEASURED AND CALCULATED RETENTION STIFFNESSES

	EXPERIMENT	2-D ANALYSIS	3-D ANALYSIS
IN-PLANE STIFFNESS (In-lbs/RAD $X10^{-6}$)	11.2	13.7	7.9
OUT OF PLANE STIFFNESS (In-lbs/RAD $X10^{-6}$)	16.3	15.5	16.9

Reasonable agreement was obtained between the experimentally determined out-of-plane stiffness and the out-of-plane stiffness calculated using both the 2-D and 3-D analysis. The experimentally determined in-plane stiffness fell midway between the stiffness calculated using the 2-D analysis and the stiffness calculated using the 3-D analysis. The measured stiffnesses were considered acceptable for the SR-7L and should prevent significant infringement of any of the blade critical speeds upon the resonance avoidance zones defined in Figure 3.6.

ORIGINAL PAGE IS
OF POOR QUALITY

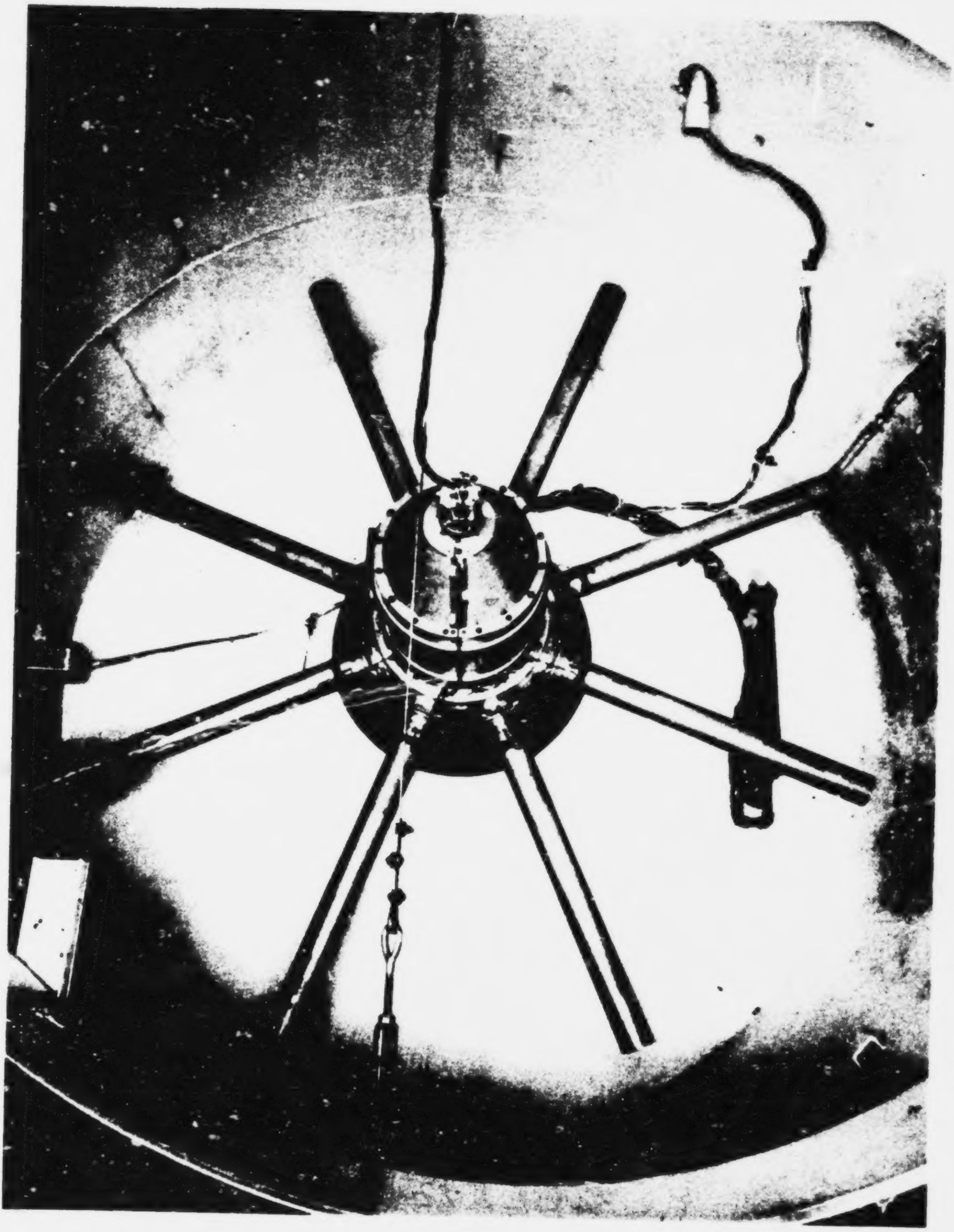

FIGURE 12.1 RETENTION STIFFNESS TEST ARRANGEMENT

E-37986

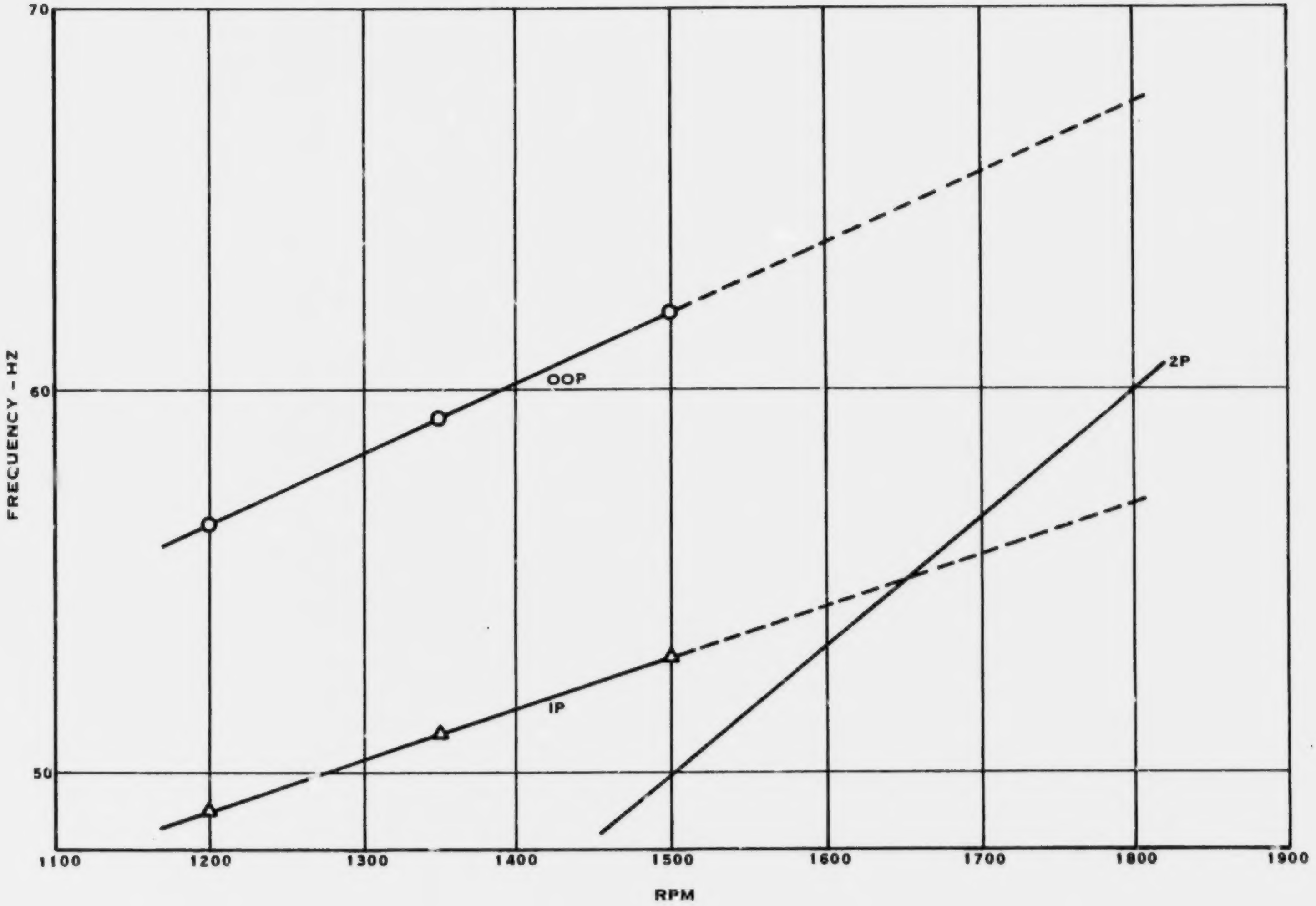

FIGURE 12.2 STUB NATURAL FREQUENCY VS. RPM

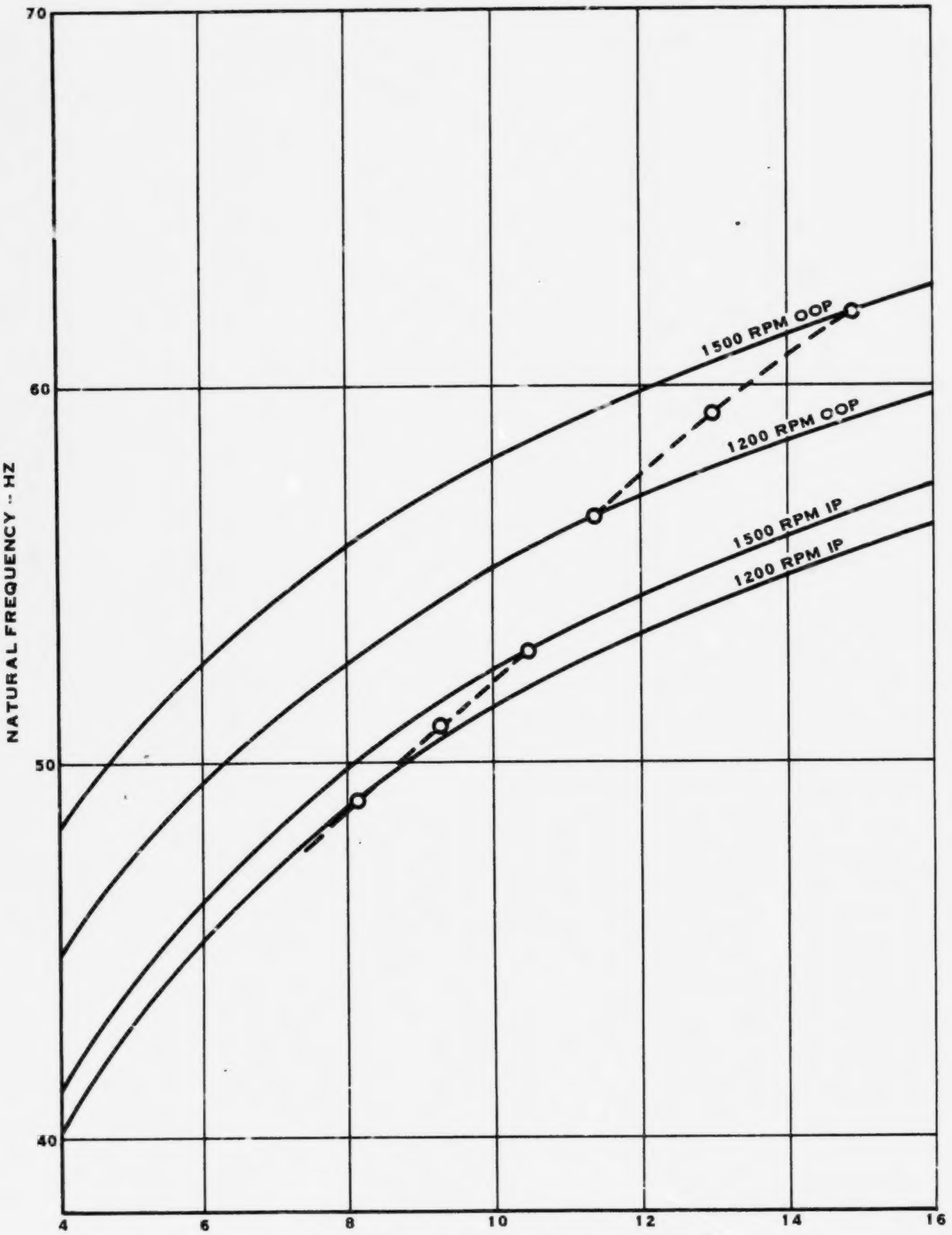

FIGURE 12.3 STUB NATURAL FREQUENCY VS. RETENTION STIFFNESS

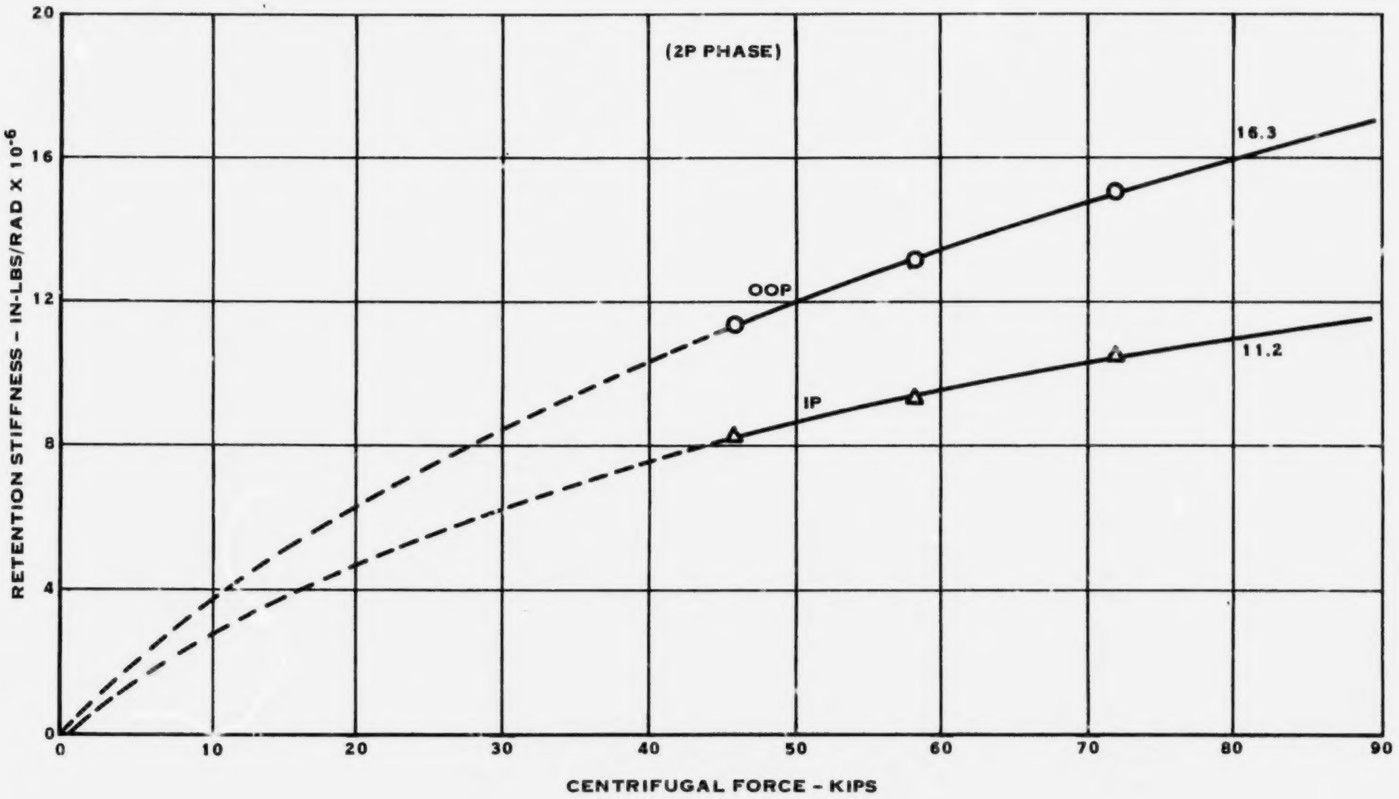

FIGURE 12.4 RETENTION STIFFNESS VS. CENTRIFUGAL LOAD

13.0 WHIRL RIG TEST

13.1 TEST DESCRIPTION

The purpose of the whirl rig test was to evaluate the performance of the LAP actuator and control. The specific characteristics that were investigated included the Prop Fan's ability to feather, the capability to introduce a speed setpoint using the control input lever, the control dead band and the overall governor gain, the accumulation of wear on the blade retention hardware during operation and the effectiveness of the pitch lock mechanism.

The Prop Fan was tested in Hamilton Standard's G-5 whirl rig. The Prop Fan was driven by a 500 H.P electric motor through a hydraulic clutch. A strut and bearing arrangement was employed to support the forward end of the Prop Fan. The support was necessary to avoid the presence of a highly undamped rig critical speed in the test operating speed range. Figure 13.1 shows a schematic of the test arrangement. Figure 13.2 shows the Prop Fan installed in the test cell without the strut and bearing arrangement.

The Prop-Fan blades were replaced by test stubs and counterweights for the whirl rig tests. The test bars and stubs apply centrifugal force and twisting moment to the actuator and blade retention, equivalent to the forces and moments that would be applied by the blades at the same rotational speed.

All of the parameters necessary to evaluate the actuator and control performance were measured during the whirl rig test. These parameters included RPM, actuator high and low pitch pressure, control supply, metered and sump pressure, sump oil temperature, blade pitch angle and control input lever position.

The whirl rig test consisted of six individual system tests. A description of each test follows:

13.1.1 Feather Test

This test determined the Prop-Fan's ability to move the blades into and out of feather. Testing was accomplished for a non-rotating Prop-Fan, using the auxiliary motor as a source of hydraulic pressure and with the Prop-Fan rotating at 1273 RPM and 1698 RPM. Feathering and unfeathering were initiated by activating and deactivating the feather solenoid valve and also by moving the control speed input lever into and out of the feather position.

13.1.2 Speed Set Point and Dead Band Test

This test evaluated the accuracy of the governor and the speed set cam and linkage in establishing a desired speed set point. The control dead band around the governor null point was also measured. The control was first calibrated at the 100% speed set point (1698 RPM). The actual speed set point and the dead band were determined by varying the test rig speed in 2 or 3 RPM increments about the speed set point selected on the Prop-Fan control input lever. The rate of change of blade angle was monitored as the rig speed was varied. The range of RPM over which no change in blade angle was observed determined the dead band and set speed. The dead band is the maximum RPM in this range minus the minimum RPM. The actual speed set point is the midpoint of the dead band speed range.

13.1.3 Governor Gain Test

The purpose of this test was to measure the pitch change governor gain at three different operating speeds (1273 RPM, 1485 RPM and 1698 RPM). The governor gain is defined by equations 1.) and 2.).

$$1.)\quad \text{Governor Gain} = \frac{\text{Rate of Change of Blade Angle}}{\%\ \text{Speed Error}}$$

Where

$$2.)\quad \%\ \text{Speed Error} = \frac{\text{Actual Speed} - \text{Set Point Speed}}{\text{Set Point Speed}} \times 100\%$$

The governor gain test was conducted by selecting a set speed on the control input lever and adjusting the test rig speed to achieve the desired speed error. The rate of change of blade angle was measured for each speed error and the governor gain was calculated.

13.1.4 Blade Angle Cycling Endurance Test

This test consisted of cycling blade angle between 35° and 60° while operating the Prop-Fan at two different rotational speeds. The change in blade angle from 35° to 60° is approximately the range that is traversed between take-off and cruise condition. This test was conceived to be an accelerated wear test for actuator and blade retention hardware.

13.1.5 Maximum CTM Endurance Test

This test consisted of cycling blade angle rapidly about 42°, while operating at 100% speed. At a blade angle of 42° the trunnions and actuator react the maximum test stub centrifugal twisting moment for a constant rotational speed. The Maximum CTM Test simulates the minor changes in blade angle that occur while the Prop-Fan is maintaining a constant RPM at cruise condition. This test was also designed to be an accelerated wear test for actuator and blade retention hardware.

13.1.6 Blade Angle Pitchlock Test

The purpose of this test was to verify the ability of the pitchlock system to maintain blade angle in the event of a loss of hydraulic pressure. The test was conducted by modifying the control feather valve, so that when the valve was actuated, supply hydraulic pressure rather than metered pressure was returned to sump, thus simulating a hydraulic failure. The pitchlock test was conducted at 1783 RPM. Hydraulic failures were simulated at blade angles of 15°, 45° and 70°.

13.2 TEST RESULTS

13.2.1 Feathering Test

Feathering and unfeathering was accomplished satisfactorily, when initiated by either the feather solenoid valve or the control input lever. A blade angle slew rate of 1.9° per second was obtained for the nonrotating Prop-Fan, feathering or unfeathering using the auxilary motor. A slew rate of 7.3° per second was obtained feathering or unfeathering with the Prop-Fan rotating at 1273 RPM or 1698 RPM.

13.2.2 Speed Set Point and Dead Band Test

The actual speed set points were determined for control input lever angles of 17.53°, 33°, 48°, 63.16°, 78.38° and 93.59° where the feather position is taken as zero degrees. The design speed set schedule and the actual speed set schedule obtained from test data are compared in Figure 13.3. The actual speed dead band measured at each speed set point is presented in Table 13-1.

TABLE 13-1
CONTROL DEAD BAND DATA

INPUT LEVER ANGLE (DEG.)	SET POINT SPEED (RPM)	APPARENT DEAD BAND (RPM)	APPARENT DEAD BAND (% RPM)
17.5	1422	± 4	± .28
32.74	1485	± 4	± .27
47.95	1553	± 3	± .19
63.20	1620	± 5	± .31
78.40	1680	± 5	± .30

13.2.3 Governor Gain Test

The measured blade angle pitch rate as a function of % speed error is presented in Figure 13.4 for a speed set point of 1698 RPM. The overall governor gain is the slope of the curve of these points at the origin. The measured governor gain resulting from this data is 1.8°/sec/% RPM.

13.2.4 Maximum CTM Endurance Test

Following 5 hours of cycling at a 42° blade angle and 100% speed, an inspection of the retention hardware, the blade trunnions and the actuator wear plates was conducted. No unusual wear patterns were observed during this inspection.

13.2.5 Blade Angle Cycling Endurance Test

Five hours of cycling was completed at 1273 RPM and 2 hours of cycling at 1485 RPM. During this testing several blade seal leaks occurred that slowed progress. The leaks were found to be the result of tears in the rubber blade seals. The tears were caused by scissoring of the seal anti-friction strip and relative motion between the seal and the blade shank. A design change was implemented to correct this problem. The new seal employs a stiffer spring to secure it to the blade shank. The anti-friction strip is also eliminated. The cross section of the seal was altered to accommodate the new spring and to provide a better static seal.

13.2.6 Blade Angle Pitchlock Test

There was no perceptible reduction in blade angle when hydraulic failures were simulated at blade angles of 15°, 45° or 70°. The data for the 45° case is presented in Figure 13.5. The data shows that actuation of the modified feather valve reduces supply pressure from 1110 psi to 180 psi and reduces the pressure differential across the actuator ($P_{hi\ pitch} - P_{lo\ pitch}$) from 660 psi to 120 psi.

13.3 COMPARISON OF DATA WITH ANALYTICAL PREDICTIONS

As seen in Figure 13.3, it was only possible to adjust the set point speed over 60% of the design speed governing range. A review of the design of the speed set cam and linkage revealed that the wrong linkage spring rate had been used in the design calculations, resulting in an incorrect speed set cam contour. A new cam was designed and fabricated which yields the correct governing speed range. The measured governor dead band averaged ± .27% RPM for the range of speed set points tested. This compared favorably with the design governing accuracy of ± .22% (ref. Section 6.2).

The measured governor gain is somewhat lower than expected. The design governor gain was 2.5°/sec/% RPM at 100% RPM as compared to the observed gain of 1.8°/sec/% RPM. The lower gain may be due to higher than expected internal leakage in the Prop Fan control. The shortfall in governor gain does not adversely affect the stability of the control system. However it does make RPM overshoots more likely during power lever transients. Therefore caution will have to be exercized not to employ abrupt changes in power lever position when introducing changes in engine power level.

The design requirement for the LAP pitchlock system was that there be less than a 1.5° loss in blade pitch angle in the event of a loss of hydraulic pressure. The test data indicates that there was essentially no loss of blade angle when a hydraulic failure was simulated.

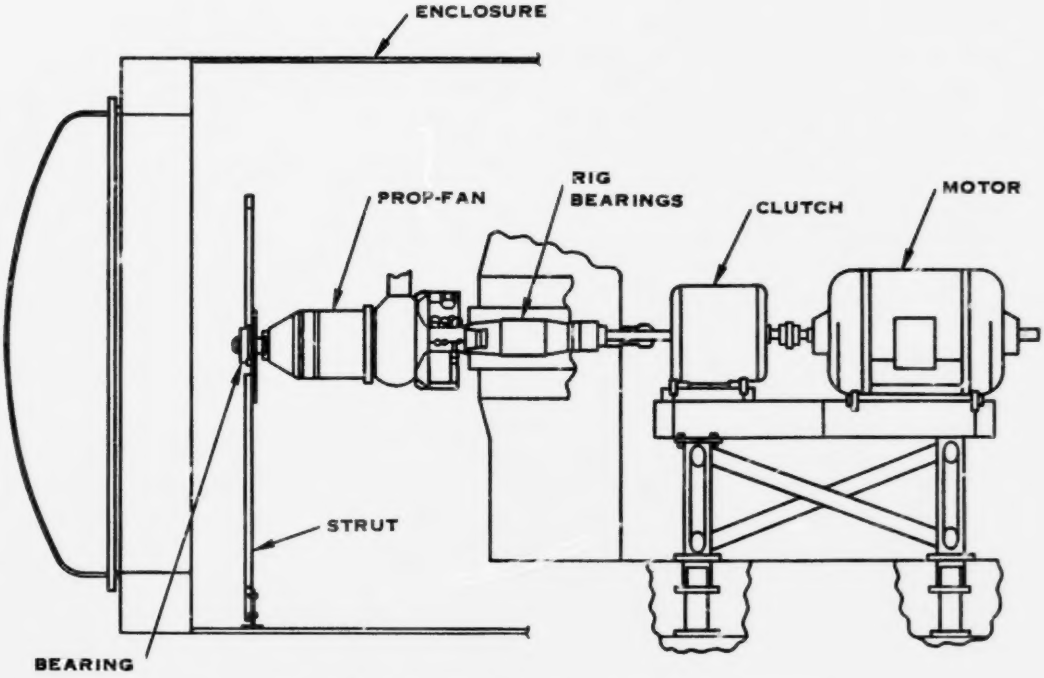
ENCLOSURE
PROP-FAN
RIG BEARINGS
CLUTCH
MOTOR
STRUT
BEARING

FIGURE 13.1 WHIRL RIG TEST ARRANGEMENT

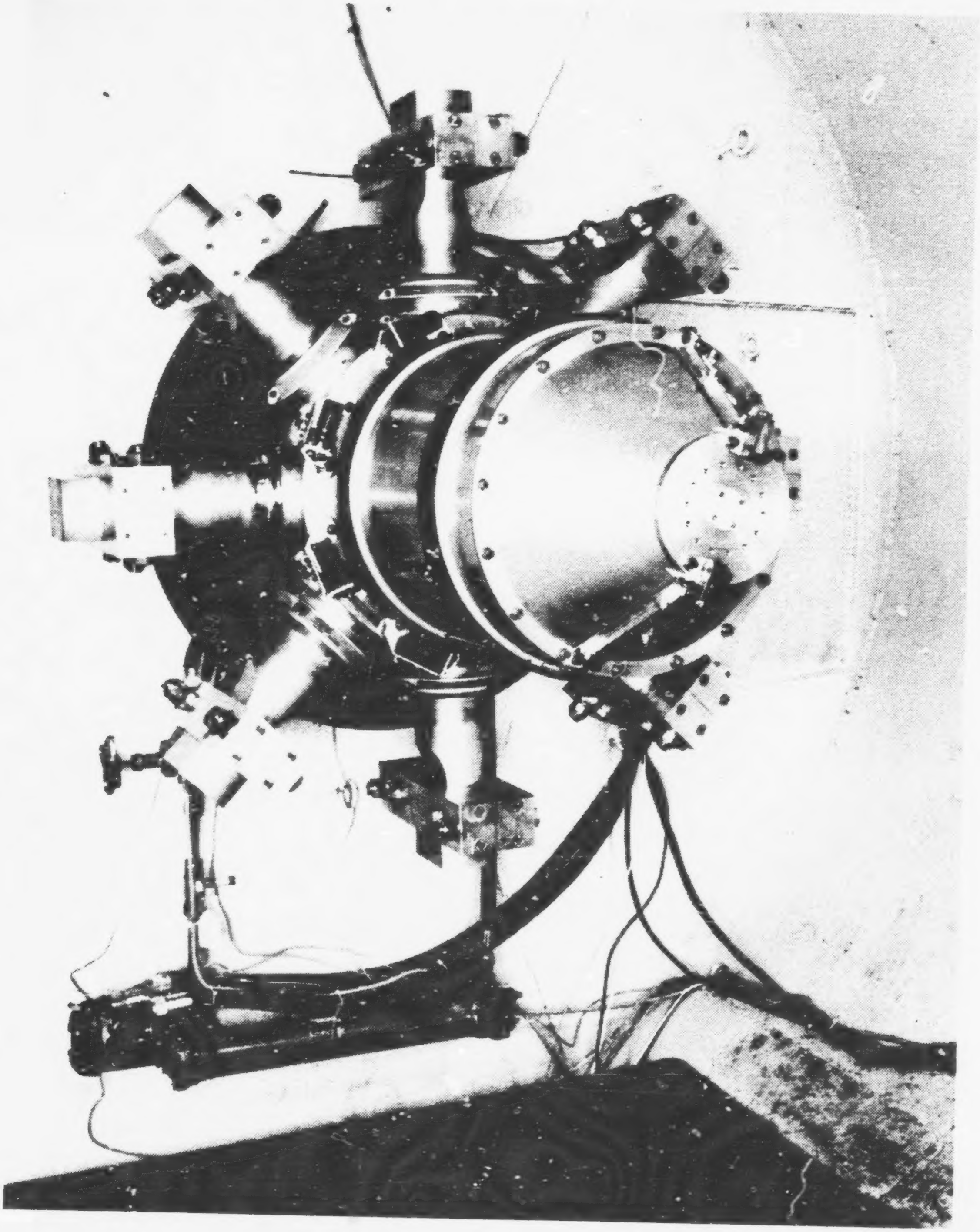

FIGURE 13.2. LAP INSTALLED IN THE G-5 WHIRL RIG

ORIGINAL PAGE IS
OF POOR QUALITY

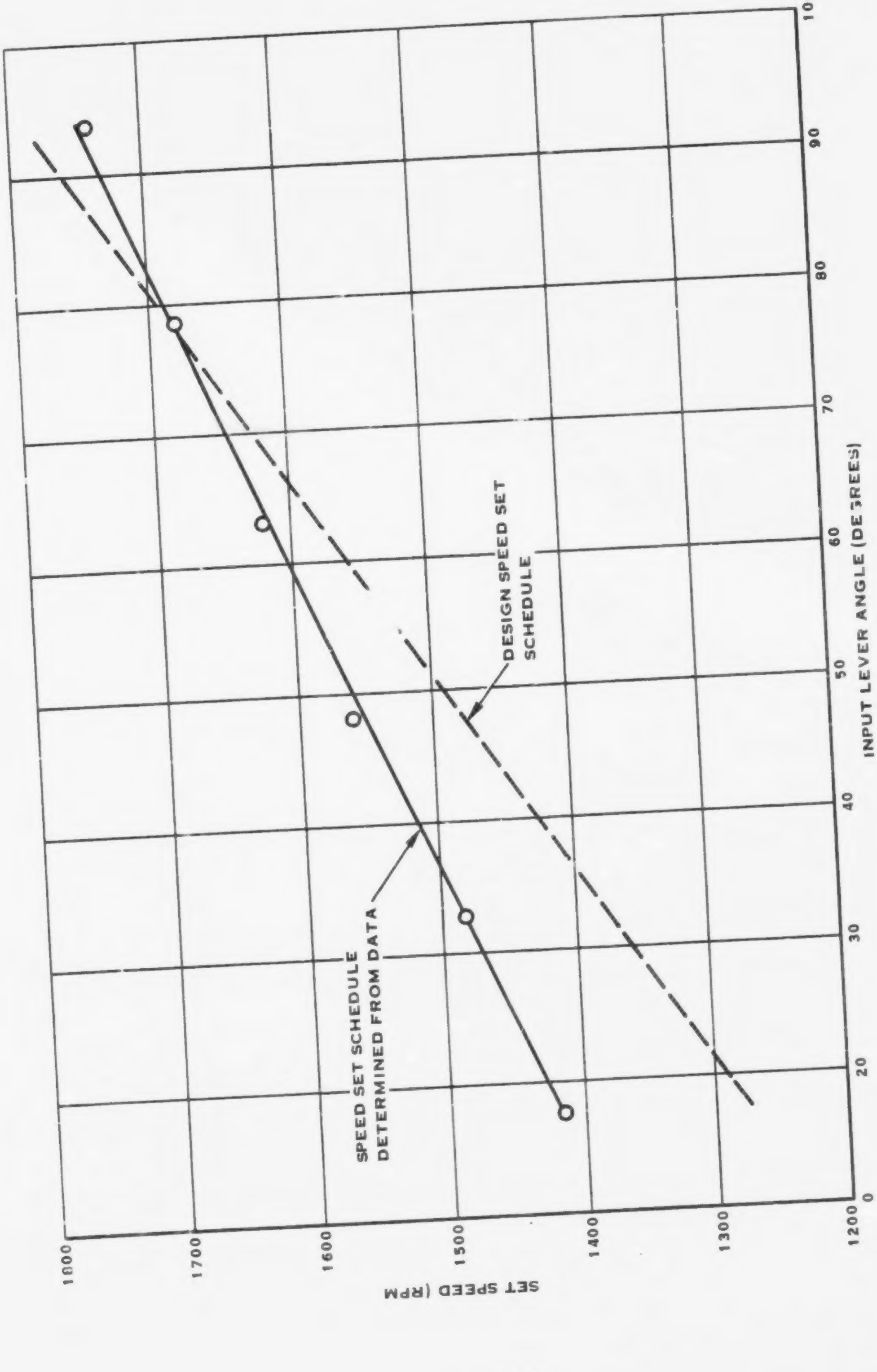

FIGURE 13.3 INPUT LEVER POSITION VS. GOVERNING SPEED

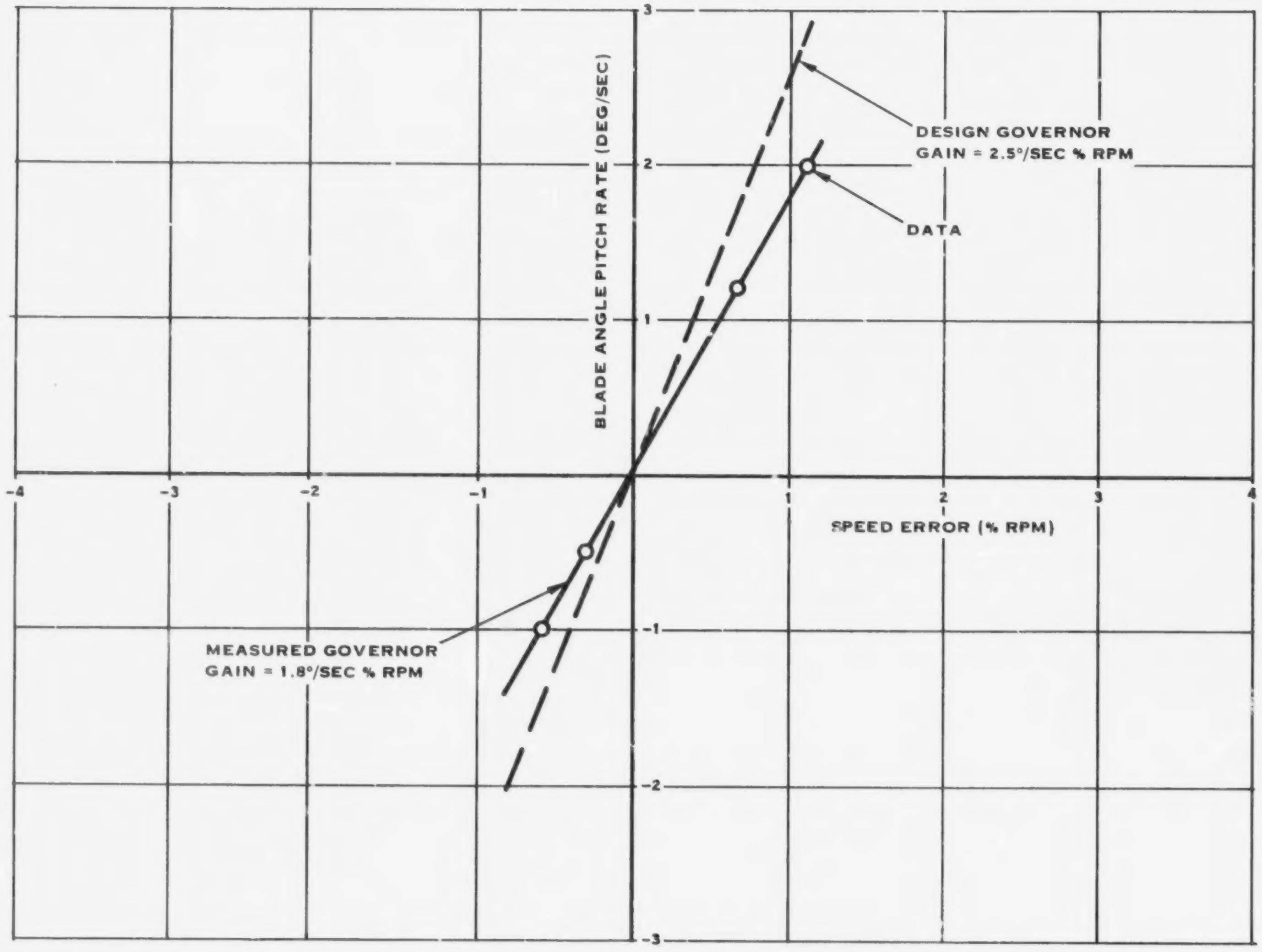

FIGURE 13.4 BLADE PITCH RATE VS. % SPEED ERROR, SET POINT = 1698 RPM

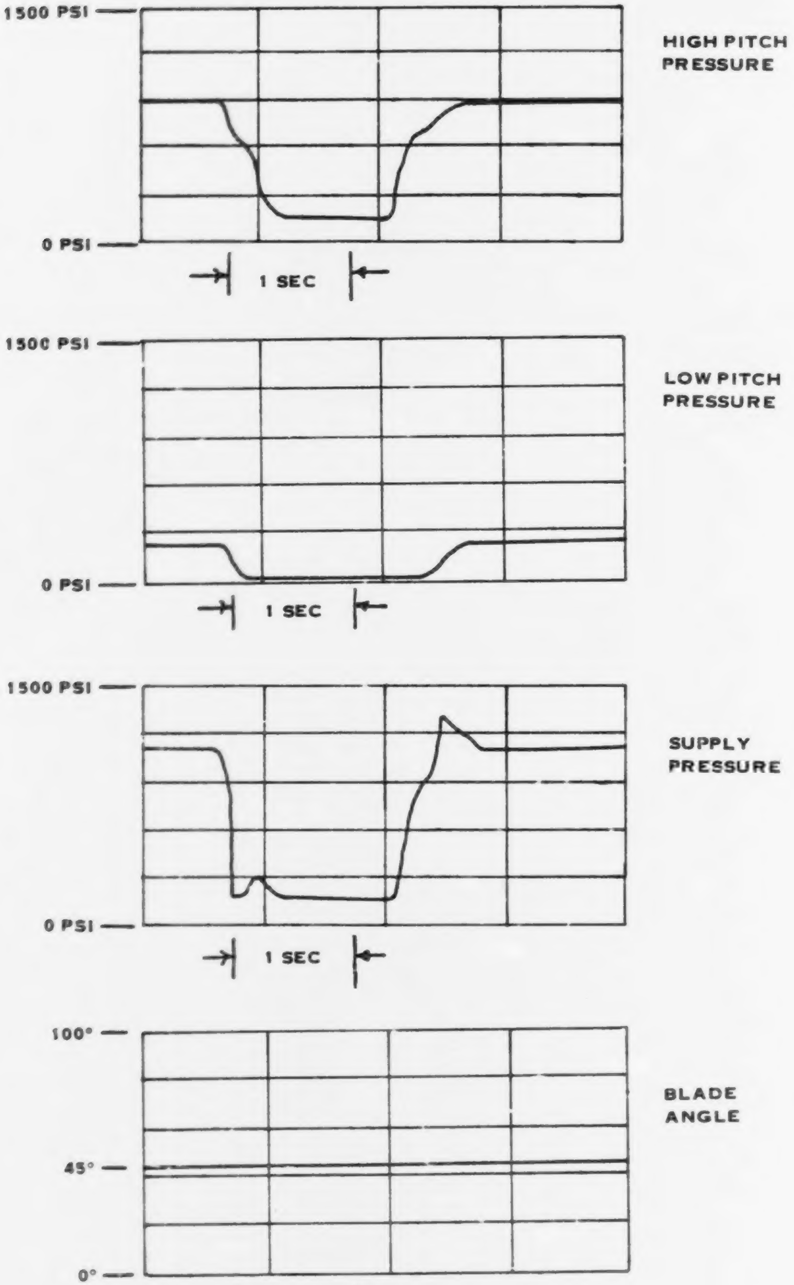

FIGURE 13.5 PITCHLOCK TEST RESULTS 1780 RPM

14.0 BLADE ESA AND FATIGUE TESTING

The goals of the LAP blade ESA (Experimented Stress Analysis) and fatigue tests were:

- Determine the Stressing in the LAP blades under static and vibratory loading.
- Determine the adequacy of analytical tools for calculating stresses.
- Determine the location of stress hot spots that might not be predicted analytically.
- Confirm the fatigue allowable stresses for the materials used in constructing the LAP blade.

14.1 TEST DESCRIPTION

14.1.1 Blade ESA Test

The blade ESA test was conducted using two methods, stress coat evaluation and strain gage testing.

Stress coat evaluation was accomplished by applying a brittle lacquer coating to the external surface of the blade up to the 99 cm (39 inch) blade station. The coated blade was installed in a test fixture and loaded first in the flatwise bending mode and then in the edgewise bending mode with respect to the 34.3 cm (13.5 inch) blade station. Static loading was applied to the blade in increments at the 104 cm (41 inch) station up to a maximum value of 2669N (600 lbs.) in the flatwise mode and 3781N (850 lbs.) in the edgewise mode. The test arrangement for the edgewise mode test is depicted in Figure 14.1.

New crack patterns observed in the brittle lacquer at each loading increment were noted by marking them with a different color. The crack patterns indicate the location and direction of the principal strains in the blade structure.

Strain gage testing of the LAP blade was conducted in both a static and dynamic mode. The strain gage arrangement employed for both the static and dynamic testing is illustrated in Figure 14.2. For the most part both the face and camber sides of the blade were identically gaged.

A U-gage with an accompanying load cell was employed for load application during the static strain gage investigation. The blade was again loaded in the flatwise and edgewise modes with respect to the 34.3 cm (13.5 inch) station. Loads up to 3781 N (850 lbs) were applied at the 104 cm (41 in)

PRECEDING PAGE BLANK NOT FILMED

PAGE 136 INTENTIONALLY BLANK

14.1.1 (Continued)

station and 2936N (660 lbs) at the 127 cm (50 in) station for the flatwise mode. The loads were applied in five equal increments. With the blade oriented in the edgewise mode loads of 2224N (500 lbs) and 667N (150 lbs) were applied to the 104 cm (41 in) and 127 cm (50 in) station respectively. These loads were also applied in five equal increments. A torsional mode was tested with 199N-M (1760 in-lbs) applied in five equal increments at the 127 cm station.

Strain gage data was recorded at all load increments for each load configuration. A finite element analysis of the blade was conducted for certain of the loading configurations in order to compare experimental data with theoretical predictions.

For the dynamic strain gage ESA testing, two blades were clamped butt to butt as a pair in the split hub test fixture. One blade was strain gaged in the same manner as for the static test. Blades were oriented in both the flatwise and edgewise modes and were driven by an electromagnetic vibrator motor. The test configuration is shown in Figure 14.3. Strain gage data was used to determine the blade resonant frequencies. A stroboscope and salt patterns were used to determine the mode shapes corresponding to the natural frequencies. Theoretical analysis was also available for comparison with the dynamic ESA data.

14.1.2 Blade Fatigue Test

Blade fatigue testing was conducted in zero mean stress and mean stress modes. For the zero mean stress test, two blades were installed butt to butt in a split hub test fixture. The spar stress levels were monitored using strain gages attached to the blade shell above the spar. Stressing of the blades was accomplished using an electromagnetic shaker to excite them at the frequency corresponding to the second flatwise resonant mode. Testing was conducted at three stress levels corresponding to 100%, 125% and 150% of the design allowable for infinite life of the spar. The test arrangement for the zero mean stress fatigue test is depicted in Figure 14.4.

Mean stress testing was conducted with four blades cropped at the 100.3 cm (39.5 in.) blade station. Fiberglass bulkheads were installed at the cropped end of the blade to facilitate introduction of steady loads at the 36.5 inch blade station. All four blades were stacked on one electromagnetic shaker with adjacent blades loaded thru a bearing arrangement at the tips. The blades were excited at the frequency corresponding to the first flatwise mode concurrently with the application of steady bending loads. The stress levels for this testing corresponded to the maximum calculated steady spar stress for the takeoff/climb condition (reference table 3-2) with vibratory stress levels of 125%, 150% and 175% of the design allowable for infinite life of the spar. The test arrangement for the mean stress testing is depicted in Figure 14.5.

14.2 TEST RESULTS

14.2.1 Blade ESA Test

The results of the stress coat evaluation are presented in Table 14-1 and Figures 14.6 and 14.7. No cracking was observed for the edgewise loading configuration. For the flatwise loading, normal crack patterns were produced at reversed loading modes where the first indication appeared at 500 lbs. load.

TABLE 14-1
STRESSCOAT ESA TEST RESULTS

1) Flatwise Mode, Camber in Tension
Sensitivity = 500 micro in/in

Load Level (lbs)	Indication
300	no
400	no
500	yes
600	yes

Flatwise Mode, Face in Tension
Sensitivity = 500 micro in/in

Load Level (lbs)	Indication
300	no
400	no
500	yes
600	yes

2) Edgewise Mode, Leading Edge in Tension
Sensitivity = 500 micro in/in

150	no
250	no
350	no
450	no
550	no
650	no
750	no
850	no

Figures 14.8 and 14.9 present the spanwise stress distribution along the blade spar and along the nickel sheath for the 150 lb load flatwise mode static strain gage ESA test. The theoretical strain distribution for this condition, based on finite element analysis are also overlayed on the data.

14.2.1 (Continued)

A comparison of the experimentally determined resonant frequencies and the predicted resonant frequencies (ref. Figure 3.6) are present in Table 14-2.

TABLE 14-2
COMPARISON OF MEASURED AND PREDICTED RESONANT FREQUENCIES

Mode Type	Test Values (Hz)	Theoretical Values (Hz)
1st Flatwise (1F)	34.32	33.95
2nd Flatwise (2F)	84.28	78.11
1st Edgewise (1E)	140.10	137.82
1st Torsional (1T)	137.20	140.86
3rd Flatwise (3F)	152.10	162.02

The modal lines for the first three flatwise modes and the torsional mode were marked on one blade and compared with the theoretical predictions. The experimentally determined mode shapes were found to be very close to the predictions.

14.2.2 Blade Fatigue Test

During the zero mean stress test, two sets of two blades completed testing at the first level. One of the blades developed a sheath crack, 32 $\times 10^6$ cycles into the first level. This blade was able to complete $50\text{X}10^6$ cycles at the first level without any additional crack propagation. At 9.17 $\text{X}10^6$ cycles into the second stress level additional propagation of the sheath crack occurred accompanied by shell cracking. Radiographic inspection revealed that a spar fracture had occurred at the same location as the sheath crack. In order to complete the zero mean stress test, the cracked blade was replaced with another blade that had also completed the first stress level. These two blades completed the $50\text{X}10^6$ cycles of the second level and $10\text{X}10^6$ cycles of the third level, without any other sheath or spar damage. Several shell/foam delaminations occurred during the course of the zero mean stress testing. These delaminations were repaired as they were detected and testing continued.

During the course of the mean stress test one blade developed a sheath crack after $29.75\text{X}10^6$ cycles. The crack extended from the face to the camber side of the sheath. This blade sustained the remainder of the $50\text{X}10^6$ cycles at the first level and $10\text{X}10^6$ cycles at both the second and third levels without further damage. A very small sheath crack was also found on a different blade at the completion of the third level of testing. Several shell/foam delaminations also occurred during the mean stress test. These delaminations were again repaired as they occurred and testing continued.

14.3 DISCUSSION OF RESULTS

14.3.1 Blade ESA Test

Generally good agreement was obtained between measured and analytically predicted blade stress distributions, natural frequencies and mode shapes.

The spanwise strain distributions measured during the static ESA test for both the spar and leading edge sheath indicates that the analytical predictions are higher than the measured strains. Discrepancies occur in a more pronounced manner in the outboard blade sections from the 88.9 cm (35 in.) station to the 127 cm (50 inch) station. Discrepancies in strain response are possible due to the complex blade configuration and local bending that may occur in the proximity of the load application point.

The discrepancies between the measured and predicted blade resonant frequencies are attributed to the infinite shank retention stiffness used in the analytical model. Despite the discrepancies between the measured and predicted resonant frequencies, the correlation between the observed and predicted mode shapes was excellent.

14.3.2 Blade Fatigue Test

The first stress level for the zero mean stress mode represents, 125% of the nickel sheath material design limit. The maximum sheath stress occurs at the 122 cm (48in) station which is the location at which the sheath crack occurred. Considering statistical scatter of fatigue allowables, the fracture of one blade sheath at this stress level is explainable. It is postulated that once the sheath cracked, a significant reduction in stiffness resulted, increasing the loading of the spar and culminating in the spar fracture. Metallurgical evaluation of the blade did not uncover any material abnormalities.

The sheath crack that occurred during the mean stress fatigue test was a statistically remote event because the stress level in the sheath was lower than in the zero mean stress fatigue test.

The shell/foam separations that occurred during the fatigue test are not uncommon in composite blades. Composite blades are known to function adequately in commercial operation for extended periods with delaminations.

The configuration of the LAP blade with the spar underneath the sheath makes the blade susceptible to a spar fracture if the sheath fractures above the spar. Therefore it is necessary to inspect the sheaths periodically during operation of the LAP and immediately replace any blade that develops a sheath crack.

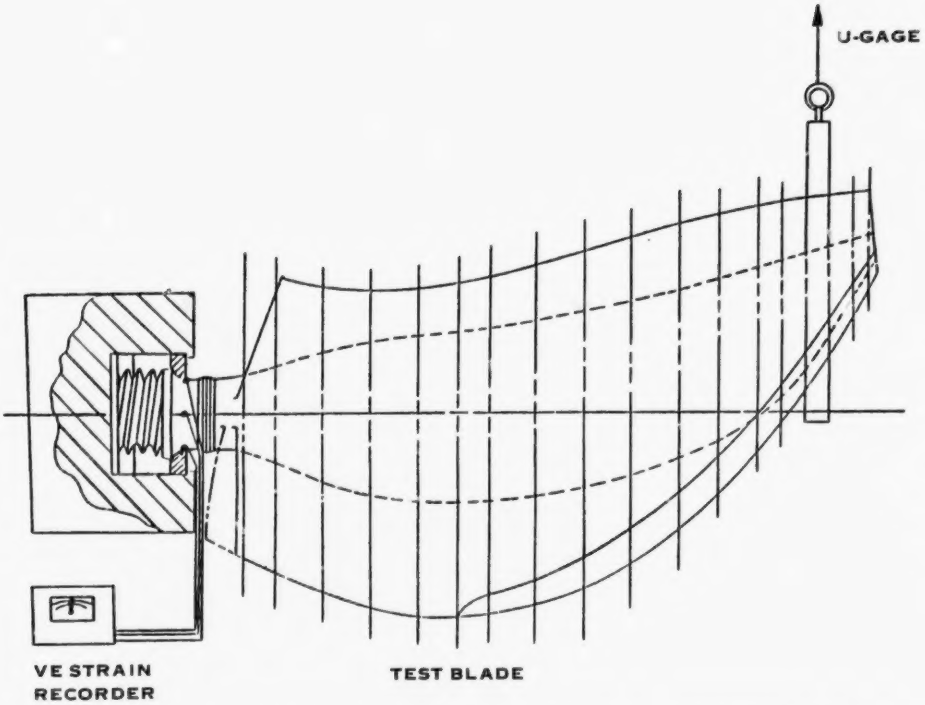
U-GAGE
VE STRAIN
RECORDER
TEST BLADE

FIGURE 14.1 STRESSCOAT TEST ARRANGEMENT - EDGEWISE MODE

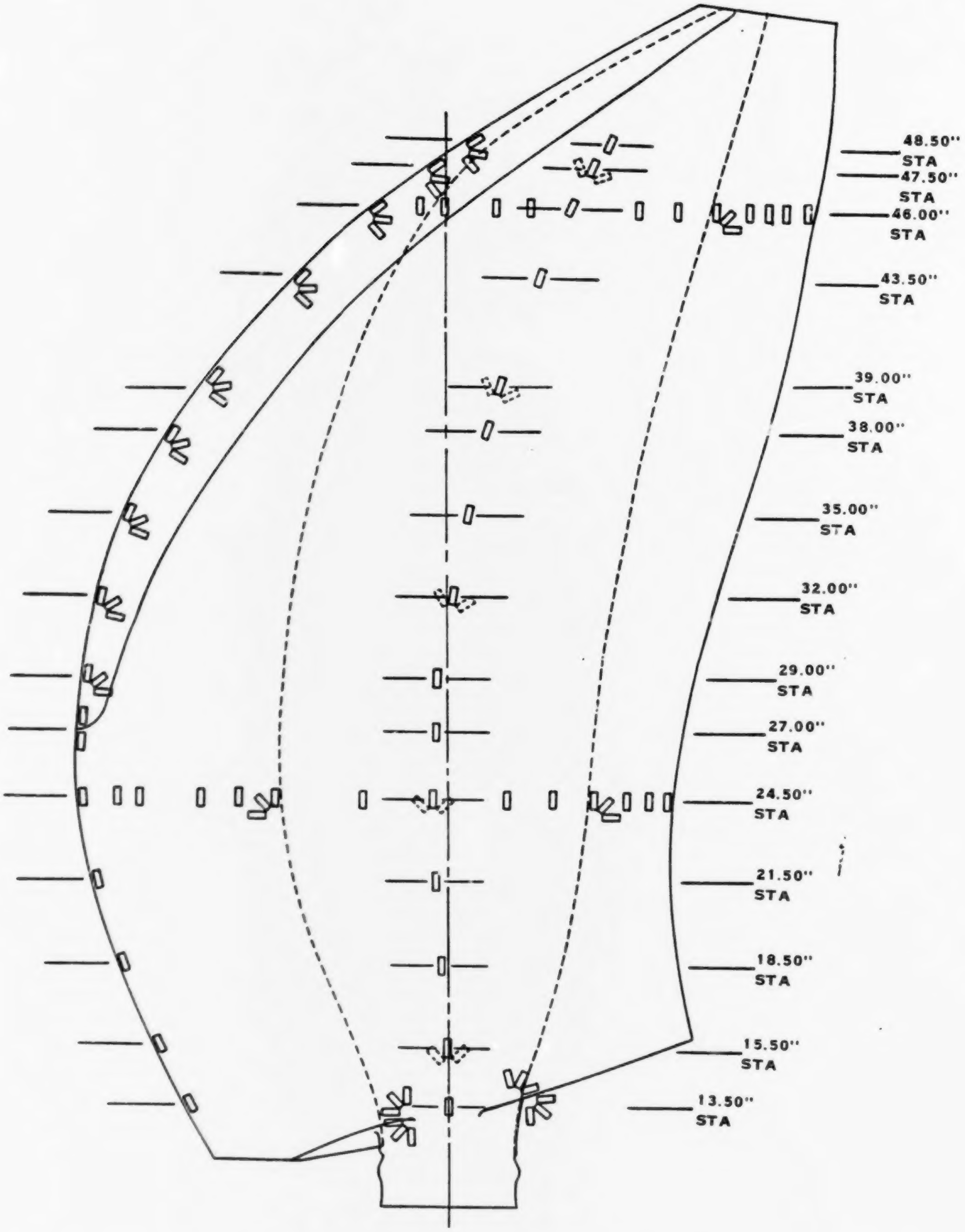
48.50" STA
47.50" STA
46.00" STA
43.50" STA
39.00" STA
38.00" STA
35.00" STA
32.00" STA
29.00" STA
27.00" STA
24.50" STA
21.50" STA
18.50" STA
15.50" STA
13.50" STA

FIGURE 14.2 STRAIN GAGE ARRANGEMENT FOR STATIC AND DYNAMIC TESTING

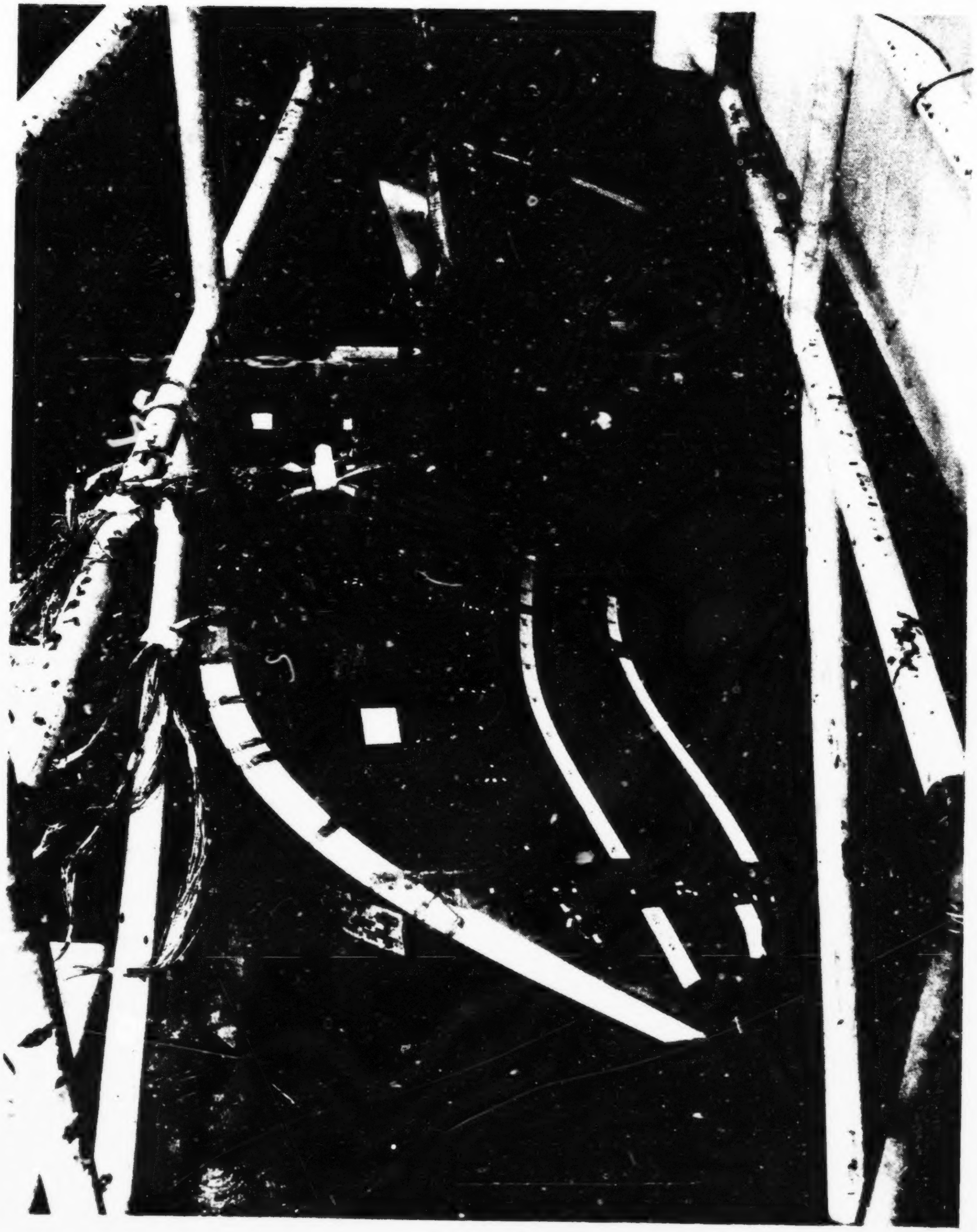

FIGURE 14.3 DYNAMIC STRAIN GAGE TEST CONFIGURATION

ORIGINAL PAGE IS
OF POOR QUALITY

ORIGINAL PAGE IS
OF POOR QUALITY

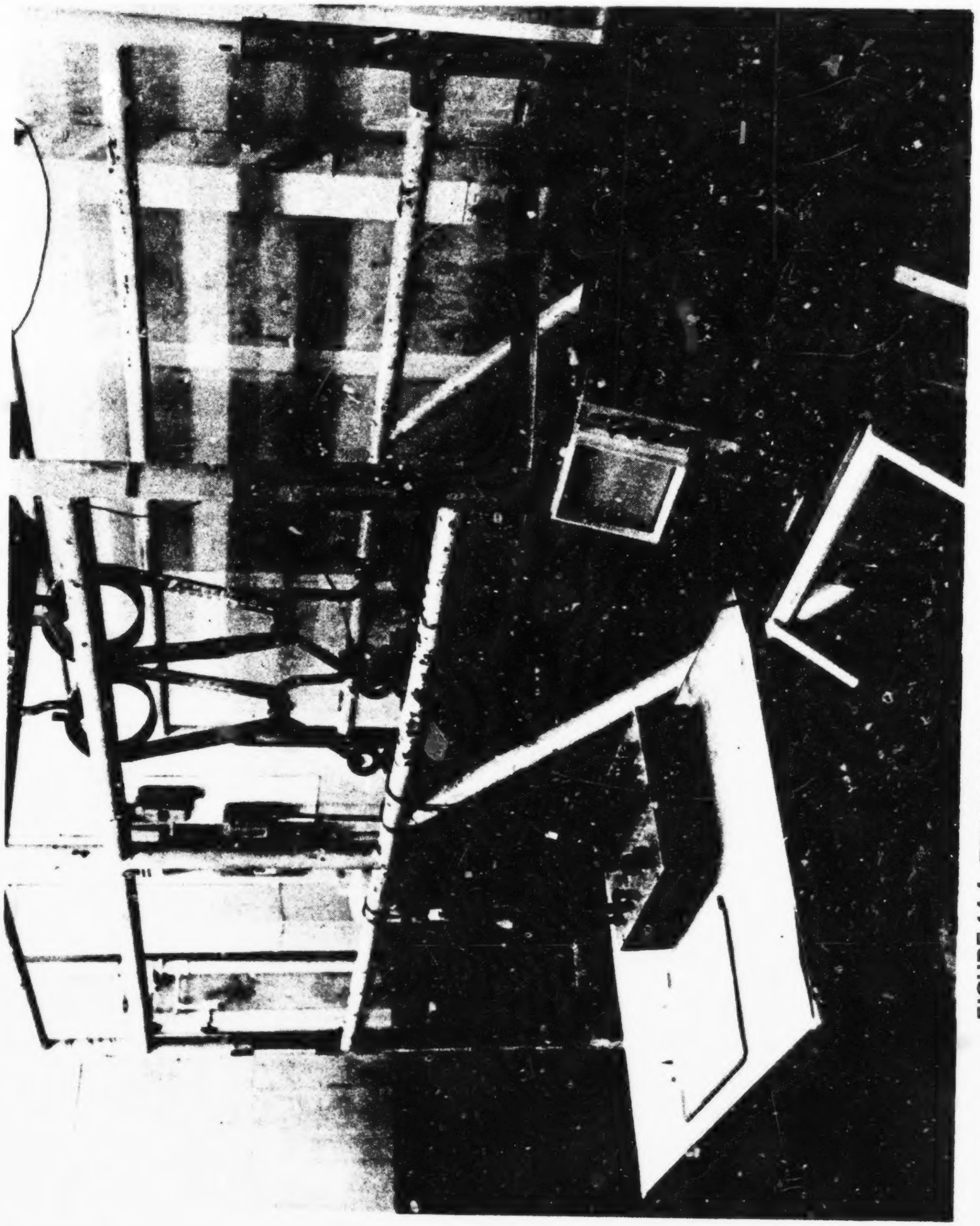

FIGURE 14.4 ZERO MEAN STRESS FATIGUE TEST ARRANGEMENT

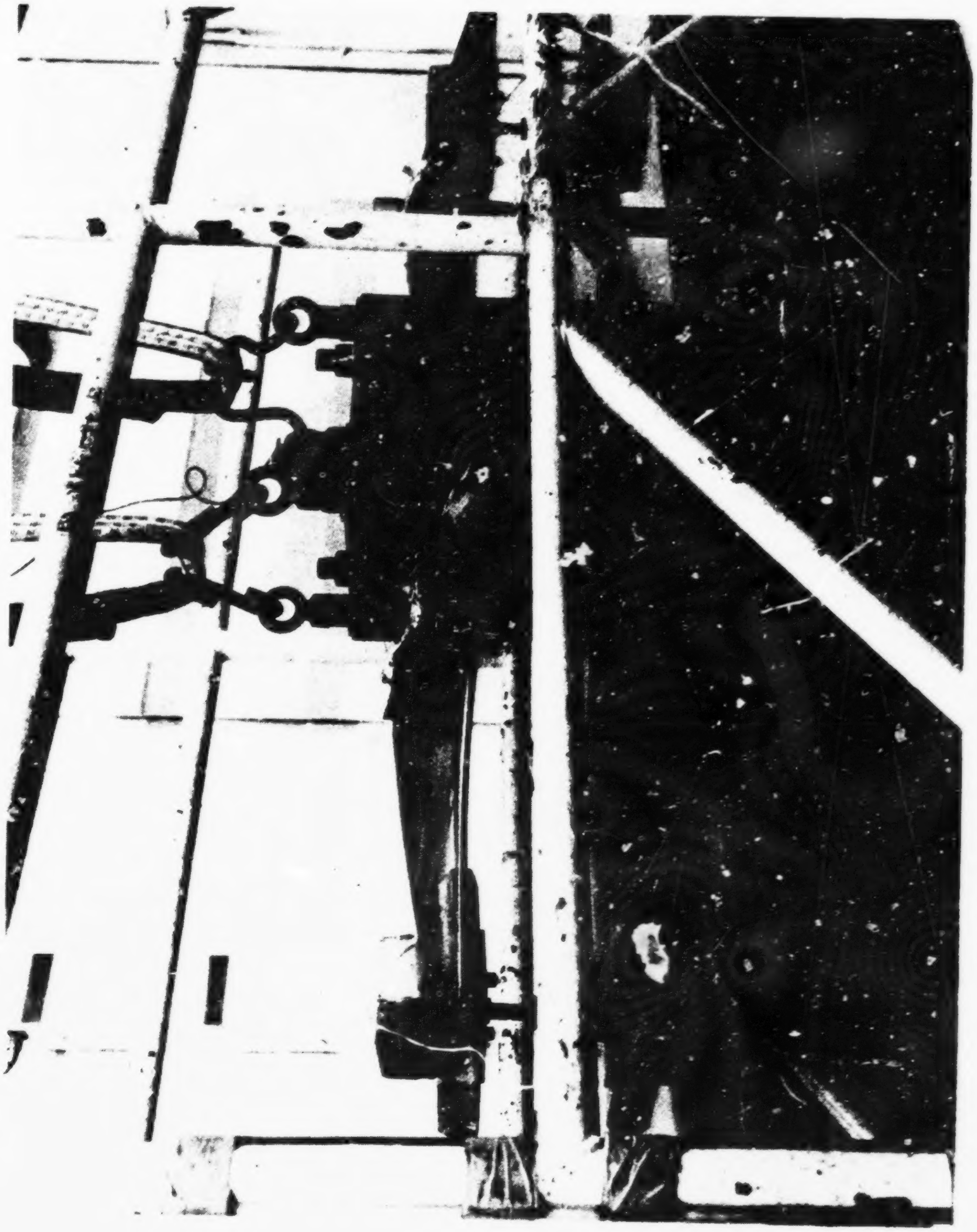

FIGURE 14.5 MEAN STRESS FATIGUE TEST CONFIGURATION

ORIGINAL PAGE IS
OF POOR QUALITY

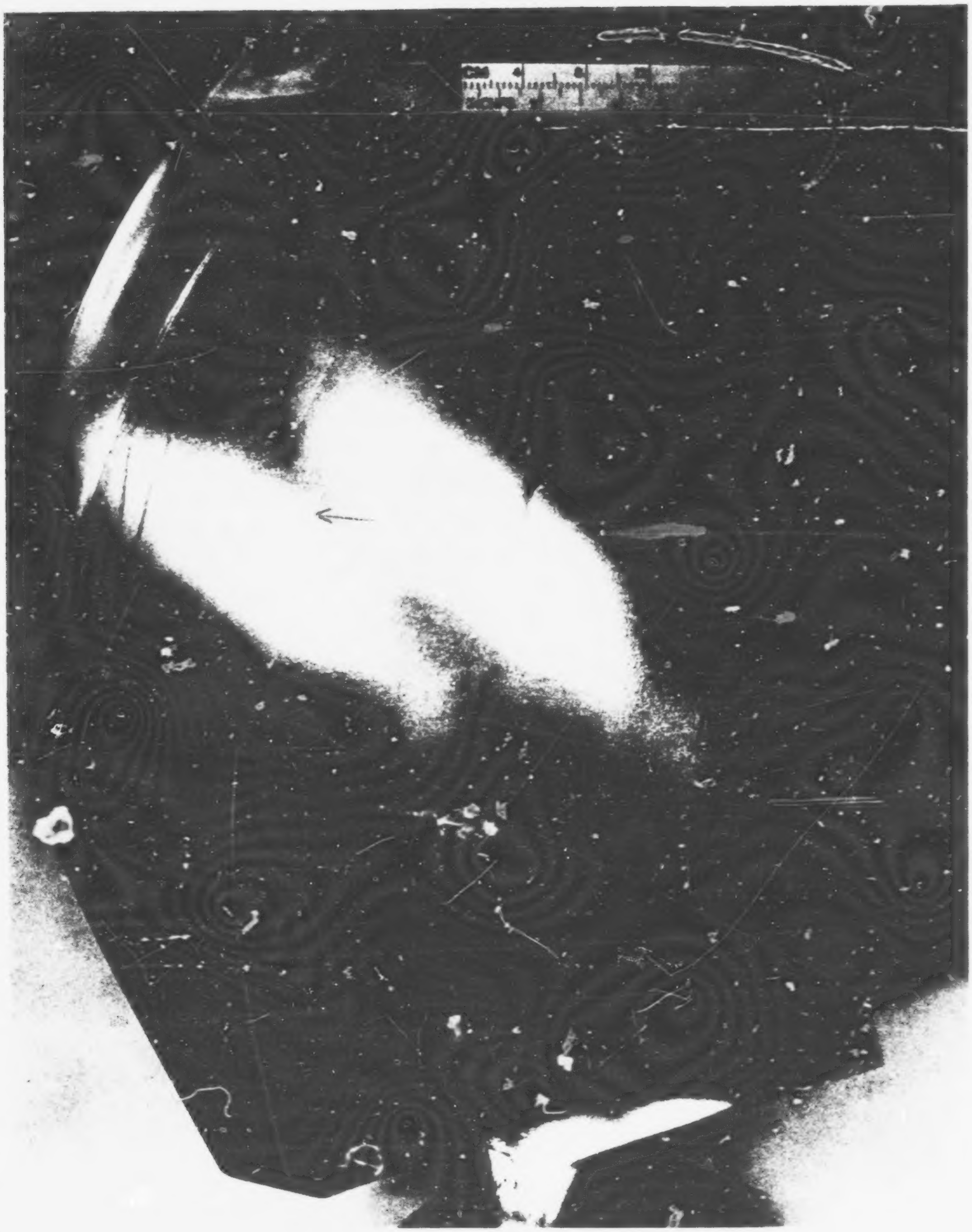

FIGURE 14.6 STRESSCOAT RESULTS, FACE SIDE

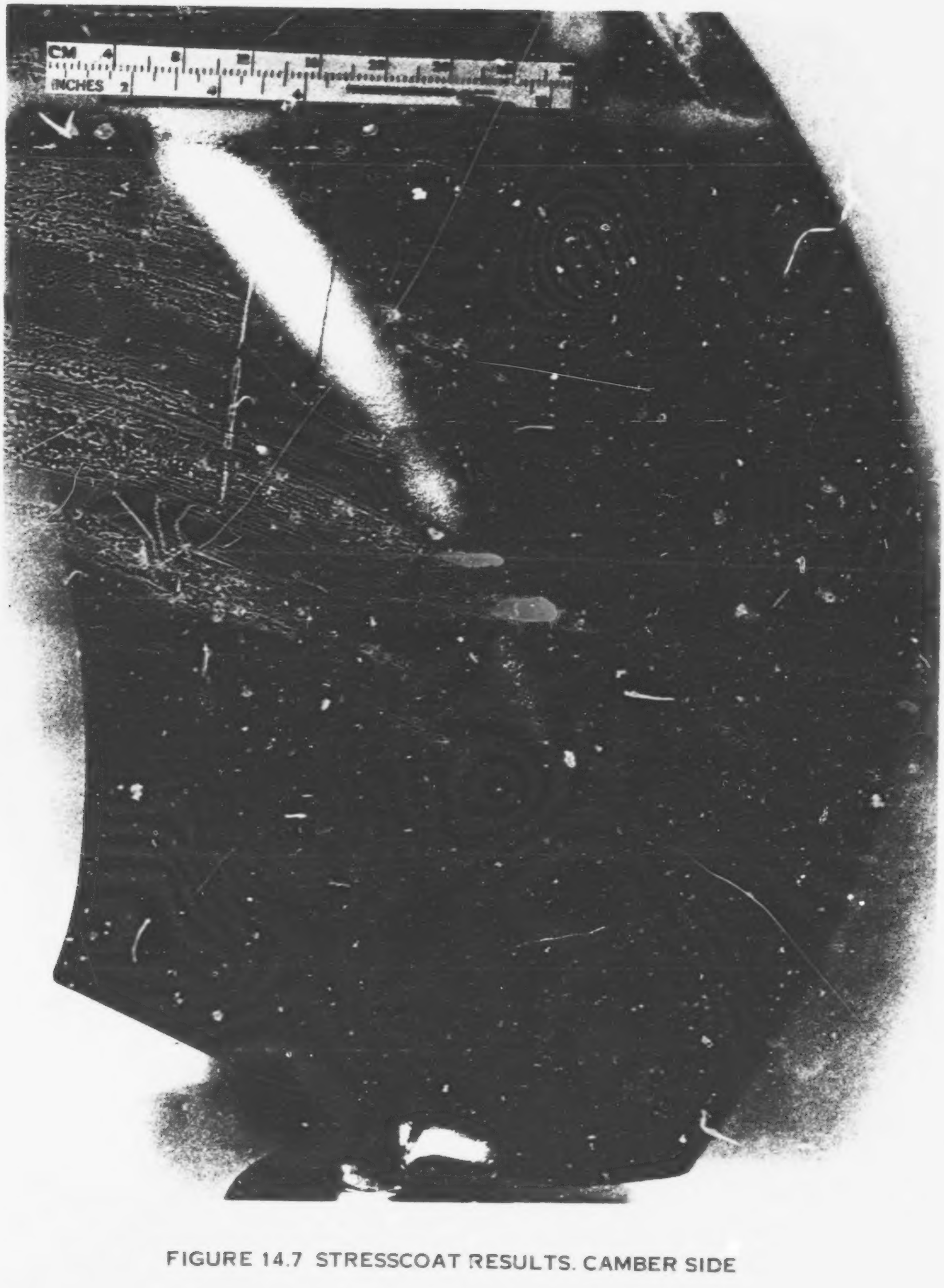

FIGURE 14.7 STRESSCOAT RESULTS. CAMBER SIDE

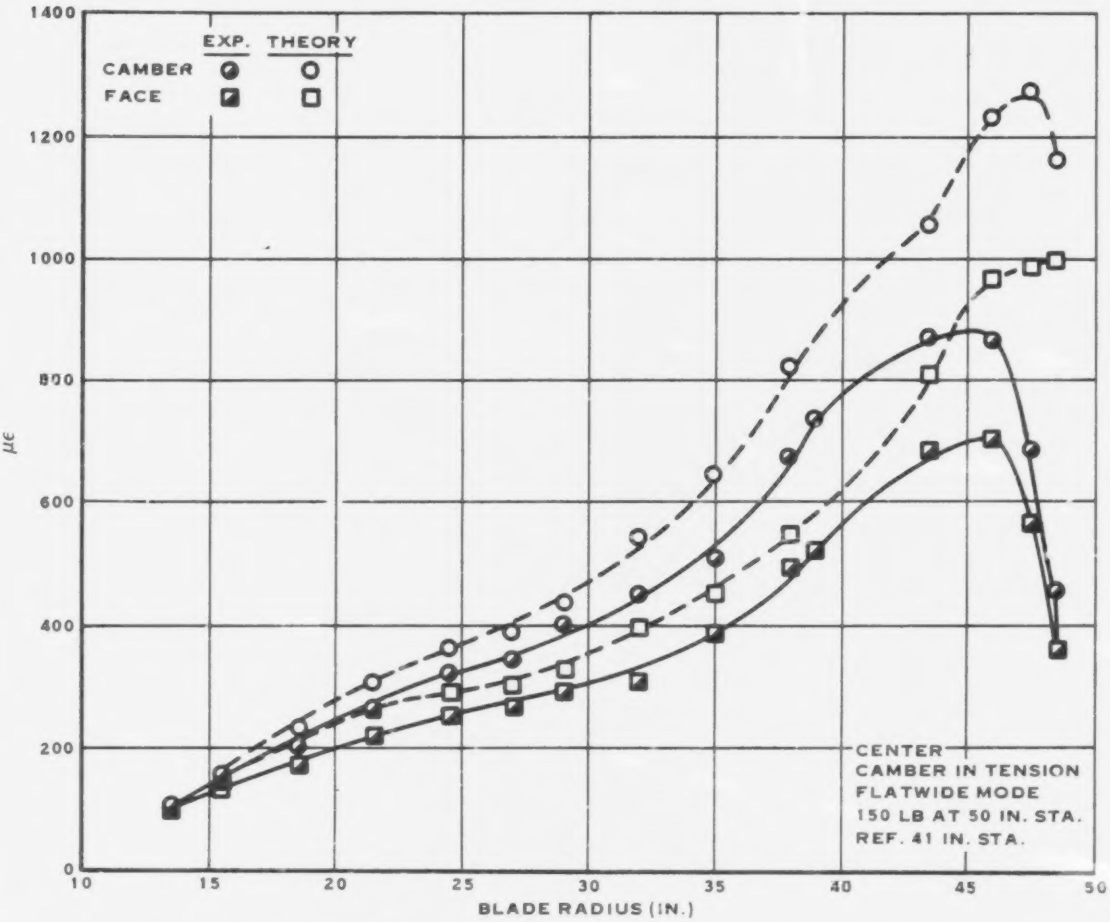

FIGURE 14.8 STATIC STRAIN GAGE ESA - SPANWISE STRAIN DISTRIBUTION ALONG SPAR

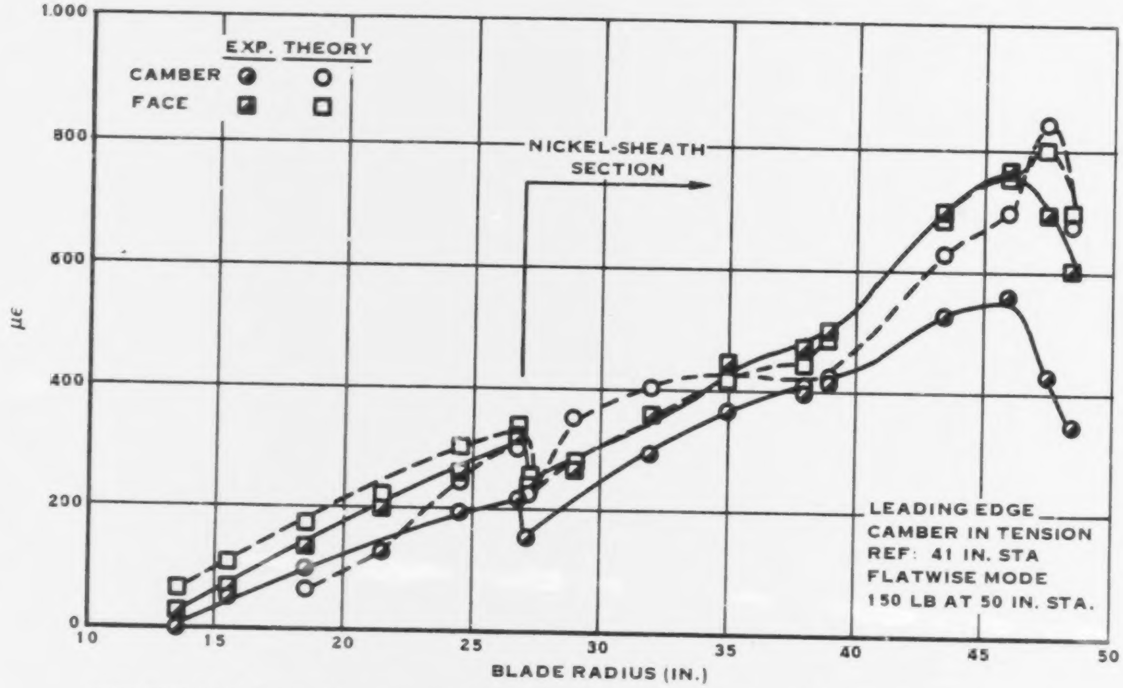

FIGURE 14.9 STATIC STRAIN GAGE ESA - SPANWISE STRAIN DISTRIBUTION ALONG SHEATH

15.0 HUB ESA AND FATIGUE TESTING

- The goals of the LAP hub ESA (experimental Stress Analysis) and fatigue test were:
  - Emperically determine high stress areas on the exterior surface of the hub using a brittle lacquer technique.
  - Quantify stresses in the peak stress areas using strain gaging and controlled loading of the barrel.
  - Evaluate the fatigue strength of the hub and blade retention when subjected to a 1P vibratory loading.

15.1 TEST DESCRIPTION

15.1.1 Hub ESA Test

The hub ESA test was accomplished with the tail shaft secured to a test post in the same manner as it is normally secured to the propeller shaft. Test bars were installed in the hub arm bores using the standard blade retention hardware. A wedge mechanism contained in the test assembly applied simulated centrifugal loads to the test bars. simulated blade bending loads were also applied to the test bars using hydraulic actuators. The magnitude of the loads were monitored by strain gages attached to the test bars. The test assembly is depicted in Figure 15.1.

The hub loading configurations employed for the ESA test were derived from the takeoff and climb design condition described in Table 3-1. The loading for this condition includes a 368690N (82,890 lb) centrifugal blade load, a 4564N-m (40,385 in-lb) blade steady bending moment (SBM); consisting of a 4340N-m (38,408 in-lbs) in plane component and a 1410N-m (12,480 in-lbs) out of plane components, and a 3880N-m (34,338 in-lb) vibratory bending moment; consisting of a 1824N-m (16,146 in-lb) out of plane component (reference Table 4-1). The steady bending moment is accounted for by increasing the centrifugal load by twice the SBM divided by the radius of the blade shank. The centrifugal load then becomes 487299N (109,556 lbs). Steady non-alternating loads corresponding to the amplitude of the vibratory bending moment, were applied to the hub for the ESA test. The nine loading configurations used in the ESA test are illustrated in Figure 15.2. Since the LAP is an 8 blade propeller, loading configurations corresponding to 1P, 4P and 8P vibration modes were included.

The ESA portion of the test consisted of both brittle lacquer and strain gage evaluation of the hub. The hub was first coated with Stresscoat®, a brittle lacquer used to determine the location and direction of principal straining. The loading conditions were tested in the order presented in Figure 15.2. The loads were applied in four or five increments for each condition and the crack pattern in the lacquer was noted at each increment. Once the centrifugal loading of condition one was applied, it was not removed until the completion of the remainder of the loading conditions. The brittle lacquer coating was replaced as required between loading conditions.

15.1.1 (Continued)

At the completion of the brittle lacquer test, strain gages were applied to the hub in the high stress areas indicated by the lacquer crack patterns. A total of 57 gages were applied to the interior and exterior hub surfaces. The loading conditions of Figure 15.2 were rerun, again applying the loads in increments. Stress levels in the barrel were measured at each strain gage location for every load increment. Each loading condition was rerun to ensure repeatability of the results.

15.1.2 Hub Fatigue Test

The hub fatigue test was conducted using basically the same test arrangement that was employed for the ESA test. The hydraulic actuators used to load the test bars were capable of applying vibratory as well as steady loads. The loading configuration used for the fatigue test consisted of the steady centrifugal load of Figure 15.2, item one and the 1P vibratory loading of item six. The 1P loading was applied at a frequency of 17 Hz and a 45° phase angle was maintained between blades by the test rig controller. The 1P loading of Figure 15.2, condition six is 25% greater than the calculated vibratory bending moment for the take off and climb design condition. A total of 50×10^6 cycles were accumulated.

15.2 TEST RESULTS

15.2.1 Hub ESA Test

Table 15-1 presents the loading conditions and increments for which lacquer crack indications were observed and the strain sensitivity of the lacquer coating. Application of the centrifugal load was halted after the second set of indications appeared, because they extended over most of the barrel surface. Typical stresscoat indications for the centrifugal loading case are presented in Figure 15.3. Based on the results of the brittle lacquer test, the peak stress areas were found to be the tailshaft to hub fillet, the blade arm faces, the blade arm aft fillets and the tailshaft.

TABLE 15-1

STRESSCOAT INDICATIONS FOUND AT TESTED LOAD CONDITIONS

% of Load	Sensitivity	Remarks
	Centrifugal Loading	
6%, 14%		No indications
23%		Indications
35%		Indications
	1P-OOP Loading	
25%, 50%, 75%		No indications
Full	.000650 in/in	Indications
	1P @ 142 Loading	
20%, 40%		No indications
60%	.000550 in/in	Indications
80%	.000600 in/in	Indications
Full		No additional indications
	1P-IP Loading	
25%, 50%, 75%, Full	.000550 in/in	No indications
	4P-IP Loading	
25%, 50%, 75%, Full	.000600 in/in	No indications
	8P-IP Loading	
50%, Full	.000475 in/in	No indications
	8P-OOP Loading	
25%, 50%, 75%, Full	.000450 in/in	No indications
	8P @ 252 Loading	
25%	.000520 in/in	Indications
50%		Indications
75%		Indications

15.2.1 (Continued)

The data taken during the strain gage portion of the ESA test exhibited repeatability and the strain response was found to be a linear function of loading. The highest measured static stress resulting from the combination of the centrifugal load steady bending moment and 1P moment was found to occur on the face of one of the arm bores. The measured stress was found to be 48% of the design yield stress for the hub material. The highest strain levels corresponding to the vibratory bending moments occurred for the 1P out of plane loading condition (ref. Figure 15.2, condition 6). This condition is more representative of actual flight than the 1P out of plane condition and is the condition used in the analysis of barrel (reference Section 4.0). The percentage of allowable stress for 10^8 fatigue cycles, resulting from the combination of the steady centrifugal loading and the vibratory loading of condition 6 is presented in Table 15-2. The percentage of allowable stress is presented at several different barrel locations.

TABLE 15-2
% OF ALLOWABLE HUB STRESS FOR 10^8 CYCLES

Location	% Allowable Stress
Shaft of Hub Fillet	27%
Blade Arm Face	35%
Aft Arm Fillet	36%

15.2.2 Hub Fatigue Test

Magnetic particle inspection of all the test hardware was conducted at the conclusion of the fatigue test. No indications of cracking were found in the hub. Ball impressions were noted in the hub races, but the level of wear was not considered excessive. Crack indications were observed on the front and rear cones.

The crack indications found on the cones were all related to fretting patterns found on the cone surfaces. The fretting is attributed to the lack of flexibility in the hub support used for the fatigue test and should not occur on the actual Prop-Fan installation.

ORIGINAL PAGE IS
OF POOR QUALITY

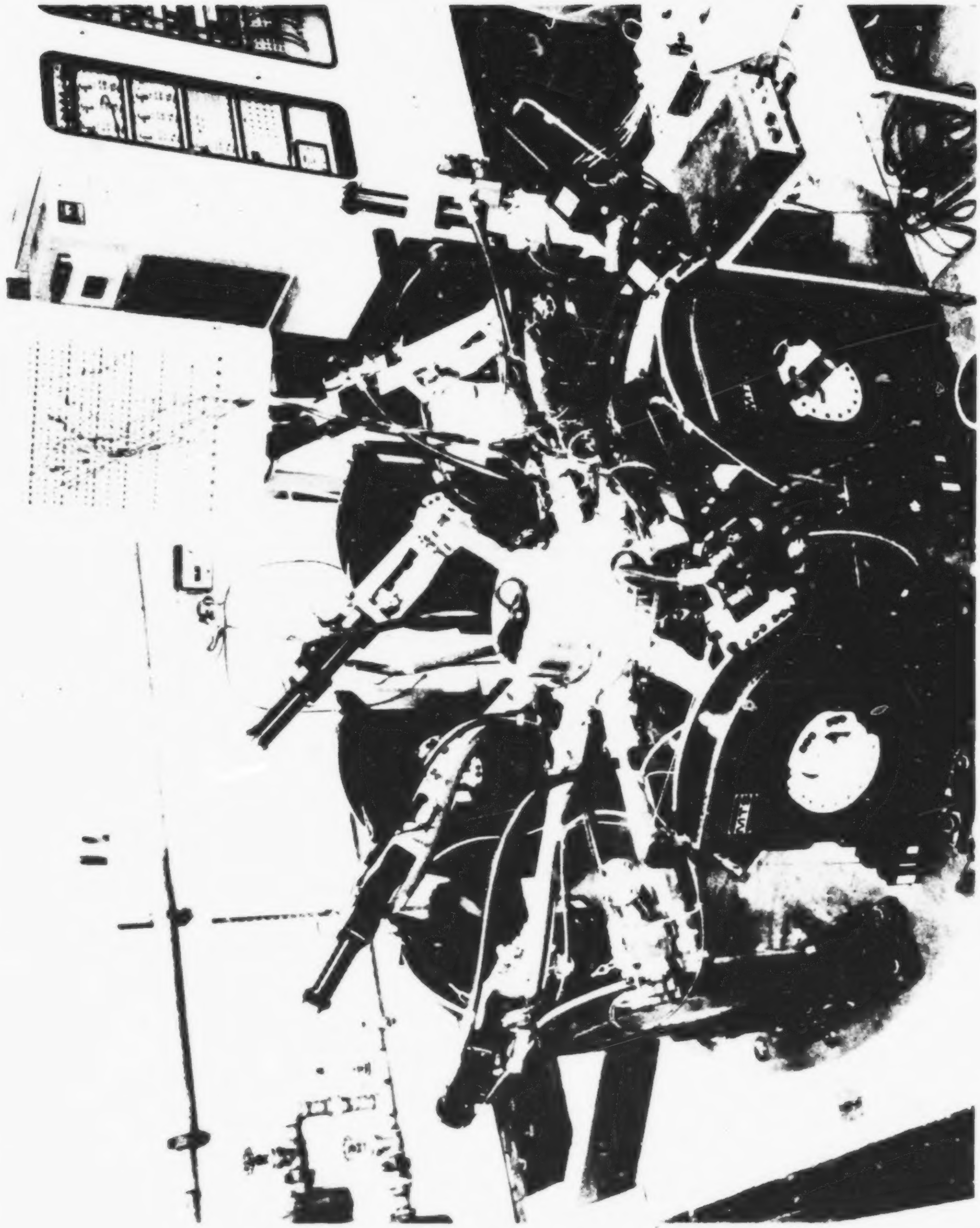

FIGURE 15.1 HUB ESA TEST ARRANGEMENT

TEST MODE	LOADING SEQUENCE	MAXIMUM LOAD OR MOMENT*
1. CENTRIFUGAL	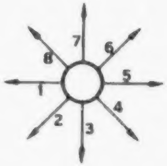	(DESIGN CENT + $\frac{2(\text{SBM})}{R}$) 109,556 LBS
2. 1P-OOP	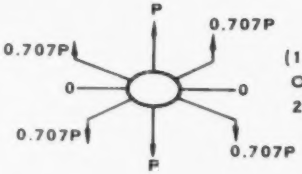 P 0.707P 0 0.707P P 0.707P 0 0.707P	(1.25 X OOP COMPONENT OF 1P) 20,183 IN-LBS
3. 1P-IP	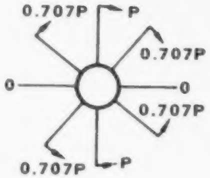 0.707P P 0.707P 0 0.707P P 0.707P 0	(1.25 X IP COMPONENT OF 1P) 27,779 IN-LBS
4. 4P-OOP	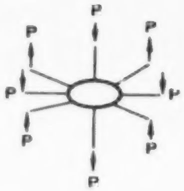	(SAME AS 2) 20,183 IN-LBS
5. 4P-IP	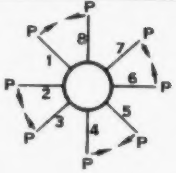 P 1 2 3 4 5 6 7 8 P P P P P P P	(SAME AS 3.) 27,779 IN-LBS
6. 1P @ 142°	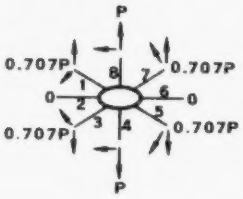 P 0.707P 0.707P 0 0 0.707P 0.707P P 1 2 3 4 5 6 7 8	(1.25 1P) 34,338 IN-LBS
7. 8P-OOP	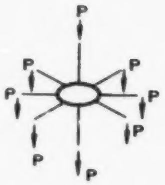	(OOP COMPONENT OF SBM) 38,408 IN-LBS
8. 8P-IP	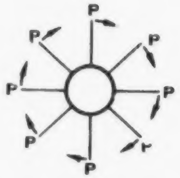	(IP COMPONENT OF SBM) 12,480 IN-LBS)
9. 8P @ 252°	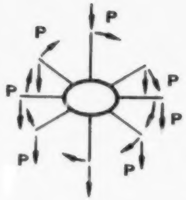	(SBM) 40,385 IN-LBS

FIGURE 15.2 LOADING CONFIGURATIONS FOR HUB ESA TESTING

ORIGINAL PAGE IS
OF POOR QUALITY

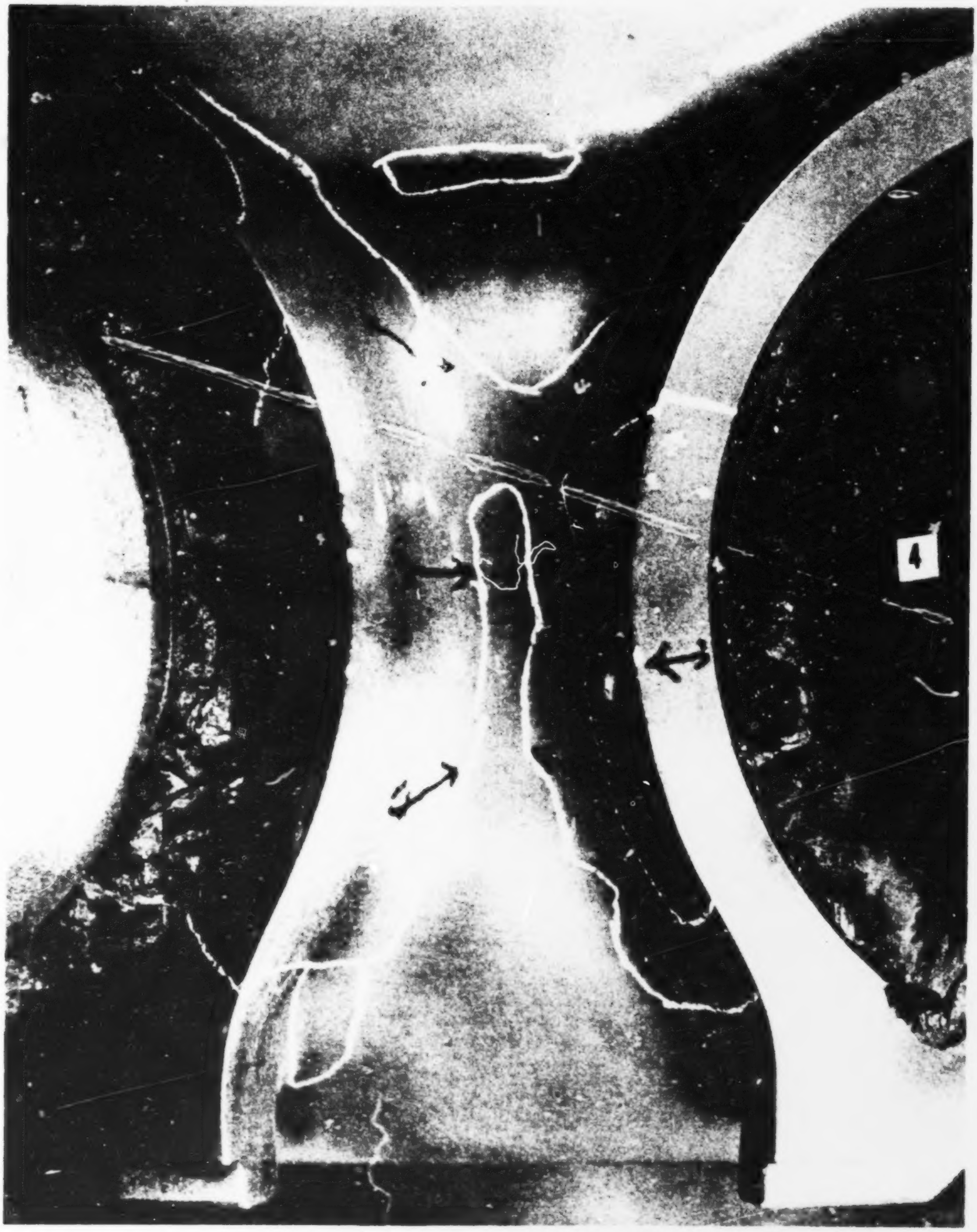

FIGURE 15.3 BRITTLE LACQUER INDICATION, CENTRIFUGAL LOADING

16.0 STATIC ROTOR TEST

16.1 TEST DESCRIPTION

The Static Rotor Test was the first test of the Large Scale Advanced Prop-Fan as a complete assembly. A detailed report of the test is presented in reference 11. The purpose of the test was to measure various Prop-Fan performance characteristics at static operating conditions ($V_\infty = 0$). The specific goals of the test were:

- Determine the static thrust produced and power absorbed by the Prop-Fan over a range of blade pitch angles and rotational speeds.
- Determine the stall flutter or stall buffet restrictions, if any, on the LAP static operating envelope and verify the calculated blade natural frequencies.
- Measure the steady state stresses and deflections of the blade structure and compare these stresses and deflections with analytical predictions.
- Establish the structural integrity of the Prop-Fan by conducting an overspeed test per MIL-P-26366A.
- Measure the steady pressure distribution on the surface of the SR-7L Prop-Fan blade for a range of blade angles and Prop-Fan rotational speeds.
- Evaluate the performance of high frequency response transducers, installed on the SR-7L blade, in measuring time varying pressures on the blade surface.

Testing was conducted on a 7460 KW (10,000 HP) electric motor driven whirl rig at the Wright Aeronautical Laboratory at Wright Patterson Air Force Base in Dayton, Ohio. The Prop Fan is shown installed on the whirl rig in Figure 16.1. No relative air velocity was supplied to the Prop Fan rotor disc. The test procedure consisted of running a series of rotational speeds, with the Prop Fan operating in a fixed pitch mode. The blade pitch angle was changed between runs.

PRECEDING PAGE BLANK NOT FILMED

PAGE 158 INTENTIONALLY BLANK

16.1.1 Aerodynamic Performance Testing

Static aerodynamic performance data was acquired over a range of blade angles from -6° to 60° and a range of rotational speeds from 600 RPM to 1900 RPM. At blade angles above 30° the maximum RPM was limited by blade vibratory stress levels. The actual test points are listed in Table 16-1. Blade angle, ambient temperature and ambient pressure were measured and recorded before and after each test run.

Net power absorbed by the Prop Fan was determined by subtracting empirically determined electrical and mechanical losses from the measured electrical power supplied to the test rig electric motor. Net power and thrust were corrected to standard conditions by multiplying them by the ratio of standard to ambient air density. The air density ratio was computed from the ambient pressure and temperature recorded before and after each run. The power and thrust data were also non-dimensionalized to coefficient form for comparison with analytically predicted static performance.

16.1.2 Structural Dynamic Testing

Structural dynamic data was gathered concurrently with the aerodynamic performance data. Structural dynamic data was acquired using the strain gage arrangement shown in Figure 16.2. A total of 54 strain gages were applied to the Prop Fan blades with thirty primary gages active at any one time. The gage locations were chosen to correspond with the analytically predicted areas of peak vibratory strain. The strain gage signals were recorded on magnetic tape for a minimum of 30 seconds at each test point.

The total vibratory strain data was digitized and statistically analyzed to produce tables of mean strain, standard deviation of strain and mean strain plus twice the standard deviation $(\bar{X} + 2\sigma)$. The terminology for the $(\bar{X} + 2\sigma)$ strain is infrequently repeating peak (IRP) strain and is referred to in this report as vibratory strain.

Spectral analysis of the data was conducted to determine the frequency content of the vibration. The spectral analysis also allowed Campbell plots to be constructed, presenting the blade natural frequencies as a function of RPM. The dependence of the blade natural frequencies on blade angle (β 3/4) was also determined.

TABLE 16-1

TEST POINTS FOR AERODYNAMIC PERFORMANCE AND STRUCTURAL DYNAMIC TESTING

Blade Angle (B 3/4)	RPM
-5.7°	600, 700, 800, 900, 1000, 1100, 1200, 1300, 1400, 1500, 1600, 1650, 1700, 1750, 1800, 1850, 1900
-2.0°	600, 700, 800, 900, 100, 1100, 1200, 1300, 1400, 1500, 1600, 1650, 1700, 1750, 1800, 1850, 1900
0.2°	600, 700, 800, 900, 1000, 1100, 1200, 1300, 1400, 1500, 1600, 1650, 1700, 1750, 1800, 1850, 1900
2.0°	600, 700, 800, 900, 1000, 1100, 1200, 1300, 1400, 1500, 1600, 1650, 1700, 1750, 1800, 1850, 1900
6.1°	600, 700, 800, 900, 1000, 1100, 1200, 1300, 1400, 1500, 1600, 1650, 1700, 1750, 1800, 1850, 1900
10.0°	600, 700, 800, 900, 1000, 1100, 1200, 1300, 1400, 1500, 1600, 1650, 1700, 1750, 1800, 1850, 1900
14.1°	600, 700, 800, 900, 1000, 1100, 1200, 1300, 1400, 1500, 1600, 1650, 1700, 1750, 1800, 1850, 1900
18.2°	600, 700, 800, 900, 1000, 1100, 1200, 1300, 1400, 1500, 1600, 1650, 1700, 1750, 1800, 1850, 1900
22.1°	600, 700, 800, 900, 1000, 1100, 1200, 1300, 1400, 1500, 1600 1650, 1700, 1750, 1800, 1850, 1900
25.8°	600, 700, 800, 900, 1000, 1100, 1200, 1300, 1400, 1500, 1600, 1650, 1700, 1750, 1800, 1850, 1900
30.3°	600, 700, 800, 900, 1000, 1100, 1200, 1300, 1400, 1500, 1600, 1650, 1700, 1750, 1800, 1850, 1900

TABLE 16-1 (Continued)

TEST POINTS FOR AERODYNAMIC PERFORMANCE
AND STRUCTURAL DYNAMIC TESTING

Blade Angle (B 3/4)	RPM
32.1°	700, 800, 900, 1000, 1100, 1200, 1300, 1400, 1500, 1600, 1700
33.5°	700, 800, 900, 1000, 1100, 1200, 1300, 1400, 1500, 1600, 1700
34.3°	600, 700, 1000, 1100, 1200, 1300
38.1°	600, 700, 800, 900, 1000, 1100, 1200
42.0°	600, 700, 800, 900, 1000, 1100, 1200
49.9°	600, 700, 800, 900, 1000, 1100, 1200
55.0°	600, 700, 800, 900, 1000, 1100
60.1°	600, 700, 800, 900, 1000, 1100

16.1.3 Blade Steady State Strain and Deflection Measurement

Steady state structural data was acquired at three operating points for which a static finite element analysis of the blade had been conducted. This permitted comparison of analytically and experimentally determined blade stresses and deflections. Operation at test point 3 was maintained for one hour, which constituted an overspeed test per MIL-P-26366A. The test points are presented in Table 16-2.

TABLE 16-2

STEADY STATE STRUCTURAL TEST POINTS

Test Point	Blade Angle (B 3/4)	RPM
1	22°	1700
2	32.1°	1700
3	25.8°	2038

16.1.3 (Continued)

The blade strain gage arrangement used during the steady state stress and deflection portion of the test is shown in Figure 16.3. The locations of gages 414 and 416 were chosen to correspond with the points of predicted maximum steady compressive and tensile stress respectively on the face side of the blade. The location of gages 415 and 417 correspond with the points of predicted maximum steady compressive and tensile stress respectively on the camber side of the blade. Strain gages 89, 81, 82, 813 and 83 provided the capability to determine the radial distribution of stress along the blade.

Blade deflection measurements were made using two separate systems, an optical system and a laser based system. The optical system consisted of a transit type telescope mounted on a carriage and track assembly, a linear scale and a strobe light. The scope was located beneath the Prop-Fan and viewed upward at the advancing blades passing through horizontal. The carriage allowed the scope to be moved back and forth parallel to the axis of rotation, as well as laterally. The axial movement of the scope was controlled by a handwheel and worm gear mechanism, which allowed precise adjustment of the scope position. The axial position of the scope was measured with the linear scale. The strobe light was triggered by the rotation of the whirl rig shaft. The phase could be adjusted to freeze the rotor with a blade in the horizontal position. The axial location of the blade leading and trailing edges at any station were determined by adjusting the position of the scope until the crosshairs were aligned with these points.

The laser deflection measurement system consisted of four helium-neon lasers and four photodetectors. One laser is reflected from a mirror on the Prop-Fan spinner back to a detector to provide a once per revolution indication. The remaining three lasers were oriented so that their beams passed obliquely through the Prop-Fan rotor disc and were received at three additional photodetectors. These laser beams intersected the blade in the six o'clock position at the 50% span, the 75% span and tip stations. As the blade intersects the beams, light going to the detectors is blocked and the detector output goes low. After the blade trailing edge passes the beam, light going to the detector is restored and the detector output goes high. Therefore the outputs of the detectors are rectangular wave forms when the Prop-Fan is rotating. The deflection of the blade is determined by relating changes in the timing of the waveforms to changes in the geometry of the blade.

16.1.4 Blade Surface Steady Pressure Testing

The purpose of steady surface pressure testing was to determine the pressure distribution around airfoil sections at ten spanwise stations on the SR-7L blade. The pressure distribution was measured over a range of rotational speeds for blade angles of 21.7°, 32° and 38.3°.

The locations of the pressure taps on the specially modified blade used for steady pressure measurement are depicted in Figure 16.4. Each column of pressure taps was connected to a radial passage embedded in the surface of the blade and leading to the shank. Each radial passage was connected to one

16.1.4 (Continued)

channel of a scanivalve. This system allowed the pressure distribution to be measured at only one radial station at a time. Pressure taps at all other stations must be capped. In order to measure the pressure distribution over the entire blade surface for one operating condition, ten separate runs were required at that condition.

The test procedure consisted of setting a blade angle and running the desired range of rotational speeds at the angle. Pressure data was recorded from every tap in the exposed chordwise row at each speed. The test rig was then shutdown, the exposed row of taps was covered and a new row of taps was uncovered. Data was then taken at the same rotational speeds as the previous run. This procedure ensured that all of the data for a pressure map of the blade at a particular operating condition was gathered at a constant blade angle.

The steady pressure test points were run at rotational speeds corrected for ambient temperature, so that the pressure data could be compared for a constant blade surface Mach number. Test data was taken at points of constant corrected RPM. The rotational speed correction is calculated per equation 16.1. The test points at which steady pressure data was acquired are listed in Table 16-3.

$$RPM_{act} = RPM_{corr} \sqrt{\frac{273° + t_{amb}}{273° + 15°}} \qquad (16.1)$$

where:

T_{amb} = ambient temperature, °C
PRM_{corr} = corrected RPM
RPM_{act} = actual RPM at which data is taken

TABLE 16-3 STEADY PRESSURE TEST POINTS

Press. Tap Row	B 3/4	Temp (°C)	RPM_{act}
10	21.7°	18	906, 1308, 1508, 1709, 1791
9	21.7°	17	903, 1305, 1505, 1705, 1786
8	21.7°	16	902, 1302, 1503, 1702, 1783
7	21.7°	16	902, 1302, 1503, 1703, 1783
6	21.7°	15	900, 1300, 1500, 1700, 1780
5	21.7°	16	902, 1302, 1503, 1704, 1784
4	21.7°	15	900, 1300, 1500, 1700, 1780
3	21.7°	14	898, 1298, 1497, 1697, 1777
2	21.7°	13	897, 1295, 1495, 1694, 1774
1	21.7°	12	895, 1293, 1492, 1692, 1771
10	32.0°	21	909, 1313, 1516, 1717
9	32.0°	21	909, 1313, 1516, 1718
8	32.0°	21	909, 1313, 1516, 1718

TABLE 16-3
STEADY PRESSURE TEST POINTS (Continued)

Press. Tap Row	ß 3/4	Temp (°C)	RPM_{act}
8	32.0°	21	909, 1313, 1516, 1718
7	32.0°	21	909, 1313, 1516, 1718
6	32.0°	21	909, 1313, 1516, 1718
5	32.0°	12	895, 1293, 1492, 1691
4	32.0°	12	895, 1293, 1492, 1691
3	32.0°	12	895, 1293, 1492, 1691
2	32.0°	12	895, 1293, 1492, 1691
1	32.0°	12	895, 1293, 1492, 1691
10	38.3°	24	914
9 thru 1	38.3°	19	906

16.1.5 Blade Surface Unsteady Pressure Testing

The primary purpose of unsteady pressure testing was to evaluate the capability of transducers installed on the SR-7L blade to measure time varying pressures on both the face and camber side surfaces of the blades. The impetus for developing the ability to monitor unsteady blade surface pressures was the wind tunnel testing planned as a follow on to the Static Rotor Test. Operation of the Prop-Fan at a yaw angle relative to the flow was included in the agenda for the High Speed Wind Tunnel test. Operation at a yaw angle results in a continuous variation of the angle of attack seen by the blade as it rotates through 360°. This theoretically yields a 1P cylical variation of the surface pressure.

Twenty six pressure transducers were installed in two rows on the face and camber sides of the blade that was specially fabricated for unsteady pressure testing. The locations of the transducers are shown in Figure 16.5. The dynamic pressure range for the transducer used in the unsteady pressure measurement blade was ± 15 psi. The frequency response of the system was 0 to 1000 HZ.

In order to produce a time variation of the pressure sensed by the transducers during a static test, an aerodynamic obstruction was erected in front of the Prop-Fan. The obstruction was a four inch diameter cylinder that spanned from the blade root to well beyond the blade tip. The centerline of the cylinder was located 24 inches in front of the blade pitch change axis. The wake generated by the inflow to the Prop-Fan, passing over the obstruction, was intended to create a once per revolution disturbance for the transducers to pass through. Data was recorded at each Prop-Fan operating condition both with the obstruction in place and the obstruction removed. Test points were run at speeds corrected for ambient temperature as described in section 16.1.4. The unsteady pressure test points are presented in Table 16-4.

TABLE 16-4
BLADE SURFACE UNSTEADY PRESSURE TEST POINTS

B 3/4 (Deg.)	RPM	Temp (°C)	Obstruction
21.9	594	9	None
21.9	891	9	None
21.9	1286	9	None
21.9	1484	9	None
21.9	1682	9	None
21.9	1880	9	None
21.9	594	9	4" diameter cylinder
21.9	891	9	4" diameter cylinder
21.9	1286	9	4" diameter cylinder
21.9	1484	9	4" diameter cylinder
21.9	1682	9	4" diameter cylinder
21.9	1880	9	4" diameter cylinder
31.7	592	8	None
31.7	887	8	None
31.7	1282	8	None
31.7	1478	8	None
31.7	1676	8	None
31.7	596	11	4" diameter cylinder
31.7	894	11	4" diameter cylinder
31.7	1291	11	4" diameter cylinder
31.7	1490	11	4" diameter cylinder
31.7	1688	11	4" diameter cylinder
38.2	596	11	None
38.2	894	11	None
38.2	1192	11	None
38.2	596	11	4" diameter cylinder
38.2	894	11	4" diameter cylinder
38.2	1192	11	4" diameter cylinder
32.0	600	15	4" cylinder with plate
32.0	900	15	4" cylinder with plate
32.0	1200	15	4" cylinder with plate
32.0	1700	15	4" cylinder with plate

16.2 RESULTS AND DISCUSSION

16.2.1 Aerodynamic Performance

Curves of corrected power and thrust versus blade angle for a constant RPM are presented in Figure 16.6. The non-dimensionalized data is also overlayed on the predicted curves of power coefficient versus blade angle and thrust coefficient versus power coefficient in Figure 16.7.

Examination of Figure 16.6 illustrates the behavior of the static thrust produced by the Prop-Fan as a function of the blade angle. A smooth increase in thrust is observed between blade angles of zero and thirty degrees. Thrust then decreases slightly between blade angle of 30° and 34° and then is essentially constant from 34° to 60°. Figure 16.7 depicts an abrupt departure of power and thrust data from predicted values as blade angle is increased beyond 30°. Both thrust produced and power absorbed by the Prop-Fan are lower than predicted above blade angles of 30°.

The reason for the shortfall in static performance at high blade angle is not clear from the data presented here. Referring to the thrust versus blade angle data in Figure 16.6 the deviation of the measured and predicted performance occurs at the same blade angle, independent of the RPM. Since the performance shortfall is observed at rotational speeds as low as 900 RPM, it is unlikely that it was caused by shock separation or compressibility. This type of behavior may be indicative of stall. However, calculations indicate angles of attack well below stall at the outboard blade sections for blade angles beyond 34°.

In view of the unusual shapes observed in LAP performance curves, the data from previous static tests of single rotation Prop-Fan wind tunnel models was carefully reviewed. Under close examination it was found that the unusual shapes of the C_P versus β 3/4 and C_T versus C_P curves were present to some degree in all prior test data for single rotation Prop-Fan configurations including the SR-2, SR-3, and SR-5 (reference Figure 2.1).

16.2.2 Structural Dynamic Test Results

Testing revealed no significant blade vibratory stress levels for blade angles in the range from -6° to 25° up to rotational speeds of 1900 RPM. The first vibratory stress limit was encountered at a 32° blade angle. An audible change in the sound produced by the Prop-Fan was perceived when the blade angle was increased over 30°. The audible sound level increased and the tonal frequency decreased. No acoustic measurements were taken during the tests to confirm these observations. The Prop-Fan speed was limited for blade angles above 30°. Figure 16.8 shows a map of the speeds and blade angles where vibratory stresses were recorded and where vibratory stress limits were reached.

The blade vibratory stress limits were encountered in the blade tip region at gage locations 23, 24, 73 and 83 (ref Figure 16.2). The vibratory stresses, measured at the other gage locations remained below their limits. The vibratory stress is characterized as buffet rather than flutter because the stress level and frequency content was unsteady in nature, the stress amplitude did not increase suddenly and no mode sustained a sinusoidal response. Buffet is caused by a flow instability and the structure responds to the broad band excitation produced by the flow instability.

Spectral analysis revealed that the frequency content of the buffet is not independent of blade angle. At a blade angle of 34° and 1300 RPM the dominant frequency of the buffet was shown to be 92.5 HZ which corresponds to the predicted second flatwise bending mode (ref Figure 3.7). At blade angles above 39° the response changed from the second flatwise mode, to the first flatwise mode, with a predominant frequency of 35HZ. The flatwise response at 35 HZ is very close to the 2P first mode critical speed. Therefore the 2P excitation may influence the blade response.

A Campbell plot of the SR-7L blade natural frequencies is presented in Figure 16.9. The figure shows good agreement between data and the calculated natural frequencies at 100% speed. The data presented in the Campbell plot is representative of all the blade angles tested and the condensed scale does not show the effect of blade angle on the blade natural frequency. To examine the blade angle effect the data was replotted versus blade angle in Figure 16.10 for three rotational speeds. The first and second flatwise bending modes decrease in frequency with increasing blade angle, the first edgewise mode increases in frequency and the first torsional mode is relatively unaffected by blade angle. These trends are typical for rotating blades.

16.2.3 Blade Steady Strain and Deflection

16.2.3.1 Steady Strain Results

At the overspeed condition of 2038 RPM and 25.8° blade angle, the normalized radial distribution of strain compares very well with the predicted blade strain as shown in Figure 16.11. The measured distribution is shown to be slightly higher in the inboard portion of the blade than predicted. A more detailed comparison of the strain distribution at all the locations where strain was measured is shown in Figure 16.12. The comparison is very good except for the measurement on the trailing edge of the blade (gage 24) and at the tip of the blade (gage 416). At gage 24 the strain is substantially higher than predicted while at gage 416 the measured strain is lower than predicted.

16.2.3.2 Steady Deflection Results

Initial testing accomplished with the optical blade deflection measurement system revealed that the 50% span and 75% span stations on the horizontal blade were obscured from view by the blade in the 45° below horizontal position. Therefore blade deflection data was only collected at the tip blade station using the optical system.

Figure 16.13 presents the blade tip twist deflection as a function of the square of the Prop-Fan rotational speed for a blade angle of 25.8°. Data acquired both with the optical and laser systems is presented in this figure. The centrifugal and aerodynamic loads on the blades are proportional to the rotational speed squared. Therefore plotting blade deflection versus RPM squared should yield a straight line. Figure 16.14 presents the deflection data taken at the 50% span, 75% span and tip blade stations overlayed on the calculated twist deflection distributions for a blade angle of 32°.

Examination of the plots of blade deflection versus RPM squared revealed that the data acquired with the laser system is well behaved and approximates a straight line. However a large amount of scatter is seen in the optical data. Comparing the measured and predicted blade deflection distribution between 50% span and the tip, some large percentage discrepancies are noted. However the actual error in terms of degrees is small. The characteristic shape of the spanwise distribution of blade twist also seems to be matched well by the data. It can therefore be concluded that the difference between the desired and actual deflected blade shapes did not significantly effect the aerodynamic performance of the Prop Fan.

16.2.4 Blade Surface Steady Pressure Results

The blade surface pressure data obtained was generally well behaved. The shape of the curves of pressure coefficient versus percent chord was reasonable for all the blade stations at which data was taken. Figures 16.15 and 16.16 present the variation of chordwise pressure coefficient distribution with blade angle for the airfoil sections closest to the blade root and tip at which pressure distribution was measured. The variation of the surface pressure distribution with blade angle suggests why the measured thrust begins to fall short of the predicted thrust for blade angles greater than 32° as discussed in section 16.2.1. Data presented in Figure 16.15 for the inboard most station ($r/R = .287$) shows that the area between the face and camber side pressure distribution curves increases continuously as blade angle is increased from 22° to 38°. This implies that the airfoil section normal force coefficient increases continuously with blade angle from 22° to 38°. Data presented in Figure 16.16 for the outboard most section at which data was collected ($r/R = .961$) reveals that the area between the face and camber side pressure distribution curves decrease continuously, as blade angle is increased from 22° to 38°, implying that the section normal force coefficient also decreases continuously. Since thrust does not increase as blade angle advances beyond 30° it is concluded that the increase in loading in the inboard portion of the blade is being offset by the unloading of the blade tip.

16.2.5 Blade Surface Unsteady Pressure Results

Initially, comparison of data with and without the obstruction did not show any indication that an aerodynamic disturbance was sensed by the transducer. This data was typical for all the functional transducers on the blade. It was concluded that either the obstruction was not generating a significant wake or the transducers were not passing through the wake, due to a large radial component of the inflow to the Prop-Fan. Radial inflow is typical of propeller static operation.

The aerodynamic obstruction was altered in order to generate a wake that would be intersected by the blade stations containing the transducers. The modification consisted of attaching plates to the cylindrical post. Tufts were also attached to the obstruction in an attempt to visualize the inflow to the Prop-Fan passing around the obstruction. The motion of the tufts was recorded on video tape.

When testing was resumed with the modified obstruction in place, a once per revolution pressure pulse was detected by most of the transducers located on blade station 35.0. The amplitude and the width of the pulses were variable from transducer to transducer at that station. Figure 16.17 shows a plot of the surface pressure versus time at the transducer location where the pressure pulse was most pronounced.

16.2.5 (Continued)

The pressure pulse was not detected by any of the transducers on blade station 49.0. A review of the videotape of the run indicated that the wake eminating from the plate obstruction may not have been intersected by blade station 49.0. Therefore the failure to detect the wake at that station does not indicate a shortcoming of the instrumentation.

The transducers demonstrated the ability to detect pressure pulses of 13.80 Pascal (.2 psig) amplitude and durations of less than 10 milliseconds. Therefore the transducer installation in the unsteady pressure measurement blade provides sufficient sensitivity and frequency response for use in wind tunnel testing.

The spectral analyses of the pressure data taken without the obstruction in place did not indicate any specific frequency content for the pressure data. Instead, an increase in pressure amplitude over a broad frequency band is noted as the blade angle is increased. Therefore the data is not instructive as to the cause of the stall buffet phenomena discussed in section 16.2.2.

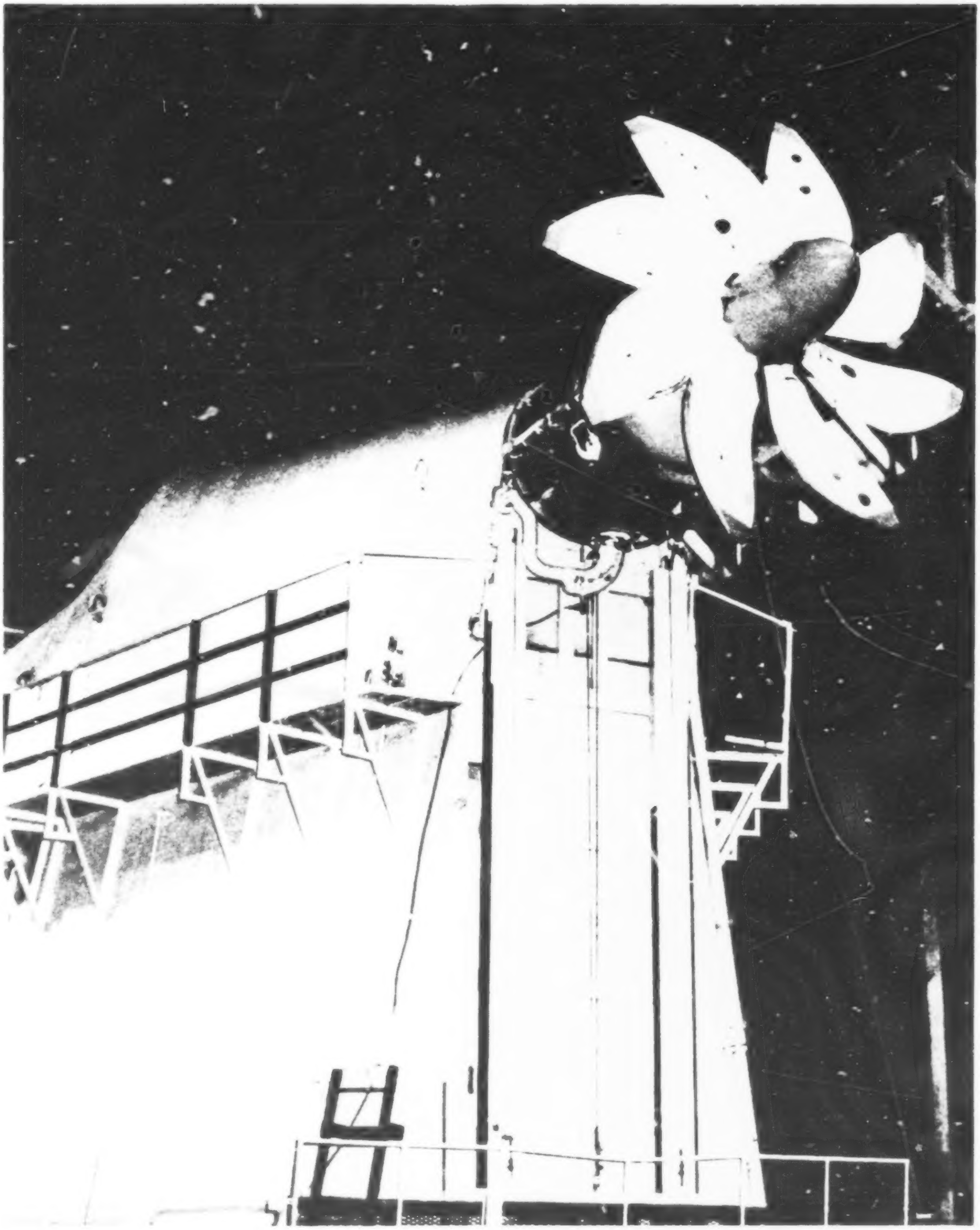

FIGURE 16.1 SR-7L PROP-FAN ON WPAFB WHIRL RIG E-37994

ORIGINAL PAGE IS
OF POOR QUALITY

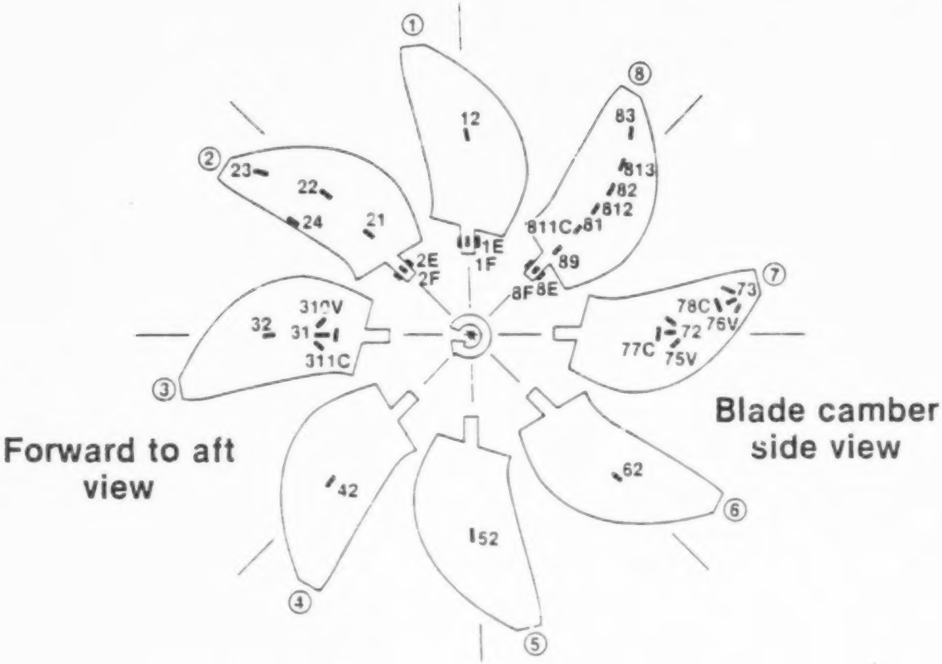
①
②
③
④
⑤
⑥
⑦
⑧
12
1E
1F
23
22
24
21
2E
2F
310V
32
31
311C
42
52
62
73
78C
76V
72
77C
75V
83
813
82
812
811C
81
89
8F
8E
Forward to aft view
Blade camber side view

FIGURE 16.2 ACTIVE STRAIN GAGE ARRANGEMENT FOR FLUTTER AND CRITICAL SPEED TESTING

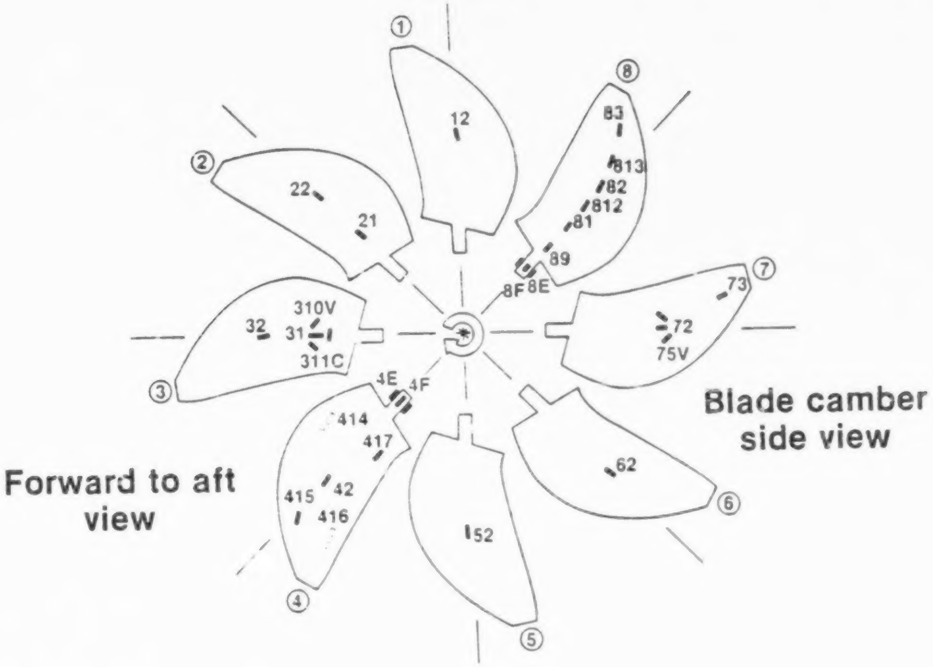
①
12
⑧
83
813
82
812
81
89
8F
8E
②
22
21
⑦
73
72
75V
310V
32
31
311C
③
4E
4F
414
417
42
415
416
④
52
⑤
62
⑥
Blade camber side view
Forward to aft view

FIGURE 16.3 ACTIVE STRAIN GAGE ARRANGEMENT FOR STEADY STRAIN AND BLADE DEFLECTION TESTING

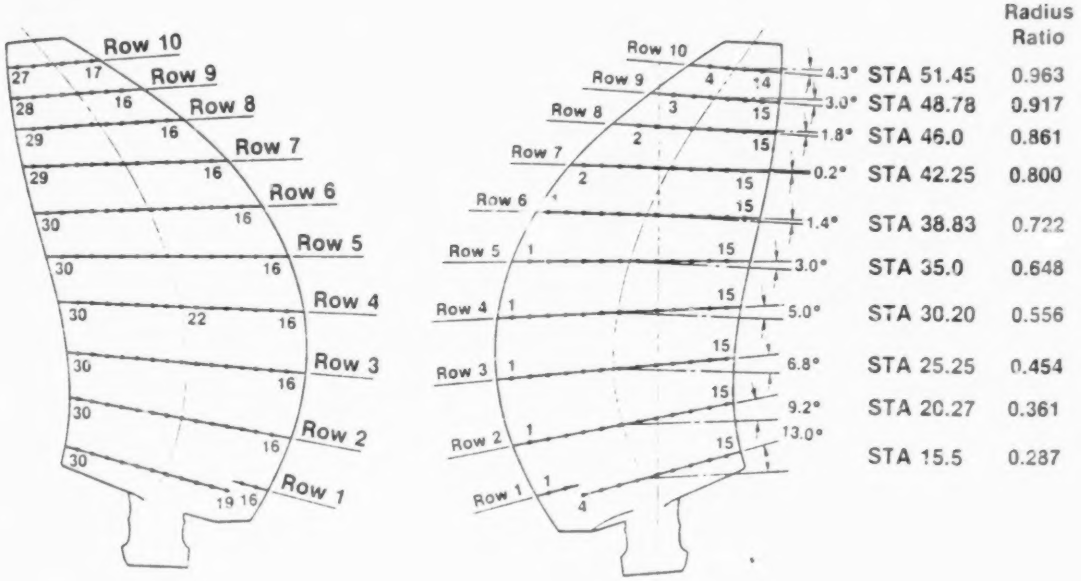
Row 10
Row 9
Row 8
Row 7
Row 6
Row 5
Row 4
Row 3
Row 2
Row 1
27
17
28
16
29
16
29
16
30
16
30
16
30
22
16
30
16
30
16
30
19
16
Row 10
Row 9
Row 8
Row 7
Row 6
Row 5
Row 4
Row 3
Row 2
Row 1
4
14
3
15
2
15
2
15
15
1
15
1
15
1
15
1
15
1
15
1
4
4.3°
3.0°
1.8°
0.2°
1.4°
3.0°
5.0°
6.8°
9.2°
13.0°
Radius
Ratio
STA 51.45
0.963
STA 48.78
0.917
STA 46.0
0.861
STA 42.25
0.800
STA 38.83
0.722
STA 35.0
0.648
STA 30.20
0.556
STA 25.25
0.454
STA 20.27
0.361
STA 15.5
0.287

Camber Side

Face Side

FIGURE 16.4 STEADY PRESSURE BLADE, PRESSURE TAP NUMBERING AND LOCATIONS

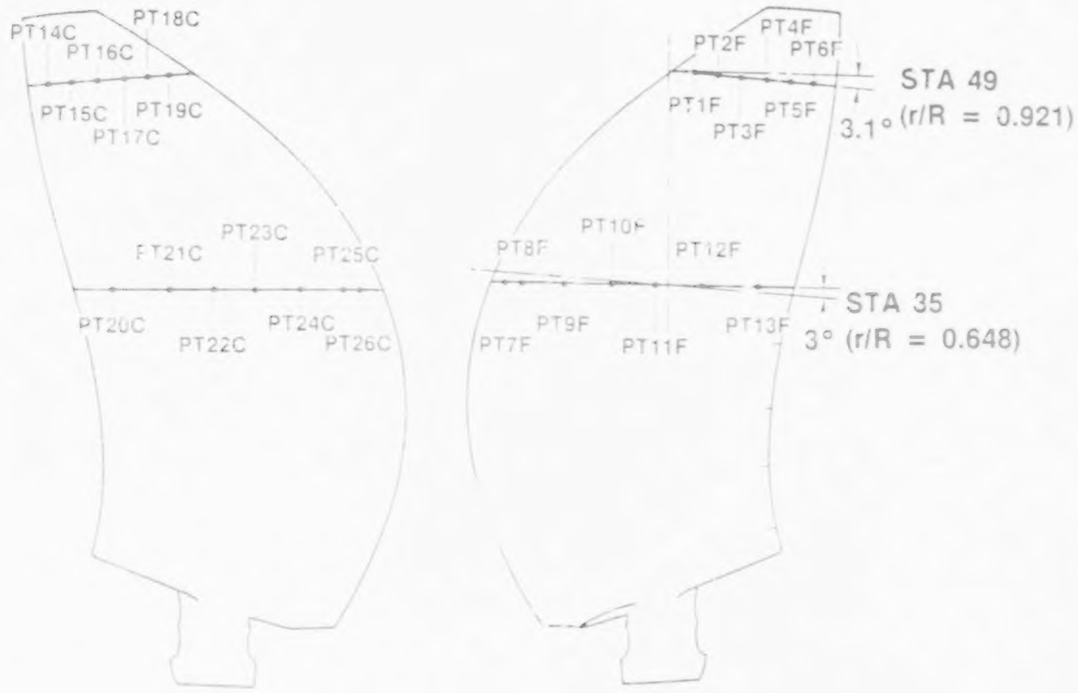
PT14C
PT18C
PT16C
PT15C
PT19C
PT17C
PT23C
PT21C
PT25C
PT20C
PT24C
PT22C
PT26C
PT4F
PT2F
PT6F
STA 49
PT1F
PT5F
PT3F
3.1° (r/R = 0.921)
PT10F
PT8F
PT12F
STA 35
PT9F
PT13F
PT7F
PT11F
3° (r/R = 0.648)

Camber Side

Face Side

Locations — % Chord	
PT1F & PT19C	16.58
PT2F & PT18C	29.85
PT3F & PT17C	43.11
PT4F & PT16C	56.38
PT5F & PT15C	69.64
PT6F & PT14C	89.54
PT7F & PT26C	4.93
PT8F & PT25C	10.00
PT9F & PT24C	23.33
PT10F & PT23C	36.66
PT11F & PT22C	49.99
PT12F & PT21C	63.32
PT13F & PT20C	83.33

FIGURE 16.5 UNSTEADY PRESSURE BLADE, TRANSDUCER LOCATIONS

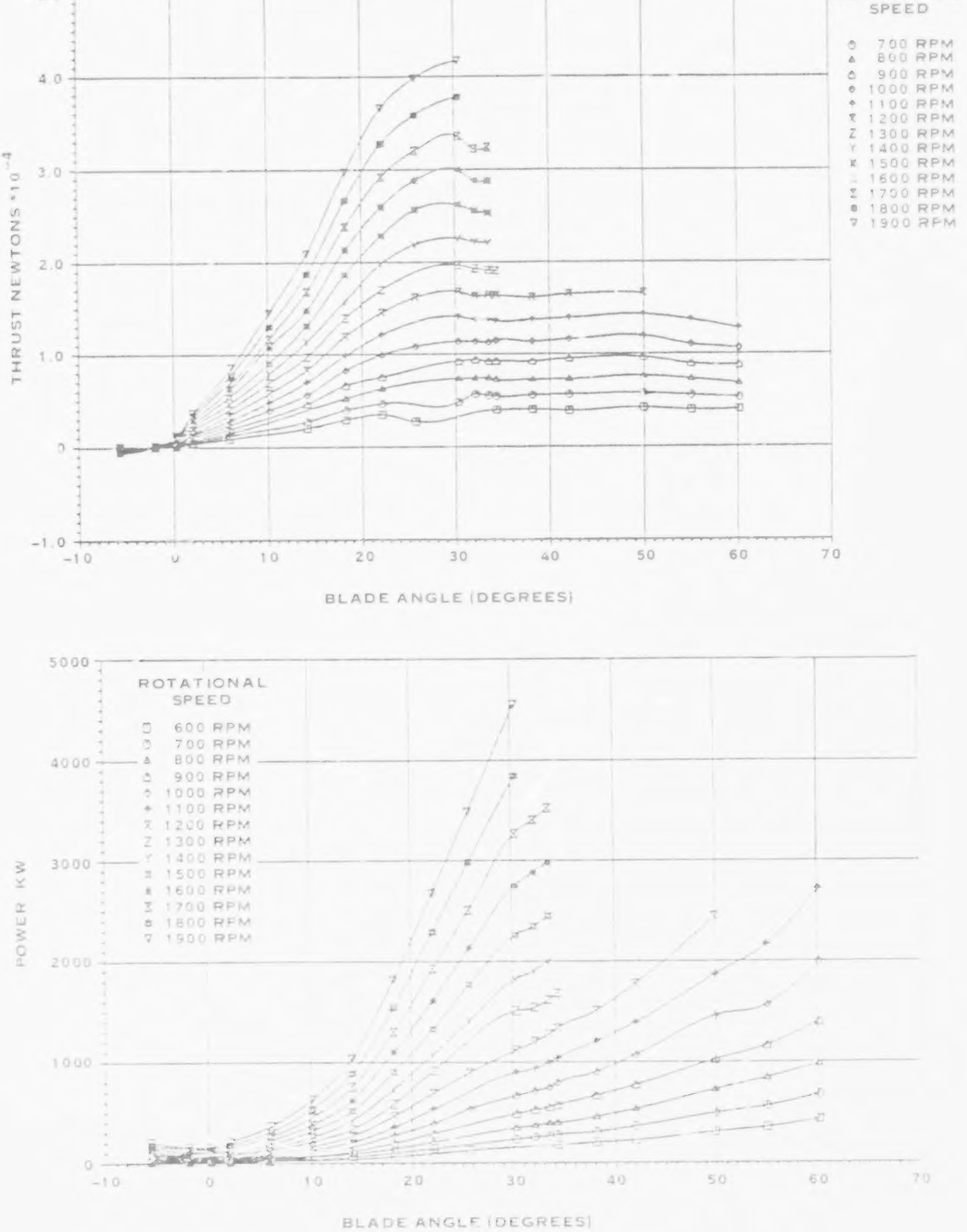

FIGURE 16.6 SR-7L CORRECTED THRUST AND POWER VS BLADE ANGLE

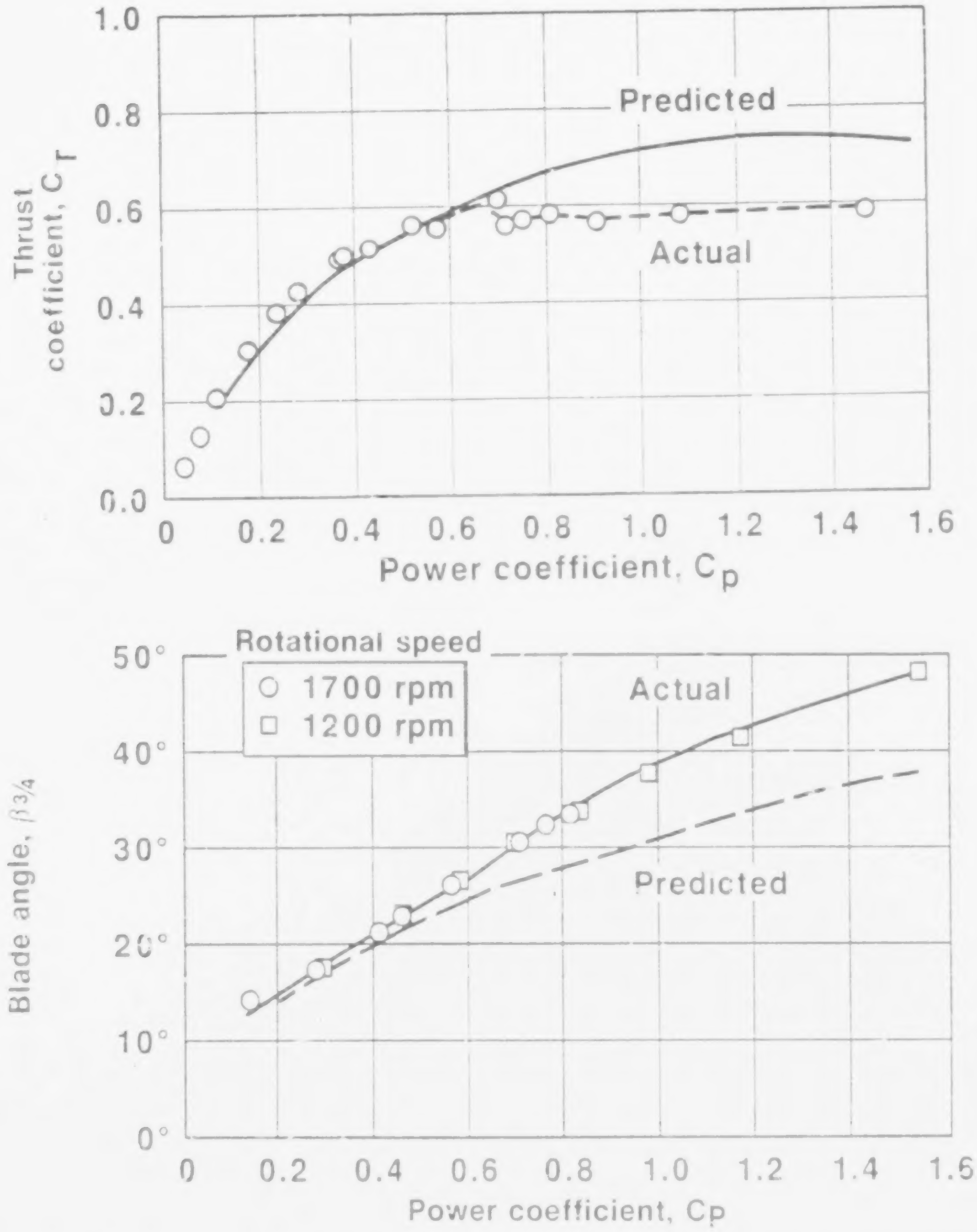

FIGURE 16.7 SR-7L PROP-FAN, COMPARISON OF MEASURED AND PREDICTED CURVES OF BLADE ANGLE VS. POWER COEFFICIENT AND THRUST COEFFICIENT VS. POWER COEFFICIENT

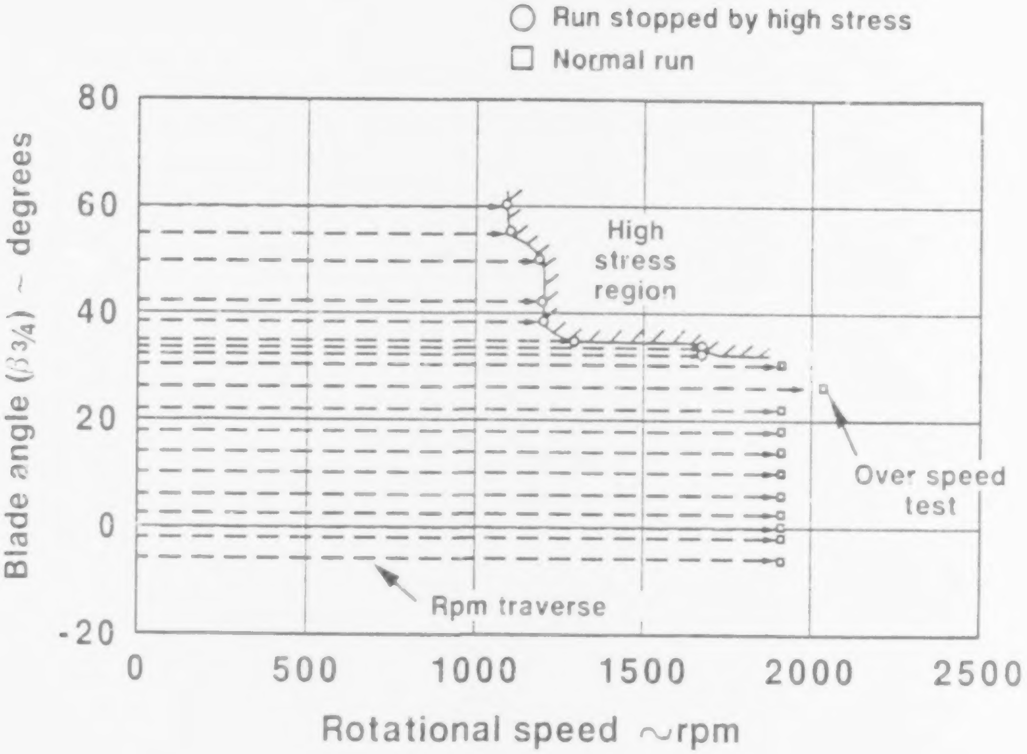

FIGURE 16.8 SR-7L STATIC ROTOR TEST SUMMARY

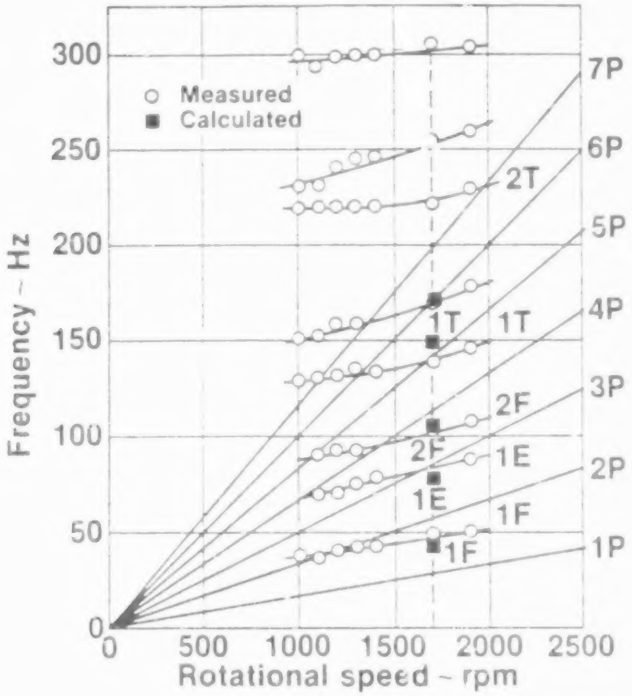

FIGURE 16.9 SR-7L BLADE NATURAL FREQUENCIES

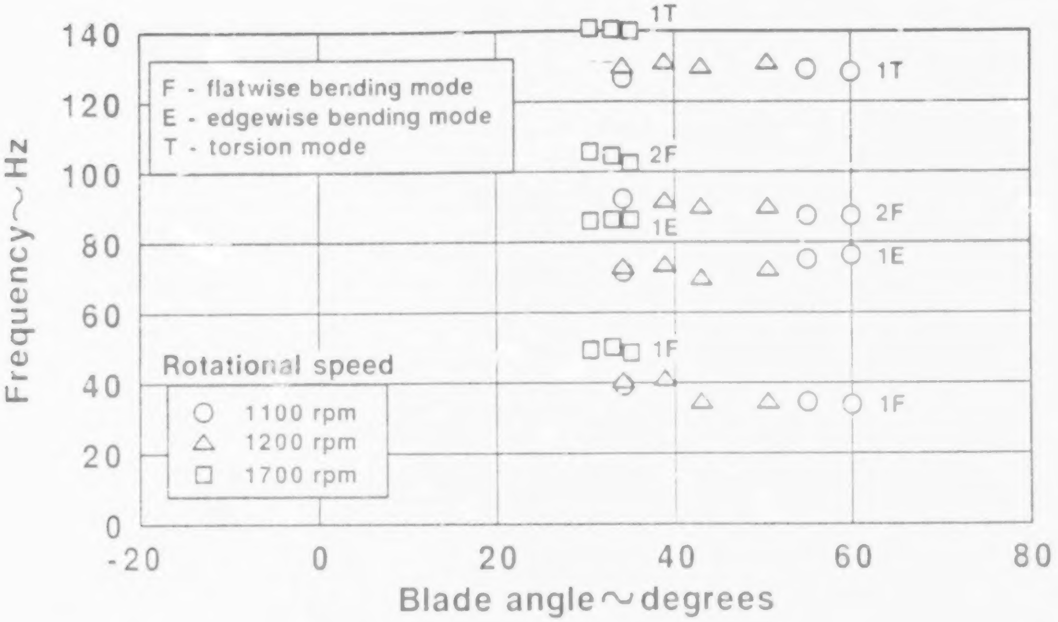

FIGURE 16.10 THE EFFECT OF BLADE ANGLE ON BLADE NATURAL FREQUENCY FOR THE SR-7L

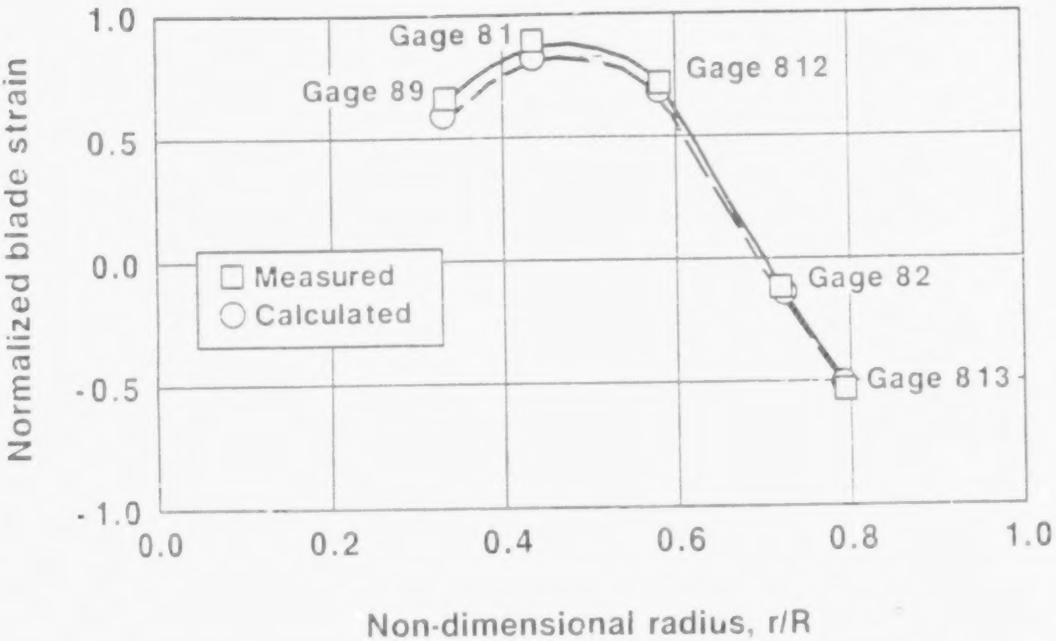

FIGURE 16.11 SR-7L STEADY STRAIN RADIAL DISTRIBUTION DURING WPAFB OVERSPEED TEST, $\beta_{3/4}$ = 25.8°, 2038 RPM, STRAIN NORMALIZED TO MAXIMUM STRAIN GAGE 417

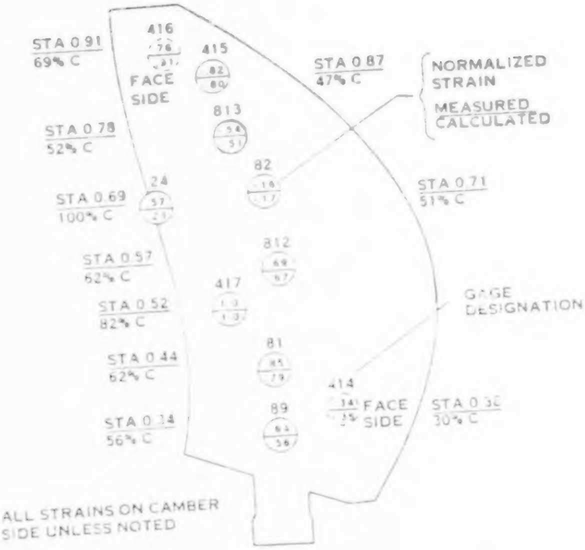
STA 0.91
69% C
416
.76
.21
FACE SIDE
415
.82
.80
STA 0.87
47% C
NORMALIZED STRAIN
MEASURED
CALCULATED
STA 0.78
52% C
813
.54
.51
82
.16
.17
STA 0.69
100% C
24
.57
.23
STA 0.71
51% C
812
.69
.67
STA 0.57
62% C
417
1.0
1.0
STA 0.52
82% C
GAGE DESIGNATION
81
.85
.79
STA 0.44
62% C
414
.34
.25
FACE SIDE
STA 0.30
30% C
89
.64
.56
STA 0.34
56% C
ALL STRAINS ON CAMBER SIDE UNLESS NOTED

FIGURE 16.12 SR-7L STEADY STRAIN DURING THE OVERSPEED TEST, $\beta\ 3/4 = 25.8°$, 2038 RPM

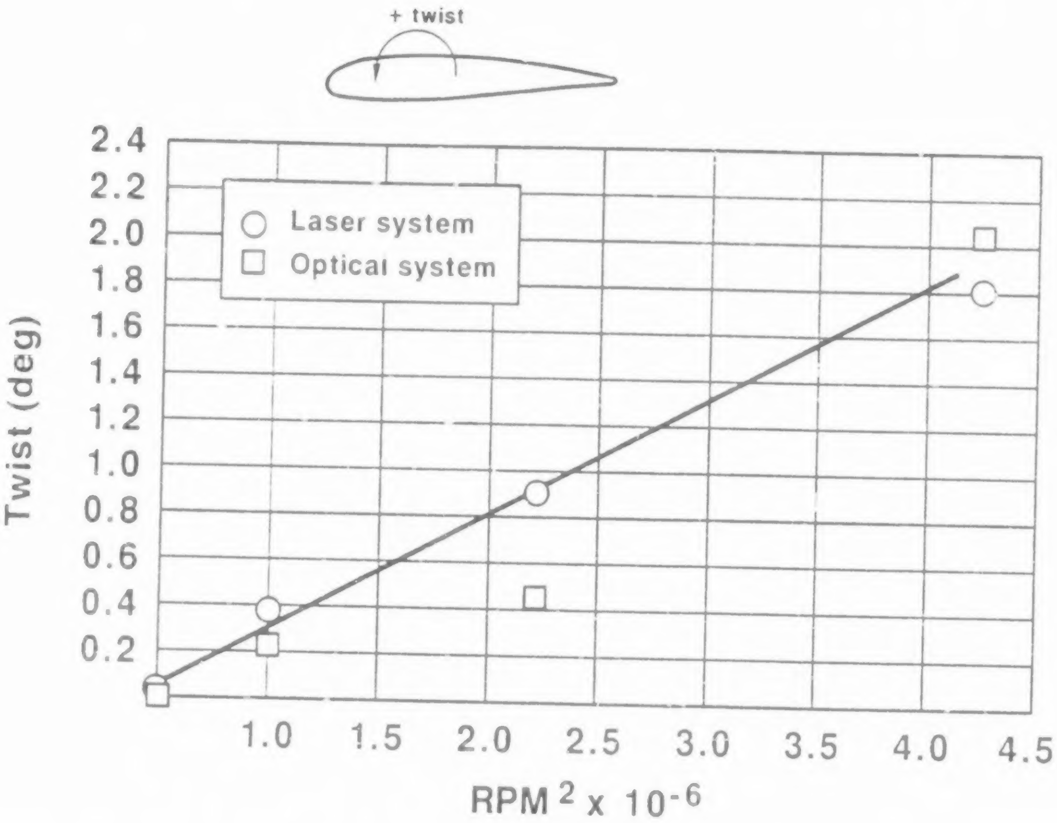

FIGURE 16.13 BLADE TIP TWIST DEFLECTION VS. ROTATIONAL SPEED, $\beta_{3/4} = 25.8°$

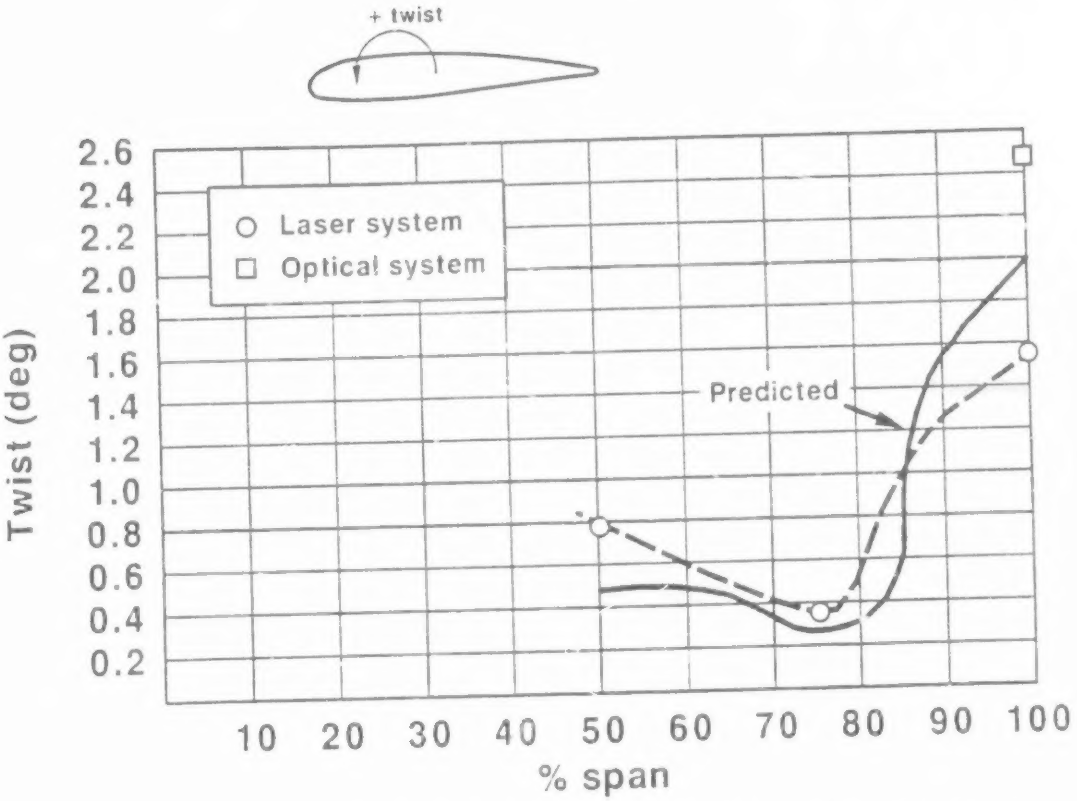

FIGURE 16.14 COMPARISON OF MEASURED & PREDICTED BLADE TWIST DEFLECTION. $\beta_{3/4} = 32°$, N = 1700 RPM

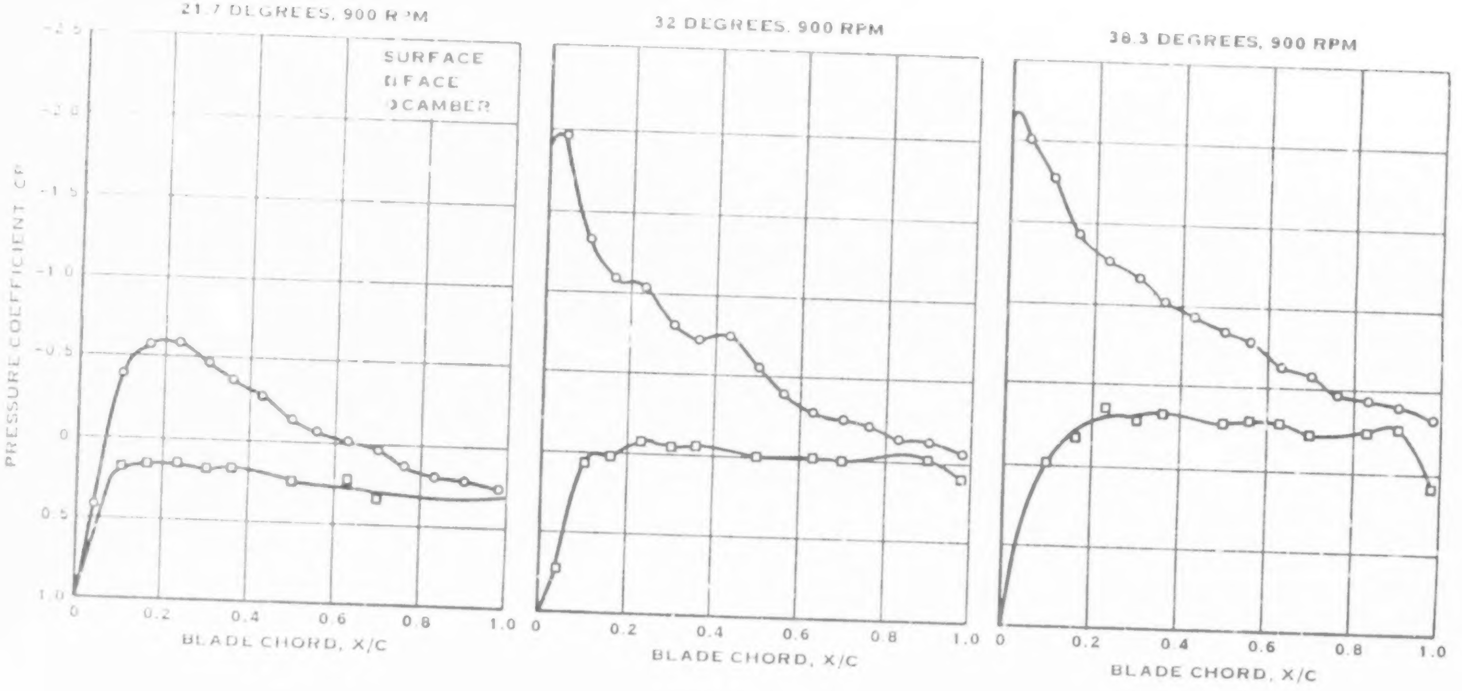

FIGURE 16.15 SR-7 PRESSURE DISTRIBUTION, r/R = 0.287

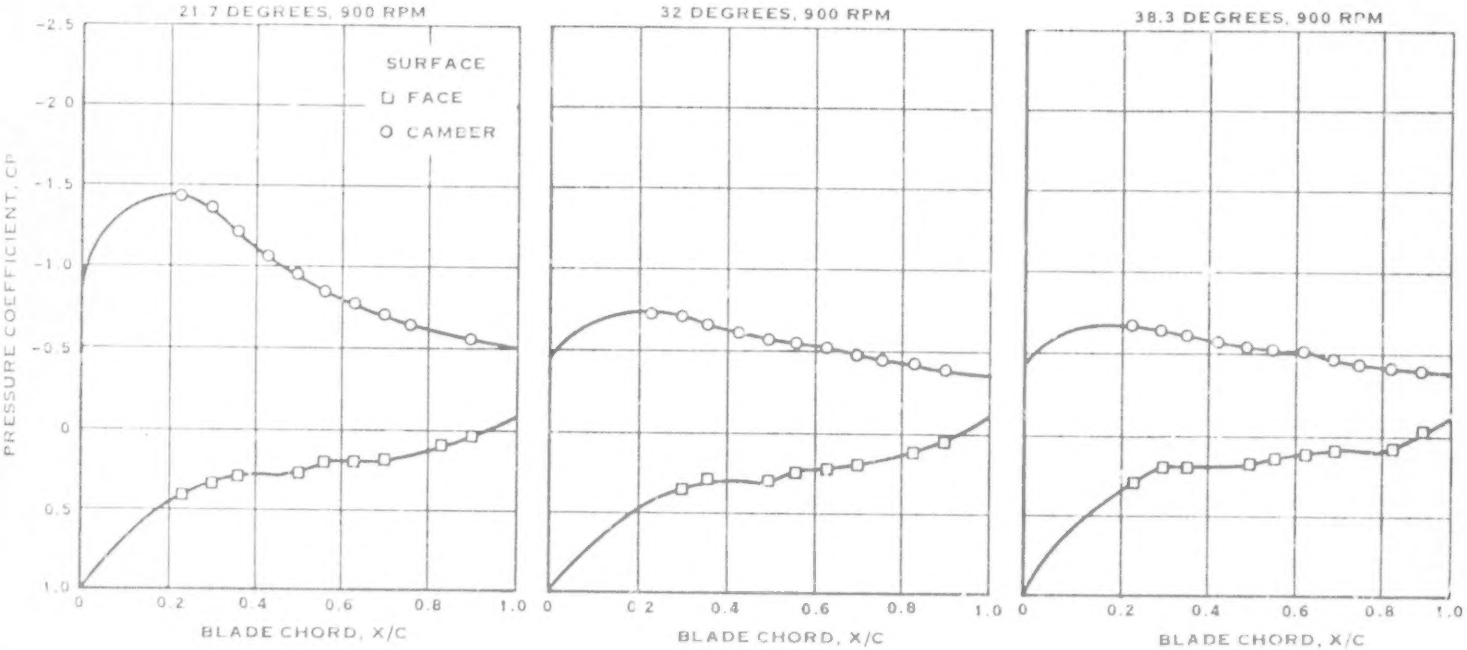

FIGURE 16.16 SR-7 PRESSURE DISTRIBUTION, r/R = 0.963

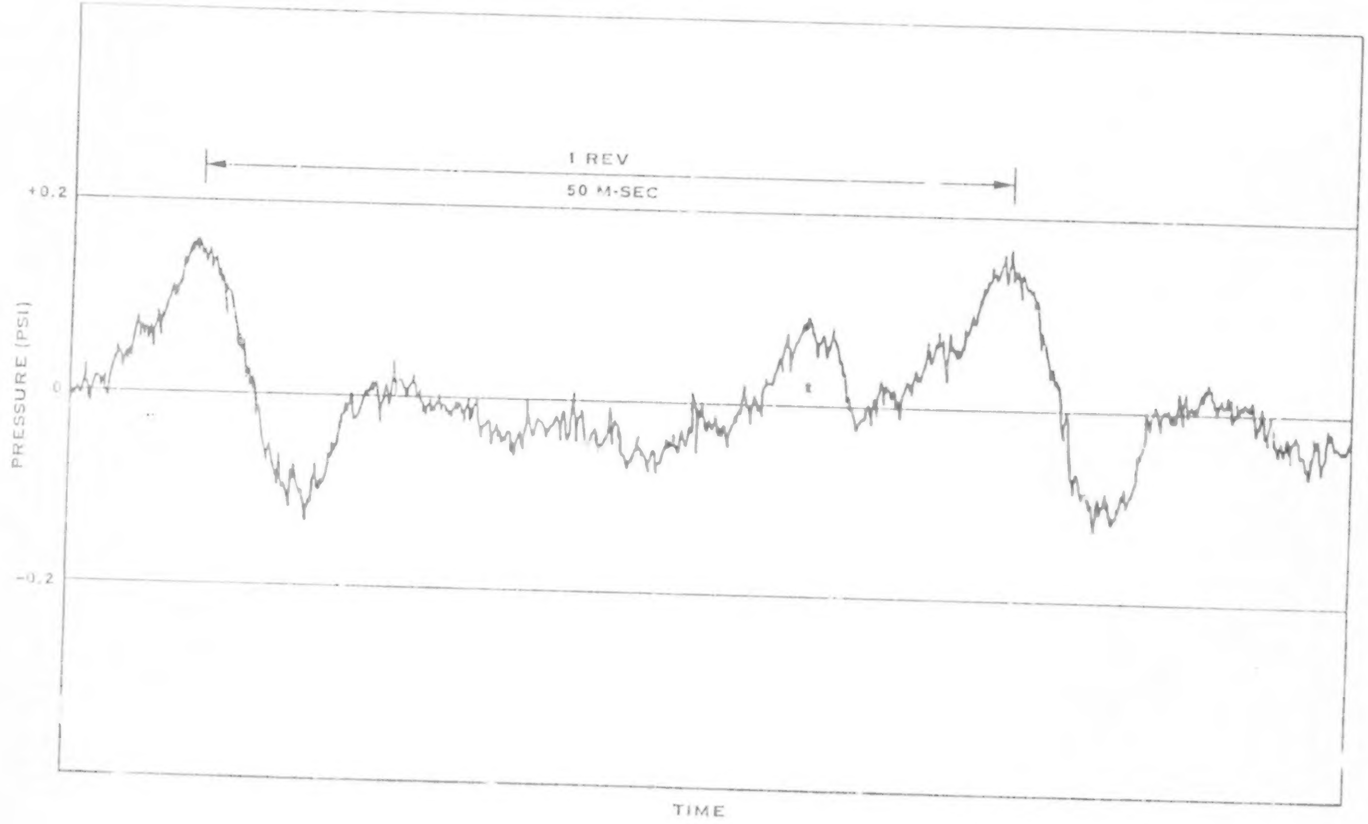

FIGURE 16.17 PRESSURE DATA, TRANSDUCER PT21C, PLATE OBSTRUCTION, $\beta_{3/4} = 32°$, 1200 RPM

17.0 HIGH SPEED WIND TUNNEL TEST

17.1 TEST DESCRIPTION

The High Speed Wind Tunnel Test was conducted in the ONERA S-1 atmospheric wind tunnel in Modane, France. A detailed report of the test is presented in reference 12. The tunnel provided the capability to achieve Mach numbers up to .85 in the test section. Testing was conducted from February thru April 1986 and in March 1987. Spinner drag, aerodynamic performance and structural dynamic testing were completed in 1986. Blade surface steady and unsteady pressure testing was completed in 1987. The specific goals of the test were as follows:

- Determine the aerodynamic drag on the Prop-Fan spinner and the test rig centerbody as a function of Mach number for Mach numbers in the range from .2 to .85.
- Measure the aerodynamic performance of the SR-7L over a range of power settings and advance ratios.
- Confirm that the SR-7L Prop-Fan is free of high speed flutter over the portion of its operating envelope that could be run in the ONERA wind tunnel.
- Evaluate the SR-7L blade 1P vibratory strain sensitivity and compare the measured and analytically predicted 1P vibratory strain response for a range of operating conditions.
- Measure the steady pressure distribution on the surface of the SR-7L blade for a range of power settings and advance ratios.
- Measure the time dependent variation of blade surface pressure for a range of power settings, advance ratios and inflow conditions.

17.1.1 Test Facility

The Prop-Fan was installed on a drive system in the 8 meter diameter test section of the tunnel. Power was provided by two gas turbine engines, which drove the Prop-Fan through a single gearbox. The engines were rated for a combined maximum power of 1000 WK (1341 HP) at standard conditions (15°C, 760 mm hg.). A balance installed in the drive line allowed the thrust, side forces and bending moments acting on the Prop-Fan to be measured. A torque meter was used to measure shaft torque. Universal joints on the drive shaft allowed the Prop-Fan to be pitched to inflow angles up to ten degrees. The test drive system is shown schematically in Figure 17.1.

A stationary aerodynamic fairing or centerbody was installed around the drive system. The centerbody provided a downstream extension of the aerodynamic contour of the Prop-Fan spinner and was designed to reduce the air velocity passing through the root sections of the Prop-Fan rotor to prevent choked flow at the blade root sections. Pressure taps were located on the surface of the centerbody and the centerbody bulkhead as shown in Figure 17.2. these taps allowed the centerbody drag and the back pressure acting on the spinner bulkhead to be determined.

17.1.2 Spinner/Centerbody Drag Test

The test arrangement for the spinner/centerbody drag test is shown in Figure 17.3. The Prop-Fan was installed on the test rig without blades. The blades were replaced with stubs, the ends of which were machined to match the contour of the spinner.

The purpose of determining the spinner and centerbody drag as a function of Mach number was to determine the corrections that must be applied to thrust measured by the balance to arrive at net thrust. Net thrust accounts for the spinner drag, the bouyancy force caused by the centerbody and the back pressure acting on the aft spinner bulkhead.

The thrust measured during wind tunnel testing was the axial force applied to the propeller shaft. Spinner aerodynamic drag results in a force applied to the shaft in the opposite direction of the blade thrust. Therefore, the spinner drag force is added to the measured thrust when determining the corrected thrust. It was desired that the measured spinner drag represent only the pressure and friction drag acting on the external surface of the spinner. Therefore the spinner drag force measured by the balance was corrected by subtracting the force acting on the rear spinner bulkhead due to the differential between the pressure in the gap between the spinner and the centerbody and the free stream static pressure. The force acting on the rear bulkhead was computed by numerically integrating the difference between the pressures measured by the tap shown in Section A-A of Figure 17.2 and free stream static pressure over the base area of the spinner.

The rotation of the Prop-Fan rotor results in an elevation of the pressure acting on the centerbody, above what would be experienced at a given Mach number without the blades in place, increasing the centerbody drag. The elevated pressure acting on the centerbody is reacted back to the rotor and results in a differential thrust equal in magnitude to the increase in centerbody pressure drag. This is the bouyancy force. There is an increase in thrust produced by the Prop-Fan due to the bouyancy force however the increase in centerbody drag negates the increase. The balance does not sense the increases in centerbody drag. Therefore, measured thrust was corrected by subtracting the difference between the centerbody drag measured at the Prop-Fan operating point of interest and the centerbody drag measured at the same Mach number without blades.

The centerbody drag was computed by numerical integration of the centerbody surface pressures determined by the pressure taps illustrated in Figure 17.2 over the external surface of the centerbody.

Spinner/centerbody drag data was collected at a total of 42 test points. All of the data was collected at a zero degree inflow angle. Table 17-1 lists the Mach numbers at which data was collected.

C-3

17.1.2 Continued

TABLE 17-1
SPINNER/CENTERBODY DRAG TEST POINTS

TEST PT.	MACH NO.
242	.499
244	.789
246	.836
248	.834
250	.833
255	.800
257	.848
260	.789
262	.739
264	.686
266	.638
268	.590
270	.494
272	.447
274	.348
276	.244
287	.201
288	.201
289	.201
290	.201
291	.201
293	.298
294	.298
295	.298
296	.298
297	.298
299	.494
300	.494
302	.590
303	.590
305	.494
308	.298
309	.298
310	.298
311	.299
312	.298
314	.201
315	.201
316	.201
317	.201
318	.201

17.1.3 Aerodynamic Performance Testing

The scope of the aerodynamic performance testing was limited because the rated power output of the drive system was significantly lower than the rated power of the Prop-Fan. Therefore, testing was conducted using two and four blade configurations as well as with eight blades. The missing blades were replaced with stubs, machined to match the spinner contour. The two and four blade configurations permitted operation at power loadings per blade that corresponded to high and intermediate power operating points respectively for the eight blade Prop-Fan design. The two, four and eight blade configurations are shown in Figure 17.4.

The Prop-Fan was operated in a Beta control mode during the aerodynamic performance testing. In this mode, Hamilton Standard personnel were able to change the blade pitch angle during testing by means of an increase/decrease pitch switch located in the control room. For a fixed Mach number and a constant power supplied by the turbines, the Prop-Fan rotational speed was varied by increasing or decreasing blade pitch angle. At the Mach numbers of interest, aerodynamic performance data was collected for two or three different power settings and over a range of rotational speeds. Approximately 140 performance data points were taken over a range of Mach numbers from .19 to .83. Data was acquired with the Prop-Fan operating at yaw angles of 0° and 3° with respect to the free stream flow.

The data acquired at each test point during aerodynamic performance testing included thrust produced and power absorbed by the Prop-Fan, RPM, Mach number, Prop-Fan forces and bending moments measured by the balance, pressures measured by the taps shown in Figure 17.2, free stream total and static pressure and free stream static temperature.

The power absorbed by the Prop-Fan was determined by multiplying the torque supplied to the Prop-Fan by the Prop-Fan rotational speed. Torque supplied to the Prop-Fan was computed by subtracting the measured torsional friction losses in the balance from the torque measured by the torquemeter.

The net thrust determined during testing is the thrust of the Prop-Fan rotor, operating in the presence of a spinner and nacelle. The net thrust is computed from equation 17.1.

$$Tnet = T + TFL - TCS + TCASS - BF \qquad (17.1)$$

where:

T = thrust measured by the balance
TFL = temperature correction
TCS = back pressure force
TCASS = spinner drag force
BF = buoyancy force

The temperature correction term compensates for the effect of changes in temperature on the balance strain gages.

17.1.3 (Continued)

The back pressure term corrects for the increase in measured thrust due to the differential between the pressure behind the spinner bulkhead and the free stream pressure. The back pressure force is calculated by multiplying the difference between the average pressure measured by the taps shown in Section AA of Figure 17.2 and the free stream pressure by the projected area of the spinner bulkhead. The spinner drag force and buoyancy force were computed from the centerbody pressure tap data and data acquired during the spinner/centerbody drag test as discussed in section 17.1.2.

Mach number was determined from the ratio of static pressure, measured four meters upstream of the Prop-Fan rotor, to stagnation pressure. Static pressure was also measured in the plane of the rotor as a backup. The ratio of static to stagnation pressure was correlated with data taken during a pre-test calibration in order to compute the Mach number. The Glauert-Young correction was applied to the computed Mach number to compensate for the effects of the tunnel walls and the thrust produced by the Prop-Fan.

17.1.4 Structural Dynamic Testing

The structural dynamic test data was acquired concurrently with the aerodynamic performance data. The data was obtained using strain gages attached to the surfaces of the blades. The strain gage arrangements used for the two, four and eight blade configurations are shown in Figure 17.5. The strain gage data was recorded on magnetic tape and monitored in real time using a four channel oscilloscope and a spectrum analyzer. Dynamic data was also acquired from accelerometers attached to the test rig drive train housing and the strain gaged elements of the balance.

The primary goals of the structural dynamic testing were to determine if classical unstalled flutter was present in the Prop-Fan operating envelope and to compare the measured and calculated blade 1P vibratory response for yawed operating conditions. The onset of classical flutter would be indicated by a sudden increase in vibratory strain at a frequency that was not an integer order of the Prop-Fan rotational speed for an operating condition well away from blade stall. Although the design range of power loadings per blade were achieved using the two and four blade Prop-Fan configurations, this methodology had the disadvantage of reducing the interblade cascade effects present in the eight blade design. These effects tend to be destabilizing in that they lower the Mach number at which the onset of classical flutter occur. The 3° yaw angle cases were run for the two blade configuration only. Operation of the Prop-Fan at a yaw angle causes a continuous variation of the blade angle of attack resulting in a 1P excitation. The 1P blade response was determined by spectral analysis of the blade strain gages. The theoretical response of the blade to these operating conditions were determined by finite element analysis.

17.1.5 Blade Surface Steady Pressure Testing

Blade surface steady pressure testing was accomplished with a specially fabricated blade and scanivalve, similar to that described in section 16.1.4 of this report. The steady pressure blade had additional rows of pressure taps installed near the tip to provide better definition of the aerodynamic phenomena in that area. The locations of the pressure taps on the blades are defined in Figure 17.6. The scanivalve was enclosed in an aerodynamic fairing in order to preserve well behaved inflow to the rotor. Blade surface steady pressure testing was conducted using the two blade configuration only. Testing was conducted over a range of Mach numbers from .01 to .78, a range of advance ratios from .08 to 3.2 and at a zero degree inflow angle. The test arrangement for blade surface steady pressure testing is shown in Figure 17.7.

17.1.6 Blade Surface Unsteady Pressure Testing

The blade surface unsteady pressure testing was accomplished using the specially fabricated blade described in section 16.1.5 of this report. Testing was again conducted using the two blade configuration only. Data was taken over a range of Mach numbers from .02 to .7 and a range of advance ratios from .14 to 3.055. Each combination of Mach number and Prop-Fan RPM was run at a zero degree inflow angle, at a 3° yaw angle and at a zero degree inflow angle with a cylindrical obstruction installed 1372 mm (4.5 ft.) upstream of the rotor. Operation at a zero degree yaw angle provides baseline surface pressure data. Operation at a 3° inflow provides a cyclical variation of blade angle of attack with a 1P period and thus a continuous variation of surface pressure to be sensed by the blade transducers. The wake caused by the cylindrical obstruction provides a twice per revolution disturbance for the transducers to sense.

17.2 TEST RESULTS

17.2.1 Spinner/Centerbody Drag Test

The spinner drag was determined at each test point and reduced to coefficient form using equation 17.2,

$$\mathrm{CTCASS} = \frac{\mathrm{DRAG\ FORCE}}{q_o\ \mathrm{As}} \qquad (17.2)$$

where q_o is the free stream dynamic pressure and As is the base area of the spinner equal to .5m^2 (4.35 ft^2). A quadratic equation was fitted to the plot of spinner drag coefficient versus Mach number shown in Figure 17.8 so that the spinner drag could be calculated for any operating condition.

17.2.1 (Continued)

The spinner drag coefficient as expected increases with Mach number for Mach numbers in the range from .3 to .85. However, an unexpected decrease in drag coefficient was observed between Mach .2 and Mach .3. The decrease in drag coefficient cannot be readily explained from the data that was collected. The large number of data points taken at Mach .2 and Mach .3 does confirm that the decrease in spinner drag coefficient is a real phenomenon.

The variation of the centerbody drag with Mach number is presented in Figure 17.8. The centerbody drag coefficient was computed from equation 17.3

$$\text{CBDWO} = \frac{\text{CENTERBODY DRAG}}{\text{qoxSref}} \qquad (17.3)$$

where the centerbody reference area, Sref, had a value of 2.368 square feet. A quadratic equation was fitted to the centerbody drag data as shown in Figure 17.7. This curve was used to compute the buoyancy force correction to measured thrust during Prop-Fan performance testing.

It is observed from the data that the centerbody drag coefficient decreases with increasing Mach number. This indicates that the centerbody surface Mach numbers are increasing at a faster rate than the free stream velocity.

17.2.2 Aerodynamic Performance Testing

The most complete aerodynamic performance data was acquired for the four blade Prop-Fan configuration. Operational problems encountered with the test rig, while running the two and eight blade configuration, limited the operating envelope for these configurations. The aerodynamic performance data was nondimensionalized for analysis according to equations 17.4, 17.5, and 17.6.

$$\text{(power coefficient)} \qquad C_p = \frac{Kw\ (\rho o/\rho)}{5.674\ (ND/1000)^3 D^2} \qquad (17.4)$$

$$\text{(net thrust coefficient)} \quad C_{T\ NET} = \frac{T_{net}\ (\rho o/\rho)}{340.42\ (ND/1000)^2 D^2} \qquad (17.5)$$

$$\text{(advance ratio)} \qquad J = \frac{60V}{ND} \qquad (17.6)$$

where

KW = power, kilowatts
Tnet = net thrust, newtons
D = Prop-Fan diameter, meters
$\rho o/\rho$ = density ratio, sea level to ambient
N = rotational speed, RPM
V = free stream velocity, meters/seconds

17.2.2 Continued

Comparisons of the calculated and experimentally determined performance of the four blade and eight blade Prop-Fan configurations are shown in Figures 17.10 and 17.11. The predicted and measured performance agree very well for the four blade configuration over the entire range of test points. Similarly good agreement between measurement and prediction was obtained for the eight blade configuration at Mach numbers of .70 and .73. The performance of the eight blade Prop-Fan design was underpredicted at Mach .5.

17.2.3 Structural Dynamic Testing

The vibratory strain data for each test point was statistically analyzed to obtain the mean amplitude and the standard deviation of the signal. The IRP (Infrequently Repeating Peak) strain, defined as the mean strain plus twice the standard deviation was calculated for each strain gage and test condition. The IRP strain was used as the conservative measure of strain amplitude. Comparison of the IRP strains from the shank bending gages showed that as expected the highest levels were obtained for the two blade 3° inflow angle case, where the excitation is the highest.

No indication of unstalled flutter were observed anywhere in the operating range that was tested. Prior to the high speed wind tunnel test, an unstalled flutter analysis had been conducted for several Prop-Fan operating cases, including three of the planned wind tunnel test points. This analysis indicated that the eight bladed wind tunnel case (Mach .8, 1698 RPM, 14000 ft) had a lower unstalled flutter Mach number than the design cruise case (Mach .8, 1698 RPM, 35000 ft). This results from the higher density attained in the wind tunnel. Due to operating restrictions, the maximum Mach number achieved for the eight blade configuration was .73. However, operation was conducted at a rotor speed of 1850 RPM for this Mach number. The combination of blade surface Mach number and density altitude for this case resulted in an unstalled flutter stability comparable to the design cruise condition.

In order to compare the 1P response of the Prop-Fan for the 3° inflow angle cases with analytical predictions, a spectrum analysis of the strain gage signals was accomplished using a Fast Fourier Transform Algorithm. The spectral analysis indicated that the vibration was predominantly 1P for the 3° inflow angle cases. A 2P component was present, which had an amplitude that was 25% of the 1P component. The excitation for the 2P response may have come from the test rig drive system rather than an aerodynamic source. The 2P vibration is characteristic of a shaft with universal joints. The comparisons of the measured and predicted 1P response showed reasonable correlation. As predicted, the highest 1P response was observed at the inboard sections of the blade and decreased toward the outboard sections. The observed trends in the variation of 1P vibratory response with power and Mach number correlated well with predictions.

17.2.4 Blade Surface Steady Pressure Testing

The surface pressure data was corrected for centrifugal effects, reduced to coefficient form and plotted by a microcomputer system during the test. The pressure coefficients were calculated according to equation 17.7.

$$Cp = \frac{Pc - Po}{.5\rho\ (Vo^2 + Vt^2)} \qquad (17.7)$$

where

Pc = corrected blade surface pressure
Po = free stream static pressure
ρ = air density
Vo = free stream velocity
Vt = tangential velocity

Figures 17.12 and 17.13 are typical of the steady pressure data that was acquired. Figure 17.12 represents a low power nominal static case and Figure 17.13 represents a low power high Mach number case.

In Figure 17.12 a suction peak is observed on the camber side of the blade at the blade tip (station 13). This is probably due to the roll up of the blade tip vortex onto the camber surface. As power was increased, the suction peak was observed to move forward on the blade and then disappear. This may be due to collapse of the vortex due to flow separation. The presence of leading edge vortex flow is indicated by the negative pressure hump that spans the leading edge. The leading edge vortex is driven by blade sweep and generates additional lift due to the low pressure in the vortex acting on the camber surface.

The outboard blade stations were operating at helical Mach numbers very close to one for the operating condition of Figure 17.13. The camber side flow was probably supersonic at these stations. The trailing edge pressure jumps that are observed at these stations in Figure 17.13 may be associated with trailing edge shock waves.

A complete set of data is included in reference 13.

17.2.5 Blade Surface Unsteady Pressure Testing

Figure 17.14 presents data measured by transducer PT16C (reference Figure 16.5) for the three inflow conditions and the operating parameters listed below. This operating point is representative of a takeoff condition.

Mach Numbers	M = .20
Advance Ratio	J = .883
Power Coefficient	Cp = .250
Blade Angle	β3/4 = 32°

17.2.5 (Continued)

The unsteady pressure data is plotted as a function of the orientation of the rotor as well as a function of time in Figure 17.14. For the trace representing undisturbed inflow, the signal level should be low, corresponding to low distortion level. However, a small 1P sinusoidal component is evident which may have been caused by residual flow angularity in the wind tunnel.

In the data for the 3° angular inflow, the angle of attack seen by the instrumented blade should be nearly a pure sine wave at the once per revolution (1P) frequency. Simplistic analysis would indicate that the blade pressure response should also be sinusoidal. The waveform and spectrum show that this is far from true.

For the data with the cylinder wake, the blade pressure should respond with a pulse each time the blade passes through a wake at the top and bottom of the revolution. This behavior is observed in the bottom trace, but the pulse magnitudes are surprisingly different at the top and bottom positions. Another interesting feature of the data for cylinder wakes is the oscillating response after the wake pulse.

A complete set of data is included in reference 14.

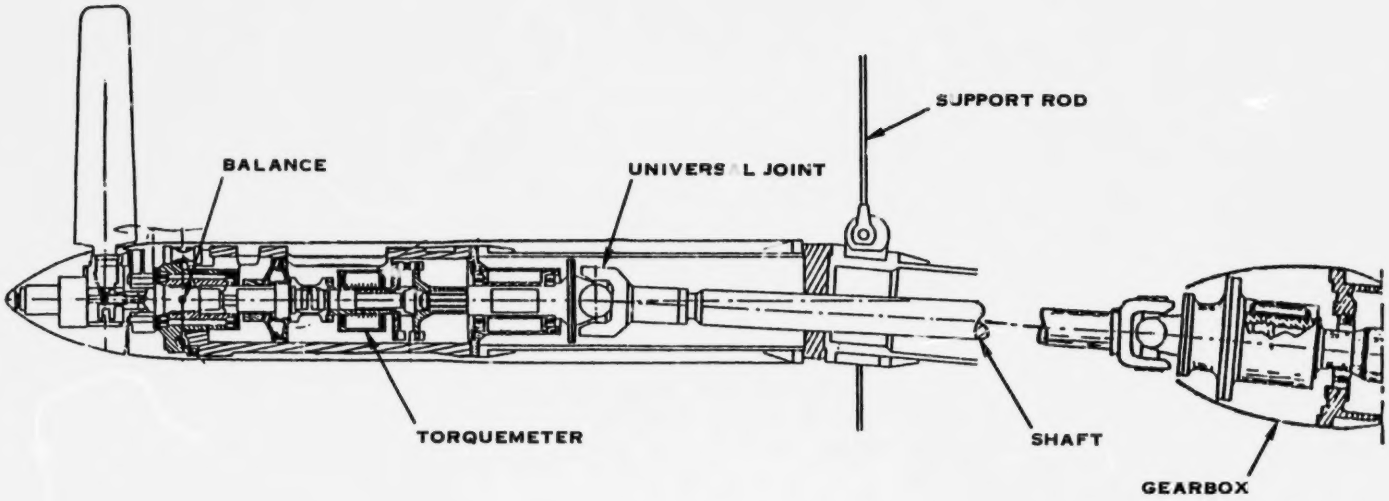
SUPPORT ROD
BALANCE
UNIVERSAL JOINT
TORQUEMETER
SHAFT
GEARBOX

FIGURE 17.1 PROP-FAN DRIVE SYSTEM ONERA S1 WIND TUNNEL

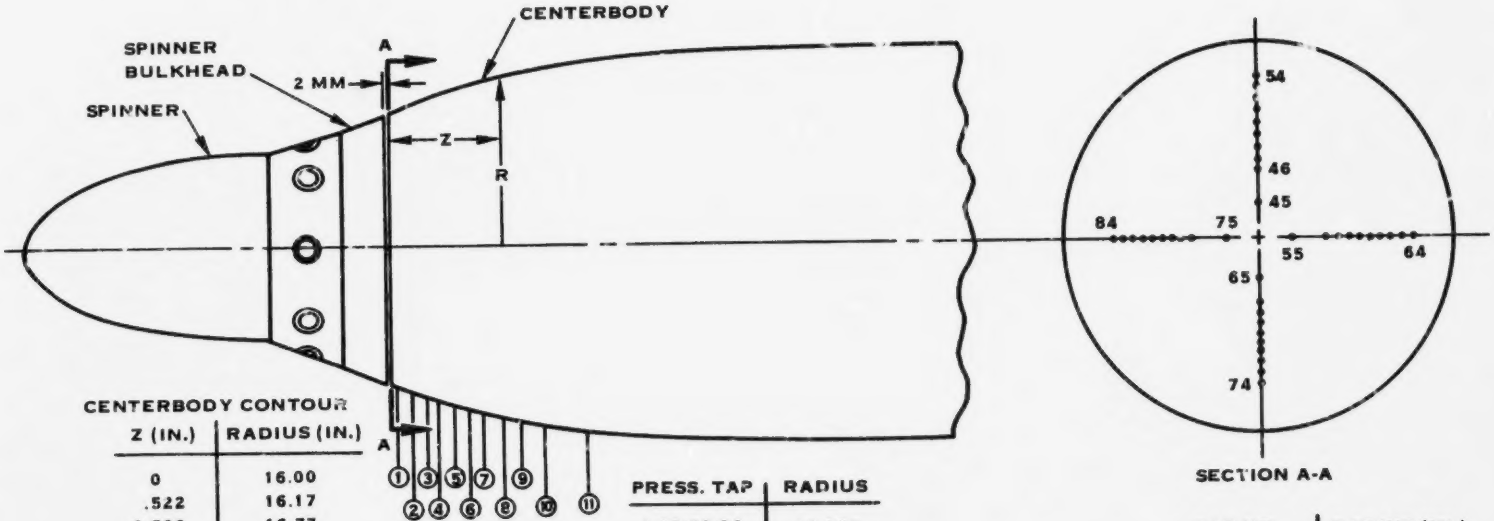

CENTERBODY
SPINNER BULKHEAD
SPINNER
2 MM
A
A
Z
R
①
②
③
④
⑤
⑥
⑦
⑧
⑨
⑩
⑪
54
46
45
84
75
55
64
65
74
SECTION A-A

CENTERBODY CONTOUR

Z (IN.)	RADIUS (IN.)
0	16.00
.522	16.17
2.522	16.77
4.522	17.33
6.522	17.80
8.522	18.15
10.522	18.45
12.522	18.70
14.522	18.90
16.522	19.01
18.522	19.08
20.522	19.10
22.522	19.10
24.522	19.10

PRESS. TAP	RADIUS
1,12,23,34	16.168
2,13,24,35	16.501
3,14,25,36	16.828
4,15,26,37	17.148
5,16,27,38	17.462
6,17,28,39	17.771
7,18,29,40	18.075
8,19,30,41	18.373
9,20,31,42	18.667
10,21,32,43	18.956
11,22,33,44	19.10

TAP NO.	RADIUS (IN.)
45,55,65,75	3.473
46,56,66,76	6.126
47,57,67,77	7.836
48,58,68,78	9.224
49,59,69,79	10.426
50,60,70,80	11.502
51,61,71,81	12.484
52,62,72,82	13.394
53,63,73,83	14.246
54,64,74,84	15.050

FIGURE 17.2 CENTERBODY PRESSURE TAP LOCATIONS, HIGH SPEED WIND TUNNEL TEST

ORIGINAL PAGE IS
OF POOR QUALITY

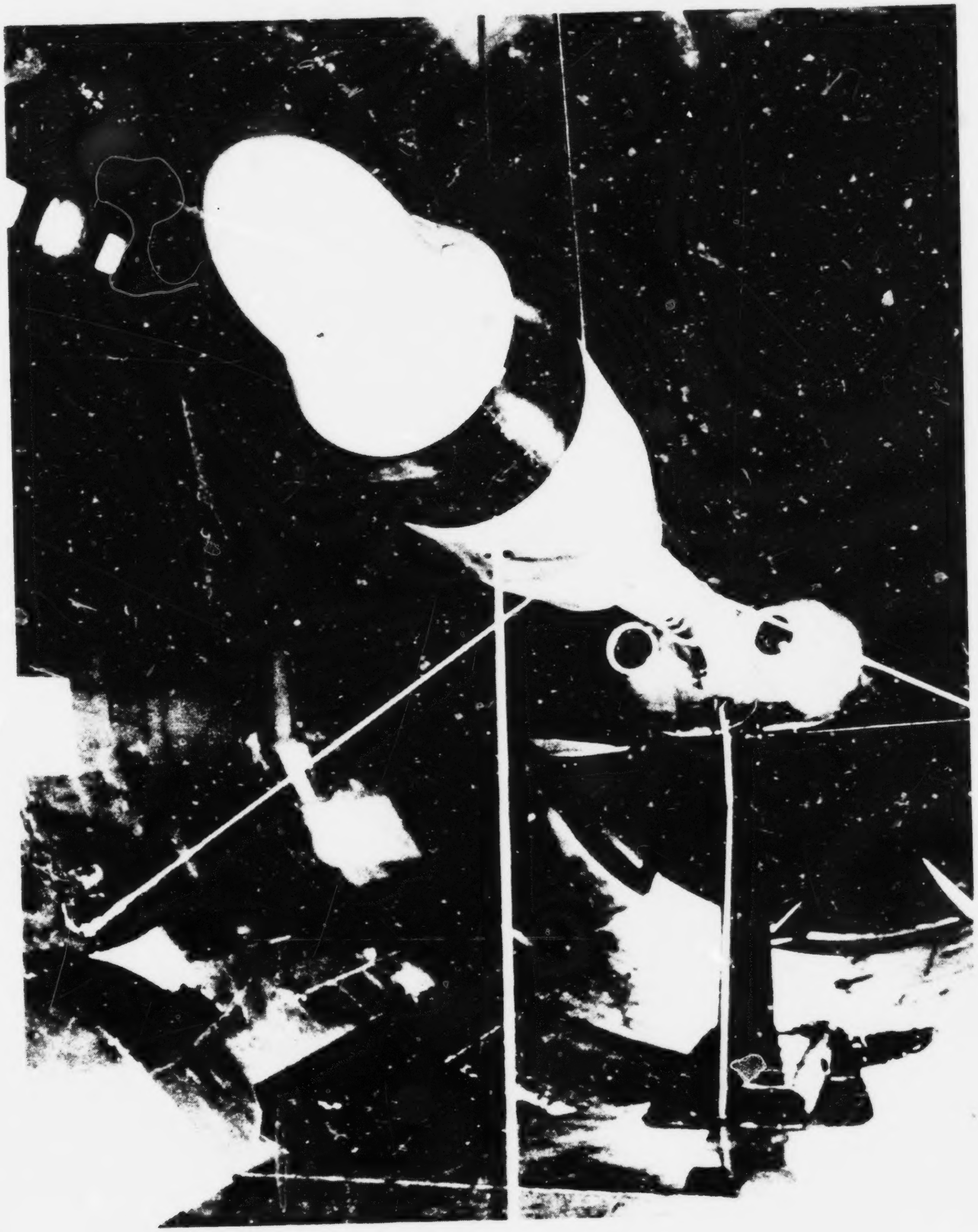

FIGURE 17.3 SPINNER DRAG TEST ARRANGEMENT

ORIGINAL PAGE IS
OF POOR QUALITY

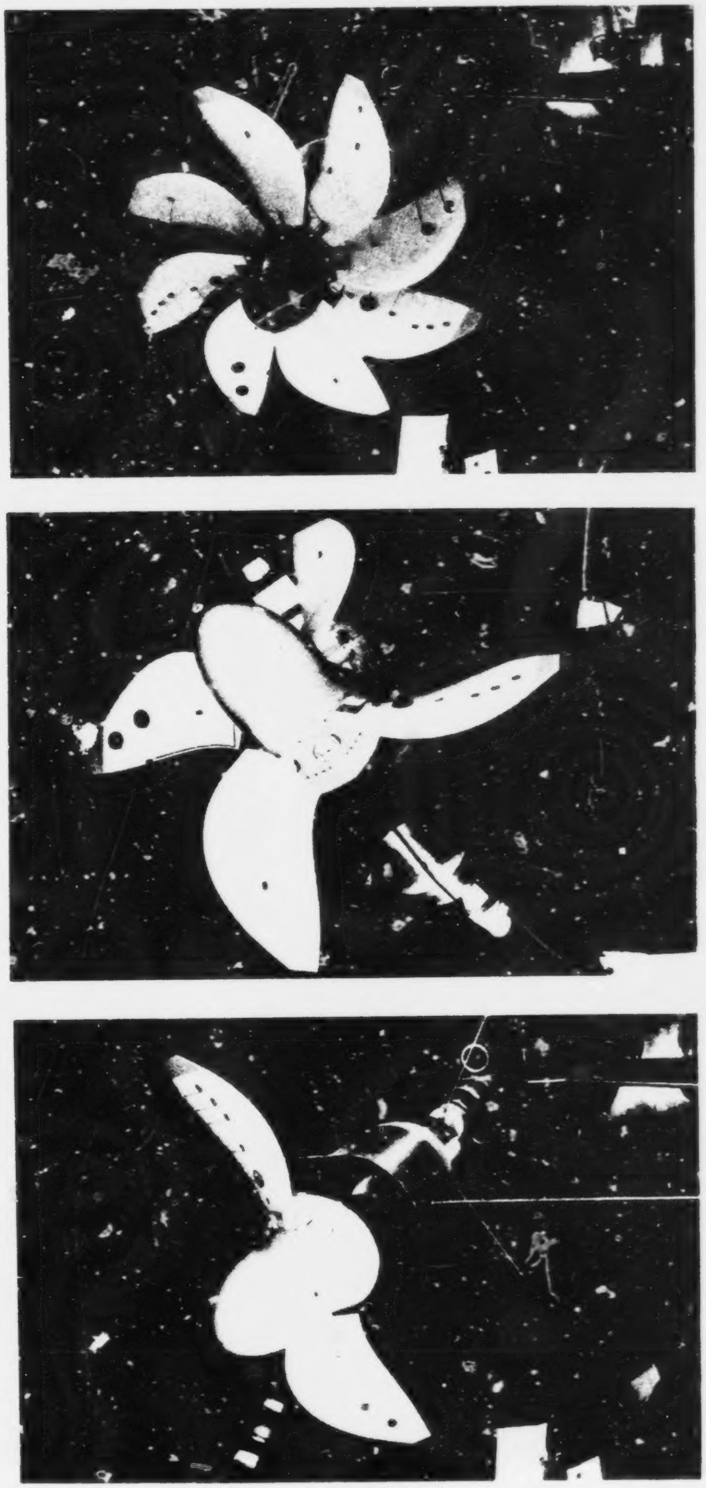

FIGURE 17.4 PROP FAN TWO, FOUR AND EIGHT BLADE CONFIGURATIONS, HIGH SPEED WIND TUNNEL TESTS

E-37987

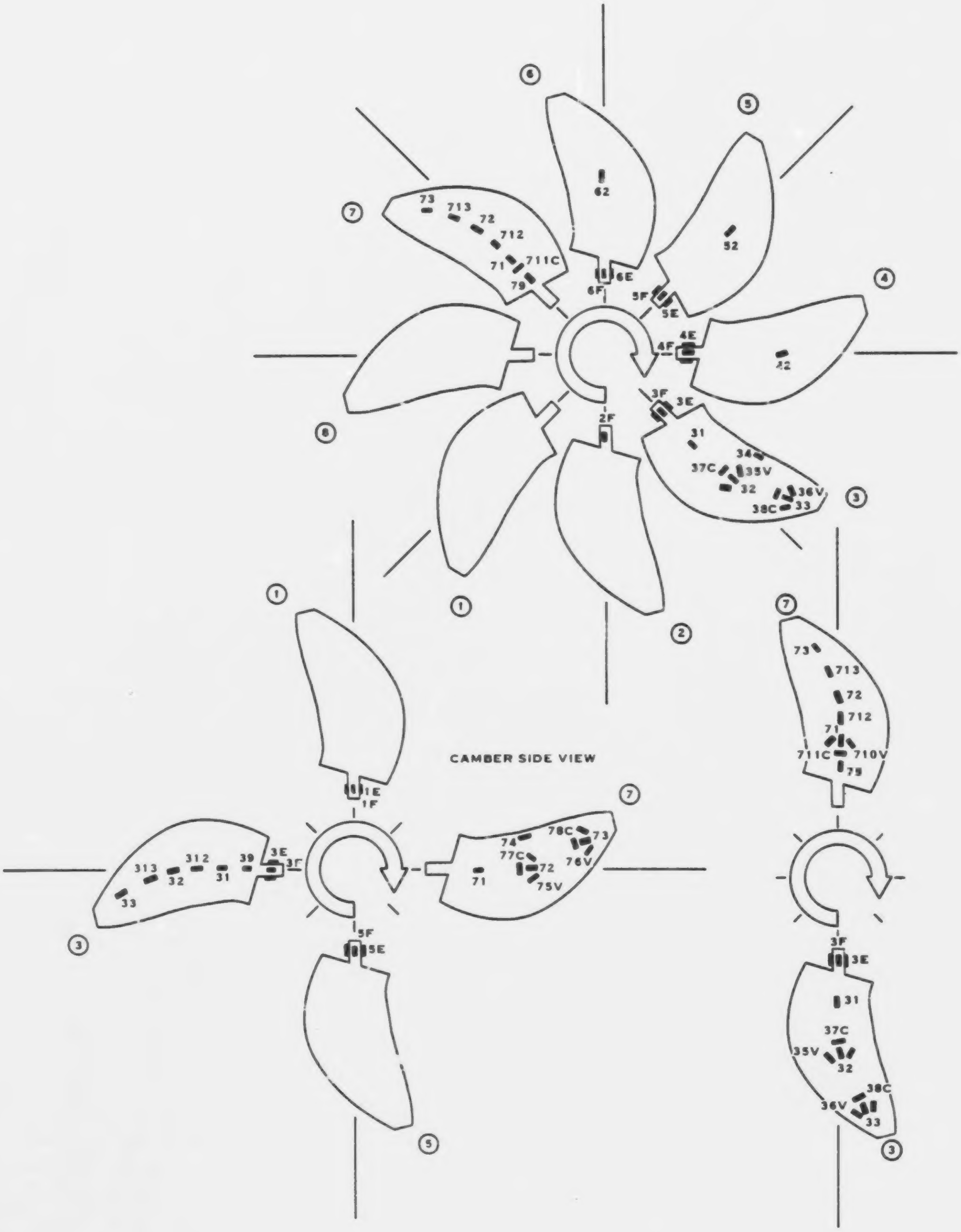
⑥
⑤
⑦
73
713
72
712
71
711C
79
62
6E
6F
52
5F
5E
④
4E
4F
42
3F
3E
2F
31
34
37C
35V
32
36V
38C
33
③
⑧
①
②
①
CAMBER SIDE VIEW
1E
1F
⑦
74
78C
73
77C
76V
72
71
75V
313
312
39
3E
3F
32
31
33
③
5F
5E
⑤
⑦
73
713
72
712
71
711C
710V
79
3F
3E
31
37C
35V
32
38C
36V
33
③

FIGURE 17.5 STRAIN GAGE ARRANGEMENTS – HIGH SPEED WIND TUNNEL TEST

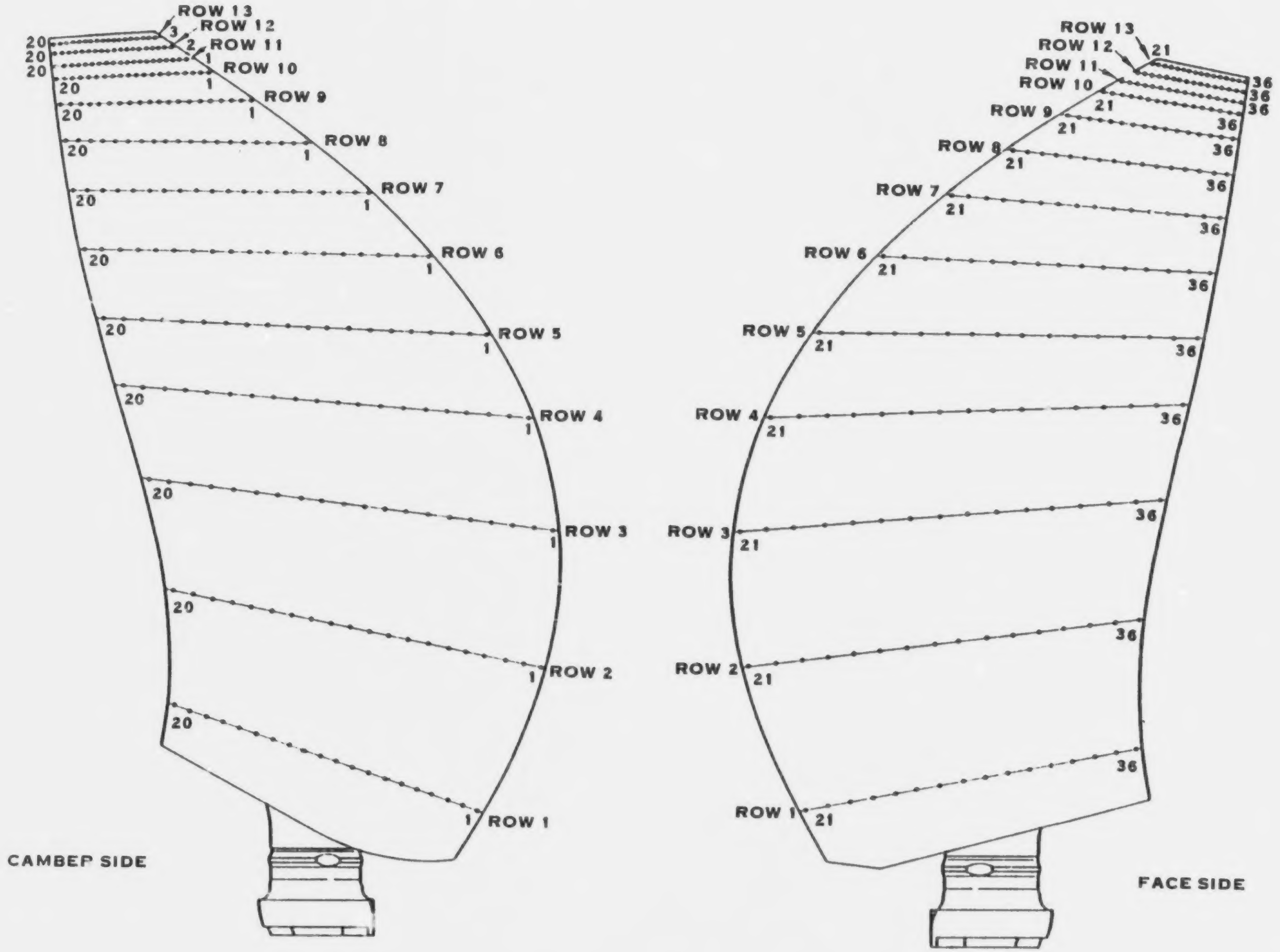
ROW 13
ROW 12
ROW 11
ROW 10
ROW 9
ROW 8
ROW 7
ROW 6
ROW 5
ROW 4
ROW 3
ROW 2
ROW 1
20
1
3
2
CAMBER SIDE
21
36
FACE SIDE

FIGURE 17.6 TAP LOCATIONS, STEADY PRESSURE BLADE, HIGH SPEED WIND TUNNEL TEST

ORIGINAL PAGE IS
OF POOR QUALITY

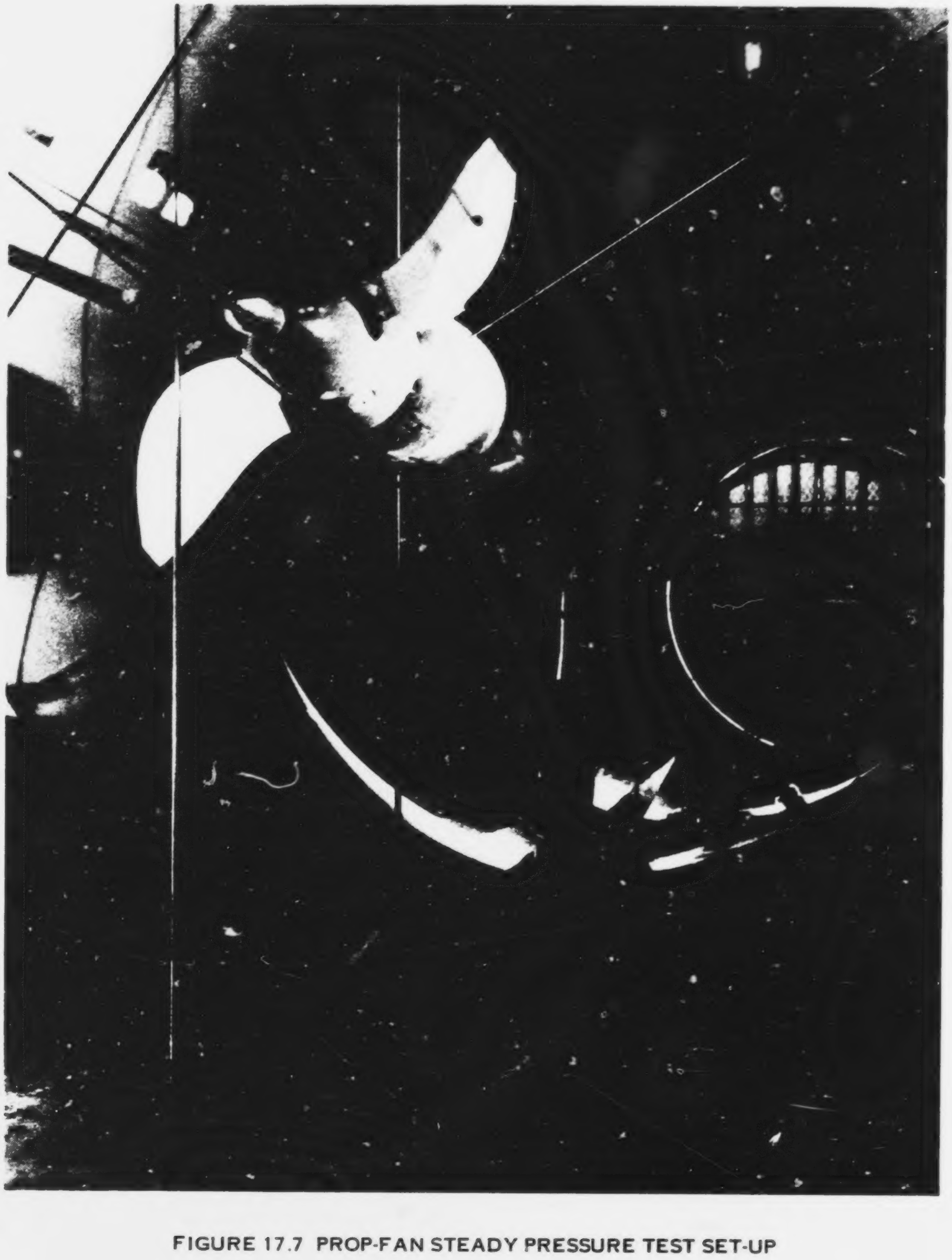

FIGURE 17.7 PROP-FAN STEADY PRESSURE TEST SET-UP

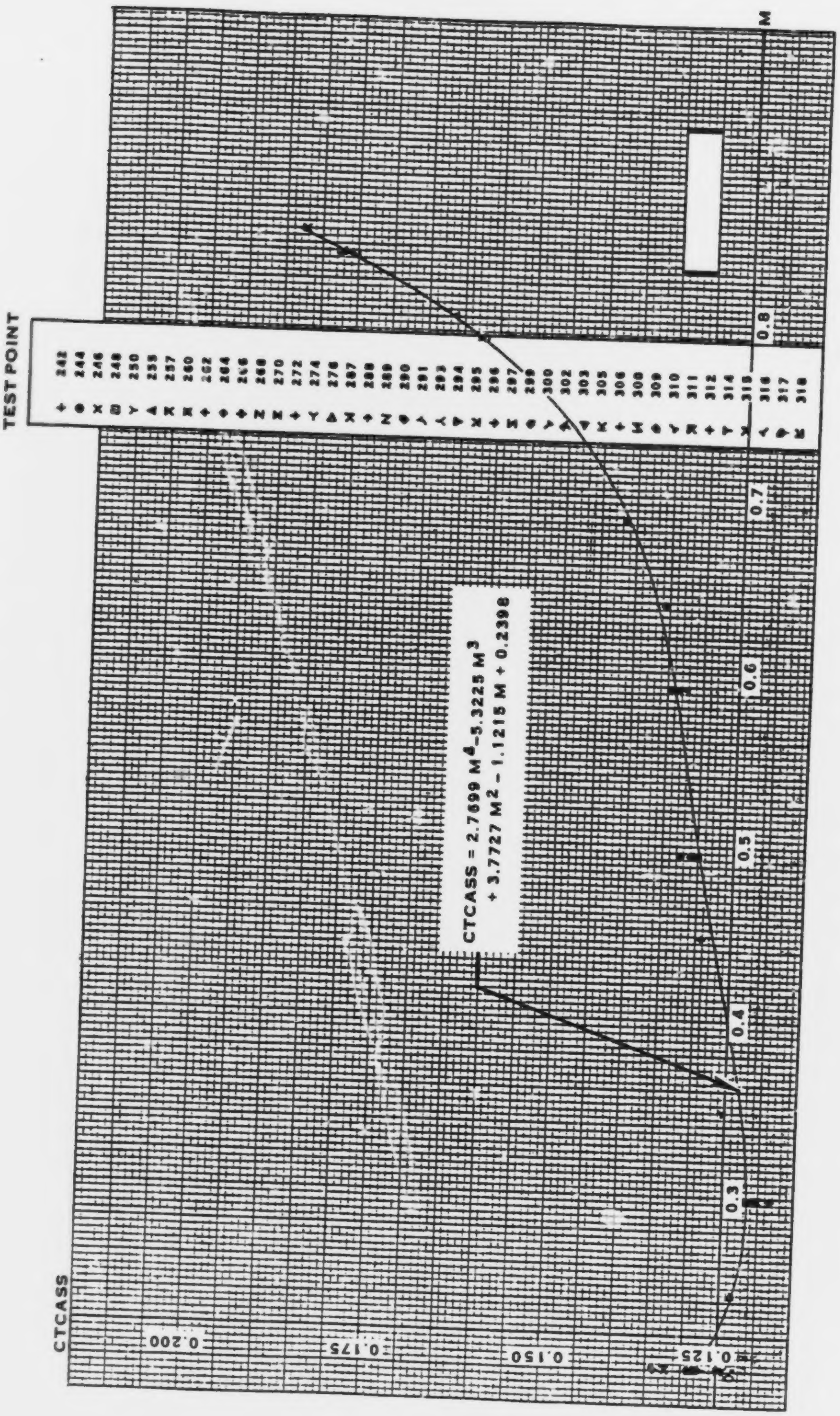

FIGURE 17.8 LAP SPINNER DRAG COEFFICIENT VS. MACH NUMBER

ORIGINAL PAGE IS
OF POOR QUALITY

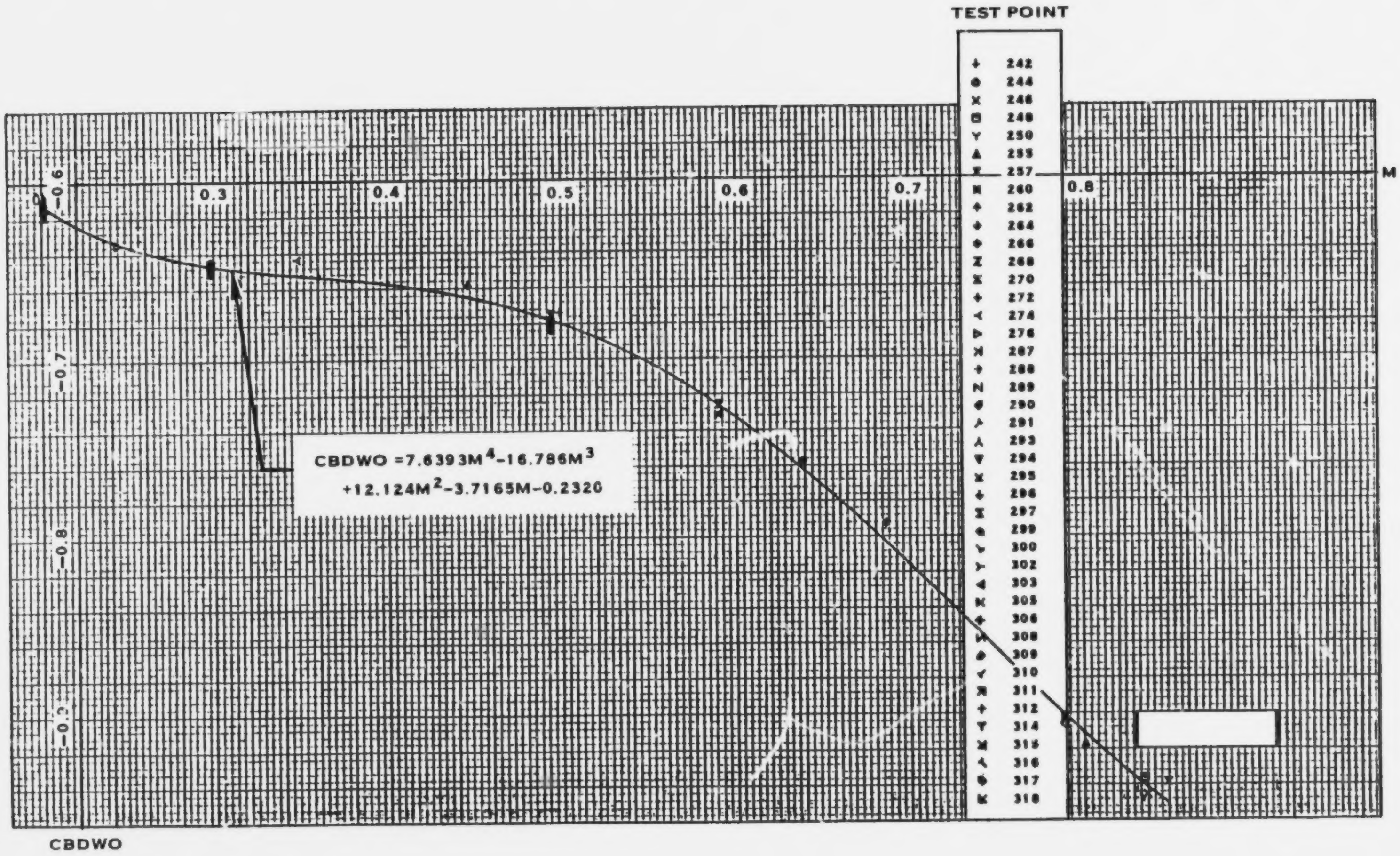

FIGURE 17.9 CENTERBODY DRAG COEFFICIENT VS. MACH NUMBER

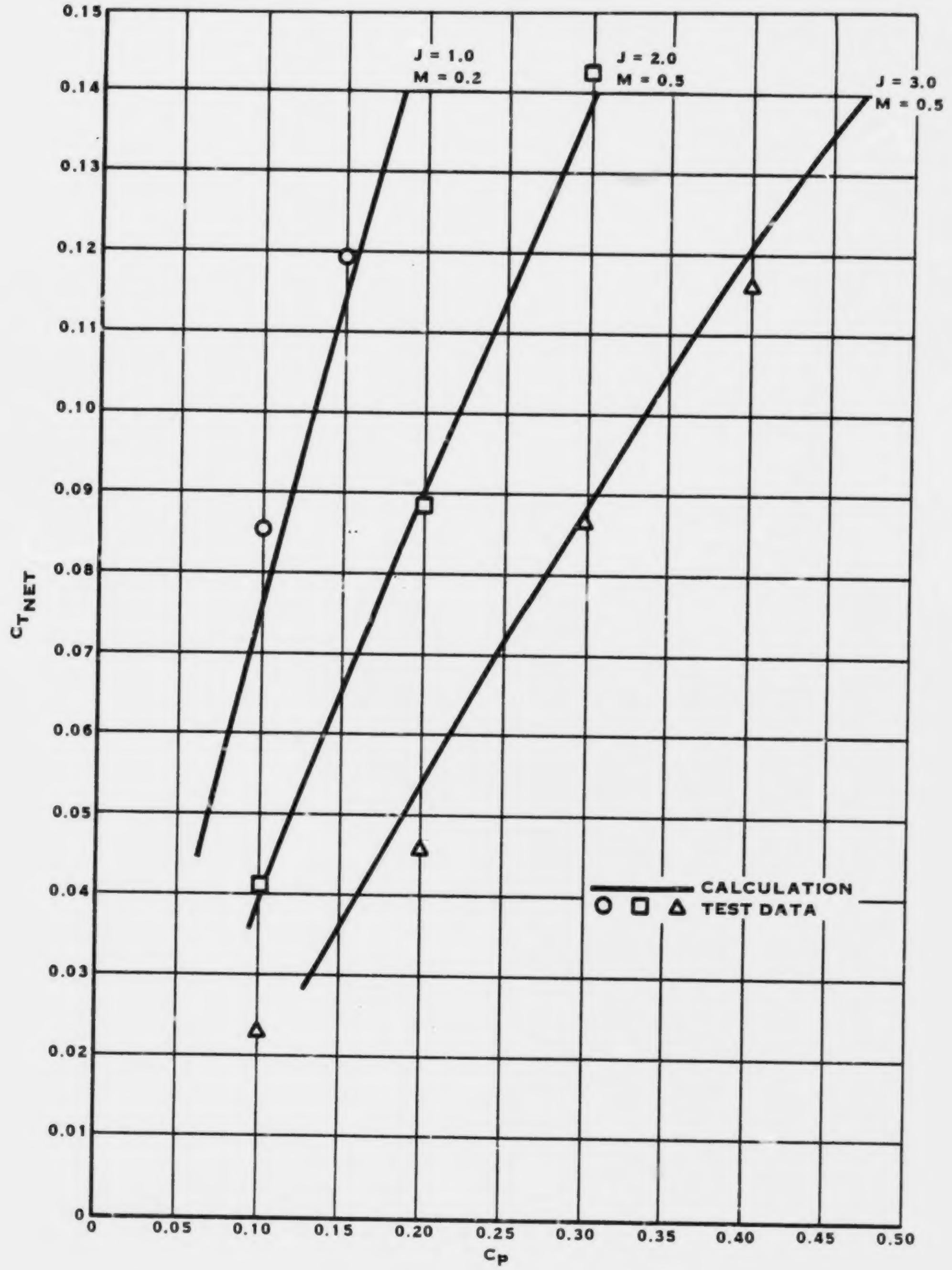

FIGURE 17.10 COMPARISON OF MEASURED AND PREDICTED PERFORMANCE 4 BLADES

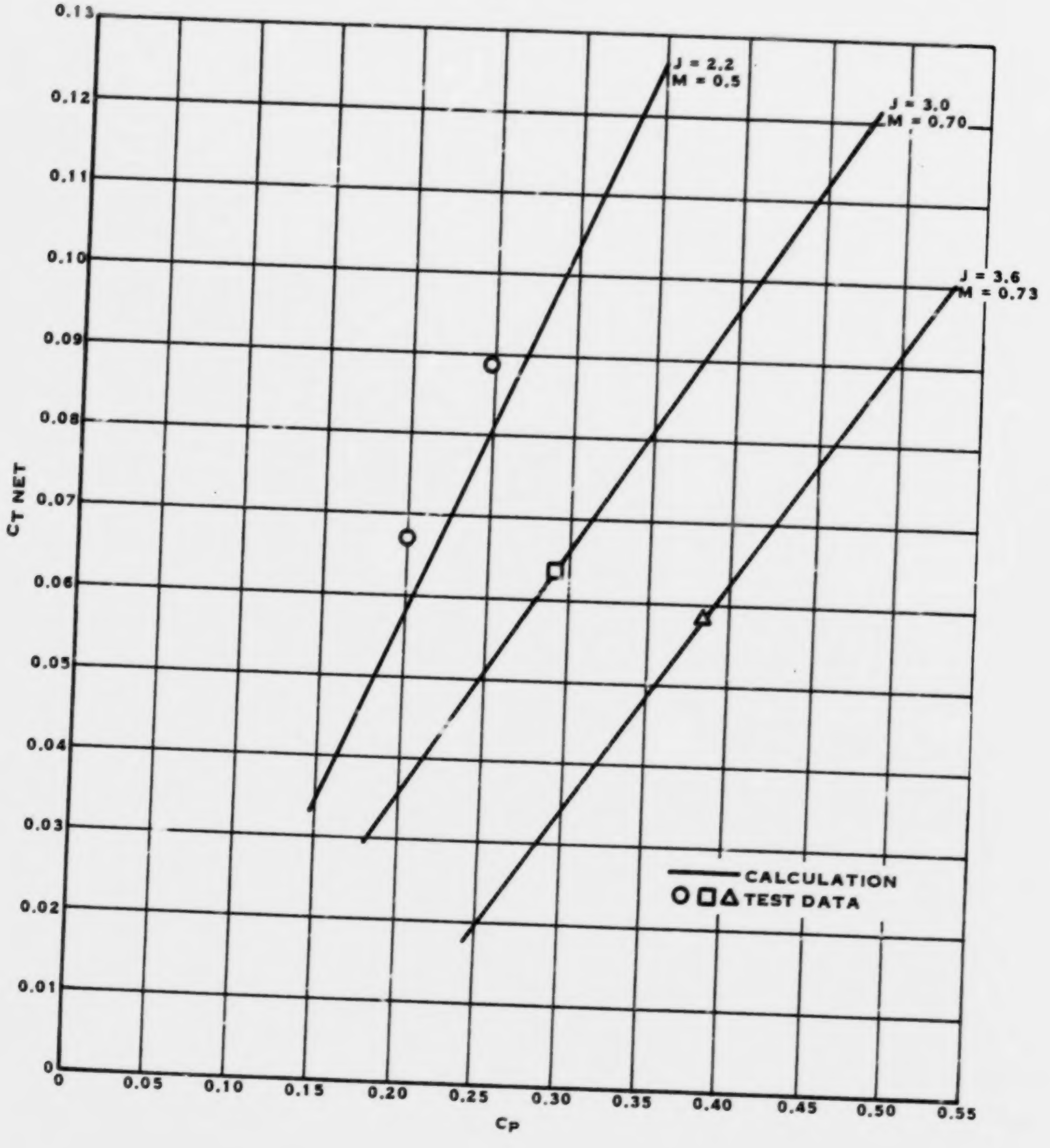

FIGURE 17.11 COMPARISON OF MEASURED AND PREDICTED PERFORMANCE, 8 BLADES

TEST CONDITION

M_N = 0.01
β = 13.8° ± 1.00°
RPM = 1200 ± 10
J = 0.08 ± 0.02
C_P = 0.079 ± 0.02

NOTES:
1. TOLERANCES SHOWN DENOTE MAXIMUM PARAMETER VARIATION FROM ONE RADIAL STATION TO THE NEXT.
2. * PLOTS CONTAIN DATA POINTS WHICH MAY BE REPLACED OR ELIMINATED.

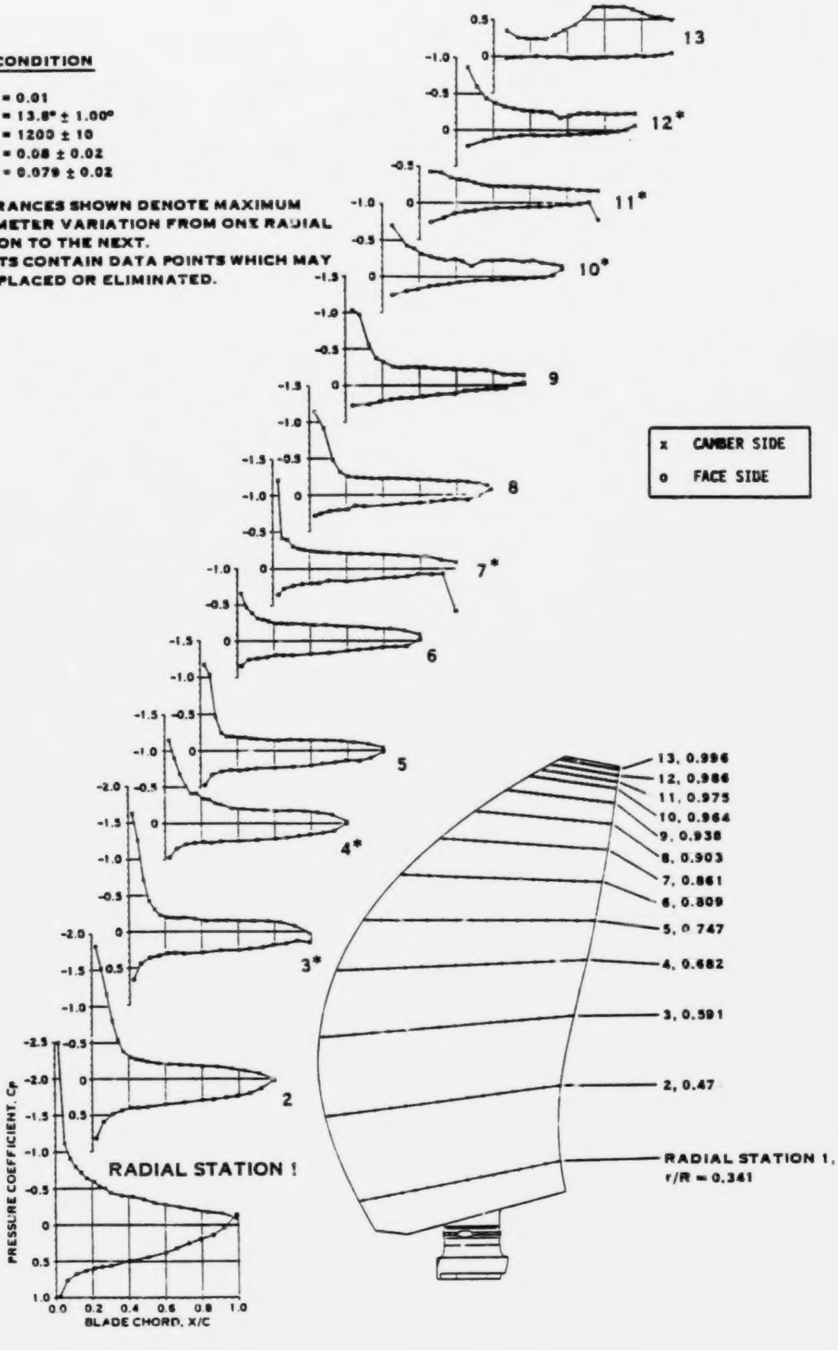

FIGURE 17.12 STEADY PRESSURE DATA - NOMINAL STATIC CASE

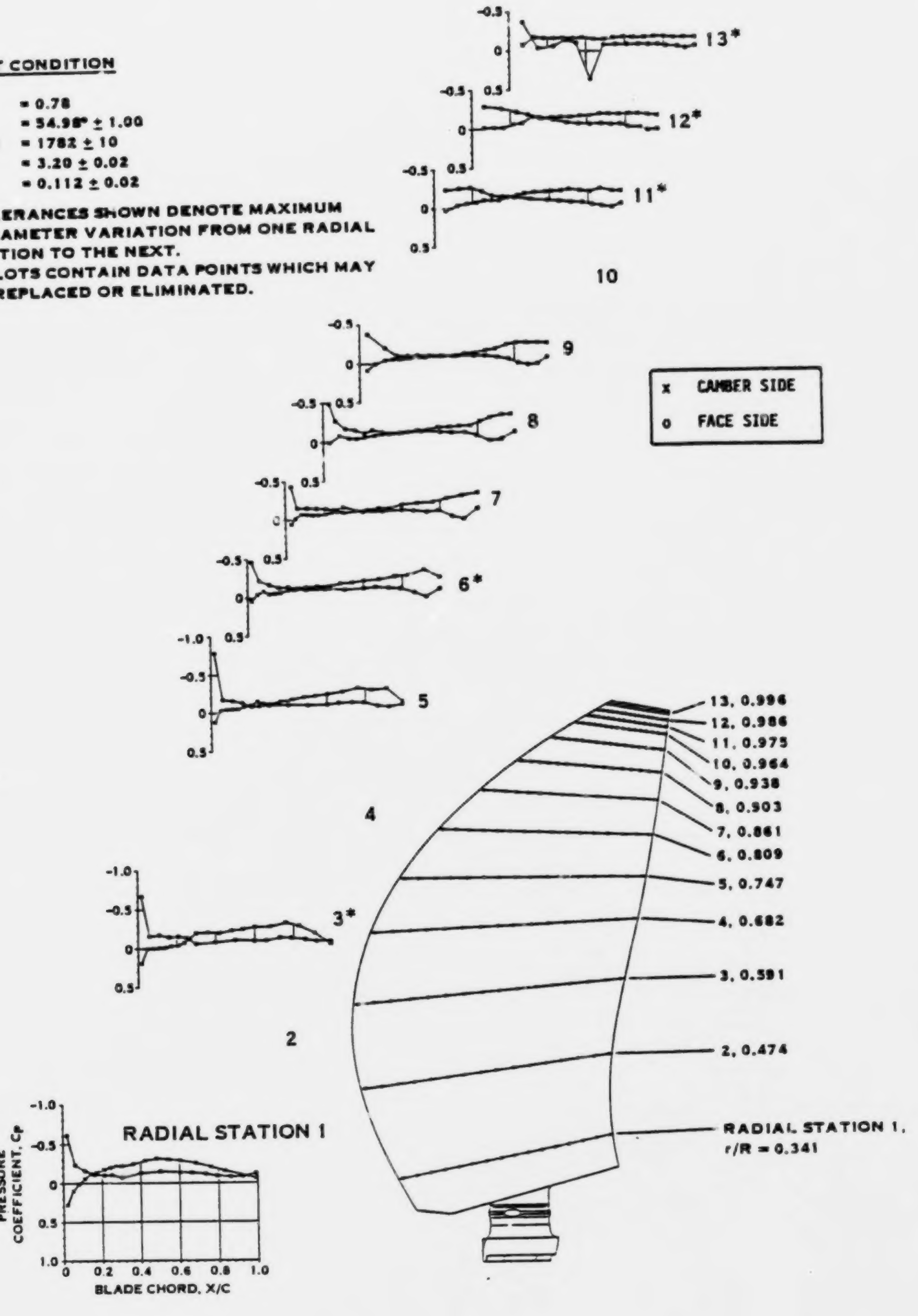

TEST CONDITION

M_N = 0.78

β = 54.98° ± 1.00

RPM = 1782 ± 10

J = 3.20 ± 0.02

C_P = 0.112 ± 0.02

NOTES:
1. TOLERANCES SHOWN DENOTE MAXIMUM PARAMETER VARIATION FROM ONE RADIAL STATION TO THE NEXT.
2. * PLOTS CONTAIN DATA POINTS WHICH MAY BE REPLACED OR ELIMINATED.

FIGURE 17.13 STEADY PRESSURE DATA - HIGH MACH NO., LOW POWER CASE

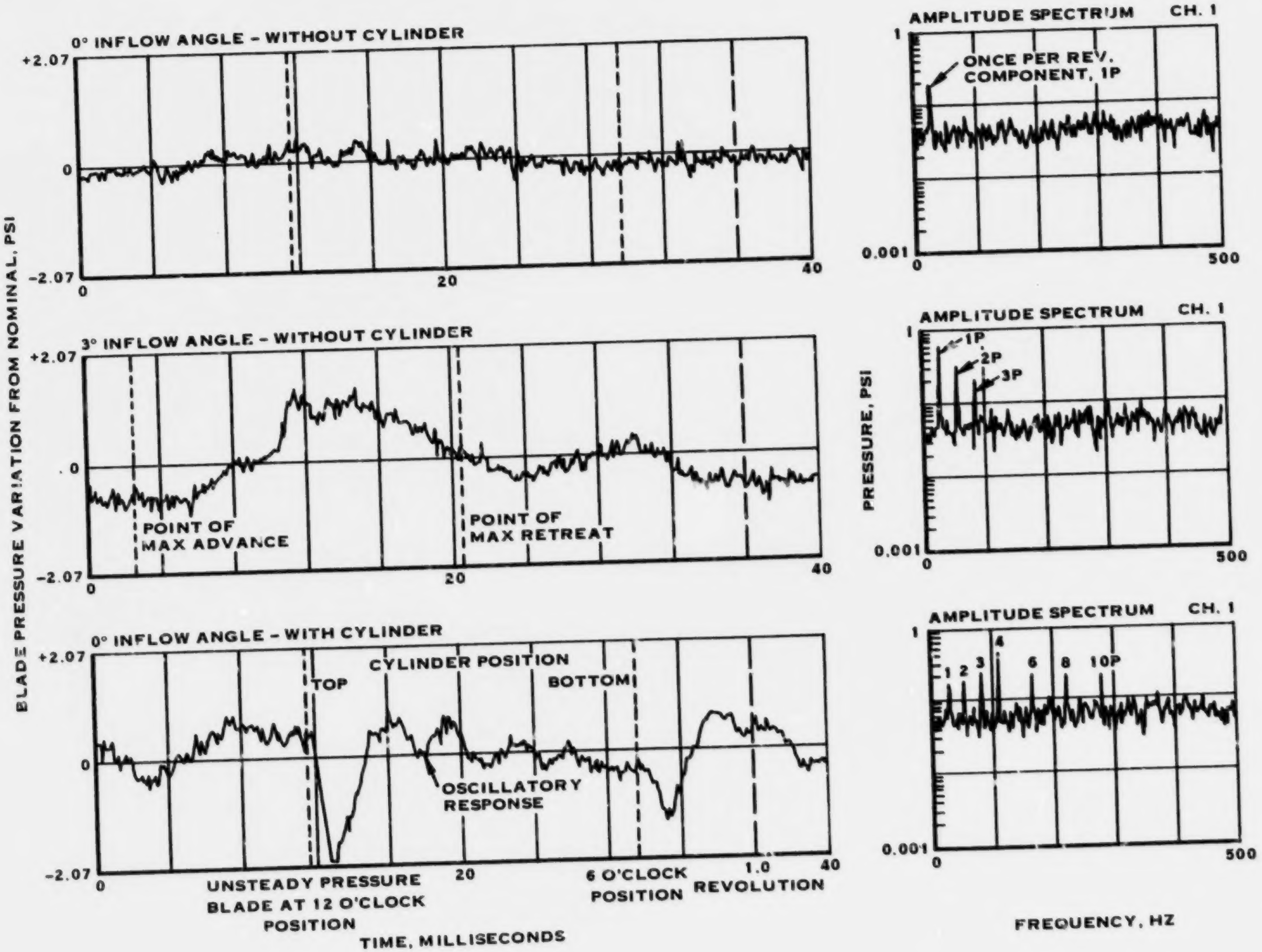

FIGURE 17.14 UNSTEADY PRESSURE DATA, HIGH SPEED WIND TUNNEL TEST
($M_n = 0.2$, J = 0.883, $C_p = 0.250$, $\beta 3/4 = 32°$)

18.0 SR-7A AEROELASTIC MODEL WIND TUNNEL TEST

Wind Tunnel testing of the SR-7A Aeroelastic Prop-Fan Model was conducted for static operating conditions, conditions simulating takeoff and climb and conditions simulating intermediate and high speed cruise. Testing was conducted at the NASA-Lewis Research Center. Static and low speed testing was conducted in the Lewis Research Center 9 X 15 wind tunnel. Intermediate and high speed testing was run in the 8 X 6 wind tunnel. This test program was designed and carried out by NASA-Lewis Research Center personnel. Hamilton Standard participated in the entire test program. This participation included a review of the NASA blade structural response measurement systems, establishing blade vibratory strain limits, determination of strain gage locations, calibration of the blade strain gage channels review of test plans with tunnel operating personnel, monitoring blade stresses during the tests and analysis of the stress data.

18.1 SR-7A AEROELASTIC MODEL INSTRUMENTATION

SR-7A model test data was acquired using strain gages installed on the blades and a speed/phase pipper. The strain gage arrangement used for SR-7A wind tunnel model testing is illustrated in Figure 18.1. Eight strain gages were installed on each of blades 1 and 5. Six of the gages, numbered 1 through 6, were installed on the camber side of these blades. The inboard bending strain was measured by gage 1, the trailing edge bending strain by gage 2, the mid-blade bending strain by gage 3, the tip bending strain by gage 4, and the tip edgewise bending and shear by gages 5 and 6. In addition, two push-pull strain gage pairs were installed on the blade shanks to measure the shank vibratory bending moments. One tip flatwise bending gage was installed on each of blades 2, 3, 4 and 6.

The constraints of the SR-7A aeroelastic model instrumentation system allowed only ten active strain gages to be monitored during any test point. The primary active gage hookup is illustrated in Figure 18.1. Strain gage signals were monitored in real time using a multichannel oscilloscope. The strain gage signals and the speed/phase pipper signal were recorded on a FM magnetic tape system. A FFT signal analyzer and a visicorder were also available for evaluating the strain signals.

18.2 SR-7A AEROELASTIC MODEL WIND TUNNEL TEST PROCEDURE

18.2.1 Static and Low Speed Testing

A schematic of the test installation for the 9 X 15 low speed wind tunnel is presented in Figure 18.2. The SR-7A aeroelastic model was powered by an air turbine rated for 634 KW (850 SHP) at 8800 RPM. The model could be operated at an inflow angle with respect to the tunnel flow by rotating the test installation about a vertical axis called the turn table axis. The range of available inflow angles was -2° to +20°. Testing was conducted at Mach numbers from 0 to .2, at blade pitch angles from -5.5° to 43.6° and at rotational speeds from 3000 RPM to 9000 RPM. The high rotational speeds were

18.2.1 (Continued)

required to obtain blade tip speeds for the SR-7A model equivalent to those in the operating range for the SR-7L. The SR-7A 1P vibratory response was calculated for three of the low speed test points using the BESTRAN finite element program. The conditions that were analyzed corresponded to takeoff and climb conditions for the SR-7L at three different power settings. The test points that were analyzed are presented in Table 18-1.

TABLE 18-1
LOW SPEED TEST POINTS FOR WHICH THE BLADE 1P RESPONSE WAS CALCULATED

Test Point	Blade Angle	Mach Number	RPM	Yaw Angle
365	29.1°	.2	7500	8°
538	34.9°	.2	7500	8°
646	43.6°	.2	7500	8°

18.2.2 Intermediate and High Speed Testing

The SR-7A Aeroelastic Model is shown installed in the NASA-Lewis 8 X 6 high speed wind tunnel in Figure 18.3. Testing was conducted over a wide range of rotational speeds (3895 RPM to 9000 RPM), Mach numbers (.36, .45, .6, .7 and .8), blade angles (42.7°, 45.5°, 48.5°, 51.3°, 54.1°, 57.3°, 59.6° and 63°) and yaw angle (0 to 7°). The SR-7L Prop-Fan was designed for cruise conditions at an altitude of 35,000 ft. at a flight speed of 0.8 Mach number, with a tip rotational speed of 800 fps. The corresponding SR-7A wind tunnel conditions were estimated as: 7520 foot altitude, 0.8 Mach number, 950 fps tip speed and a rotational speed of 8886 rpm. The blade 1P vibratory response was calculated for three of the test points using the Hamilton Standard BESTRAN finite element program. These points are listed in Table 18.2. Test point 723 was also analyzed using the NASTRAN computer program.

TABLE 18-2
HIGH SPEED TEST POINTS FOR WHICH THE BLADE 1P RESPONSE WAS CALCULATED

Test Point	Blade Angle	Mach Number	RPM	Yaw Angle
338	54.1°	.60	8004	2.08°
545	57.3°	.80	8004	2.45°
723	59.6°	.80	8006	2.13°

This allowed the comparison of the analytical and measured blade response for a range of excitation factors, as well as a comparison of the accuracy of the two different analytical techniques.

18.3 SR-7A AEROELASTIC MODEL TEST RESULTS

18.3.1 Static and Low Speed Test Results

One purpose of the low speed wind tunnel test was to investigate the effect of forward velocity on the operating envelope defined by blade high vibratory strains. Figure 18.4 shows the vibratory strain boundaries, plotted as blade angle versus rotational speed, for a range of Mach numbers from 0 to .2. The boundaries represent the operating conditions at which the vibratory strains in the blade structure reached their predetermined limits. The boundaries for the Mach .15 and Mach .2 are shown as dashed lines since the vibratory strain limit was encountered at only one point below the 9000 RPM rotational speed limit. Figure 18.4 also indicates the predominant vibratory frequency occurring at various points along the vibratory strain boundaries and the vibratory modes with which they correspond. At high blade angle static conditions the blade vibratory strains are dominated by the first edgewise and second flatwise modes. The maximum response was observed at 328 Hz corresponding to the first edgewise mode. As discussed in section 16.2.2 of this report, the stall buffet response mode of the SR-7L was found to be a function of blade angle. The SR-7L response frequency corresponded to the second flatwise mode at blade angles below 34° and the first flatwise mode at blade angles above 39°. Similar behavior was exhibited by the SR-7A aeroelastic model as illustrated by the change in response mode along the 0 Mach number vibratory strain boundary curve. For Mach numbers from .05 to .20 and high blade angle, blade buffet was dominated by higher frequency vibration corresponding to the blade second torsional mode.

Figure 18.4 indicates that an area of high vibratory strain was encountered at low blade angles for Mach numbers from 0 to .10. This behavior was not observed during Static Rotor Testing of the SR-7L Prop-Fan. The response frequency for the low blade angle buffet was 590 Hz which corresponds to the first torsional mode. A possible explanation for the onset of buffet at low blade angle is wake flutter. Wake flutter is a self excited blade vibration believed to be caused by a given blade passing through the wake of the preceding blade. The theory of wake turbulence is based on the idea of a blade natural mode being reinforced periodically by the wake pattern. It is therefore expected that such a flutter condition would occur at those rotational speeds where integral multiples of the rotational frequency are equal to a natural frequency of the blade. As seen in Figure 18.4 for a rotational speed of 7000 RPM the vibratory response was at 590Hz. The 5P frequency at 7000 RPM is 583 Hz. Therefore these results compare favorably with the wake flutter theory. It is uncertain why the wake flutter phenomenon was observed during static testing of the SR-7A Aeroelastic Model but not during the SR-7L Static Rotor Test. Reynolds number effects could be one explanation.

Figure 18.5 shows the vibratory strain boundaries for the SR-7A at 0° inflow angle and 0 Mach number overlayed on the vibratory strain boundaries determined for the SR-7L during the Static Rotor Test. For the high blade angle cases, good correlation was obtained between the SR-7A and SR-7L.

18.3.1 (Continued)

The blade 1P response, measured at several different strain gage locations, is presented as a function of inflow angle in Figure 18.6. The figure indicates that the 1P vibratory strain levels are nearly a linear function of inflow angle and that the 1P vibratory response is more pronounced at the inboard sections of the blade than the outboard sections. The total vibratory strain for the zero degree inflow angle cases was observed to be higher at the blade tip sections than at the inboard sections for the entire range of rotational speeds run. For operation at an inflow angle the total vibratory strain was generally higher at the inboard sections below 6000 RPM and then became predominant at the outboard section above 6000 RPM. This behavior is explained by the 1P response being dominant at low RPM and vibratory strain due to buffet or resonance being dominant at the higher RPM's. The critical speeds that were significant at the higher RPM's were the 5P first torsional mode crossover at 7000 RPM and the 4P first torsional mode crossover at 9000 RPM.

Significant 2P response was also observed for the inflow angle conditions at Mach .2. This was especially significant near the 2P first flatwise critical speed at 6000 RPM, where the 2P response exceeded the 1P response.

Analytical prediction of the 1P response compared well with test results for the inboard, mid-blade and tip bending strain gage locations with analytical values slightly lower than actual measured strain. Calculated shank flatwise moments compared well with test results, while the edgewise moments compared poorly. However, the edgewise moments were small and a small variation in value can be a large percentage error.

18.3.2 Intermediate and High Speed Results

Spectral analysis of the high speed wind tunnel test data was accomplished to determine the blade natural frequencies as a function of RPM. The experimentally determined variation of blade natural frequency as a function of RPM is presented in Figure 18.7. The data is also compared with predictions of the natural frequency variation with RPM for the first four vibratory modes. Good agreement was observed between test data and predictions. The variations of the 1P mid-blade vibratory bending strain with inflow angle and RPM are presented in Figures 18.8 and 18.9 for a Mach number of .7 and a 57.3° blade angle. The 2P and 3P components of vibratory strain are also presented as a function of RPM in Figure 18.9. The strains presented in these figures are data sample averages of the peak vibratory strain amplitudes. The variation of the 1P vibratory strain with blade angle is found to be linear which is the expected trend. Figure 18.9 shows that the 1P blade response is predominant which was expected for the case of a pure inflow angle. For the Mach .7, 57.3° blade angle and 2.5° inflow angle case the mid-blade 1P vibratory bending strains were found to be 30% to 50% greater than the blade tip 1P bending strains over the whole range of rotational speeds that were tested. The trend of a lower 1P response at the

18.3.2 (Continued)

outboard section of the blade is consistent with the trends observed during the LAP High Speed Wind Tunnel Test. Comparison of data with analysis showed that the mid-blade 1P response was overpredicted by from 4% to 32% for the 3 cases for which a finite element solution was generated. The overprediction of the 1P response at this station also correlates with the LAP wind tunnel test. Analysis both underpredicted and overpredicted the tip 1P response for the different cases that were analyzed. The BESTRAN and NASTRAN analyses were found to correlate well.

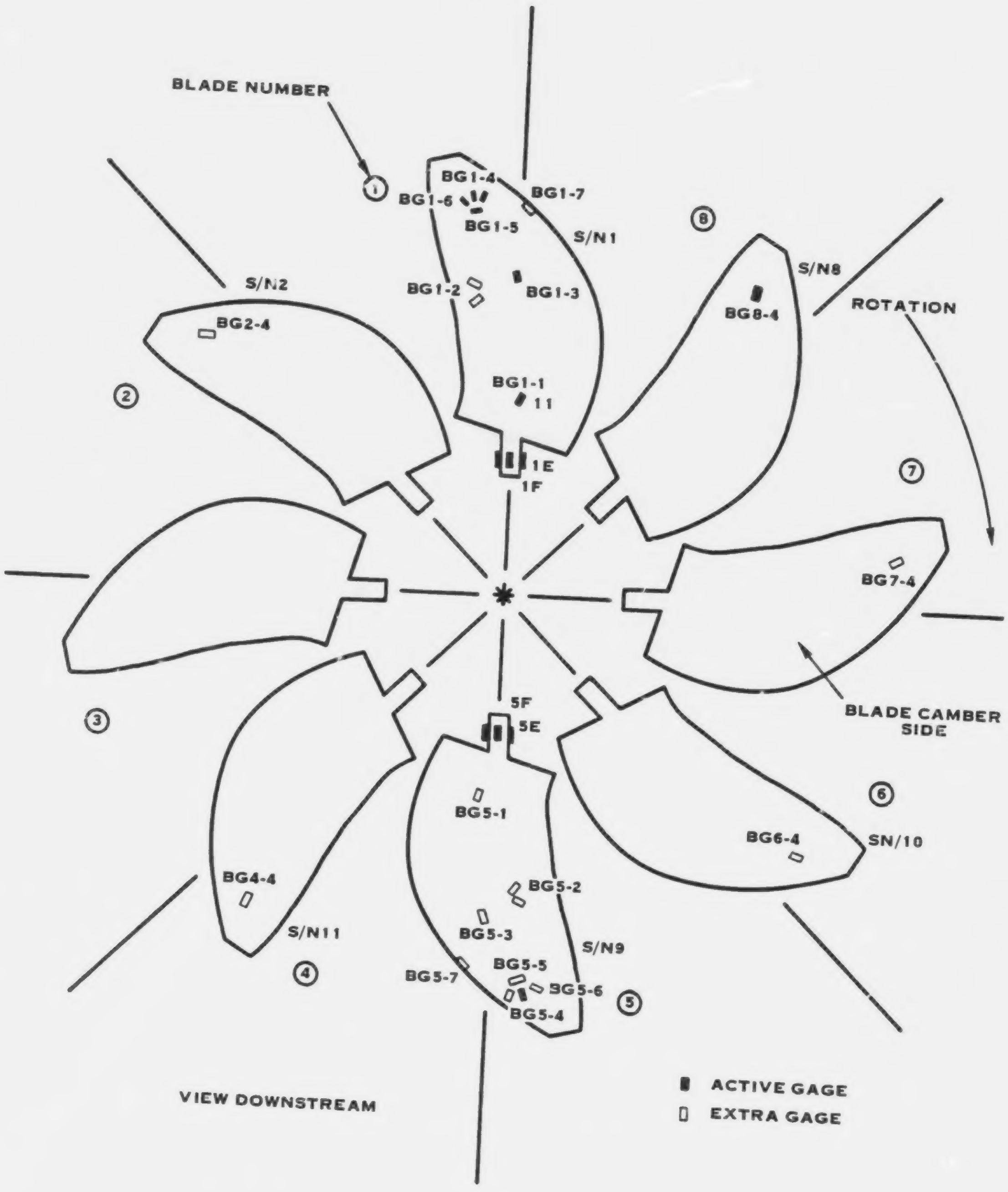
BLADE NUMBER
①
BG1-4
BG1-6
BG1-7
BG1-5
S/N1
⑧
S/N2
BG1-2
BG1-3
S/N8
BG2-4
BG8-4
ROTATION
BG1-1
11
②
1E
1F
⑦
BG7-4
5F
5E
BLADE CAMBER SIDE
③
⑥
BG5-1
BG6-4
SN/10
BG4-4
BG5-2
BG5-3
S/N11
S/N9
BG5-5
④
BG5-7
BG5-6
⑤
BG5-4
VIEW DOWNSTREAM
▮ ACTIVE GAGE
▯ EXTRA GAGE

FIGURE 18.1 SR-7A STRAIN GAGE ARRANGEMENT

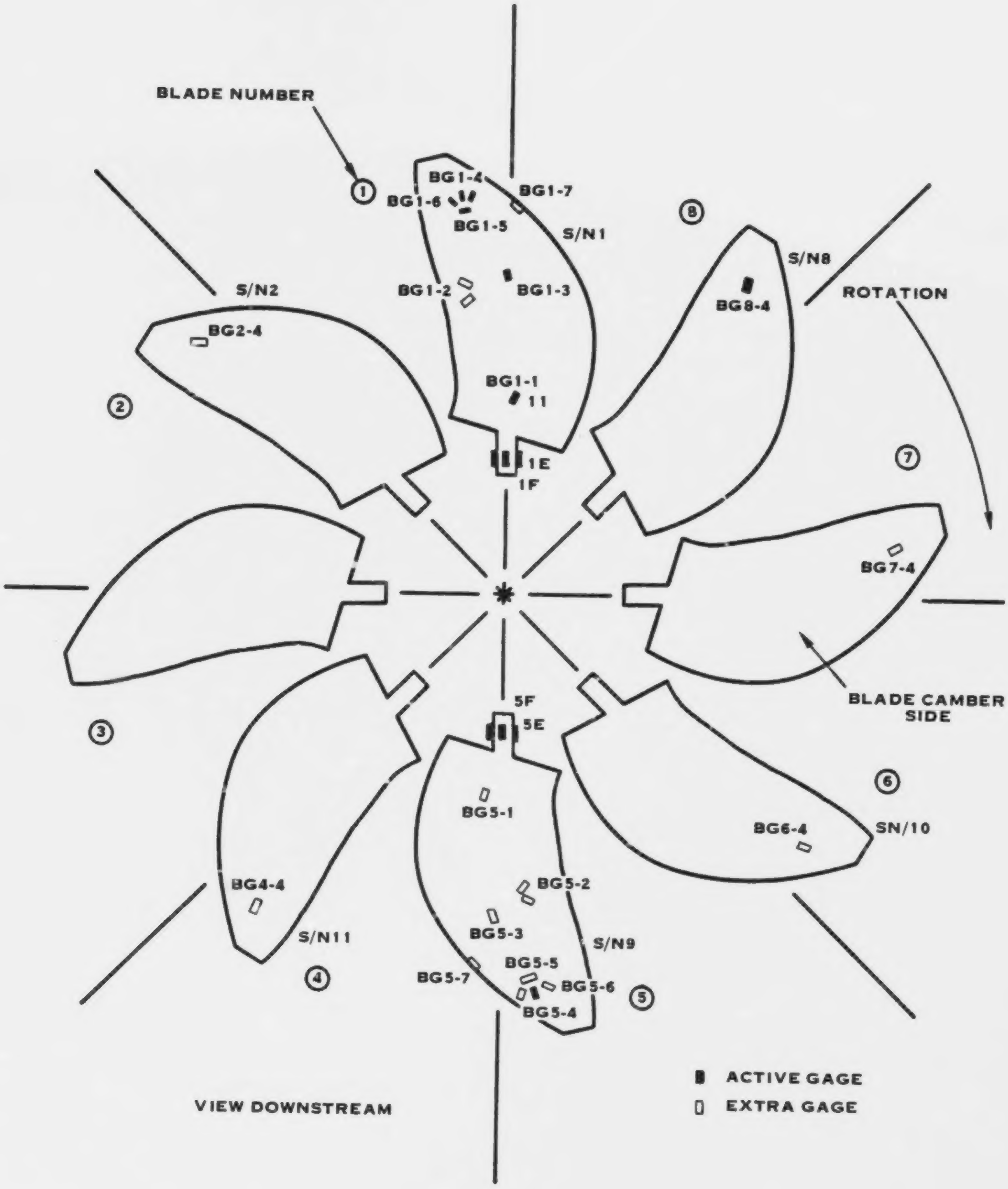
BLADE NUMBER
①
BG1-4
BG1-7
BG1-6
BG1-5
S/N1
⑧
S/N8
S/N2
BG1-2
BG1-3
BG8-4
ROTATION
BG2-4
BG1-1
11
②
1E
1F
⑦
BG7-4
BLADE CAMBER SIDE
5F
5E
③
⑥
BG5-1
BG6-4
SN/10
BG4-4
BG5-2
BG5-3
S/N9
S/N11
BG5-5
BG5-7
BG5-6
④
⑤
BG5-4
ACTIVE GAGE
EXTRA GAGE
VIEW DOWNSTREAM

FIGURE 18.1 SR-7A STRAIN GAGE ARRANGEMENT

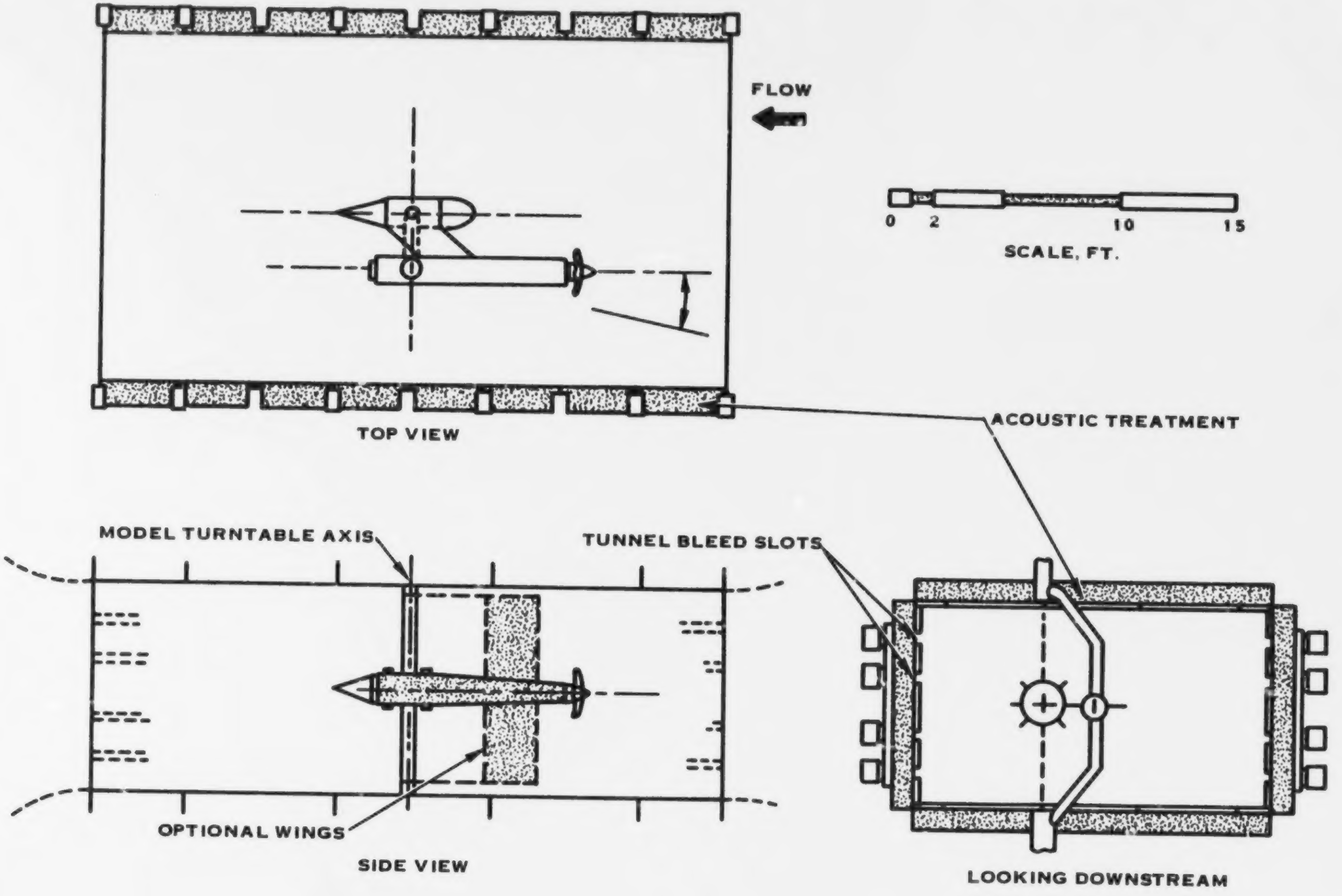
FLOW
0
2
10
15
SCALE, FT.
TOP VIEW
ACOUSTIC TREATMENT
MODEL TURNTABLE AXIS
TUNNEL BLEED SLOTS
OPTIONAL WINGS
SIDE VIEW
LOOKING DOWNSTREAM

FIGURE 18.2 SR-7A INSTALLED IN 9 X 15 LOW SPEED WIND TUNNEL

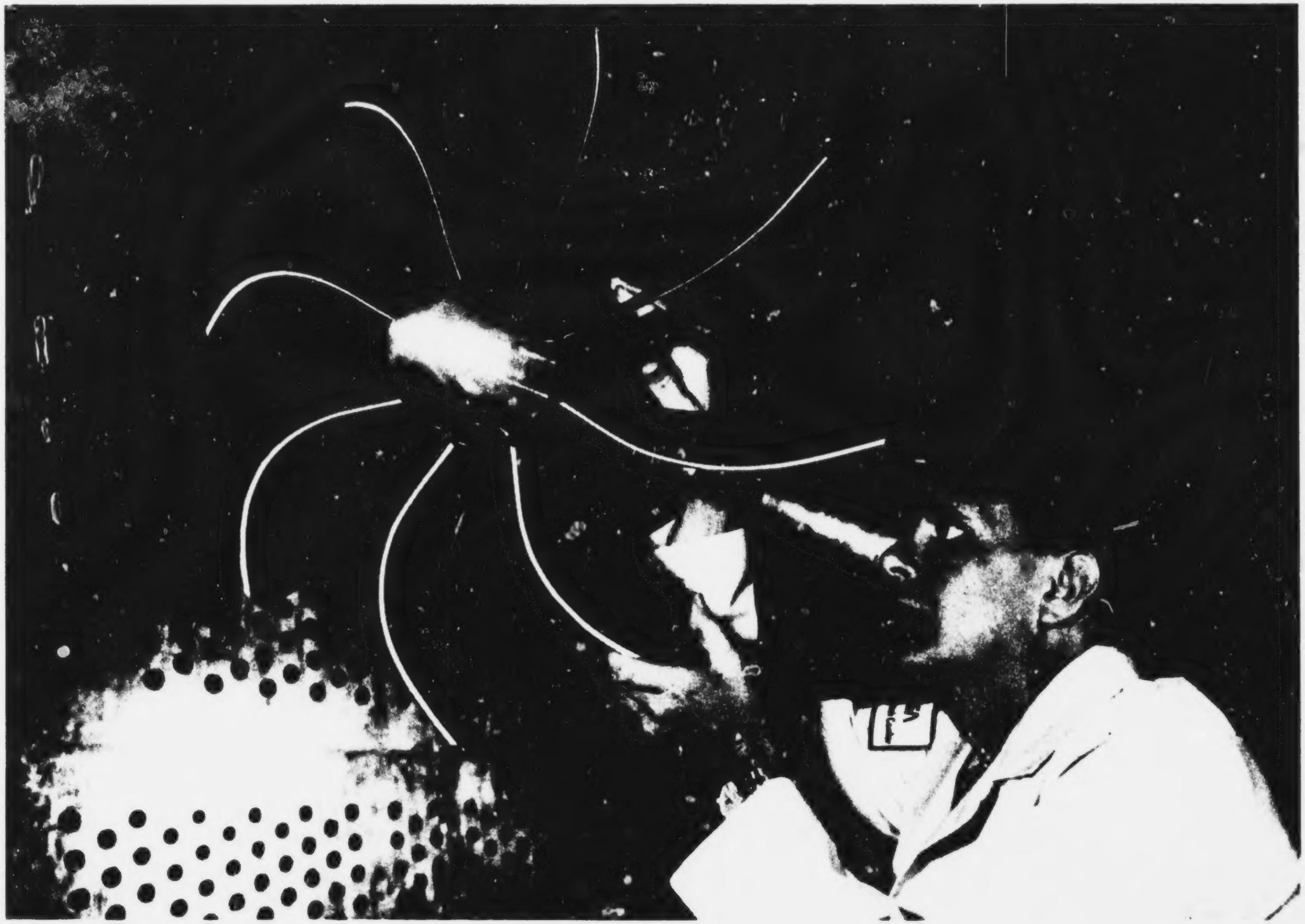

FIGURE 18.3 SR-7A MODEL PROP-FAN IN 8 X 6 FOOT NASA-LEWIS WIND TUNNEL E-37988

IGINAL PAGE IS
OF POOR QUALITY

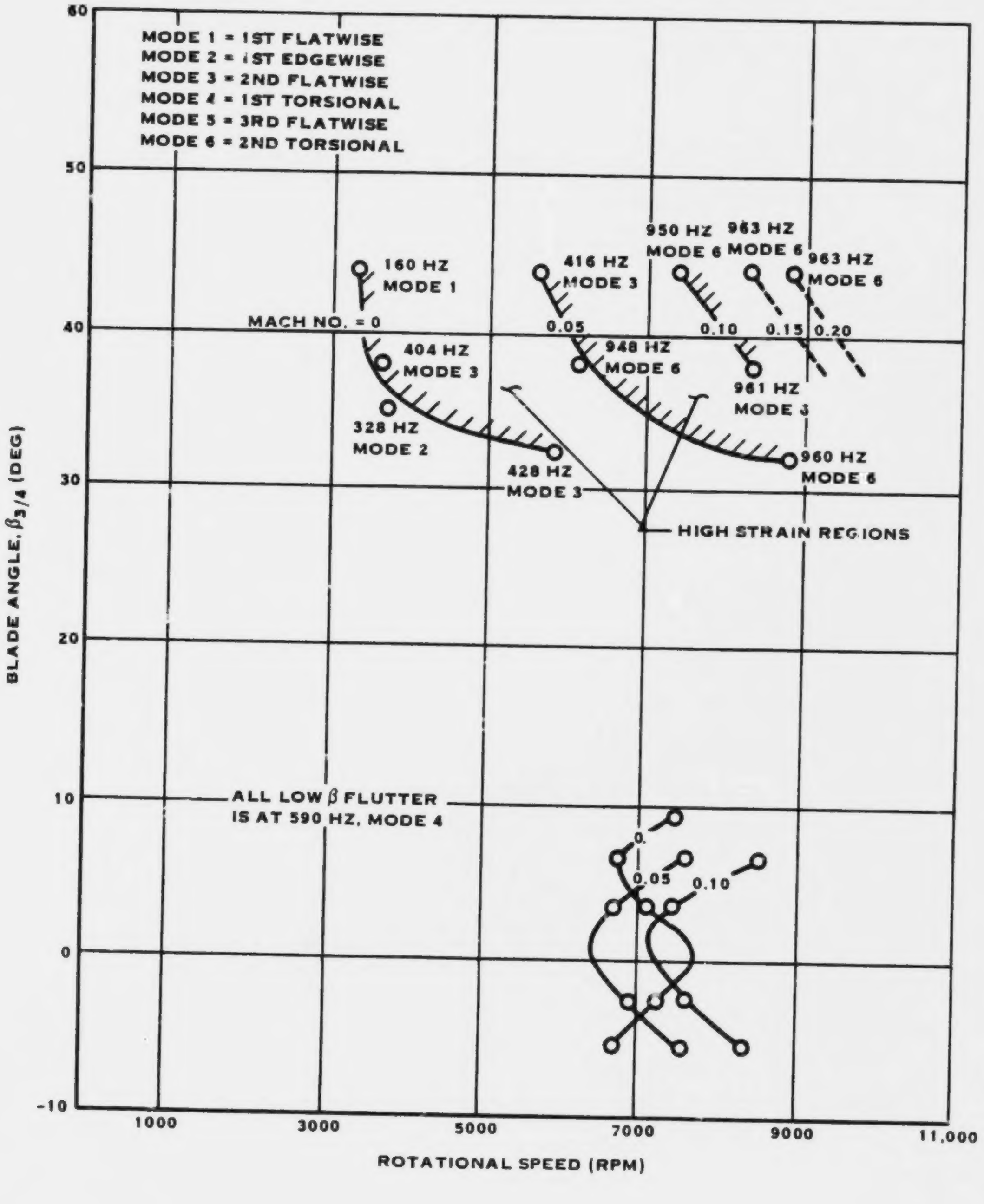

FIGURE 18.4 SR-7A HIGH VIBRATORY STRAIN OPERATING LIMITS

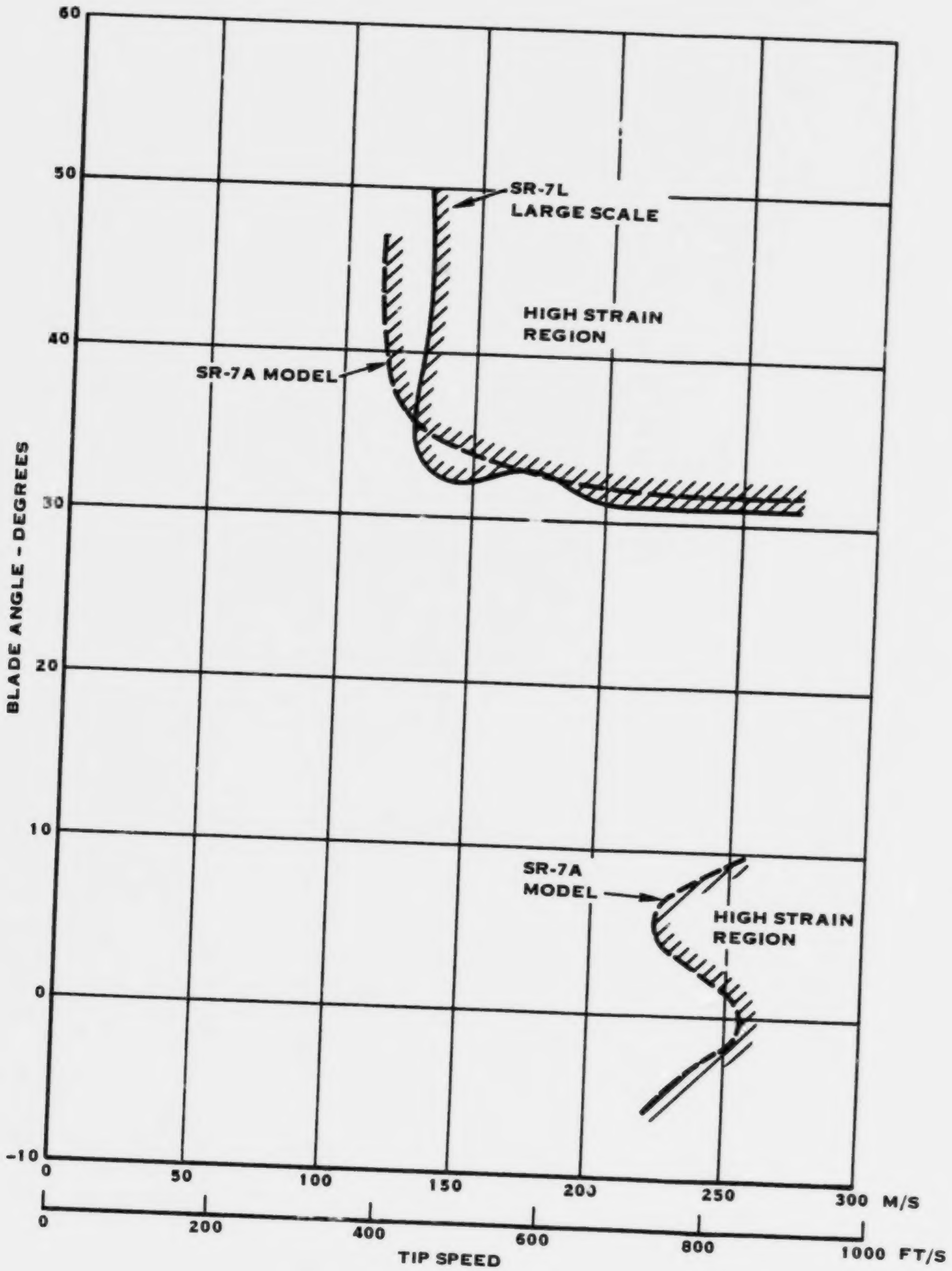

FIGURE 18.5 COMPARISON OF HIGH VIBRATORY STRAIN OPERATING BOUNDARIES FOR SR-7A AND SR-7L

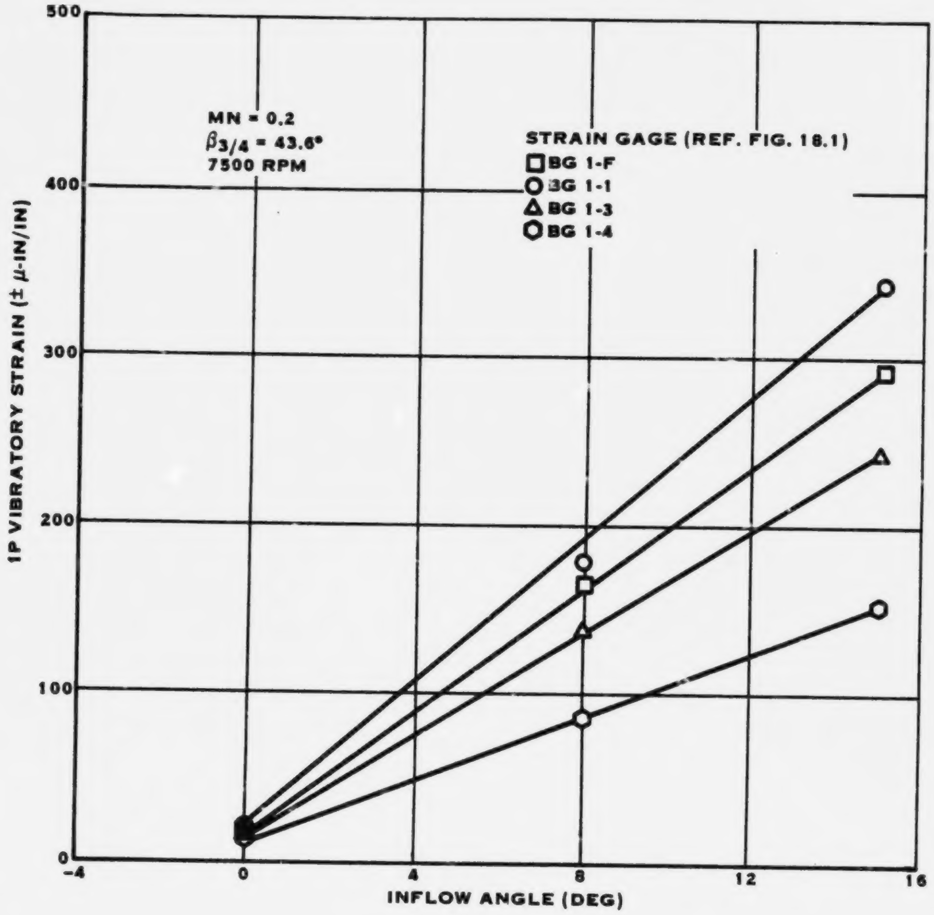

FIGURE 18.6 1P VIBRATORY STRAIN RESPONSE AS A FUNCTION OF INFLOW ANGLE

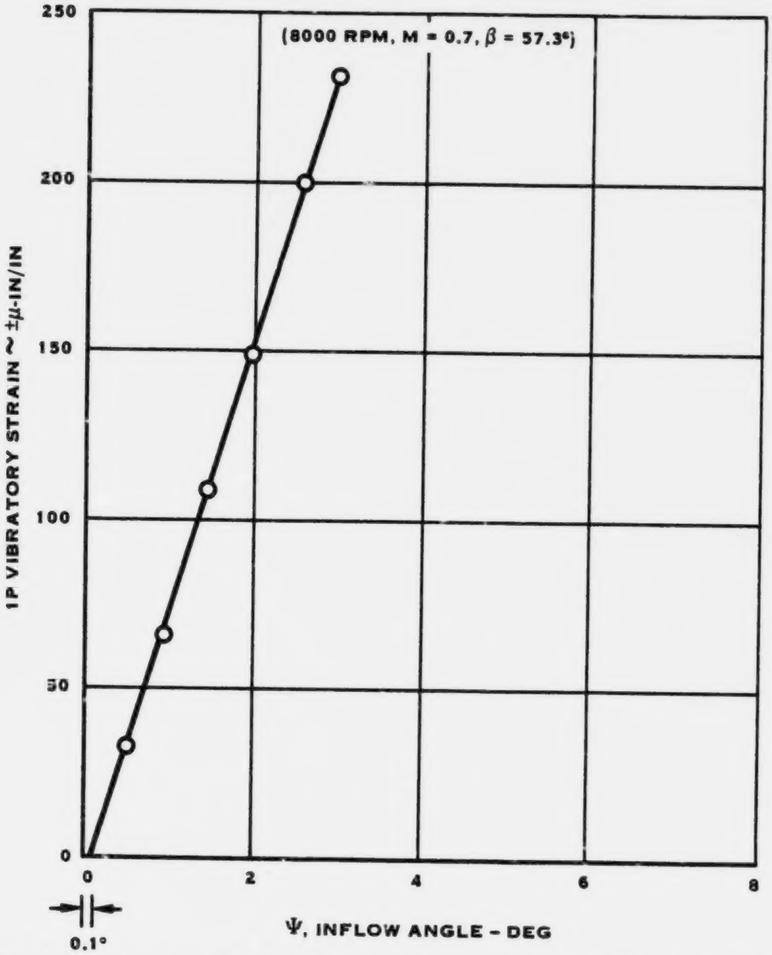

FIGURE 18.8 MID-BLADE 1P VIBRATORY STRAIN VS. INFLOW ANGLE

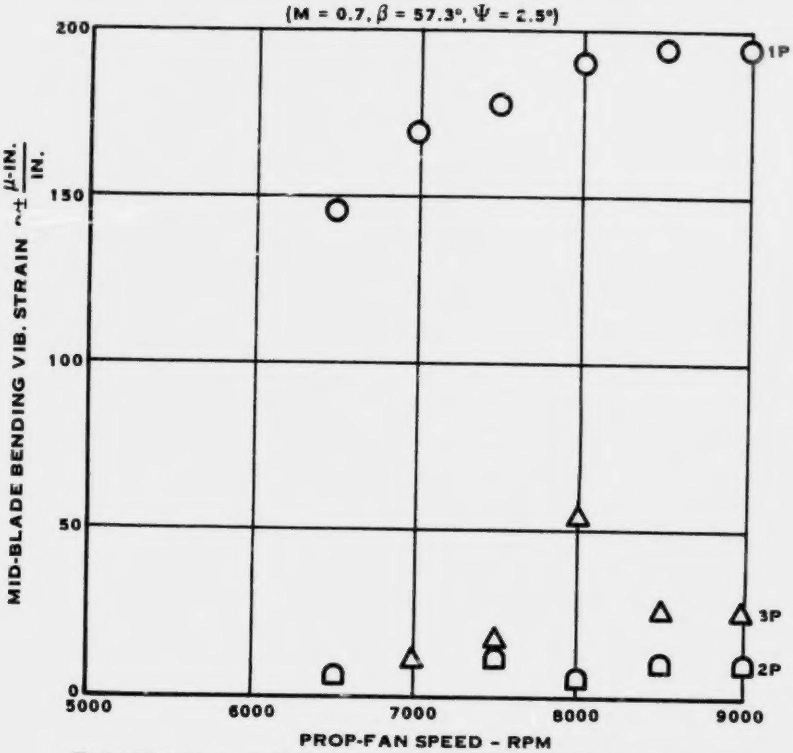

FIGURE 18.9 MID BLADE VIBRATORY STRAIN VS. RPM

19.0 INTERFACE COORDINATION

The purpose of the interface coordination effort conducted under the LAP program was to provide airframe and turbine engine manufacturers with a unified Prop Fan data package that could be used in the design of a test bed aircraft and drive system for flight test evaluation of the Large Scale Advanced Prop Fan. Four categories of Prop Fan data were provided in this data package. These categories included the physical characteristics of the Prop Fan, (mass and dimensional properties), definition of the utilities required by the Prop Fan, the interconnections between the Prop Fan and the aircraft and turbine engine systems and the Prop Fan aerodynamic and acoustic performance characteristics.

19.1 INSTALLATION DRAWING

Installation drawing SK 108280, Figure 19.1, was prepared to illustrate the areas where interface coordination between the Prop Fan and the airframe or drive system are required.

19.2 PROP-FAN PHYSICAL PROPERTIES

The mass of the LAP is 660 kg (1455 lbs.) of which 584 kg (1287 lbs.) is rotating. The weight includes eight blades, the hub, pitch control and actuator, spinner, instrumentation and hydraulic oil. It does not include any pitch control/airframe interface devices or linkages. The center of gravity of the Prop Fan is located 46.2 cm (18.2 in.) forward of the rear cone seat as illustrated in drawing SK 108280. The polar mass moment of inertia of the rotating assembly about the Prop Fan axis of rotation is 82.5 kg m^2 (1959 lb ft^2) and 87.2 kg m^2 (2071 lb ft^2) about a normal to the axis of rotation through the center of gravity.

The spinner contour is defined in drawing SK 108280. It is recommended that a minimum axial gap of 2mm (.08in) be allowed between the aft plane of the spinner and the stationary aircraft nacelle.

The dimensional envelope for the stationary Prop Fan pitch control is also defined in drawing SK108280. The envelope includes clearances that must be allowed for removal of such items as the oil dip stick, oil filler cap and valve housing access cover. The maximum static diameter of the Prop Fan blades is 272.5 cm (107.3 in). The trailing edge of the blade at the tip swings through a radius of 35.2 cm (13.84 in) from the blade pitch axis as the blade pitch angle changes from low pitch to feather.

19.3 INTERCONNECTIONS AND UTILITIES

19.3.1 Mechanical

The LAP is designed to be mounted on a standard 60A splined propeller shaft. The configuration of the shaft is defined in Aeronautical Design Standard AND 10152.

In order to prevent the pitch control from rotating with the Prop Fan, a control drive bracket must be provided on the aircraft or engine stationary structure. The bracket engages a female clip bolted to the control housing. The design of the anti-torque bracket as well as its required position with respect to the control are illustrated in drawing SK108280.

An external heat exchanger must be provided for cooling, the Prop Fan MIL-H-5606 hydraulic oil. The oil leaves and returns to the Prop Fan through two ports on the rear of the pitch control. The location and configuration of these ports are illustrated in the installation drawing. The heat exchanger must be designed for a heat rejection rate of 7.6KW (10.2 H.P.) at a flow rate of .87 liters/sec (55 QPM) and a maximum return oil temperature of 77°C (170°F). The maximum pressure drop through the heat exchanger, including all piping and fittings, must be less than 137,900 pa (20 psi).

An oil collection system is provided on the Prop Fan to collect any static oil leakage from the control forward and rear lip seals. The leakage is routed to a manifold block on the side of the control. A line must be provided to route the leakage from the manifold to a collection reservoir. The port on the manifold block is configured per MS33649-06.

The Prop Fan governing speed is set by means of a single mechanical input lever on the rear of the pitch control. The Prop Fan can also be feathered using this lever. The location and configuration of the lever are shown in drawing SK108280. The angular orientations of the lever corresponding to the governing speed range and the feather position are also indicated. A torque of 1.1 N-m (10 in lbs) is required to move the input lever in the governing range. A torque of 6.8 N-m (60 in-lbs) is requirement to move the lever into the feather position.

19.3.2 Electrical

The auxiliary motor and pump provide hydraulic pressure for static cycling and feathering of the propeller. A three pin military connection (RB 1302-18-22P.) is provided on the pitch control for supplying electric power to the auxiliary motor. The motor is three phase delta connected and rated for 200 volts and 400 HZ. The maximum steady state power draw is 3350 Watts. The duty cycle for the motor is 20 seconds on and 15 minutes off. Control logic must be provided that activates the motor in conjunction with the feather/unfeather command and turns it off after 20 seconds of operation.

19.3.2 (Continued)

The feather solenoid allows the feather command to be input to the Prop Fan by an electrical signal. A two pin, military type connector (MS3102R-125-3P) is provided on the top of the control valve housing cover for the feather solenoid. The feather solenoid operates on 24 volt DC power and has a maximum current draw of 1 amp.

A flow switch is contained in the pitch control which detects the loss of flow from the standby hydraulic pump. The switch is normally closed and provides continuity to ground when oil flow falls below the minimum specified level. A connection to the flow switch can be made at pin D of a ten pin military connector (RB 3102-18-1P). The location of the connector is specified on the installation drawing.

Figure 19.2 presents the calculated reverse thrust as a function of airspeed for a blade angle of -5° and an engine power level of 310 kw (415 SHP). The variation of Prop Fan speed with airspeed is also presented. The -5° is a typical reverse thrust angle for the Prop Fan and the 310 kw in close to the maximum power that can be applied in the reverse configuration without risking a significant overspeed.

The drag of the Prop Fan in the feathered/configuration is presented as a function of Mach no. in Figure 19.3. The feathered configuration corresponds to a blade pitch angle of approximately 87°.

The windmilling drag and rotational speed for the Prop Fan at 35000 ft and Mach .8 are presented in Figure 19.4. The calculations assume that the Prop Fan is at steady state operation at the power level listed along the abscissa of the figure and the blade tip speed listed above the curve. A 1° loss of block angle prior to pitchlocking is also assumed to occur with the removal of engine power.

FOLDOUT FRAME

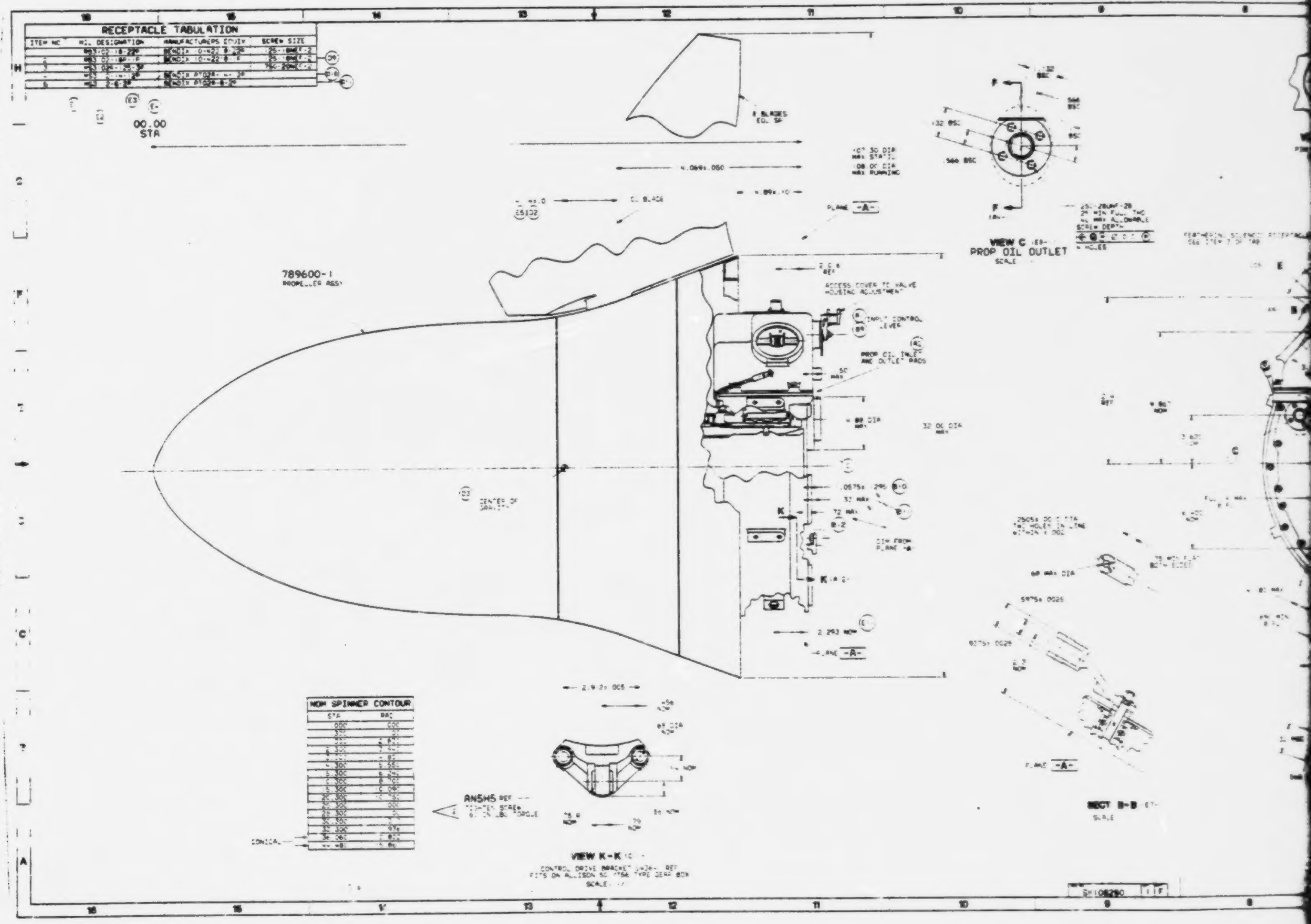
RECEPTACLE TABULATION
ITEM NO
MIL DESIGNATION
MANUFACTURERS EQUIV
SCREW SIZE
00.00
STA
8 BLADES
4.069±.050
PLANE -A-
VIEW C
PROP OIL OUTLET
789600-1
PROPELLER ASSY
ACCESS COVER TO VALVE HOUSING ADJUSTMENT
INPUT CONTROL LEVER
PROP OIL INLET AND OUTLET PADS
32.00 DIA
CENTER OF GRAVITY
K
K
2.293 NOM
PLANE -A-
NOM SPINNER CONTOUR
STA
RAD
CONICAL
AN5H5 REF
TIGHTEN SCREW
VIEW K-K
CONTROL DRIVE BRACKET
FITS ON ALLISON T56 TYPE GEAR BOX
SECT B-B
PLANE -A-
FEATHERING SOLENOID RECEPTACLE
E
B
C
SH108290
16
15
14
13
12
11
10
9
8
H
G
F
E
D
C
B
A

2 FOLDOUT FRAME

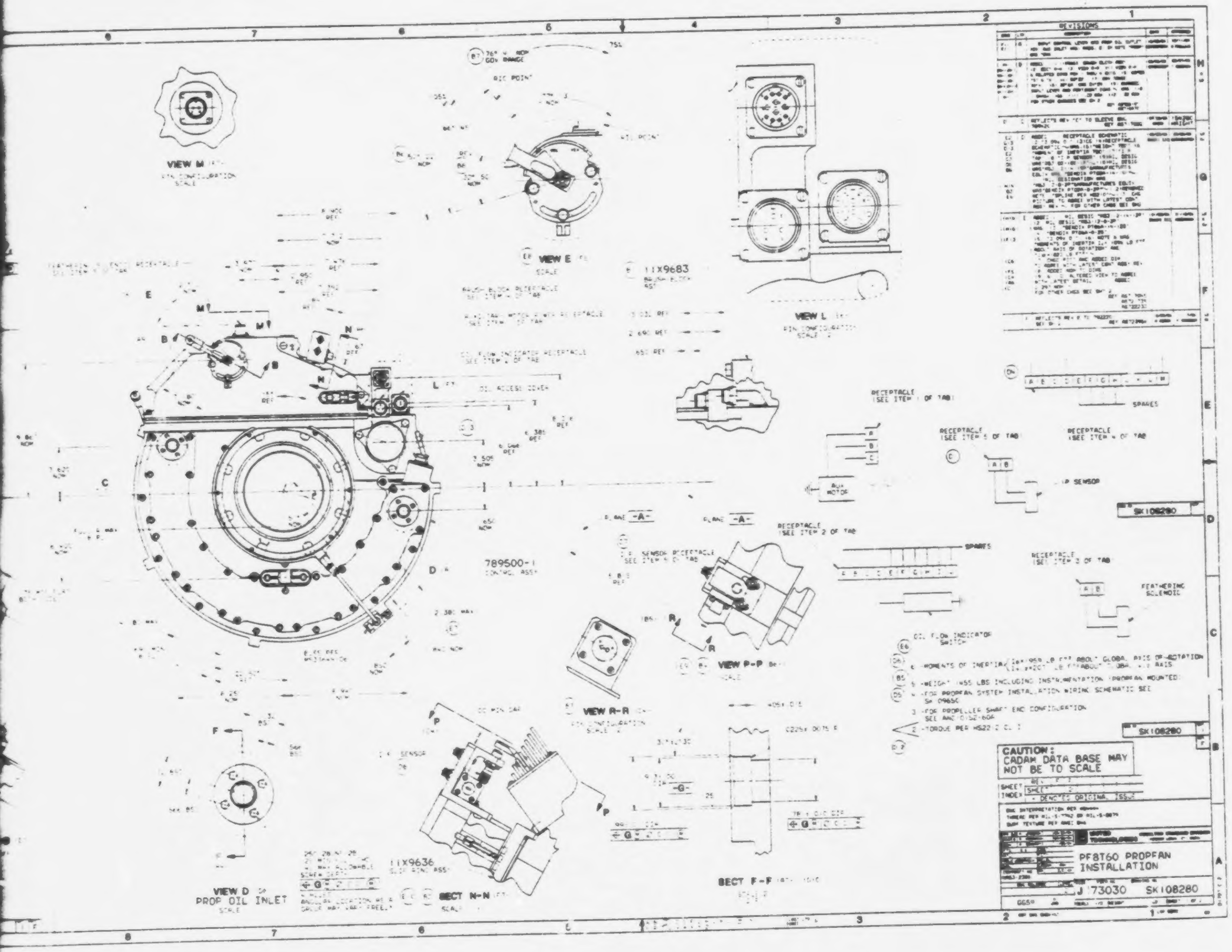
REVISIONS
VIEW M
PIN CONFIGURATION
VIEW E
11X9683
BRUSH BLOCK ASSY
VIEW L
PIN CONFIGURATION
789500-1
CONTROL ASSY
RECEPTACLE (SEE ITEM 1 OF TAB)
RECEPTACLE (SEE ITEM 5 OF TAB)
RECEPTACLE (SEE ITEM 4 OF TAB)
RECEPTACLE (SEE ITEM 2 OF TAB)
RECEPTACLE (SEE ITEM 3 OF TAB)
SPARES
AUX MOTOR
LP SENSOR
FEATHERING SOLENOID
OIL FLOW INDICATOR SWITCH
PLANE -A-
VIEW P-P
VIEW R-R
PIN CONFIGURATION
VIEW D
PROP OIL INLET
11X9636
SLIP RING ASSY
SECT N-N
SECT F-F
SK108280
CAUTION:
CADAM DATA BASE MAY NOT BE TO SCALE
PF8T60 PROPFAN INSTALLATION
73030
SK108280

PRECEDING PAGE BLANK NOT FILMED

FIGURE 19.1 LAP INSTALLATION DRAWING

PAGE 230 INTENTIONALLY BLANK

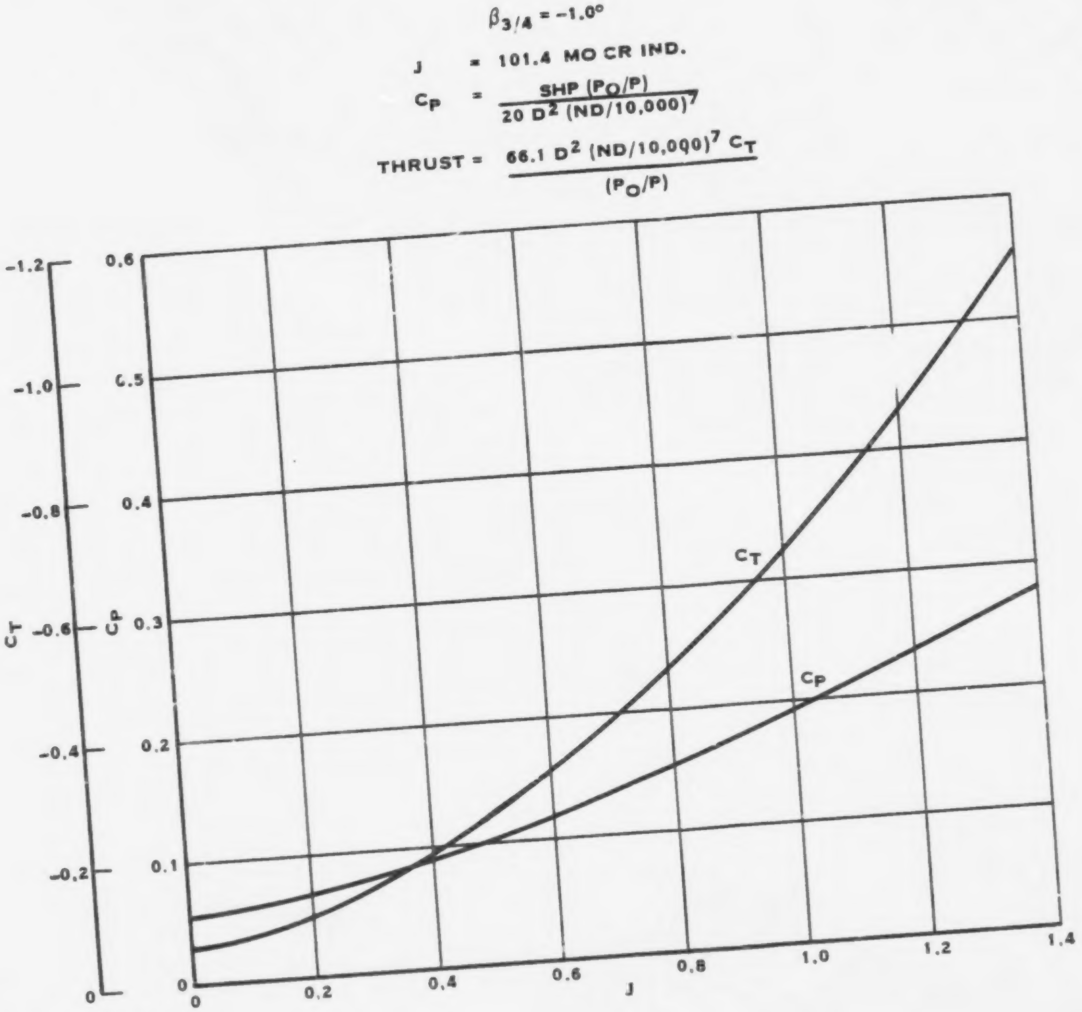

$\beta_{3/4} = -1.0°$

J = 101.4 MO CR IND.

$$C_P = \frac{SHP\ (P_O/P)}{20\ D^2\ (ND/10{,}000)^7}$$

$$THRUST = \frac{66.1\ D^2\ (ND/10{,}000)^7\ C_T}{(P_O/P)}$$

FIGURE 19.2 LAP REVERSE THRUST PRODUCED AND POWER ABSORBED

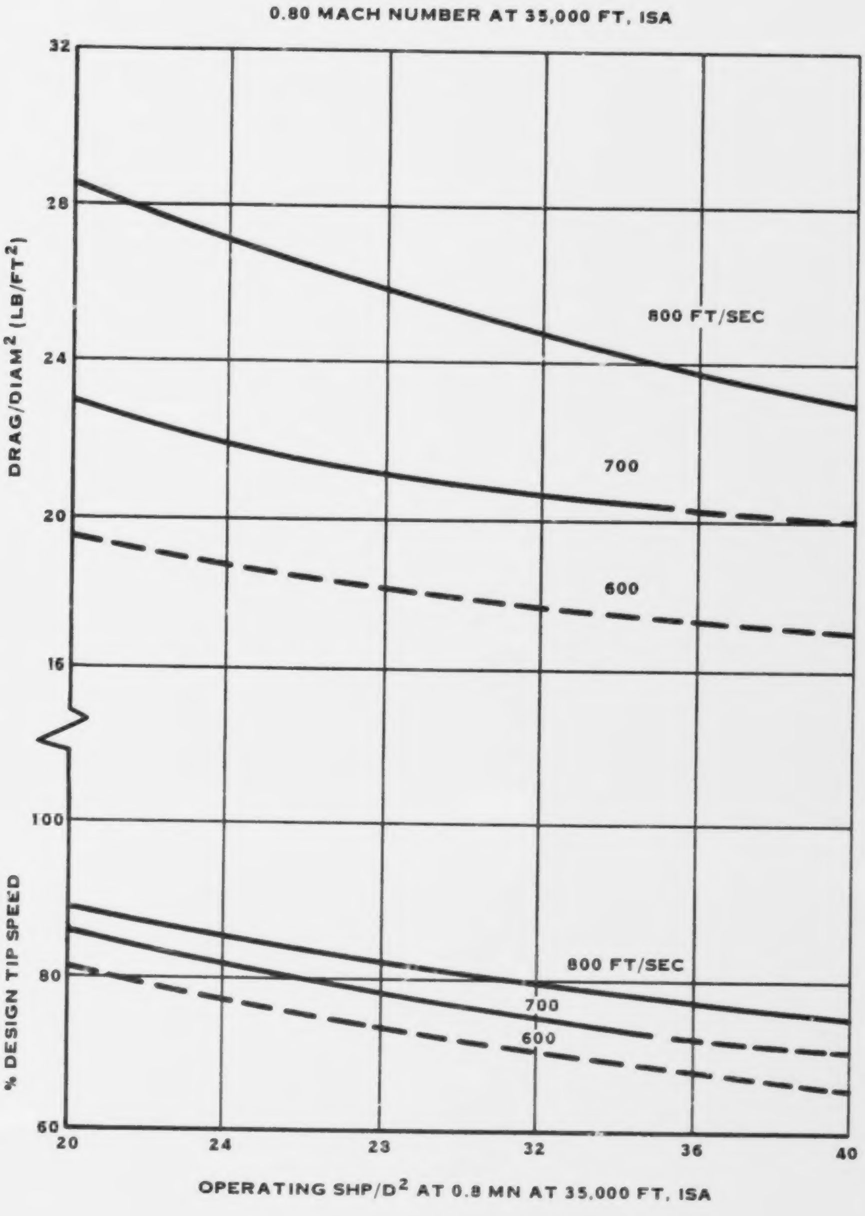

FIGURE 19.4 LAP WINDMILLING DRAG

20.0 CONCLUSIONS AND RECOMMENDATIONS

The overall goal of the Large Scale Advanced Prop-Fan (LAP) program was to demonstrate that the aeroacoustic performance, previously attained with Prop-Fan wind tunnel models, could be achieved with a full scale Prop-Fan structure designed and fabricated using state of the art propeller technology.

The specific objectives, established to achieve this overall goal, were listed in the introductory section of this report. Each of these objectives has been accomplished. The LAP program has taken a significant step toward demonstrating the feasibility of using single rotation, tractor type Prop-Fans for propulsion of large commercial and military transport aircraft in the Mach .8 flight regime.

A significant amount of data was also collected, analyzed and documented during the course of the LAP program. This data should serve as a guide for future Prop-Fan designs and also should allow the analytical tools used in the design process to be fine tuned.

The conclusions derived from the research performed during the Large Scale Advanced Prop-Fan Program are listed below. Some of the findings of the program point to the need for additional investigation and research. Recommendations for additional effort are also presented.

20.1 CONCLUSIONS

- The design objectives for the Large Scale Advanced Prop-Fan were completely satisfied in almost every case. Resonance avoidance criteria, structural dynamic stability, required component ultimate and yield strengths and specified low and high cycle fatigue lives were analytically demonstrated to have been achieved. The exceptions were the low cycle fatigue lives of the blade shell for the reverse thrust case and the blade retention ball bearing for the takeoff and climb case. These calculated low cycle fatigue lives were below 50,000 hours but were more than adequate for the foreseen usage of the Large Scale Advanced Prop-Fan. The blade second vibratory mode was also found to impinge slightly on the 3P resonance avoidance zone, however no source of 3P excitation is expected to be present.

- Failure modes and effects analysis of the SR-7L Prop-Fan system identified no catastrophic failure modes. Critical failure modes identified were determined to be highly unlikely.

236 INTENTIONALLY BLANK

20.1 (Continued)

- The SR-7A model Prop-Fan was designed assuming that aeroelastic similarity with the SR-7L Large Scale Advanced Prop-Fan could be achieved by matching the SR-7A blade mass and stiffness distributions to the SR-7L and scaling the SR-7A retention stiffness from the SR-7L by the ratio of the SR-7A to SR7L blade loads. Analysis indicated that this approach would achieve good correlation between the flutter stability and resonance characteristics of the SR-7A and SR-7L.

- The SR-7L blade retention stiffness test demonstrated that the measured stiffness fell midway between the stiffnesses determined by 2-D and 3-D analysis. The correlation with analysis was sufficient that blade resonance problems were not a concern.

- The Whirl Rig Test of the Large Scale Advanced Prop-Fan revealed two areas requiring redesign, the control speed set cam and the blade seal. The overall control governor gain was found to be lower than predicted but acceptable.

- The static and vibratory experimental stress analysis of the SR-7L blade showed reasonable agreement with finite element analyses. The SR-7L blade fatigue test provided confidence in the fatigue allowables used for blade design. However, the configuration of the blade, with the sheath overlapping a portion of the spar, makes the blade susceptible to a crack in the sheath propagating into the spar. Periodic inspection of the sheath for crack initiation is therefore required to protect against spar fracture.

- Fatigue testing and experimental stress analysis conducted on the hub demonstrated that the fatigue and static strength of the hub are more than adequate. This was as expected since the hub was designed to meet stiffness requirements.

- The static aerodynamic performance of the SR-7L Large Scale Advanced Prop-Fan corresponded well with analytical predictions for blade angles up to 30°. At blade angles above 30° the measured thrust produced and power absorbed were lower than predicted. The measured pressure loading distribution on the blade surface was also significantly different than predicted. Blade vibratory stresses were found to increase significantly as blade angle was increased beyond 30°. This increase in vibratory stress is characterized as stall buffet and is believed to be related to the fall off in aerodynamic performance, though the mechanism by which this occurs is not clear from the data that has been acquired. The correlation between measured and predicted blade deflections indicated that discrepancies between measured and predicted static aerodynamic performance are not the result of an unexpected deflected blade shape.

20.1 (Continued)

- Wind tunnel testing of the SR-7L demonstrated that the Prop-Fan was free of unstalled flutter at operating conditions comparable to the Mach .8 design cruise case. The measured aerodynamic performance of the SR-7L, over a range of Mach numbers to .8, compared favorably with predictions. Comparison of measured and predicted performance was restricted to low power points due to the operating limitations of the test facility. The measured blade surface pressure distributions showed evidence of leading edge and tip vortex flow at low Mach numbers and shocks attached to the camber surface at high Mach numbers.

- Wind tunnel testing of the SR-7A aeroelastic model showed good correlation between the aeroelastic performance of the model and the SR-7L Large Scale Advanced Prop-Fan.

20.2 RECOMMENDATIONS

- The stall buffet phenomena observed during Static Rotor Testing of the SR-7L prevents the Prop-Fan from absorbing design power at design rpm statically due to high vibratory blade stress. Additional research is necessary to understand the mechanisms causing this phenomena and to formulate single rotation Prop-Fan designs that avoid it.

- Static test results showed that the aerodynamic performance of the SR-7L Prop-Fan was not accurately predicted for high power static cases. The measured blade loading distribution was also not accurately predicted by analysis. More effort is needed to improve the analytical tools used to predict Prop-Fan static aerodynamic behavior. Research into the wake configuration for Prop-Fan blades is one area that might help improve the accuracy of the analytical tools. Improved understanding of the static aerodynamics of Prop-Fans may also lead to a better understanding of stall buffet.

- The LAP High Speed Wind Tunnel tests resulted in the acquisition of extensive blade surface pressure data. This data affords the opportunity to significantly improve the analytical tools used in aerodynamics, acoustics, and structural design. Predictions of the SR-7L blade surface pressure distribution, devised from various analytical techniques should be correlated with this data to determine how these techniques could be fine tuned to improve their accuracy.

REFERENCES

1. "Large Scale Advanced Prop-Fan (LAP) Performance, Acoustic and Weight Estimation", NASA CR 174782.

2. L.C. Billman, etal, "Large Scale Prop-Fan Structural Design Study", Volume I Initial Concepts, NASA CR 174992

3. L.C. Billman, etal, "Large Scale Prop-Fan Structural Design Study", Volume II Preliminary Design of SR-7, NASA CR 174993

4. W.E. Sullivan, J.E. Turnberg, J.A Violette, "Large Scale Advanced Prop-Fan (LAP) Blade Design", NASA CR174790

5. J.E. Turnberg, "Classical Flutter Stability of Swept Propellers", AIAA/ASME/ASCE/AHS 24th Structures, Structural Dynamics and Materials Conference, May 1983

6. M. Soule, "Large Scale Advanced Prop-Fan (LAP) Hub/Blade Retention Design Report", NASA CR 174786

7. R.A. Schwartz, P. Carvalho, M.J. Cutler, "Large Scale Prop-Fan (LAP) Pitch Change Actuator and Control Design Report", NASA CR 174788

8. B.P. Huth, "System Design and Integration of the Large Scale Advanced Prop-Fan", NASA CR 174789

9. M. Gruber, "LAP Instrumentation Design Report", HSER 9790

10. D. Nagle, S. Auyeung, J.E. Turnberg, "SR-7A Aeroelastic Model Design Report", NASA CR 174791

11. C.L. DeGeorge, J.E. Turnberg, H.S. Wainauski, "Large Scale Advanced Prop-Fan (LAP) Static Rotor Test Report", NASA CR 180848

12. P.J. Arseneaux, W.A. Campbell, H.S. Wainauski "Large Scale Advanced Prop-Fan (LAP) High Speed Wind Tunnel Test Report" NASA CR 182125

13. P. Bushnell, "Measurement of the Steady Pressure Distribution on a Single Rotation Large Scale Advanced Prop-Fan Blade" NASA CR 182124.

14. P. Bushnell, "Measurement of the Unsteady Pressure Distribution on a Single Rotation Large Scale Advanced Prop-Fan Blade", NASA CR 182123.

APPENDIX A

The definition of "Hazard Category" and "Hazard Probability" were taken from MIL-STD-1629A and are listed below for reference.

Hazard Category:

Category I - Catastrophic - A failure which may cause death or system loss (i.e., aircraft, missile, ship, etc.)

Category II - Critical - A failure which may cause severe injury, major property damage, or major system damage which will result in mission loss.

Category III - Marginal - A failure which may cause minor injury, minor property damage, or minor system damage which will result in delay or loss of availability or mission degradation.

Category IV - Minor - A failure not serious enough to cause injury, property damage, or system damage, but which will result in unscheduled maintenance or repair.

Hazard Probability:

Level A - Frequent. A high probability of occurrence during the item operating time interval. High probability may be defined as a single failure mode probability greater than 0.20 of the overall probability of failure during the item operating time interval.

Level B - Reasonably Probable. A moderate probability of occurrence during the item operating time interval. Probable may be defined as a single failure mode probability of occurrence which is more than 0.10 but less than 0.20 of the overall probability of failure during the item operating time.

Level C - Occasional. An occasional probability of occurrence during item operating time interval. Occasional probability may be defined as a single failure mode probability of occurrence which is more than 0.01 but less than 0.10 of the overall probability of failure during the item operating time.

Level D - Remote. An unlikely probability of occurrence during item operating time interval. Remote probability may be defined as a single failure mode probability of occurrence which is more than 0.001 but less than 0.01 of the overall probability of failure during the item operating time.

Level E - Extremely Unlikely. A failure whose probability of occurrence is essentially zero during item operating time interval. Extremely unlikely may be defined as a single failure mode probability of occurrence which is less than 0.001 of the overall probability of failure during the item operating time.

PRECEDING PAGE BLANK NOT FILMED

PAGE 244 INTENTIONALLY BLANK

The definition of "Hazard Category" and "Hazard Probability" were taken from MIL-STD-1629A and are listed below for reference.

Hazard Category:

Category I - Catastrophic - A failure which may cause death or system loss (i.e., aircraft, missile, ship, etc.)

Category II - Critical - A failure which may cause severe injury, major property damage, or major system damage which will result in mission loss.

Category III - Marginal - A failure which may cause minor injury, minor property damage, or minor system damage which will result in delay or loss of availability or mission degradation.

Category IV - Minor - A failure not serious enough to cause injury, property damage, or system damage, but which will result in unscheduled maintenance or repair.

Hazard Probability:

Level A - Frequent. A high probability of occurrence during the item operating time interval. High probability may be defined as a single failure mode probability greater than 0.20 of the overall probability of failure during the item operating time interval.

Level B - Reasonably Probable. A moderate probability of occurrence during the item operating time interval. Probable may be defined as a single failure mode probability of occurrence which is more than 0.10 but less than 0.20 of the overall probability of failure during the item operating time.

Level C - Occasional. An occasional probability of occurrence during item operating time interval. Occasional probability may be defined as a single failure mode probability of occurrence which is more than 0.01 but less than 0.10 of the overall probability of failure during the item operating time.

Level D - Remote. An unlikely probability of occurrence during item operating time interval. Remote probability may be defined as a single failure mode probability of occurrence which is more than 0.001 but less than 0.01 of the overall probability of failure during the item operating time.

Level E - Extremely Unlikely. A failure whose probability of occurrence is essentially zero during item operating time interval. Extremely unlikely may be defined as a single failure mode probability of occurrence which is less than 0.001 of the overall probability of failure during the item operating time.

PRECEDING PAGE BLANK NOT FILMED

PAGE 244 INTENTIONALLY BLANK

FAILURE MODE & EFFECT ANALYSIS

SYSTEM LAP 108 Prop-Fan
SUBSYSTEM Control Housing
DRAWING NO. L-14325-3

REPORT
DATE 6/29/84 PAGE 1 OF 9
PREPARED BY T. Sutek/R. Schwartz
FILE REF 6970A, 6971A

ITEM	PART OR ASSEMBLY DESCRIPTION	MODE OF FAILURE	EFFECT OF FAILURE ON THE SYSTEM	HAZ. CAT.	HAZ. PROB.	REMARKS
1.0	Main Pump	Low or No Pump Output	Supply Pressure decreases. Main and Standby Regulating Valve shifts to maintain supply pressure. Standby Pump Check Valve opens. System continues to function normally on Standby Pump. Maximum slew rate of propeller is reduced. Response to transients may be slowed. Control operating temperature increases slightly.	IV	C	A Standby Pump provides operating pressure in the event of a Main Pump failure.
2.0	Standby Pump	Low or No Pump Output	System continues to function normally dn Main Pump. Low output from Standby Pump causes flow switch to close illuminating a warning light. Maximum slew rate of propeller is reduced. Response to transients may be slowed.	IV	C	In the event of a Main and Standby Pump failure, the propeller can be feathered by the Auxiliary Pump which is actuated by the airframe mounted emergency feather button.
3.0	Scavenge Pump	Low or No Output	Normal oil leakage or drainage collecting in Atmospheric Sump will not be returned to Pressurized Sump. Sump pressurization will be lost. Main or Standby Pump cavitation is possible. Maximum slew rate of propeller is reduced. Response to transients may be slowed. If total loss of supply oil occurs, propeller will pitchlock.	IV	C	
4.0	Auxiliary Pump	Low or No Pump Output	Loss of ground handling capability. No feather capability in case of loss of primary hydraulics.	IV	D	
5.0	Auxiliary Scavenge Pump	Low or No Pump Output	Sump cannot be pressurized for ground handling operations. Normal oil leakage or drainage will not be returned to the pressurized sump. Auxiliary Pump cavitation is possible. No feather capability in case of loss of primary hydraulics.	IV	D	
6.0	Auxiliary Motor	No or Low Torque Output	Little or no Auxiliary Pump output. Little or no Auxiliary Scavenge Pump output. Loss of ground handling capability. No feather capability in case of loss of primary hydraulics.	IV	C	

FAILURE MODE & EFFECT ANALYSIS

SYSTEM LAP 10B Prop-Fan
SUBSYSTEM Control Housing
DRAWING NO. L-14325-1

REPORT
DATE 6/29/84 PAGE 2 OF 9
PREPARED BY T. Sutak/R. Schwartz
FILE REF 6970A, 6971A

ITEM	PART OR ASSEMBLY DESCRIPTION	MODE OF FAILURE	EFFECT OF FAILURE ON THE SYSTEM	HAZ. CAT.	HAZ. PROB.	REMARKS
7.0	Sump Relief Valve	Valve fails open	Sump pressurization is lost. Main and Standby Pump cavitation is possible. Maximum slew rate of propeller is reduced. Response to transients may be slowed.	IV	D	
		Valve fails closed	Sump and actuator pressure increases. Seal or sump failure occurs. System pressure is lost. Propeller pitchlocks.	III	F	The Sump Relief Valve is a ball type check valve. A failure of this type is considered extremely unlikely. System pressure acts to open valve.
8.0	Main Pump Check Valve	Valve fails closed	Main Pump pressure increases. Main Pump or seal failure occurs.	IV	E	System pressure acts to open valve. This type of failure is considered extremely unlikely.
		Valve fails open	Operation other than feather, system operates normally. Ground handling and Auxiliary Pump feathering capability is lost.	IV	[illegible]	
9.0	Standby Pump Check Valve	Valve fails closed	Standby Pump pressure increases. Standby Pump or seal failure occurs.	IV	E	System pressure acts in a direction to open the valve. This type of failure is considered extremely unlikely.
		Valve fails open	Operation other than feather, system operates normally. Ground handling and Auxiliary Pump feathering capability is lost. Standby Pump operating temperature increases.	IV	D	
10.0	Auxiliary Pump Check Valve	Valve fails closed	Auxiliary Pump cannot supply oil to pitch change actuator for ground handling operations or feathering. Propeller may still be feathered with primary hydraulics.	IV	[illegible]	Auxiliary Pump pressure acts to open valve.
		Valve fails open	Supply pressure leaks to drain. Maximum slew rate of propeller is reduced. Response to transients may be slowed. Propeller may pitchlock.	IV	[illegible]	

ORIGINAL PAGE IS
OF POOR QUALITY

FAILURE MODE & EFFECT ANALYSIS

SYSTEM LAP 108 Prop-Fan
SUBSYSTEM Control Housing
DRAWING NO. L-14325-3

REPORT
DATE 6/29/84 PAGE 3 OF 9
PREPARED BY T. Sutak/R. Schwartz
FILE REF 6970A, 6971A

ITEM	PART OP ASSEMBLY DESCRIPTION	MODE OF FAILURE	EFFECT OF FAILURE ON THE SYSTEM	HAZ. CAT.	HAZ. PROB.	REMARKS
11.0	Auxiliary Scavenge Pump Check Valve	Valve fails closed	Auxiliary Scavenge Pump pressure increases. Auxiliary Scavenge Pump or seal failure occurs.	IV	E	Auxiliary Scavenge Pump pressure acts in a direction to open the valve. The Auxiliary Scavenge Pump Check Valve is a ball type check valve. This type of failure is considered extremely unlikely.
		Valve fails open	Sump pressurization is lost. Cavitation of Main, Standby, or Auxiliary Pump is possible.	IV	D	
12.0	High Pressure Relief Valve	Valve fails open	Maximum slew rate of propeller is reduced. Response to transients may be slowed.	IV	D	
		Valve fails closed	Operation other than feather: System operates normally.	III	E	The High Pressure Relief Valve acts as a backup pressure regulating device for the Main and Standby Regulating Valve.
			Feather Operation: System experiences abnormally high pressures. Seal or structural damage is possible.	III	E	Propeller must continue to rotate after feather position is reached for failure to occur. A failure of this type is considered unlikely.
13.0	Main Filter	Filter clogs	Filter Bypass Valve opens. Control continues to function on unfiltered oil.	III	D	All critical downstream components have individual screens of finer mesh than that used in the Main Filter. Additionally, the pumps are equipped with inlet screens.
14.0	Standby Filter	Filter clogs	Filter Bypass Valve opens. Control continues to function on unfiltered oil.	III	D	All critical downstream components have individual screens of finer mesh than that used in the Standby Filter.
15.0	Filter Bypass Valve	Valve fails closed	If filters are clear: No affect on system. If filters are clogged: Pump damage or structural failure is possible.	IV	E	

FAILURE MODE & EFFECT ANALYSIS

SYSTEM LAP 108 Prop-Fan
SUBSYSTEM Control Housing
DRAWING NO. L-14325-3

REPORT
DATE 6/29/84 PAGE 4 OF 9
PREPARED BY T. Sutak/R. Schwartz
FILE REF 6970A, 6971A

ITEM	PART OR ASSEMBLY DESCRIPTION	MODE OF FAILURE	EFFECT OF FAILURE ON THE SYSTEM	HAZ. CAT.	HAZ. PROB.	REMARKS
16.0	Heat Exchanger Bypass Valve	Valve fails open	Propeller oil temperature increases. Seal and bearing degradation possible. Potential Transfer Bearing seizure. Propeller may pitchlock or feather dependent upon bearing damage location.	[illegible]	[illegible]	
		Valve fails closed	If extreme low oil temperatures exist, excessive flow restriction in the heat exchanger can occur. Supply pressure increases until High Pressure Relief Valve opens.	IV	E	The system will operate at the High Pressure Relief Valve setting. As oil temperature increases, it will begin to flow through heat exchanger. Supply pressure is monitored for failure detection.
17.0	Delta Pressure Valve	Upstream orifice clogs (P supply)	Supply pressure decreases. Propeller pitchlocks.	IV	[illegible]	The system is equipped with a Main and Standby filter. In addition, the orifices have their own screens.
		Downstream orifice clogs (P drain)	Backup pressure increases. Main and Standby Regulating Valve shifts to bypass less flow. Supply pressure increases until High Pressure Relief Valve opens.	IV	[illegible]	The system is equipped with a Main and Standby filter. In addition, the orifices have their own screens. The system will operate at the High Pressure Relief Valve setting. Supply pressure is monitored for failure detection.
18.0	Main and Standby Regulating Valve	Seized (No Supply pressure bypass position)	System pressure increases to cracking pressure of High Pressure Relief Valve.	IV	[illegible]	The system will operate at the High Pressure Relief Valve setting.
		Seized (Supply pressure bypass position)	Main and Standby Pump output is bypassed to drain. Propeller will pitchlock.	IV	C	
19.0	Servo Governor	Valve seizes in increase pitch position or Speeder Spring/Speed Set Linkage failure causes valve to go to increase pitch position.	Propeller will feather.	IV	E	This is a rotating valve and thus a seizure is extremely unlikely. The linkage and spring are conservatively designed.
		Valve seizes in decrease pitch position or loss of fly weights or Governor drive.	Blade pitch moves to decrease pitch position. Propeller overspeeds.	IV	[illegible]	This is a rotating valve and thus a seizure is extremely unlikely. The aircraft supplied electrical overspeed governor will activate the Feather Solenoid and maintain RPM at overspeed setting. Pilot may feather the propeller.

NAL PAGE IS
OF POOR QUALITY

FAILURE MODE & EFFECT ANALYSIS

SYSTEM [illegible]
SUBSYSTEM [illegible]
DRAWING NO. [illegible]

REPORT
DATE 6/29/84 PAGE 6 OF 9
PREPARED BY T. Sufak/R. Schwartz
FILE REF 6970A, 6971A

ITEM	PART OR ASSEMBLY DESCRIPTION	MODE OF FAILURE	EFFECT OF FAILURE ON THE SYSTEM	HAZ. CAT.	HAZ. PROB.	REMARKS
[illegible]	Seals (Leaks)	[illegible]	Maximum slew rate of propeller is reduced. Response to transients may be slowed. If leakage is severe, supply pressure will decrease and propeller may pitch lock.	IV	D	System Supply pressure is monitored.
		Supply Pressure leaks to Metered Pressure.	If leakage is minimal, maximum slew rate of propeller is reduced. Drift in operating RPM occurs. Response to transients may be slowed. If leakage is severe, piston will move to decrease pitch position. The propeller overspeeds.	IV	D	The aircraft supplied electrical overspeed governor will activate feather solenoid and maintain RPM at overspeed setting. Pilot may feather the propeller. Where probability is higher (i.e. dynamic seals) Supply and Metered pressure are separated by drain pressure.
		Metered Pressure leaks to drain.	If leakage is excessive, the propeller will feather. Drift in operating RPM occurs. Response to transients may be slowed.	IV	E	
		Supply Pressure leaks to Delta P valve signal	Main and Standby Regulating Valve function is lost. System continues to function normally on the High Pressure Relief Valve.	IV	D	
24.0	Delta Pressure Regulating Valve	Valve Seizes (Supply Pressure ported to Metered Pressure)	Metered pressure rises to Supply pressure. Propeller overspeeds.	IV	D	Valve generates sufficient force to overcome 20 lbs of resistance. The aircraft supplied electrical overspeed governor will activate feather solenoid and maintain RPM at overspeed setting. Pilot may feather the propeller.
		Valve Seizes (Metered Pressure ported to Sump)	Metered pressure is ported to sump. Piston moves to increase pitch.	IV	[illegible]	
		Valve seizes in null position.	Excessive forces are applied to the actuator linkage.	III	E	

ORIGINAL PAGE IS
OF POOR QUALITY

FAILURE MODE & EFFECT ANALYSIS

SYSTEM [illegible]
SUBSYSTEM Pitch Change Actuator
DRAWING NO. [illegible]

REPORT
DATE 6/29/84 PAGE 7 OF 9
PREPARED BY T. Sutak/R. Schwartz
FILE REF 6970A, 6971A

ITEM NO.	PART OR ASSEMBLY DESCRIPTION	MODE OF FAILURE	EFFECT OF FAILURE ON THE SYSTEM	HAZ. CAT.	HAZ. PROB.	REMARKS
[illegible]	Actuator Valve	Valve sticks in null position	Actuator valve and pitch change actuator remain in position at time of failure. Propeller remains in fixed position.	IV	D	
		Valve sticks in position other than null	Actuator moves in direction of last called for signal until valve moves or actuator linkage failure occurs. If failure is in decrease pitch direction, propeller will pitchlock. If failure is in increase pitch direction, propeller will feather.	III	D	Very large actuator force is available to move Actuator Valve.
[illegible]	Ballscrew/Spline Shaft	Ballscrew spline shaft fails open	Servo output does not drive Actuator Valve. Dependent upon vibration levels, and friction, Actuator Valve may move to increase pitch, decrease pitch, or null position. If increase or decrease direction, blade angle changes slowly. The blade angle is limited by the low pitch stop in the decrease pitch direction.	III		Actuator valve seal friction acts to hold valve in position. Propeller speed is controllable by reduction in engine power level and aircraft speed.
[illegible]	Pitchlock Screw	Pitchlock Screw fails open	Servo output does not drive Actuator Valve. Dependent upon vibration levels, and friction, Actuator Valve may move to increase pitch, decrease pitch, or null position. If increase or decrease direction, blade angle changes slowly. The blade angle is limited by the low pitch stop in the decrease pitch direction.	IV	E	There is a high probability of loads overcoming valve seal friction. Propeller speed is controllable by reduction in engine power level and aircraft speed.
[illegible]	Actuator Valve Drive Rod	Actuator Valve Drive rod fails open	Servo output does not drive Actuator Valve. Dependent upon vibration levels, and friction, Actuator Valve may move to increase pitch, decrease pitch, or null position. If increase or decrease direction, blade angle changes slowly. The blade angle is limited by the low pitch stop in the decrease pitch direction.	IV	E	There is a low probability of loads overcoming Actuator Valve seal friction. Propeller speed is controllable by reduction in engine power level and aircraft speed.
[illegible]	Servo	Jams	Servo becomes locked in position. Propeller will remain fixed in position at time of failure.	IV	D	

FAILURE MODE & EFFECT ANALYSIS

SYSTEM LAP [illegible]
SUBSYSTEM Pitch Change Actuator
DRAWING NO. 1-14525-3

REPORT
DATE 6/29/84 PAGE 8 OF 9
PREPARED BY T. Sutek/R. Schwartz
FILE REF 6970A, 6971A

ITEM	PART OR ASSEMBLY DESCRIPTION	MODE OF FAILURE	EFFECT OF FAILURE ON THE SYSTEM	HAZ. CAT.	HAZ. PROB.	REMARKS
[illegible]	Pitch Control Actuator	Actuator jammed	Actuator remains fixed in position at time of failure. No pitch change possible, propeller remains at fixed pitch.	IV	D	
		Fails open	Propeller goes to low pitch. Propeller overspeeds, blade angle is uncontrollable.	II	E	Pitch Control Actuator is designed as a primary structure and as such, this failure is considered unlikely.
[illegible]	Actuator Outer Wall	Fails open	Actuator will rotate with respect to blade trunnions until blade disengage. Propeller overspeeds, blade angle is uncontrollable.	II	E	Pitch Control Actuator is designed as a primary structure and as such, this failure is considered unlikely.
[illegible]	Yoke Actuator	Fails open (loss of Barrel lubricating oil)	Loss of lubrication oil for ballscrew bearings, trunnion rollers, [illegible]. Wear increases.	IV	E	External leakage is visually detected on normal walk around check.
[illegible]	Seals and Transfer Tubes	Supply to Governor Metered Pressure leakage	Propeller goes to decrease pitch. Propeller will overspeed.	II	E	All dynamic seals for Supply to Governor Metered pressure are separated by drain pressure. The aircraft supplied electrical overspeed governor will activate feather solenoid and maintain RPM at overspeed setting. Pilot may feather the propeller.
		Governor Metered Pressure to Pressurized Sump leakage	Shift in operating RPM occurs. Maximum slew rate of propeller is reduced. Response to transients may be slowed. If leakage is severe, propeller will feather.	IV		
		Actuator Metered Pressure leaks High to Low	Maximum slew rate of propeller is reduced. Response to transients may be slowed. If leakage is severe, propeller will pitchlock.	IV	C	
		Any leakage to Barrel cavity	Maximum slew rate of propeller may be reduced. Response to transients may be slowed. If leakage is severe, control may run dry, propeller will pitchlock. Barrel pressure increases with blade seal leakage possible.	IV		Oil level in Barrel and Control should be checked periodically.

ORIGINAL PAGE IS
OF POOR QUALITY

FAILURE MODE & EFFECT ANALYSIS

SYSTEM [illegible] Propeller
SUBSYSTEM Pitch Change Actuator
DRAWING NO. [illegible]

REPORT
DATE 6/29/84 PAGE 9 OF 9
PREPARED BY T. Sutak/R. Schwartz
FILE REF 6970A, 6971A

ITEM	PART OR ASSEMBLY DESCRIPTION	MODE OF FAILURE	EFFECT OF FAILURE ON THE SYSTEM	HAZ. CAT.	HAZ. PROB.	REMARKS
34.0	Transfer Bearing	Seizure (Supply Pressure leaks to drain)	Maximum slew rate of propeller is reduced. Response to transients may be reduced.	IV	C	
		Seizure (Supply Pressure leaks to Metered Pressure)	Propeller moves toward decreased pitch. Propeller rpm increases.	IV	C	Propeller speed is controllable by reduction in engine power level and aircraft speed. Propeller may be feathered by the feather valve.
		Seizure (Metered Pressure leaks to drain)	Propeller feathers.	IV	[illegible]	
35.0	Barrel	Fracture (cracks through the wall)	Loss of blade retention and trunion lubricating oil	II	E	Barrel is designed as a primary structure and as such this failure is considered unlikely. External leakage will be visible during normal walk around check.
36.0	Blade Retention	Fracture of Balls/Races or Spalling	Maximum slew rate of propeller is reduced. Response to transients may be slowed.	III	F	
37.0	Trunion	Fracture	No response to pitch change inputs for affected blade.	III	E	Remaining blades will respond to pitch change inputs.
38.0	Propeller Blade	Separation of shell	Loss of blade performance.	III	E	Propeller can be moved to the feather position.
		Spar separation	Loss of blade retention and trunion lubricating oil.	II	E	Blade Spar is designed as a prime structure and as such this failure is considered unlikely.

1. Report No. CR 182112

2. Government Accession No.

3. Recipient's Catalog No.

4. Title and Subtitle
Large Scale Advanced Prop-Fan (LAP)

5. Report Date

6. Performing Organization Code
73030

7. Author(s)
C. L. DeGeorge

8. Performing Organization Report No.

9. Performing Organization Name and Address
Hamilton Standard Division, UTC
P. O. Box 1000
Windsor Locks, CT 06096

10. Work Unit No.
HSER 11803

11. Contract or Grant No.
NAS3-23051

12. Sponsoring Agency Name and Address
NASA Lewis Research Center
21000 Brookpark Road
Cleveland, OH 44135

13. Type of Report and Period Covered
Contractor Report

14. Sponsoring Agency Code

15. Supplementary Notes
Project Managers: J. Notardonato, D. Sagerser, I. Sumner
Advanced Turboprop Project Office
NASA Lewis Research Center, Cleveland, OH 44135

16. Abstract

In recent years, considerable attention has been directed toward improving aircraft fuel efficiency. Analytical studies and research with wind tunnel models have demonstrated that the high inherent efficiency of low speed turboprop propulsion systems may now be extended to the Mach .8 flight regime of today's commercial airliners. This can be accomplished with a propeller, employing a large number of thin highly swept blades. The term Prop-Fan has been coined to describe such a propulsion system.

In 1983 the NASA-Lewis Research Center contracted with Hamilton Standard to design, build and test a near full scale Prop-Fan, which was designated the Large Scale Advanced Prop-Fan (LAP). This report provides a detailed description of the Large Scale Advanced Prop-Fan program. The assumptions and analytical procedures used in the design of the Prop-Fan system components are discussed in detail. The manufacturing techniques used in the fabrication of the Prop-Fan are presented. Each of the tests run during the course of the program are also discussed and the major conclusions derived from the tests are stated.

17. Key Words (Suggested by Author(s))
Prop-Fan

18. Distribution Statement

19. Security Classif. (of this report)

20. Security Classif. (of this page)

21. No. of Pages
256

22. Price*

* For sale by the National Technical Information Service, Springfield, Virginia 22161

NASA-C-168 (Rev. 10-75)